

Contribution of HIV-1 subtype C envelope glycoprotein conformations in apoptosis of uninfected bystander CD4⁺ T lymphocytes

Nelia Phuti Manamela (736237)



A dissertation submitted to the Faculty of Health Sciences, University of the Witwatersrand, Johannesburg, in fulfilment of the requirements for the degree of Master of Science in Medicine.

November 2019

Declaration

I, Nelia Phuti Manamela declare that this dissertation is my own work. It is being submitted for the degree of Master of Science in Medicine in the University of the Witwatersrand, Johannesburg. It has not been submitted before for any degree or examination at this or any other University.

Nelia Phuti Manamela

_____ day of November, 2019

Dedication

This dissertation is dedicated to my amazing grandmother, parents, sister and brother, for their valuable support, sacrifices, encouragements and believing in my capabilities even when I did not. You have made me yearn to excel beyond my background and for that I am eternally grateful. This work is dedicated to you as a sign of my love and appreciation for all that you have done.

Conference presentations arising from this study

1. **Manamela, N.P**, Khanyile, T, and Papathanasopoulos, M. A. Contribution of HIV-1 subtype C envelope glycoprotein conformations in apoptosis of uninfected bystander CD4⁺ T lymphocytes. November 2018, Molecular Biosciences Research Thrust (MBRT), University of the Witwatersrand, Johannesburg, South Africa. Oral presentation.

Achievement: 1st prize for best oral presentation.

2. **Manamela, N.P**, Khanyile, T, and Papathanasopoulos, M. A. Contribution of HIV-1 subtype C envelope glycoprotein conformations in apoptosis of uninfected bystander CD4⁺ T lymphocytes. October 2018, 9th cross-faculty postgraduate symposium, University of the Witwatersrand, Johannesburg, South Africa. Poster presentation.

Abstract

HIV-1 primarily infects CD4-expressing T lymphocytes causing their progressive depletion, ultimately leading to acquired immunodeficiency syndrome (AIDS). Interestingly, uninfected bystander CD4⁺ T cells are also implicated in the depletion. This bystander effect is attributed to the interaction of uninfected CD4⁺ T cells with viral proteins such as the envelope glycoproteins (Env) leading to programmed cell death commonly known as apoptosis. However, HIV-1 Env is dynamic and exists in monomeric and trimeric conformations, but the contribution of each conformation to bystander apoptosis remains controversial. Therefore this study evaluated the contribution of HIV-1 subtype C Env conformations to bystander apoptosis, specifically mediated via CD4 signalling. The Env conformations used included matched monomeric gp120_{FVC}, trimeric gp140_{GCN4} and gp140_{SOSIP} (based on founder virus sequence).

Env recombinant proteins were expressed in HEK 293T and HEK 293F cells, as confirmed by SDS-PAGE and Western blots analyses. Subsequently, Env monomers and trimers were purified to homogeneity by lectin affinity and size exclusion chromatography, which were further confirmed by blue native PAGE. Structural integrity and functionality of each Env conformation was then validated using conformation-specific antibodies (CAP256-VRC26.25, 10E8, IgG1b12) and binding to antibody 17b in the presence of soluble CD4 in ELISAs, respectively. Bystander apoptosis induction of Jurkat T cells was measured by flow cytometry up to 72 hours post addition of a range (50 to 500 nM) of each functional Env conformation, using Annexin V/7-AAD stain, Mitopotential dye, Caspase 3/7 activation antibodies and Multicolor DNA damage assays.

Overall, the trimeric gp140_{SOSIP} and gp140_{GCN4} induced bystander apoptosis via mitochondrial membrane depolarization (intrinsic pathway) with onset reversible DNA fragmentation, in the absence of caspase 3/7 activation. Interestingly, only apoptosis induction by gp140_{GCN4} was associated with phosphatidylserine translocation. By contrast, the monomeric gp120_{FVC} induced bystander apoptosis via both mitochondrial membrane depolarization (intrinsic pathway) and caspase 3/7 activation (extrinsic pathway) with low levels of phosphatidylserine translocation and negligible DNA fragmentation. Collectively, these results confirmed the ability of both

monomeric and trimeric Env conformations to induce CD4-mediated bystander apoptosis via varied mechanisms. The observed differences in apoptosis-inducing capacity of monomeric and trimeric Envs imply possible variations in CD4 binding affinities and signal activation, and warrant further investigation.

Acknowledgements

Beyond everything, I would like to thank God for granting me the opportunity, strength and courage to do this project to my fullest potential.

I would also like to sincerely appreciate the following people for their contributions towards the success of my project;

To my exceptional supervisors Ms Thulile Khanyile and Prof. Maria Papathanasopoulos, a special thank you for your unconditional support, guidance, patience, words of wisdom, sharing your expertise with me and most importantly, pushing me out of my comfort zone. I am really grateful and honoured to have learnt from phenomenal academics such as you.

To Ms Nancy Tumba, Dr Mark Killick, Dr Gavin Owen and Dr Adriaan Basson, thank you for always being so selfless and sacrificing your time to help where you can. The ideas you have suggested and efforts you all made in assisting me in this study are highly valued.

A special thank you to Ms Natasha James and Mr John Walters from Merck, for supplying the Muse mini flow cytometer. To Ms Genevieve Mezoh and Dr Jaclyn Mann from the HIV Pathogenesis Programme (Hasso Plattner Research Laboratory, Nelson R. Mandela School of Medicine), thank you for providing the Jurkat T cells, without which I would not have been able to conduct experiments in this study.

To my colleagues at the HIV Pathogenesis Research Unit (HPRU), my deepest gratitude for your friendship, great support, motivation and for creating a positive, nurturing working environment. Simone Smith and Ashlyn Davis, God knows without your giggles and moral support I would have not come this far. Tumelo Moshoele and Melanie Moodie, thank you for your advices, guidance and prompt assistance in plenty of my experiments.

To my grandmother, parents, sister, brother, nieces, nephew and family at large, thank you for your prayers, love, for always being my biggest cheerleaders and critics. Mom, your desire to see your children excel and achieve beyond what life circumstances deprived you of, has inspired me to unapologetically chase my dreams and be the best version of myself, for that I am grateful.

Last but foremost, I would like to express my deepest appreciation to my closest friends for their companionship, support, understanding, enthusiasm and always being there for me when I needed you the most. Tlakale Mogebeisa and Poppy Mashilo, thank you for your proof reading skills.

Table of Contents

| | |
|--|-------|
| Declaration | ii |
| Dedication | iii |
| Conference presentations arising from this study | iv |
| Abstract | v |
| Acknowledgements | vii |
| List of Figures..... | xiv |
| List of Tables..... | xviii |
| List of Abbreviations | xix |
| 1. Introduction..... | 25 |
| 1.1 HIV/AIDS history and pandemic..... | 25 |
| 1.2 HIV-1 Pathogenesis; role of viral and host proteins | 27 |
| 1.2.1 Virus entry; Envelope-CD4 and co-receptor interactions | 28 |
| 1.2.2 HIV-1 replication; reverse transcription, integration, transcription, translation, assembly and budding | 30 |
| 1.2.3 Clinical course of HIV-1 infection; disease progression to AIDS..... | 33 |
| 1.3 Mechanisms of CD4 ⁺ T cell depletion during HIV-1 infection..... | 35 |
| 1.3.1 HIV-1 mediated bystander apoptosis..... | 36 |
| 1.3.2 Intrinsic pathway and HIV-1 mediated CD4 ⁺ T cell depletion..... | 38 |
| 1.3.3 Extrinsic pathway and HIV-1 mediated CD4 ⁺ T cell depletion..... | 41 |
| 1.3.4 Nef, Tat, Vpr, Vpu and protease mediated bystander apoptosis..... | 42 |
| 1.3.5 Env-mediated bystander apoptosis..... | 44 |
| 1.3.6 Membrane expressed Env-mediated hemifusion, syncytial and contagious apoptosis leading to bystander CD4 ⁺ T cell loss..... | 45 |
| 1.3.7 Soluble gp120 -mediated bystander apoptosis..... | 46 |
| 1.4 Research motivation | 50 |
| 1.5 Research aim and objectives | 51 |

| | |
|---|----|
| 2. Materials and Methods | 52 |
| 2.1 Reagents used in this study | 52 |
| 2.1.1 Recombinant plasmids | 52 |
| 2.1.2 Bacterial strains | 52 |
| 2.1.3 Mammalian cell lines | 52 |
| 2.1.4 Antibodies used in the Indirect ELISAs and Western blot analyses | 53 |
| 2.1.5 Recombinant proteins | 53 |
| 2.2 Plasmid DNA propagation and maintenance | 54 |
| 2.2.1 Preparation of chemically competent cells | 54 |
| 2.2.2 Transformation of chemically competent cells | 54 |
| 2.3 Plasmid DNA isolation | 55 |
| 2.3.1 Qiagen maxi prep | 55 |
| 2.3.2 Quantification of isolated plasmid DNA | 56 |
| 2.3.3 Analysis of plasmid DNA isolation | 56 |
| 2.4 Mammalian and bacterial protein expression | 57 |
| 2.4.1 General mammalian cell culture | 57 |
| 2.4.1.1 Maintenance of HEK 293T, HEK 293F and Jurkat T cells | 57 |
| 2.4.1.2 Preparation of HEK 293T, HEK 293F and Jurkat T cells stocks | 58 |
| 2.4.2 Optimization of transient transfection of HEK 293T cells for recombinant gp140 _{SOSIP} expression | 58 |
| 2.4.3 Expression of gp120 _{FVC} and gp140 _{GCN4} from stable HEK 293F cell line | 60 |
| 2.4.4 Expression of 2dCD4 WT | 60 |
| 2.5 Confirmation of protein expression | 61 |
| 2.5.1 SDS-PAGE | 61 |
| 2.5.2 Western blot analysis | 62 |
| 2.6 Protein purification | 63 |
| 2.6.1 Purification of recombinant gp140 _{SOSIP} , gp140 _{GCN4} and gp120 _{FVC} Env proteins | 63 |

| | | |
|---------|--|----|
| 2.6.1.1 | Lectin affinity chromatography | 63 |
| 2.6.1.2 | Size exclusion chromatography (SEC) | 64 |
| 2.6.2 | Nickel affinity chromatography purification of 2dCD4 WT | 65 |
| 2.7 | Concentration and quantification of purified proteins | 66 |
| 2.7.1 | Bicinchoninic acid assay (BCA) | 66 |
| 2.8 | Biochemical characterization of purified Env; confirmation of correct structural orientation and functionality | 67 |
| 2.8.1 | Blue native-PAGE | 67 |
| 2.8.2 | Indirect ELISA: confirmation of Env conformation integrity and functionality | 68 |
| 2.9 | Flow cytometry detection of apoptosis by the Muse Cell analyser | 72 |
| 2.9.1 | Flow cytometer set up and maintenance..... | 73 |
| 2.9.2 | Set up of assays for apoptosis induction and detection | 74 |
| 2.9.2.1 | Annexin V assay | 76 |
| 2.9.2.2 | Mitopotential assay | 77 |
| 2.9.2.3 | Caspase 3/7 assay | 79 |
| 2.9.2.4 | Multicolor DNA damage assay..... | 81 |
| 2.9.2.5 | Data analysis | 84 |
| 3. | Results..... | 85 |
| 3.1 | Expression and purification of recombinant gp140 _{SOSIP} , gp120 _{FVC} , gp140 _{GCN4} and 2dCD4 WT | 85 |
| 3.1.1 | Large scale propagation of recombinant gp140 _{SOSIP} VRC 3831 and Furin pCDNA 3.3 plasmids | 85 |
| 3.1.2 | Purification of propagated gp140 _{SOSIP} VRC 3831 and Furin pcDNA 3.3 plasmids | 86 |
| 3.1.3 | Optimization of transient transfections of HEK 293T cells for gp140 _{SOSIP} expression, and expression of gp120 _{FVC} , gp140 _{GCN4} from stably transfected HEK 293F cell lines..... | 87 |

| | |
|---|-----|
| 3.1.4 Purification of expressed gp140 _{SOSIP} , gp140 _{GCN4} and gp120 _{FVC} by lectin affinity and size exclusion chromatography | 90 |
| 3.1.5 Bacterial expression and purification of 2dCD4 WT..... | 95 |
| 3.2 Characterization of purified Env for conformational integrity and functionality assessment..... | 96 |
| 3.3 Flow cytometry assessment of Env- mediated bystander apoptosis of uninfected Jurkat T cells | 99 |
| 3.3.1 Annexin V detection of apoptotic uninfected Jurkat T cells post treatment with varying concentrations of gp140 _{SOSIP} , gp140 _{GCN4} and gp120 _{FVC} | 99 |
| 3.3.2 Mitopotential assay detection of apoptosis via intrinsic pathway post treatment of uninfected Jurkat T cells with varying concentrations of gp140 _{SOSIP} , gp140 _{GCN4} and gp120 _{FVC} | 103 |
| 3.3.3 Caspase 3/7 activation in uninfected Jurkat T cells post treatment with varying concentrations of gp140 _{SOSIP} , gp140 _{GCN4} and gp120 _{FVC} | 106 |
| 3.3.4 DNA fragmentation in uninfected Jurkat T cells treated with varying concentrations of gp140 _{SOSIP} , gp140 _{GCN4} and gp120 _{FVC} | 109 |
| 4. Discussion..... | 114 |
| 4.1 Transient and stable expression and purification of recombinant HIV-1 Env conformations (gp140 _{SOSIP} , gp140 _{GCN4} , gp120 _{FVC})..... | 114 |
| 4.2 Purified recombinant FVC gp140 _{SOSIP} , gp140 _{GCN4} and gp120 _{FVC} are conformationally intact and functional | 118 |
| 4.3 Apoptosis-inducing ability of monomeric and trimeric FVC Envs in uninfected Jurkat T cells..... | 120 |
| Appendix A: Composition of solutions used in this study | 130 |
| Appendix B- Quantification of purified plasmid DNA | 139 |
| Appendix C- Annexin V data | 141 |
| Appendix D- Mitopotential data | 147 |
| Appendix E- Caspase 3/7 activation data..... | 153 |
| Appendix F- DNA fragmentation data..... | 159 |
| Appendix G - Ethics waiver..... | 193 |

References..... 165

List of Figures

| | |
|--|----|
| Figure 1.1: Global HIV prevalence. | 27 |
| Figure 1.2: An overview of HIV-1 viral entry into target CD4 -expressing T cells during infection..... | 29 |
| Figure 1.3: A schematic representation of the HIV-1 replication cycle. | 32 |
| Figure 1.4: Time based clinical course of HIV-1 infection from initiation of infection to AIDS defining symptoms..... | 33 |
| Figure 1.5: A schematic representation of the intrinsic and extrinsic apoptotic pathways..... | 37 |
| Figure 1.6: A schematic representation of the mitopotential in non-apoptotic and apoptotic cells. | 39 |
| Figure 2.1: Schematic representation of an Indirect ELISA experimental set up for confirmation of Env structural/conformational integrity..... | 70 |
| Figure 2.2: Schematic representation of an Indirect ELISA experimental set up for confirmation of Env functionality..... | 71 |
| Figure 2.3: Schematic representation of apoptosis induction- experiment set-up in Jurkat T cells and detection of apoptotic hall marks using flow cytometry..... | 75 |
| Figure 2.4: Representative scatter dot plot acquired from Muse mini flow cytometer for Annexin V assay analysis..... | 77 |
| Figure 2.5: Representative scatter dot plot acquired from Muse mini flow cytometer for Mitopotential depolarization assay analysis. | 79 |
| Figure 2.6: Representative scatter dot plot acquired from Muse mini flow cytometer for caspase 3/7 activation analysis..... | 81 |
| Figure 2.7: Representative scatter dot plot acquired from Muse mini flow cytometer for DNA damage analysis..... | 83 |
| Figure 3.1: Transformation of chemically competent <i>E.coli</i> DH5 α cells with gp140 _{SOSIP} VRC 3831 and Furin pCDNA 3.3..... | 85 |
| Figure 3.2: Agarose gel analysis of Qiagen maxi kit DNA purification procedure used for extraction of gp140 _{SOSIP} VRC 3831 and Furin pCDNA 3.3 recombinant plasmids. | 86 |
| Figure 3.3: Western blot validation of recombinant Env (gp140 _{SOSIP} , gp140 _{GCN4} and gp120 _{FVC}) expression..... | 89 |

| | |
|--|-----|
| Figure 3.4: Western blot and SDS-PAGE analysis of lectin affinity chromatography purification of FVC Env conformations (gp140 _{SOSIP} , gp140 _{GCN4} and gp120 _{FVC})..... | 91 |
| Figure 3.5: SEC profiles of Envs post purification by lectin affinity chromatography.. | 92 |
| Figure 3.6: Blue native PAGE analysis of SEC purified Envs..... | 94 |
| Figure 3.7: SDS-PAGE analysis of 2dCD4 WT post Ni affinity purification. | 95 |
| Figure 3.8: Confirmation of conformational integrity of purified Envs.. | 97 |
| Figure 3.9: Functionality assessment of purified Envs. | 98 |
| Figure 3.10: Representative scatter plots of Annexin V and 7- AAD staining results post 24 hours of Jurkat T cells treatment. | 100 |
| Figure 3.11: Apoptosis detection by Annexin V and 7- AAD analysis. | 101 |
| Figure 3.12: Representative scatter dot plot results from Mitopotential assay. | 103 |
| Figure 3.13: Apoptosis induced via the intrinsic pathway, as detected by mitopotential assay analysis..... | 104 |
| Figure 3.14: Representative caspase 3/7 activation analysis in Jurkat T cells. | 106 |
| Figure 3.15: Apoptosis via caspase 3/7 activation in Env treated Jurkat T cells.... | 107 |
| Figure 3.16: Representative DNA fragmentation results post 24 hours of Jurkat T cells treatment..... | 109 |
| Figure 3.17: DNA fragmentation analysis in Env treated uninfected Jurkat T cells.. | 110 |
| Figure 3.18: Env protein stability analysis through heat denaturation curves..... | 113 |
| Figure 3B1: Spectra analysis and quantification of QIAGEN maxi kit isolated plasmid DNA..... | 140 |
| Figure 3C1: Annexin V flow cytometry scatter plots post 24 hours of Jurkat T cells treatment with 50 to 500 nM concentrations of gp140 _{SOSIP} , gp140 _{GCN4} and gp120 _{FVC} . | 141 |
| Figure 3C2: Annexin V flow cytometry scatter plots post 24 hours of Jurkat T cells treatment with 50 to 500 nM of gp140 _{SOSIP} , gp140 _{GCN4} and gp120 _{FVC} | 142 |
| Figure 3C3: Annexin V flow cytometry scatter plots post 48 hours of Jurkat T cells treatment with 50 to 500 nM of gp140 _{SOSIP} , gp140 _{GCN4} and gp120 _{FVC} | 143 |
| Figure 3C4: Annexin V flow cytometry scatter plots post 48 hours of Jurkat T cells treatment with 50 to 500 nM of gp140 _{SOSIP} , gp140 _{GCN4} and gp120 _{FVC} | 144 |
| Figure 3C5: Annexin V flow cytometry scatter plots post 72 hours of Jurkat T cells treatment with 50 to 500 nM of gp140 _{SOSIP} , gp140 _{GCN4} and gp120 _{FVC} | 145 |

| | |
|---|-----|
| Figure 3C6: Annexin V flow cytometry scatter plots post 72 hours of Jurkat T cells treatment with 50 to 500 nM of gp140 _{SOSIP} , gp140 _{GCN4} and gp120 _{FVC} ... | 146 |
| Figure 3D1: Mitopotential assay flow cytometry scatter plots post 24 hours of Jurkat T cells treatment with 50 to 500 nM of gp140 _{SOSIP} , gp140 _{GCN4} and gp120 _{FVC} | 147 |
| Figure 3D2: Mitopotential assay flow cytometry scatter plots post 24 hours of Jurkat T cells treatment with 50 to 500 nM of gp140 _{SOSIP} , gp140 _{GCN4} and gp120 _{FVC} | 148 |
| Figure 3D3: Mitopotential assay flow cytometry scatter plots post 48 hours of Jurkat T cells treatment with 50 to 500 nM of gp140 _{SOSIP} , gp140 _{GCN4} and gp120 _{FVC} | 149 |
| Figure 3D4: Mitopotential assay flow cytometry scatter plots post 48 hours of Jurkat T cells treatment with 50 to 500 nM of gp140 _{SOSIP} , gp140 _{GCN4} and gp120 _{FVC} | 150 |
| Figure 3D5: Mitopotential assay flow cytometry scatter plots post 72 hours of Jurkat T cells treatment with 50 to 500 nM of gp140 _{SOSIP} , gp140 _{GCN4} and gp120 _{FVC} | 151 |
| Figure 3D6: Mitopotential assay flow cytometry scatter plots post 72 hours of Jurkat T cells treatment with 50 to 500 nM of gp140 _{SOSIP} , gp140 _{GCN4} and gp120 _{FVC} | 152 |
| Figure 3E1: Caspase 3/7 activation flow cytometry scatter plots post 24 hours of Jurkat T cells treatment with 50 to 500 nM of gp140 _{SOSIP} , gp140 _{GCN4} and gp120 _{FVC} | 153 |
| Figure 3E2: Caspase 3/7 activation flow cytometry scatter plots post 24 hours of Jurkat T cells treatment with 50 to 500 nM of gp140 _{SOSIP} , gp140 _{GCN4} and gp120 _{FVC} | 154 |
| Figure 3E3: Caspase 3/7 activation flow cytometry scatter plots post 48 hours of Jurkat T cells treatment with 50 to 500 nM of gp140 _{SOSIP} , gp140 _{GCN4} and gp120 _{FVC} | 155 |
| Figure 3E4: Caspase 3/7 activation flow cytometry scatter plots post 48 hours of Jurkat T cells treatment with 50 to 500 nM of gp140 _{SOSIP} , gp140 _{GCN4} and gp120 _{FVC} | 156 |
| Figure 3E5: Caspase 3/7 activation flow cytometry scatter plots post 72 hours of Jurkat T cells treatment with 50 to 500 nM of gp140 _{SOSIP} , gp140 _{GCN4} and gp120 _{FVC} . . | 157 |
| Figure 3E6: Caspase 3/7 activation flow cytometry scatter plots post 72 hours of Jurkat T cells treatment with 50 to 500 nM of gp140 _{SOSIP} , gp140 _{GCN4} and gp120 _{FVC} . . | 158 |

| | |
|---|-----|
| Figure 3F1: DNA fragmentation flow cytometry scatter plots post 24 hours of Jurkat T cells treatment with 50 to 500 nM of gp140 _{SOSIP} , gp140 _{GCN4} and gp120 _{FVC} | 159 |
| Figure 3F2: DNA fragmentation flow cytometry scatter plots post 24 hours of Jurkat T cells treatment with 50 to 500 nM of gp140 _{SOSIP} , gp140 _{GCN4} and gp120 _{FVC} | 160 |
| Figure 3F3: DNA fragmentation flow cytometry scatter plots post 48 hours of Jurkat T cells treatment with 50 to 500 nM of gp140 _{SOSIP} , gp140 _{GCN4} and gp120 _{FVC} | 161 |
| Figure 3F4: DNA fragmentation flow cytometry scatter plots post 48 hours of Jurkat T cells treatment with 50 to 500 nM of gp140 _{SOSIP} , gp140 _{GCN4} and gp120 _{FVC} | 162 |
| Figure 3F5: DNA fragmentation flow cytometry scatter plots post 72 hours of Jurkat T cells treatment with 50 to 500 nM of gp140 _{SOSIP} , gp140 _{GCN4} and gp120 _{FVC} | 163 |
| Figure 3F6: DNA fragmentation flow cytometry scatter plots post 72 hours of Jurkat T cells treatment with 50 to 500 nM of gp140 _{SOSIP} , gp140 _{GCN4} and gp120 _{FVC} | 164 |

List of Tables

| | |
|---|-----|
| Table 1: Solutions for bacterial cell culture and transformation | 131 |
| Table 2: Buffer solutions used during plasmid DNA isolation. | 132 |
| Table 3: Solutions and buffers used for agarose gel electrophoresis | 133 |
| Table 4: SDS-PAGE reagents | 134 |
| Table 5: Western blot buffers | 135 |
| Table 6: Lectin affinity chromatography buffers..... | 136 |
| Table 7: Size exclusion chromatography buffers..... | 136 |
| Table 8: CD4 purification buffers | 137 |
| Table 9: CD4 refolding buffers | 137 |
| Table 10: BCA protein standards | 138 |

List of Abbreviations

| | |
|-------------------|--------------------------------------|
| AIDS | Acquired immunodeficiency syndrome |
| AIF | Apoptosis-inducing factor |
| ATM | Ataxia telangiectasia mutated kinase |
| ART | Antiretroviral therapy |
| BCA | Bicinchoninic acid assay |
| BSA | Bovine serum albumin |
| Bcl2 | B cell lymphoma 2 |
| bp | Base pairs |
| bnAb | Broadly neutralizing antibody |
| 2dCD4 WT | Wild type two domain CD4 |
| C- terminal | Carboxyl terminal |
| CD4 | Cluster of differentiation 4 |
| CD8 | Cluster of differentiation 8 |
| CD4i | CD4 induced epitopes |
| CO ₂ | Carbon dioxide |
| CTL | Cytotoxic T lymphocyte |
| CCR5 | Chemokine co-receptor type 5 |
| CXCR4 | Chemokine co-receptor type 4 |
| CHO | Chinese hamster ovary cell line |
| DI | Deionized water |
| DISC | Death inducing signalling complex |
| dH ₂ O | Distilled water |

| | |
|----------------|--|
| DNA | Deoxyribonucleic acid |
| dNTP | Deoxyribonucleotide triphosphate |
| DMSO | Dimethyl sulfoxide |
| DMEM | Dulbecco's Modified Eagle Medium |
| DEVD | Aspartic acid-Glutamic acid-Valine-Aspartic acid peptide |
| DSB | Double stranded breaks |
| dsDNA | Double stranded deoxyribonucleic acid |
| DR4 | Death receptor 4 |
| DR5 | Death receptor 5 |
| <i>E.coli</i> | <i>Escherichia coli</i> |
| Env | Envelope |
| ELISA | Enzyme-linked immunosorbent assay |
| EDTA | Ethylenediaminetetraacetic acid |
| FADD | Fas associated death domain |
| F _C | Fragment crystallization regions |
| FCS | Fetal calf Serum |
| FVC | Founder virus subtype C |
| 6HB | Six helix bundle |
| Gag | Group specific antigen |
| GC | Guaninine-Cytosine |
| GFP | Green fluorescence protein |
| GNL | <i>Galanthus nivalis</i> lectin |
| G418 | Geneticin 418 |

| | |
|------------------------|--|
| GSH | Reduced glutathione |
| GSSG | Oxidised glutathione |
| gp120 _{FVC} | Envelope glycoprotein 120 from subtype C founder virus |
| gp120 _{BaL} | Subtype B envelope glycoprotein 120 |
| gp140 _{SOSIP} | Envelope glycoprotein 140 with SOSIP mutations |
| gp140 _{GCN4} | Envelope glycoprotein 140 with GCN4 motif |
| HIV | Human immunodeficiency virus |
| His | Histidine |
| HEK 293T/F | Human embryonic kidney 293 T/F cells |
| HRP | Horse Radish peroxidase |
| HR | Heptad regions |
| HUVEC | Human umbilical cord vein |
| H2A.X | Histone variant 2A.X |
| 7-AAD | Seven amino actinomycin D stain |
| ICF | Instrument cleaning fluid |
| IN | Integrase |
| IL-1 β | Interlukin 1 beta |
| KDa | KiloDaltons |
| LB | Luria Bertani |
| M- group | Main group |
| MHC | Major histocompatibility complex |
| Mitopotential | Mitochondrial membrane potential |
| MPER | Membrane proximal external region |

| | |
|-------------|---|
| MMP | Methyl- α -D-manno-pyranoside |
| mRNA | Messenger ribonucleic acid |
| MTP | Membrane transition pore |
| N- terminal | Amino terminal |
| N-group | Non-main group |
| Nef | Negative regulatory factor |
| NIH | National institutes of health |
| NaCl | Sodium chloride |
| Ni | Nickel |
| O- group | Outlier group |
| OD | Optical density |
| P-group | Putative group |
| PBMC | Peripheral mononuclear cells |
| PBS | Phosphate buffered saline |
| PBS-T | Phosphate Buffered Saline containing Tween-20 |
| PE | Phycoerythrin dye |
| PECy5 | Phycoerythrin-Cyanine 5 conjugate dye |
| PEI | Polyethylenimine |
| PIC | Pre-integration complex |
| Pol | DNA polymerase |
| PS | Phosphatidylserine |
| PSA | Penicillin-Streptomycin antibiotic |
| Q | Quadrant |

| | |
|----------|--|
| Rev | Responsive viral protein |
| Rip | Receptor interacting serine/threonine protein kinase |
| Rpm | Revolutions per minute |
| RPMI | Roswell Park Memorial Institute medium |
| RT | Room temperature |
| RNA | Ribonucleic acid |
| SDS-PAGE | Sodium dodecyl sulphate polyacrylamide gel electrophoresis |
| SEC | Size exclusion chromatography |
| SOSIP | Disulphide bond (SOS) between gp41 and gp120 with a substitution of Isoleucine to Proline (IP) |
| SIV | Simian immunodeficiency virus |
| SHIV | Simian-human immunodeficiency virus chimera |
| ssRNA | Single stranded ribonucleic acid |
| Tat | Transactivator of transcription |
| tBid | Truncated bid |
| T cells | Thymus lymphocytes |
| TdT | Deoxyribonucleotidyl transferase |
| T-TBS | Tween-Tris buffered saline |
| TMB | 3,3', 5,5;-tetramethylbenzidine |
| TNF | Tumour necrosis factor |
| TEMED | Tetramethylethylenediamine |
| TRADD | TNFR – associated death domain |
| TRAIL | TNF related apoptosis-inducing ligand |

| | |
|--------|--|
| Tris | Hydroxymethyl aminomethane |
| TUNNEL | Deoxynucleotidyl transferase dUTP nick labelling |
| UNAIDS | United Nations acquired immunodeficiency syndrome programme |
| UV | Ultraviolet light |
| V38E | Valine 38 glutamic acid substitution |
| V1V2 | Variable regions one and two |
| WB1 | Wash buffer 1 |
| WB2 | Wash buffer 2 |
| Z-VAD | Benzyloxycarbonyl valine-alanine-aspartic acid broad caspase inhibitor |

1. Introduction

1.1 HIV/AIDS history and pandemic

Human Immunodeficiency Virus (HIV) is a pathogen discovered in the early 1980s (Barré-Sinoussi et al., 1983, Popovic et al., 1984) as a causative agent of Acquired immunodeficiency syndrome (AIDS), a disease commonly defined by a progressive decline in cluster of differentiation 4 thymus lymphocytes (CD4⁺ T cells). Following its discovery, HIV was later characterized as a *Lentivirus* from the *Retroviridae* family (Fields et al., 1996) of viruses which induce infection through integration of their genetic material into the host genome. As a result of the viral genetic variation and difference in viral antigens, HIV is classified into two types; HIV-1 and HIV-2 (Lemey et al., 2003, Nyamweya et al., 2013, Sharp and Hahn, 2011).

HIV-1 originated from a zoonotic transmission of Simian immunodeficiency virus (SIV) from Chimpanzee subspecies *Pan troglodytes* to humans while HIV-2 originated from zoonotic transmission of SIV from Sooty Mangabey monkeys (Gao et al., 1999). HIV-2 is mostly restricted to West Africa and in contrast to HIV-1, it results in a slow progression to immunodeficiency and is less transmissible (Sharp and Hahn, 2011). HIV-1 zoonotic transmissions occurred within three events in Central Africa, which resulted in formation of distinct groups; M (main), O (outlier), N (non-M/O) with group M being responsible for the global HIV epidemic (Aguchi et al., 2000, Chen et al., 1997, Gao et al., 1994, Marx et al., 2001, Sharp and Hahn, 2011). In addition, a putative group called Group P was discovered in infected Cameroon patients, and has been found to be closely related to the SIV found in gorillas (Plantier et al., 2009, Vallari et al., 2011). Infections by this group are rare and show less infectivity relative to other main HIV-1 groups such as group M (Alessandri-Gradt et al., 2018).

HIV-1 group M further diversified into subgroups/types A-D, F-H, J and K which are distributed to different global regions (Spira et al., 2003). Moreover, there are currently 98 existing circulating recombinant forms that are contributing to the global burden of HIV-1 infection (<http://www.hiv.lan.gov/content/sequence/HIV/CRFs/CRFs.html>). However, for the

purpose of this study, subtype C is of particular interest due to its high prevalence in India, Brazil and Sub-Saharan Africa.

HIV-1 infection has a high global prevalence. In 2017 alone, approximately 36.9 million people were living with HIV globally, with 1.8 million global new infections and 940 000 deaths from AIDS-related illness (UNAIDS and WHO, 2017). As shown in Figure 1.1, the developing world continents such as Africa bear the biggest disease burden, as indicated by the highest HIV prevalence. In particular, the East and Southern African countries contributed to 54 % of the global population living with AIDS (19.6 million), 44 % new infections (800 000) and 40 % AIDS related deaths in 2017 (WHO, 2017). However, of all East and Southern African countries, South Africa has the highest number of people living with HIV-1 infection; approximately 7.9 million individuals were predominantly infected by HIV-1 subtype C (WHO, 2018).

AIDS-related death is attributed to the fact that HIV-1 progressively infects and depletes important immune cells such as CD4⁺ T cells, macrophages, monocytes, microglia and dendritic cells, and, in the absence of antiretroviral therapy (ART), an infected individual ultimately succumbs to opportunistic infections (Bowen et al., 2016, Masur, 2015, Chinyowa et al., 2018).

ART is a combinatorial therapy of two or more classes of drugs targeting different stages of the HIV-1 life cycle to suppress viral replication and reduce viral load i.e. viral copies in the infected individuals, so as to boost the immune system, prolong progression to AIDS and lower chances of HIV transmission to uninfected counterparts (Cohen et al., 2011, Powers et al., 2014, Reynolds et al., 2011, Thompson et al., 2012, Saag et al., 2018). However, the ART treatment is not curative i.e. cannot entirely eradicate latent viral reservoirs (Cummins and Badley, 2015, Jubault et al., 1998, Ruiz et al., 2000, Smith et al., 2014, Bender et al., 2019), the treatment efficacy is dependent on daily adherence and lack of adherence thereof, results in virus resistance to ART (Gandhi et al., 2007, Mtambo et al., 2012, Wensing et al., 2016, Bachmann et al., 2019, Altice et al., 2019). For these reasons, HIV/AIDS remains a health burden. This raises the need to understand the structural biology of HIV-1 and its pathogenesis in order to improve existing treatment modalities.

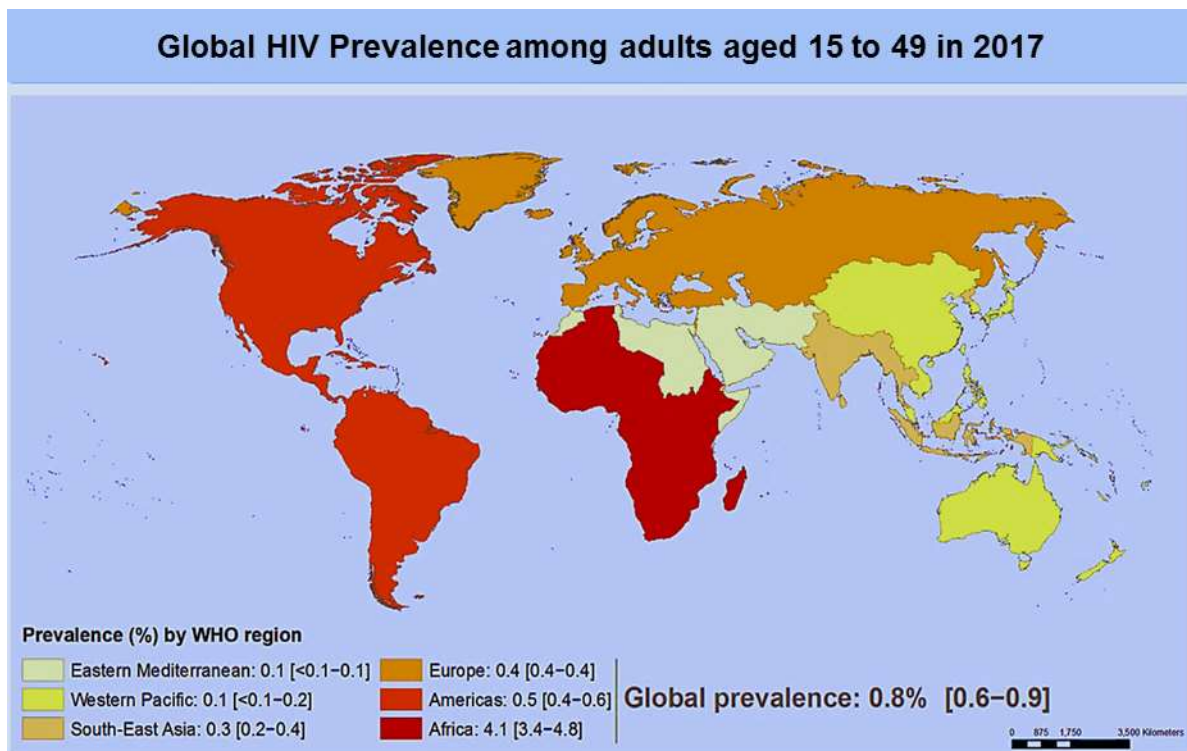


Figure 1.1: Global HIV prevalence distribution among adults aged 15 to 49. The HIV prevalence is represented as a percentage in each region indicated by various colours. Lighter colours show a low to moderate prevalence while darker colours demonstrate high prevalence. Africa has the highest prevalence for adults aged 15 to 49 as indicated by the dark red region. This image was adapted from the Global HIV annual report, WHO 2017.

1.2 HIV-1 Pathogenesis; role of viral and host proteins

HIV-1 transmission from infected to uninfected individuals occurs through transfer of the virus particles contained in body fluids such as blood, semen and breast milk. This process commonly results from exposure of the virus to mucosal surfaces (Shattock and Moore, 2003) and is facilitated by unprotected sexual intercourse, sharing of contaminated needles or injections, blood transfusions and breast feeding. During transmission, HIV-1 undergoes various stages of the life cycle to establish infection. This entails virus attachment and entry into target immune cells, reverse transcription of its genome, integration of the genome into host DNA, translation, viral assembly and budding (Figure 1.3), briefly described below. Each stage of the

life cycle (Figure 1.3) involves interaction between the viral and host encoded proteins.

1.2.1 Virus entry; Envelope-CD4 and co-receptor interactions

HIV-1 virions exist as nearly spherical nanoparticles (Sougrat et al., 2007) coated with a virus membrane comprising host membrane, embedded with the viral envelope glycoproteins (Env). The HIV-1 Env is expressed in infected cells as a gp160 precursor protein which undergoes proteolytic maturation into a heterotrimer of three receptor binding gp120 subunits non-covalently linked to equivalent transmembrane gp41 subunits (Hallenberger et al., 1992, Klasse, 2012, Willey et al., 1988, Wyatt and Sodroski, 1998).

During viral entry, the gp120 subunit facilitates fusion between the virus and target immune cells (Figure 1.2). Since HIV-1 primarily infects CD4⁺ T cells (Klatzmann et al., 1984), the virus initiates entry via binding of gp120 to CD4 receptors (Figure 1.2, step 2) on target T cells (Maddon et al., 1986, McDougal et al., 1986). CD4 receptors are membrane glycoproteins expressed on T cells and normally interact with major histocompatibility complex class II antigens (MHC class II) to initiate early stages of T cell activation (Bour et al., 1995, Brady and Barclay, 1996). Engagement of the viral gp120 subunit with these CD4 receptors triggers conformational changes in the Env which promotes binding of the gp120 to chemokine co-receptors CCR5 or CXCR4 (Figure 1.2, step 3) on target T cells (Gern, 1997, Kwong et al., 1998, Wilen et al., 2012).

CCR5 and CXCR4 are structurally related chemokine co-receptors from a superfamily of seven transmembrane G proteins coupled receptors and have been previously identified as major HIV-1 entry co-factors (Deng et al., 1996, Dragic et al., 1996, Feng et al., 1996). The primary function of these co-receptors is to recruit immune cells during inflammation (Fanales-Belasio et al., 2010). However during HIV-1 infection, co-receptor preference and usage determines classification of HIV-1 into various strains; CCR5 (R5 tropic), CXCR4 (R4 tropic), or dual (R5/X4) strains (Broder and Berger, 1995, Coakley et al., 2005). Successful co-receptor binding to HIV-1 Env results in exposure of amino (N) and carboxyl (C) terminal heptad regions (HR) in the gp41 subunit which increases the fusogenic potential of gp41 through a six helix bundle (6HB) formation (Chan et al., 1997, Eckert and Kim, 2001, Skehel

and Wiley, 2000). The 6HB is a highly stable trimer of gp41 hairpins made up of three N-terminal HR repeat segments and equivalent C-terminal helical segments (Markosyan et al., 2003). To promote complete fusion between the virus and target T cells (Figure 1.2, step 4), the 6HB trimer brings the viral and target T cell membranes into close proximity and forms a stable fusion pore (Cohen and Melikyan, 2004, Gallo et al., 2003, Wild et al., 1994). Complete membrane fusion results in subsequent delivery of viral contents encapsulated in the p24 into the cytoplasm of the target T cells for viral replication.

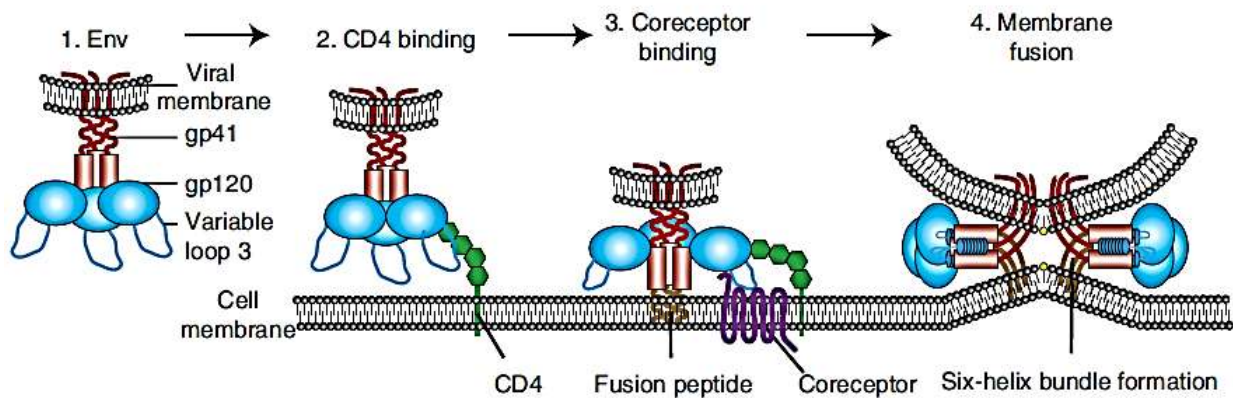


Figure 1.2: An overview of HIV-1 viral entry into target CD4-expressing T cells during infection. To transfer viral contents into target T cells, HIV-1 utilizes surface Env protein to facilitate fusion between the virus and the target cells. The Env consists of gp120-gp41 heterotrimer complex (step 1). To initiate viral entry, the gp120 subunit binds to CD4 receptors on CD4⁺ T cells (step 2). This gp120-CD4 interaction then induces conformational changes in the Env which further facilitates its binding to co-receptors on the target T cells (Step 3). Subsequently, co-receptor binding promotes fusion of viral and target T cell membranes through insertion of gp41 transmembrane region into target T cell membrane and formation of a six helix bundle which ensures complete membrane fusion. The diagram was copied from (Wilens et al., 2012).

1.2.2 HIV-1 replication; reverse transcription, integration, transcription, translation, assembly and budding

The HIV-1 viral core exists as a cone-shaped p24 capsid (Briggs et al., 2006) which contains the viral replication enzymes such as reverse transcriptase (RT), integrase (IN) and most importantly, two single plus stranded viral genomic ribonucleic acid (ssRNA) genomes (Coffin et al., 1997). This cone-shaped capsid is a polymer of approximately 250 hexamers and 12 pentamers (Ganser et al., 1999, Mattei et al., 2016, Zhao et al., 2013) linked via C and N terminal interactions (Ganser-Pornillos et al., 2007, Pornillos et al., 2009). Upon delivery of the viral core into target CD4⁺ T cells, these capsid proteins uncoat/disassemble into monomers, opening up the capsid to release the HIV-1 RNA genome and associated viral proteins into the host T cell cytoplasm (Figure 1.3). This process is commonly known as uncoating (Ambrose and Aiken, 2014) and crucial for viral replication (Fitzon et al., 2000, Forshey et al., 2002). Mutations destabilizing the viral capsid and its morphology resulted in reduced viral infectivity (Forshey et al., 2002, Tang et al., 2001), further emphasizing the essentiality of viral capsid in infection and replication.

Since the HIV-1 genome exists as RNA, to allow replication using the host cell's machinery, the viral genome is reverse transcribed into a double stranded deoxyribonucleic acid (dsDNA) genome (Rankovic et al., 2017). The reverse transcription is conducted by HIV-1 RT (Figure 1.3) using host cell deoxyribonucleotide triphosphates commonly known as dNTPs (Miller et al., 1997, Masuda et al., 2015). The HIV-1 is error prone, leading to the emergence of multiple quasispecies within an infected individual and the extensive viral diversity seen globally. Following reverse transcription, the viral dsDNA, together with viral proteins such as IN and host proteins such as LEDGF/p75, forms a preintegration complex (PIC), which moves into the nucleus (Figure 1.3). The viral dsDNA is then irreversibly integrated into the host cell's DNA using viral IN (Nisole and Saïb, 2004). The resulting integrated DNA is referred to as a provirus which serves as an exclusive template for production of more virions during the course of HIV-1 infection (Freed, 2001, Hindmarsh and Leis, 1999).

Upon provirus formation, the integrated viral genome is transcribed into messenger RNA (mRNA); a process regulated by viral transactivator of transcription (Tat) and

host cell DNA transcription factors (Cullen, 1998, Wei et al., 1998, Wu, 2004). Tat protein promotes transcription and synthesis of longer viral RNA transcripts (Charnay et al., 2009, Zhou and Yik, 2006). Once transcribed, the viral RNA is transported out of the nucleus into the host cell's cytoplasm through the functioning of responsive viral (Rev) protein (Cullen, 1998, Felber et al., 1990). During transfer from the nucleus into the cytoplasm, the transcribed RNA is either transported in its full length to serve as a viral genome for new virions or partially or completely spliced. Both spliced and unspliced versions of RNA encode for the synthesis of different viral proteins such as group specific antigen (Gag), DNA polymerase (Pol), negative regulatory factor (Nef), viral protein R (Vpr), and Env within host cell ribosomes (Figure 1.3).

Since all Pol, Gag and Env structural proteins are synthesized from longer viral mRNAs, they undergo proteolytic cleavage for production of functional i.e. infectious virions. Proteolytic cleavage using viral protease (PR) of Gag and Pol precursor protein results in formation of structural proteins p24, p17, p9 and p7 (Fanales-Belasio et al., 2010). In contrast, cleavage of the 160 kD Env precursor by host proteases such as Furin results in formation of a gp120-gp41 trimer complex with the ability to engage CD4 receptors on target T cells during infection.

Once all viral proteins are synthesized, they are arranged or assembled at the surface of the cell membrane (Figure 1.3). This entails association of two identical viral RNA with replication enzymes and further assembly of viral core proteins (Gag, Pol, Nef and Vpr) around the viral RNA genome forming the p24 capsid (Zimmerman et al., 2002). To release the virions, Gag facilitates fusion of the assembled viral particles with the host cell membrane (within which are embedded the Env trimers) and budding out of an immature virion (Garnier et al., 1999). The released immature virions undergo further proteolytic cleavage by the viral PR to form mature virions capable of infecting new cells, thereby repeating the viral life cycle.

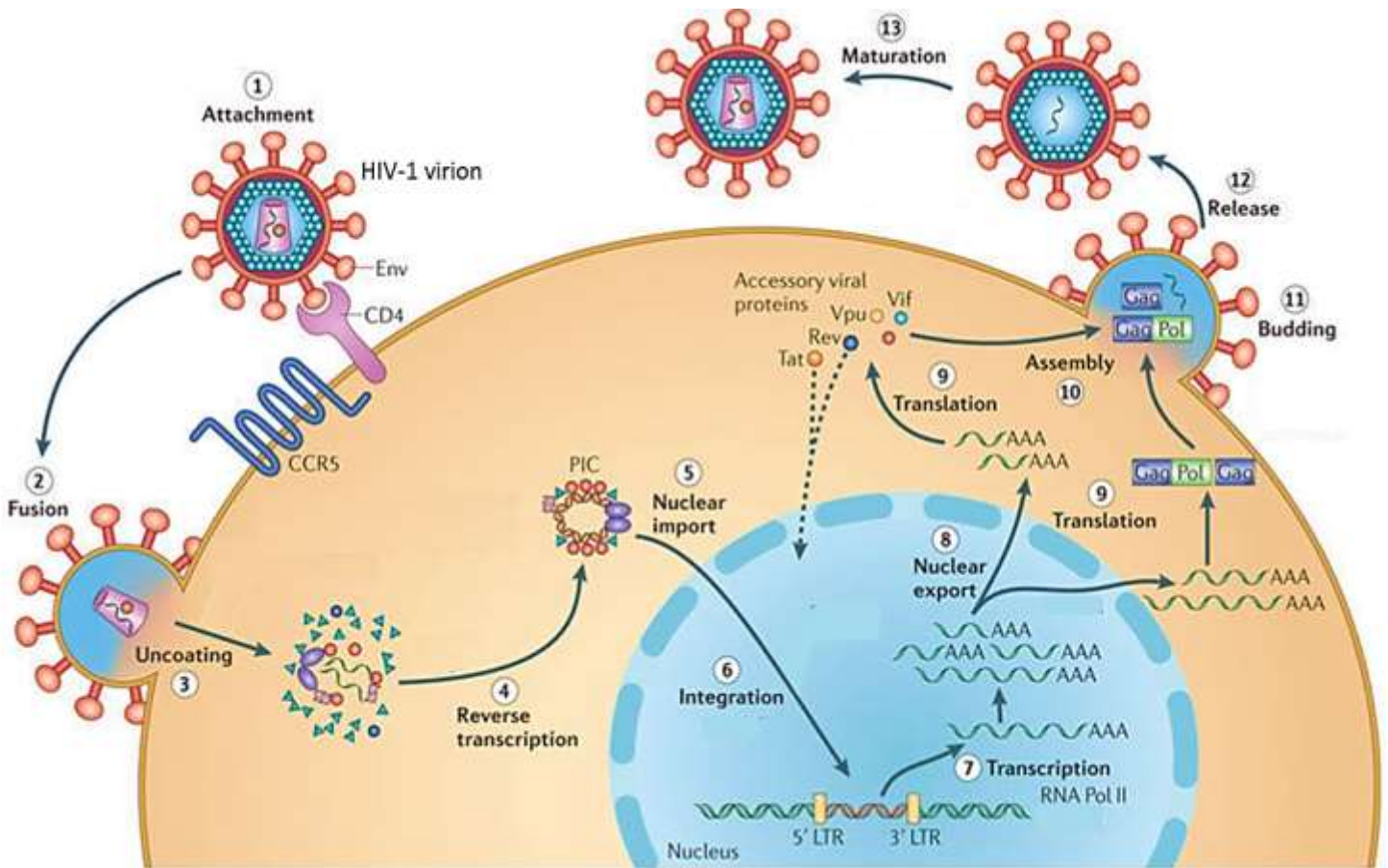


Figure 1.3: A schematic representation of the HIV-1 replication cycle. The diagram was copied from (Laskey and Siliciano, 2014). The HI virus initiates infection through interaction with host receptors (step1), fusion with the host membrane and release of viral contents into the target cell cytoplasm (step 2-3). The virus reverse transcribes its RNA genome into DNA (step 5) which is then transported into the nucleus for integration with the host genome (step 5-6) to form a provirus. This integrated viral genome is then transcribed to produce mRNA which is then exported into the cytoplasm and translated into viral proteins (steps 7-9). The latter proteins along with viral RNA are assembled and the resulting immature virions are released from the host cell through budding to mature and further infect new cells (steps 10-13).

1.2.3 Clinical course of HIV-1 infection; disease progression to AIDS

HIV-1 is a chronic infection; because the virus persists despite the presence of an anti HIV immune response, and gradually depletes immune cells, primarily CD4⁺ T cells until the infected individual succumbs to opportunistic infections. Following transmission from infected to uninfected individuals, HIV-1 establishes infection through its life cycle described in section 1.2.2. As a result of infection, latent reservoirs are established early, and over time CD4⁺ T cells in peripheral blood progressively decline (measured as CD4⁺ T cells/ μ l) in relation to the amount of viral particles (viral load, measured as RNA copies/ml) produced by viral replication (Brenchley et al., 2004). This process occurs in three stages namely acute/primary infection, clinical latency and AIDS, as illustrated in Figure 1.4.

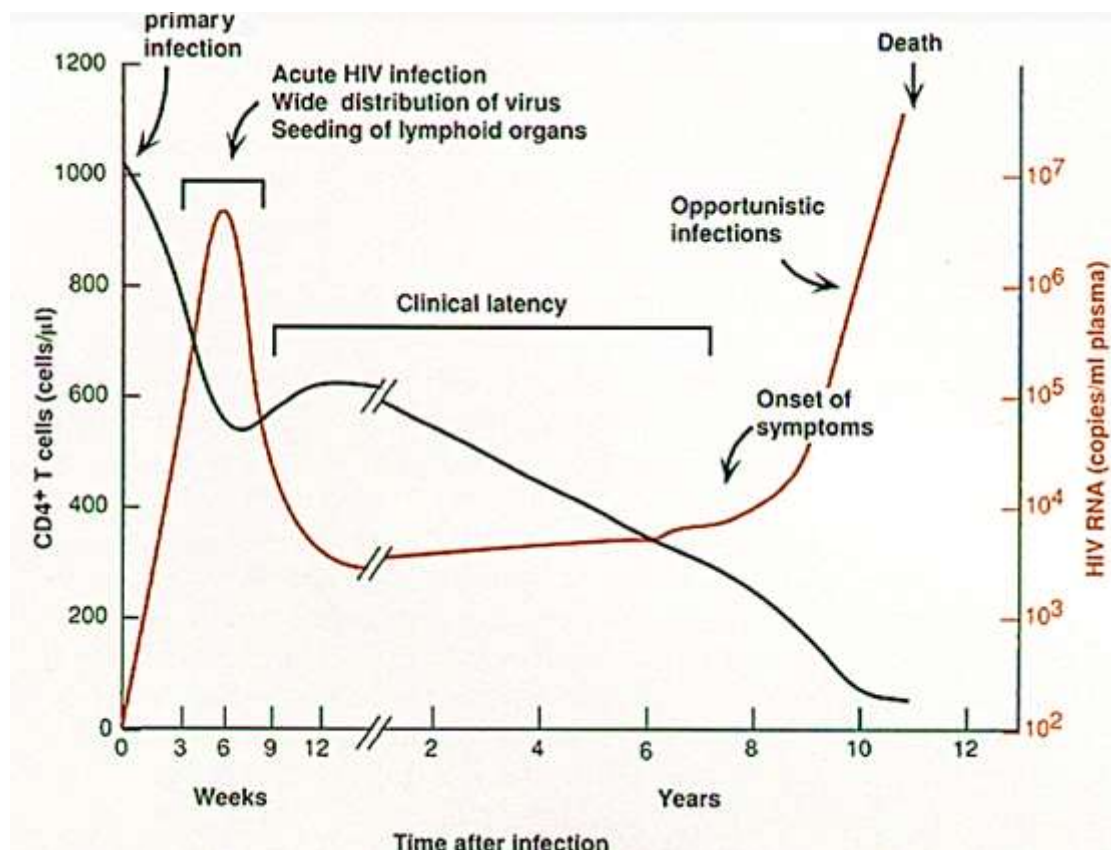


Figure 1.4: Time based clinical course of HIV-1 infection from initiation of infection to AIDS defining symptoms. The y axis illustrates CD4⁺ T cell counts

(black curve) and viral load (red curve) over a period of 3 weeks to 12 years (x axis). The diagram was copied from (Pantaleo et al., 1993b).

Acute infection occurs within three to six weeks of transmission and is characterized by rapid replication of the virus which spreads throughout the body causing a significant decline in CD4⁺ T cells (Clark et al., 1991, Daar et al., 1991, Gaines et al., 1990, Tindall and Cooper, 1991). Due to exponential rise in viral titers as a result of increased viral replication rates, individuals acutely infected with HIV-1 have high risks of transmitting the virus. Moreover, acute HIV-1 infection triggers host's humoral and cellular immune responses in an attempt to suppress the virus (Cooper et al., 1987, Chiodi and Scarlatti, 2018, Gaines et al., 1987, Ho et al., 1985). During the acute phase, the virus establishes latent reservoirs, which are not eradicated with current ART regimens.

As a result of the emergence of HIV-1 specific CD8⁺ Cytotoxic T lymphocyte (CTL) responses, the immune system manages to somewhat control viral replication, as seen by a decrease in the viral load to a set point (Figure 1.4). There is a long period of little to no clinical symptoms known as clinical latency or chronic HIV-1 infection. Clinical latency occurs after the acute stage of infection, and is associated with low levels of viral replication (Figure 1.4). During this stage of HIV-1 infection, there is ongoing viral replication resulting in a steady decline in CD4⁺ T cells which, in a typical progressor, persists over 10 years without ART intervention. The number of CD4⁺ T cells gradually decrease over time and the infected individuals eventually succumb to AIDS (Ward et al., 1993). This is the last stage of HIV-1 infection where the virus rapidly replicates and the immune system is significantly depleted, with very low CD4⁺ T cell counts (Figure 1.4). The compromised immune system renders the infected individuals susceptible to opportunistic diseases such as tuberculosis, pneumococcal meningitis and cancers (Swanstrom and Coffin, 2012). In the absence of ART, this state of infection can last up to two to three years until death dependent on the levels of CD4⁺ T cells in the body, and opportunistic infections the individual is exposed to. However, individuals taking successful ART will control their viral loads, with very low to undetectable levels of virus being reported, and will not progress to AIDS (Hendriks et al., 1998, Lackner et al., 2012, Muñoz et al., 1989).

Since CD4⁺ T cell depletion is a major driver of AIDS progression, it is of paramount importance to study the mechanisms of CD4⁺ T cell depletion in order to understand its contribution to pathogenesis and mitigate this health burden.

1.3 Mechanisms of CD4⁺ T cell depletion during HIV-1 infection

The loss of CD4⁺ T cells after HIV-1 infection is linked to several mechanisms such as CD8⁺ CTL induced killing of infected cells and cytotoxic effects directed by the virus (Alimonti et al., 2003). The primary role of CD8⁺ CTLs is to mediate destruction of damaged or infected immune cells. Therefore, during early stages of HIV-1 infection, anti-HIV CD8⁺ CTL responses are activated as an immune defence to reduce viral load and this results in the killing of infected CD4⁺ T cells (Appay et al., 2002). This CD8⁺ CTL induced killing is promoted by excessive activation of immune cells (Douek et al., 2009). Other studies have implicated the CD4 loss to pyroptosis which induces cell death by producing inflammatory cytokine IL-1 β that causes the infected cells to swell and burst (Doitsh et al., 2014, Galloway et al., 2015).

CD4⁺ T depletion via viral imposed cytotoxic effects include alterations of host cell membrane permeability as a result of excessive viral budding during its life cycle (Stevenson et al., 1988). In addition, HIV-1 infection also impairs the ability of the host thymus to produce more CD4⁺ T cells (Gaardbo et al., 2012), decreasing the input of naïve CD4⁺ T cells in peripheral blood compared to uninfected individuals (Bandera et al., 2010). This contributes to inadequate levels of circulating CD4⁺ T cells observed during the course of HIV-1 infection.

Above all the mentioned strategies contributing to CD4 loss, apoptosis has been extensively described as a major mechanism of HIV-1 mediated CD4⁺ T cell depletion (Ameisen and Capron, 1991, Cummins and Badley, 2010, Holm et al., 2004, Herbeuval et al., 2006, de Oliveira Pinto et al., 2002, Terai et al., 1991). Apoptosis is a regulated form of programmed cell death with a pivotal role of eliminating diseased, worn-out or damaged cells through self-destruction (Bai et al., 2014, Jacobson et al., 1997, Vaux and Strasser, 1996). In support of its role in CD4⁺ T cell depletion, lymphocytes isolated from HIV-1 infected individuals showed accelerated apoptosis which accelerated T cell death in both symptomatic and asymptomatic stages of infection (Meyaard et al., 1992). Its significance was further

illustrated in Macaque animal models, where infections with a pathogenic strain of SIV resulted in increased apoptosis compared to infections with a non-pathogenic counterpart (Cumont et al., 2008, Meythaler et al., 2008, Meythaler et al., 2009, Silvestri et al., 2003). Moreover, multiple studies have reported a correlation between apoptosis of peripheral mononuclear cells (PBMCs) and CD4⁺ T cell loss in HIV-1 infected individuals and SIV/HIV chimera (SHIV) infected Macaques (Joshi et al., 2016, Iida et al., 2000, Oyaizu et al., 1993, Reinberger et al., 1999, Sternfeld et al., 2009). All of these studies prove the essential role of apoptosis in the pathogenesis of HIV-1 infection leading to AIDS.

Although the role of apoptosis in CD4⁺ T cell loss is well established, the number of apoptotic cells significantly exceeds those of HIV-1 infected cells and therefore does not account for the significant loss of CD4⁺ T cells *in vivo* (Ameisen and Capron, 1991, Holm et al., 2004, Jekle et al., 2003, Meygaard et al., 1992, Muro-Cacho et al., 1995). To explain this observation, an early study by (Finkel et al., 1995) demonstrated that a majority of the cells undergoing apoptosis during HIV-1 infection were uninfected cells in close proximity to infected cells, thus implicating the apoptosis of uninfected CD4⁺ T cells in pathogenesis. This phenomenon was later referred to as bystander apoptosis and plays a crucial role in HIV-1 pathogenesis (Ahr et al., 2004, Cummins and Badley, 2010, Garg et al., 2012, Perfettini et al., 2005a).

1.3.1 HIV-1-mediated bystander apoptosis

Bystander apoptosis of neighbouring uninfected cells is a major driver of CD4⁺ T cell depletion during HIV-1 infection leading to AIDS. Evidence of this phenomenon was shown in *in vitro* cultures of blood cells isolated from HIV-1 infected individuals, which revealed accelerated apoptosis of uninfected cells relative to infected cells (Debatin et al., 1994, Garg et al., 2011, Holm et al., 2004, Holm and Gabuzda, 2005, Lecoeur and Gougeon, 1996, Tsao et al., 2016). In addition, Rhesus Macaques infected with a pathogenic dual strain of SIV and HIV called SHIV89.6P also demonstrated predominant apoptosis of uninfected memory CD4⁺ T cells (Matrajt et al., 2014). These studies ignited interest in determining the mechanisms of bystander apoptosis during HIV-1 infection later discussed in the current study. The

intrinsic and extrinsic pathways of apoptosis are implicated in these mechanisms of bystander apoptosis (Figure 1.5). The role of each pathway is briefly described below.

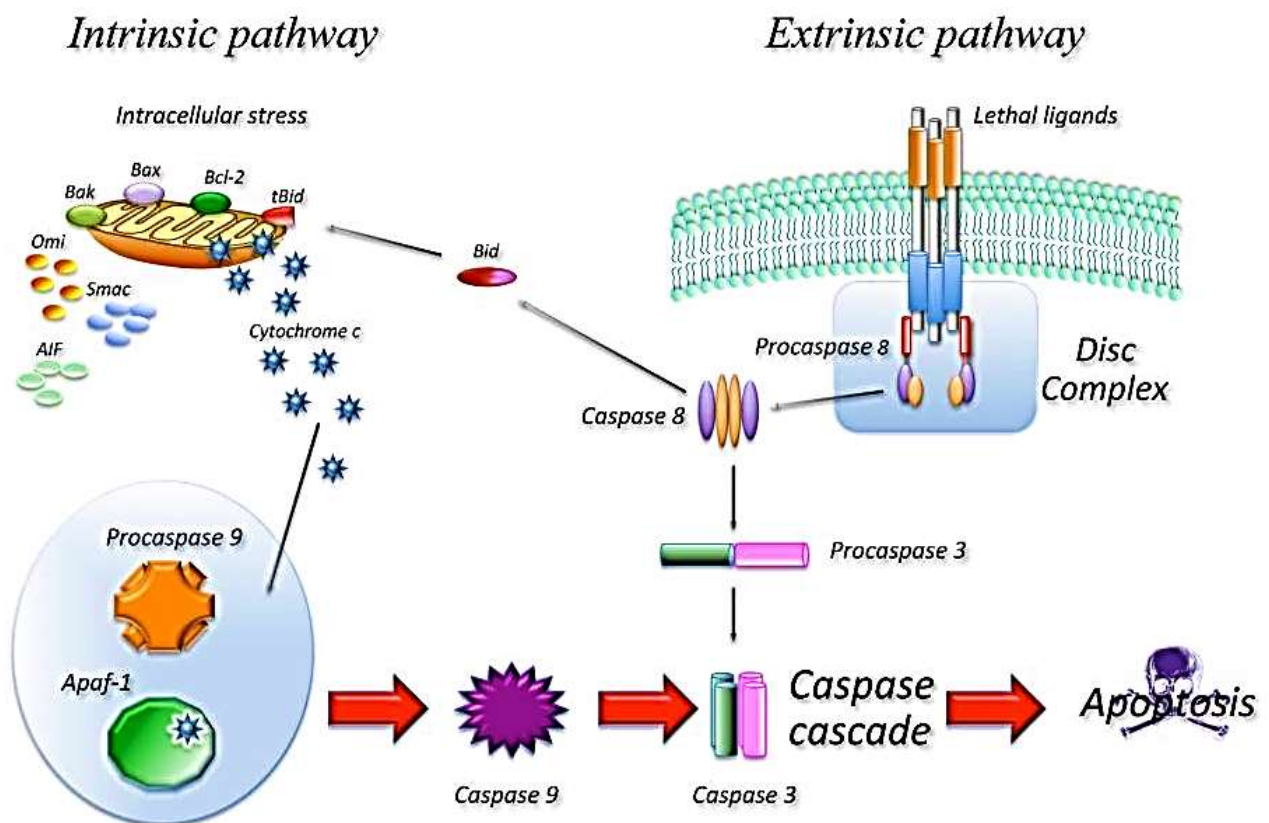


Figure 1.5: A schematic representation of the intrinsic and extrinsic apoptotic pathways. The intrinsic pathway (left) is triggered by intracellular stress which changes mitochondrial morphology and release pro-apoptotic proteins to commit the cell to death mediated by a downstream caspase cascade. The extrinsic (right) pathway is initiated in response to external stimuli such as binding of death ligands to death receptor which also activates a cascade of downstream caspases to induce cell death. Both pathways cause biochemical and morphological changes in the

affected cells which ultimately results in complete cell death. The diagram was copied from (Favaloro et al., 2012).

1.3.2 Intrinsic pathway and HIV-1 mediated CD4⁺ T cell depletion

The intrinsic pathway, commonly known as mitochondrial apoptosis is initiated by intracellular stress such as oxidative stress and DNA damage which changes the morphology of the mitochondria (Figure 1.5). During initiation of mitochondrial apoptosis, these pro-apoptotic signals trigger activation of proteins within the B-cell lymphoma 2 (Bcl2) family (Bak and Bax) which increases the permeability of the mitochondrial membrane (Boya et al., 2001, Tait and Green, 2010).

The transformation in mitochondrial membrane permeability in turn triggers a series of apoptosis-promoting events. Initially, the mitochondrial membrane transition pore (MTP) opens up causing loss of mitochondrial membrane potential i.e. mitopotential (Boya et al., 2001, Galluzzi et al., 2012, Pietro and Zauli, 2004, Saelens et al., 2004). Mitopotential is a charge gradient which measures differences in ion concentrations on opposite sides of the mitochondrial membrane and is considered a fundamental biomarker of the intrinsic pathway (Chikando et al., 2011). As a result of disrupted membrane permeability, apoptotic cells have reduced negative charge, hence are referred to as a depolarized mitopotential (Figure 1.6).

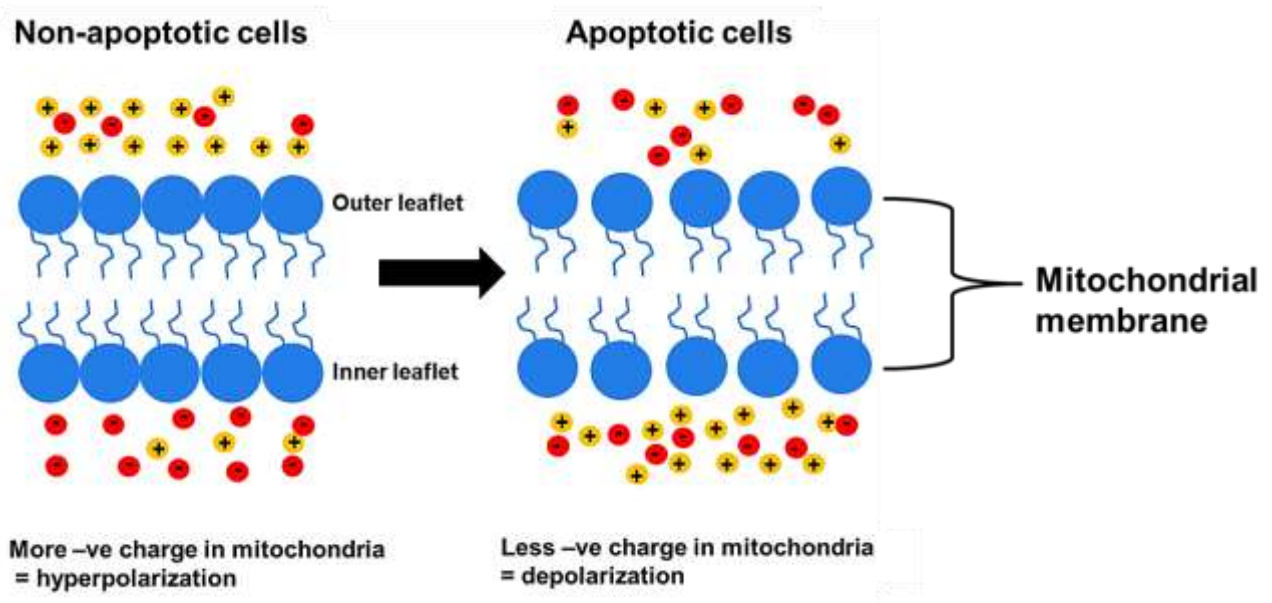


Figure 1.6: A schematic representation of the mitopotential in non-apoptotic and apoptotic cells. Non-apoptotic cells (left) have intact mitochondrial membranes, hence contain a hyperpolarized mitopotential i.e. more negative charge within the mitochondria. Apoptotic cells have increased mitochondrial membrane permeability which allows an influx of positive charge resulting in a depolarized mitopotential i.e. less negative charge within the mitochondria. The diagram was adapted from (<http://www.vet.purdue.edu/depts/bms/courses/bms511/coursework/nervous/n3.htm>) and drawn by student.

The depolarized mitopotential mediates release of pro-apoptotic proteins such as cytochrome C and Apoptosis-Inducing Factor i.e. AIF (Boya et al., 2001, Galluzzi et al., 2012, Pietro and Zauli, 2004, Saelens et al., 2004). Subsequently, cytochrome C initiates formation of a death complex called the apoptosome (Chinnaiyan, 1999, Green and Llambi, 2015) through activation of Apaf 1 and cleavage of procaspase 9 into an active caspase 9 (Hill et al., 2004). Thereafter, downstream effectors are activated by a cascade of caspases which become active upon cleavage of Aspartate residues (Figure 1.5). Caspase 9 initiates this cascade by cleaving caspase 3 and 7 responsible for ultimate execution of the cell (Reed, 2000). The executioner caspases then trigger further release of AIF and endonuclease G which are translocated to the nucleus to induce DNA fragmentation. AIF degrades DNA into 50-300 kb fragments and condensate surface chromatin (Joza et al., 2001) while

endonuclease G causes oligonucleosomal DNA fragments (Li et al., 2001). As a result of induced DNA fragmentation, the cells eventually die and this process is regulated by anti-apoptotic proteins Bcl-X_L, Bcl-2, Bcl-W, A1, and Mcl-1 (Czabotar et al., 2014, Dai et al., 2016).

HIV-1 infection mediates the depletion of CD4⁺ T cells and other cell types by promoting mitochondrial damage (Avdoshina et al., 2016, Fields et al., 2016). This damage entails changes in mitochondrial morphology and function mediated by altering expression levels of pro and anti-apoptotic proteins within the intrinsic pathway. Evidence of this is found in previous studies which showed that pro-apoptotic proteins Bim and Bak were upregulated in CD4⁺ T cells from chronically infected HIV-1 patients and in Rhesus Macaques infected with SIV compared to the healthy counterparts (Arnoult et al., 2003, Fraietta et al., 2013). Anti-apoptotic proteins Bcl2 and BclXL are also down-regulated in HIV-1 acutely infected monocytic U937 and J.Jhan human lymphoblastoid CD4⁺ T cell lines to allow pro-apoptotic proteins to induce changes in mitochondrial membrane which lead to apoptosis (Aillet et al., 1998).

Although these variations in protein expression contribute to apoptosis via changes in mitochondrial morphology, other studies have suggested the role of the biochemical status of the mitochondria in apoptosis induction during HIV-1 infection (Bennett et al., 2014, Ferri et al., 2000a, Garg et al., 2011). Accordingly, PBMCs isolated from untreated HIV-1 patients showed a depolarized mitopotential relative to uninfected controls (Sternfeld et al., 2007, Sternfeld et al., 2009). In addition, *in vitro* treatment of HIV-1 infected CD4⁺ T cells with a broad caspase inhibitor-Z-VAD and caspase 3 inhibitor-Ac-DEVD-CHO repressed mitopotential depolarization resulting in decreased apoptosis (Garg and Blumenthal, 2006b, Petit et al., 2002). Recently, another broad caspase inhibitor called Q-VD-OPH has prevented CD4⁺ T cell death and delayed AIDS progression in SIV infected Rhesus Macaques (Laforge et al., 2018). Overall, these studies suggest an essential role of caspases in mediating mitopotential depolarization and CD4⁺ T cell apoptosis during HIV-1 infection. Hence, therapies that could block caspase activation and mitochondrial depolarization by upregulating anti-apoptotic proteins could potentially reduce HIV-1 induced CD4⁺ T cell depletion.

1.3.3 Extrinsic pathway and HIV-1 mediated CD4⁺ T cell depletion

Extrinsic pathway, also known as receptor-mediated apoptosis, is initiated by ligand-receptor interactions (Figure 1.5). Upon binding of death initiating ligands; Tumor Necrosis Factor (TNF), Fas ligand and TNF-related apoptosis-inducing ligand (TRAIL) to their death receptors, adaptor proteins are recruited (Ashkenazi and Dixit, 1998, Galluzzi et al., 2012, Locksley et al., 2001, Wajant, 2002). Fas-associated death domain (FADD) adaptor protein is recruited when the initiating ligand in the pathway is Fas while TNFR-associated death domain (TRADD) binds to the TNF-TNF receptor complex with recruitment of FADD and Receptor-interacting serine/threonine-protein (RIP) kinase (Hsu et al., 1995). FADD adaptor protein subsequently uses the death effector domain to interact with procaspase 8 to form the Death Inducing Signalling Complex (DISC) and allow autocatalytic activation of procaspase 8 into caspase 8 (Kischkel et al., 1995, Martin-Villalba et al., 2013, Peter et al., 2015). Active caspase 8 subsequently transmits the signal through proteolytic cleavage of downstream effector caspases such as caspase 3 (Tait and Green, 2010, Walczak and Krammer, 2000). At this point of the pathway the execution phase of apoptosis is induced and causes DNA fragmentation which ultimately results in complete cell death.

Since the initiation of the extrinsic pathway relies on ligand-receptor interactions, HIV-1 infection exploits the expression levels of these molecules to induce apoptosis (Cummins and Badley, 2014). Levels of Fas receptor/ Fas-ligand and TRAIL along with its DR5 receptor are highly elevated in lymph nodes and peripheral blood of HIV-1 infected individuals relative to their uninfected counterparts (Herbeuval et al., 2005, Huang et al., 2006, Li et al., 2009, Mitra et al., 1996, Kim et al., 2007, Kottlilil et al., 2007). In addition, TNF was found to be upregulated in lymphocytes of symptomatic HIV-infected individuals and increased apoptosis in these cells (Herbein and Khan, 2008). The heightened levels of Fas/Fas ligand expression have also been shown to contribute to bystander apoptosis of uninfected CD4⁺ T cells (Nardacci et al., 2015). Interestingly, these levels of Fas/Fas ligand expression correlate with HIV-1 progression to AIDS (Aries et al., 1995, Dockrell et al., 1999, Ipp et al., 2014, Mitra et al., 1996). Inhibition of this pathway with monoclonal antibodies targeting Fas ligand during acute SIV infection resulted in reduced disease

progression to AIDS (Salvato et al., 2007). Moreover, PBMCs isolated from HIV-1 infected individuals exhibited decreased apoptosis when treated with retinoic acid which prevents overexpression of Fas and activation-induced T cell apoptosis (Yang et al., 1995a, Yang et al., 1995b). These studies emphasize the importance of Fas/Fas ligand expression and interactions in HIV-1 mediated apoptosis of CD4⁺ T cells. Therefore, targeting the Fas mediated apoptosis pathway in HIV-1 infected individuals could be a potential therapy for AIDS.

In addition to facilitating events that promote HIV-1 infection, soluble or membrane bound viral encoded proteins such as Nef, Tat, Vpr, Vpu, PR and Env have been shown to modulate extrinsic and intrinsic pathways to mediate apoptosis of both infected and uninfected CD4⁺ T cells (Arnoult et al., 2003, Arnoult et al., 2004, Abbas and Herbein, 2013, Cummins and Badley, 2010, Ferri et al., 2000a). However, of all viral encoded proteins, HIV-1 Env is deemed a principal cause of bystander apoptosis. The mechanisms and contributions of each protein to bystander apoptosis leading to CD4⁺ T cell loss are defined below, with more emphasis on Env.

1.3.4 Nef, Tat, Vpr, Vpu and PR mediated bystander apoptosis

Nef is an accessory protein that is expressed in abundant levels during the earliest stages of HIV-1 infection. This protein is multifunctional with both anti-apoptotic and pro-apoptotic properties (Cummins and Badley, 2010, Jacob et al., 2017). During the early stages of infection, Nef promotes viral replication by preventing cell death through inhibiting pro-apoptotic proteins such as ASK1, Bad or p53 (Baur et al., 1994, Geleziunas et al., 2001, Greenway et al., 2002, Wolf et al., 2001). However, during later stages of infection, Nef is secreted in exosomes from HIV-1 infected cells and induces bystander apoptosis of CD4⁺ T cells (Lenassi et al., 2010). Evidence of this stems from detection of the Nef protein in serum of HIV-1 infected individuals (Caby et al., 2005, Zhang and Crumpacker, 2001). It has been reported that this soluble secreted Nef induces bystander apoptosis of CD4⁺ T cells through direct interaction with their CXCR4 receptor (James et al., 2004). The Nef-CXCR4 interactions subsequently trigger the intrinsic pathway by down-regulating expression of anti-apoptotic proteins Bcl2, Bclxl and increasing caspase activity (Rasola et al.,

2001). Binding of Nef to uninfected CD4⁺ T cells also recruits anti-Nef antibodies which prime these cells for apoptosis (Fujii et al., 1996a, Fujii et al., 1996b, Otake et al., 1994). Indirect mechanisms include overexpression of the Fas ligand on infected CD4⁺ T cells which induce apoptosis of uninfected CD4⁺ T cells through contagious apoptosis (Andreau et al., 2004, Xu et al., 1999).

Tat is a regulatory protein which primarily facilitates viral transcription. However, when secreted into the plasma of HIV-1 infected individuals, Tat crosses membranes of uninfected CD4⁺ T cells via clathrin mediated endocytosis to trigger extrinsic and intrinsic pathways of apoptosis (Frankel and Pabo, 1988, Gougeon, 2003, Vendeville et al., 2004, Wang et al., 2010a). In the extrinsic pathway, secreted Tat induces overexpression of TRAIL, Fas/Fas ligand and caspase 8 thus rendering the uninfected cells susceptible to Fas/ TRAIL mediated cell death (Bartz and Emerman, 1999, Li et al., 1995, McCloskey et al., 1997, Westendorp et al., 1995, Zhang et al., 2001a). Tat has also demonstrated the ability to induce apoptosis via generation of oxidative damage which triggers the intrinsic pathway (Manes and Cota-Gomez, 2016). In this pathway, Tat also upregulates expression of pro-apoptotic Bax, downregulates Bcl2 and disrupts calcium levels within mitochondria thus causing mitopotential depolarization (Buccigrossi et al., 2011, Macho et al., 1999, Perry et al., 2005, Sastry et al., 1996, Shedlock et al., 2008).

The Vpr accessory protein is responsible for transport of the PIC into the nucleus during HIV-1 replication and activation of transcription. During HIV-1 infection, Vpr secreted from infected cells mediates cleavage of pro-apoptotic Bid into active truncated Bid (tBid) which increases the permeability of mitochondrial membrane (Snyder et al., 2010). Previous studies demonstrated that this Vpr-induced increase in mitochondrial membrane permeability releases cytochrome C and mediates bystander apoptosis via the caspase 9 dependent intrinsic pathway (Jacotot et al., 2001, Muthumani et al., 2002). Furthermore, Vpr activates Bax to promote apoptosis via the intrinsic pathway (Andersen et al., 2006). In the extrinsic pathway, Vpr-augmented Fas ligand expression of activated PBMCs (Arokium et al., 2009).

The Vpu accessory protein prevents superinfection during the early stages of HIV-1 infection by downregulating expression of CD4 receptors (Tanaka et al., 2003). This

is necessary to promote viral replication and budding out of new virions without killing the cells during the early stages of infection. During later stages of infection, soluble Vpu decreases potassium levels in uninfected CD4⁺ T cells making the cells susceptible to apoptosis stimuli (Strebel, 2014). Moreover, Vpu interacts with tetherin to promote viral budding which disrupts the cell membrane resulting in cell death (Azad, 2000).

HIV-1 PR plays a crucial role of truncating immature precursor proteins into mature viral proteins during HIV-1 replication. Over and above its role in the virus life cycle, the protease promotes apoptosis during HIV-1 infection by inactivating anti-apoptotic Bcl2 protein and cleaving procaspase 8 into a novel peptide called casp8p41 (Nie et al., 2007, Strack et al., 1996). This peptide triggers intrinsic apoptosis through mitochondrial depolarization and nuclear fragmentation (Nie et al., 2007, Strack et al., 1996).

1.3.5 Env-mediated bystander apoptosis

The primary role of Env during HIV-1 infection is to facilitate virus entry into target CD4⁺ T cells. In addition to its role in initiation of infection, this protein has been extensively implicated as a major mediator of bystander apoptosis leading to CD4⁺ T cell loss associated with HIV/AIDS (Ahr et al., 2004, Cummins and Badley, 2010, Garg and Blumenthal, 2008, Garg et al., 2012, Sourisseau et al., 2007). Evidence of its role in bystander apoptosis is supported by numerous observations. Firstly, since loss of immune cells is significantly limited to CD4⁺ T cells and Env utilizes CD4 as a primary receptor for entry, it is most likely that this protein is able to induce bystander apoptosis. Secondly, previous studies have demonstrated that Env is expressed on the surface of infected cells where it is able to interact with CD4 receptor and CXCR4/CCR5 co-receptors on the surface of bystander uninfected CD4⁺ T cells to mediate bystander apoptosis (Biard-Piechaczyk et al., 2000, Blanco et al., 2003, Garg and Blumenthal, 2006a, Joshi et al., 2011, Joshi et al., 2016, Laurent-Crawford et al., 1995, Li and Pauza, 2011). In addition, after viral entry, gp120 spontaneously dissociates from the virus and is shed into the circulatory system where it accumulates in the lymphoid tissue (Santosuosso et al., 2009, Finzi et al., 2010).

Here it interacts with uninfected CD4⁺ T cells, hence inducing bystander apoptosis. Accordingly, substantial amounts of gp120 are detected in blood and tissues of HIV-1 infected patients (Oh et al., 1992, Rychert et al., 2010).

The structural biology of Env determines its ability to induce bystander apoptosis. As previously mentioned and reiterated here, Env exists as a heterotrimer of three gp120 CD4 binding subunits non-covalently linked to three transmembrane gp41 subunits responsible for fusing viral and host cell membranes (Wyatt and Sodroski, 1998). When expressed on membranes of infected cells, the gp120-gp41 heterotrimer induces bystander apoptosis through interaction with CD4 and/ co-receptors via varied mechanisms. These mechanisms include hemifusion, syncytium mediated and contagious apoptosis defined below.

1.3.6 Membrane expressed Env-mediated hemifusion, syncytial and contagious apoptosis leading to bystander CD4⁺ T cell loss

Hemifusion entails interactions between membrane expressed Env on infected cells and CD4 with or without CXCR4/CCR5 on uninfected CD4⁺ T cells which results in partial membrane fusion and lipid exchange between infected and uninfected cells (Chernomordik and Kozlov, 2005, Nardacci et al., 2015). The fusion and exchange of lipids leads to loss of membrane integrity which triggers apoptosis of both infected and uninfected cells (Perfettini et al., 2005a).

In contrast to hemifusion, complete fusion between membranes of infected and uninfected cells results in merging of the two cells to form a multinucleated cell called syncytium (Spijkerman et al., 1998). As an outcome of syncytia formation, the two nuclei within this multinucleated cell fuse into a single nucleus in a process called karyogamy (Nardacci et al., 2005, Perfettini et al., 2004, Spijkerman et al., 1998). Subsequently, the process of nuclei fusion introduces DNA lesions such as double stranded breaks (DSB) which trigger pro-apoptotic signals (Ferri et al., 2000a, Perfettini et al., 2008, Roumier et al., 2003). These signals include inactivation of an anti-apoptotic tumour-suppressor protein p53, activation of pro-apoptotic proteins such as Bax and Bak within the intrinsic pathway (Nakano and Vousden, 2001). This activated apoptotic pathway results in apoptosis of both infected and uninfected CD4⁺ T cells commonly known as syncytial apoptosis. A study by (Ferri et al., 2000a)

has reported the presence of syncytia in lymphoid organs and brains of HIV-1 infected individuals. Interestingly, syncytium and hemifusion formation correlates with CD4⁺ T cell loss and progression to AIDS in HIV-1 infected individuals (Blaak et al., 2000, Castedo et al., 2002, Garg and Blumenthal, 2006a, Garg et al., 2007, Maas et al., 2000).

Similarly to hemifusion and syncytium-induced bystander cell death, contagious apoptosis also requires fusion between membranes of virally infected and uninfected cells. However, the virally infected cells are already undergoing apoptosis due to infection and rapidly transmit their apoptotic signals to uninfected cells causing bystander apoptosis (Andreau et al., 2004).

Even though the gp120 subunit is the first point of interaction between Env-expressing infected cells and CD4 on uninfected cells, previous studies have highlighted the importance of the gp41 subunit in bystander apoptosis (Blanco et al., 2003, Garg and Blumenthal, 2006b). This subunit mediates hemifusion and syncytial apoptosis by facilitating fusion between membranes of infected and uninfected cells (Perfettini et al., 2005b). Its significance in bystander apoptosis was demonstrated in studies where treatment with a gp41 antagonist Enfuvirtide in HIV-infected patients, inhibited gp41-mediated cell death (Barretina et al., 2004), the V38E mutation in gp41- inhibited bystander apoptosis *in vitro* (Garg et al., 2009) and resulted in slower CD4⁺ T cell decline in humanized mice (Garg et al., 2011). Thus therapies that prevent HIV-1 mediated gp41 fusion through fusion inhibitors could be beneficial in inhibiting bystander apoptosis and CD4⁺ T cell loss associated with HIV/AIDS.

1.3.7 Soluble gp120-mediated bystander apoptosis

Granting the relevance of membrane expressed Env in bystander apoptosis, the role of shed soluble gp120 cannot be ignored. Similarly to Env expressed on the surface of infected cells, the shed soluble gp120 also mediates apoptosis via interactions with CD4 and or CXCR4/CCR5 co-receptors on uninfected cells (Ahr et al., 2004, Joshi et al., 2011, Joshi et al., 2014). This suggests that signalling via host-derived receptors is a requirement in soluble gp120-mediated bystander apoptosis. In agreement with this suggestion, previous *in vitro* studies have demonstrated that blocking gp120-CD4 interactions inhibited bystander apoptosis (Biard-Piechaczyk et

al., 2000, Guillerm et al., 1998, Moutouh et al., 1998). Furthermore, inhibition of gp120-co-receptor binding by a CXCR4 antagonist AMD3100 and CCR5 inhibitor Tak 779 also abrogated bystander apoptosis (Blanco et al., 2000, Tsao et al., 2016). These studies serve as further evidence that bystander apoptosis has a potential to be therapeutically blocked via CD4 and co-receptor inhibitors, hence reducing CD4⁺ T cell loss and slow down disease progression to AIDS.

The gp120-CD4/co-receptor interactions trigger pro-apoptotic signals within the intrinsic and extrinsic pathways to mediate bystander apoptosis. In the extrinsic pathway, gp120 causes overexpression of death receptors and ligands such as Fas, Fas ligand, TNF, TRAIL, DR5, DR4 and plausibly acts as a Fas mimic (Herbeuval et al., 2006, Poonia et al., 2009, Silvestris et al., 1996). In the intrinsic pathway, gp120 causes formation of reactive oxygen species, caspase 3-dependent mitopotential depolarization and downregulates expression of anti-apoptotic proteins such as Bcl2 and p53 (Cicala et al., 2000, Castedo et al., 2002, Garg and Blumenthal, 2006b, Reshi et al., 2014, Wang et al., 2010b). In addition to mediating loss of uninfected CD4⁺ T cells, soluble gp120 has been implicated in depletion of other cells such as neurons, cardiomyocytes, renal tubular cells, human vascular endothelial cells (HUVEC) and keratinocytes (Chen et al., 2013, Février et al., 2011, Green et al., 2013, Vashistha et al., 2009).

Apoptosis-inducing potential of soluble gp120 is driven by its ability and efficiency to bind receptors on uninfected cells commonly known as fusogenicity. This phenomenon directly correlates with CD4⁺ T cell loss in SHIV models of HIV-1 infection, humanized mice, *in vitro* cell lines and HIV-1 infected individuals (Etemad-Moghadam et al., 2000, Etemad-Moghadam et al., 2001, Garg and Blumenthal, 2006a, Garg et al., 2009, Garg et al., 2011, Joshi et al., 2014). The gp120 fusogenicity is linked to varied factors such as binding affinity to CD4, co-receptor expression levels and Env phenotype (Joshi et al., 2014, Joshi et al., 2016). Accordingly, several studies reported that during the course of HIV-1 infection *in vivo*, gp120-gp41 heterotrimers developed mutations which altered CD4 binding affinities and its fusogenicity (Gray et al., 2005, Li et al., 1999, Sterjovski et al., 2011, Thomas et al., 2007). Moreover, increasing binding affinity of gp120 to the CD4 receptor increased bystander apoptosis (Meissner et al., 2005). In addition to CD4 binding affinities, expression levels of CCR5 and CXCR4 contribute to varied Env

fusogenicity. Previous studies have demonstrated a direct correlation between CCR5 and CXCR4 expression levels, Env fusogenicity and bystander apoptosis (Anton et al., 2000, Holm et al., 2004, Joshi et al., 2011, Platt et al., 1998, Reeves et al., 2002).

HIV-1 Env is conformationally dynamic and the amino acid sequence continuously evolves during the course of infection (Curlin et al., 2010, Korber et al., 2001). Hence primary Envs isolated from HIV-1 infected individuals are highly variable in their genetic signatures and phenotypes (Edo-Matas et al., 2012, Joshi et al., 2014, Navis et al., 2008, van Gils et al., 2011). This variability influences their fusogenicity and ability to induce bystander apoptosis. Evidence of this was observed in primary Envs from HIV-1 infected individuals which demonstrated highly variable apoptosis-inducing potentials due to differences in their genetic sequences (Joshi et al., 2014). In addition to the influence of Env phenotype, fusogenicity and ability to induce bystander apoptosis is also associated with the stages of HIV-1 infection (Sterjovski et al., 2007). This concurs with the observation made by Wade et al, 2010 which demonstrated that primary Envs isolated from late-stage HIV-1 infected individuals were more fusogenic and induced significantly higher levels of bystander CD4⁺ T cell apoptosis relative to the early-stage Envs (Wade et al., 2010). Findings from these studies do not only emphasize the pivotal role of the Env phenotype in bystander apoptosis but also highlight its essentiality in driving HIV-1 progression to AIDS.

The effective study of the role that soluble shed Env-mediated bystander apoptosis plays in HIV-1 infection *in vitro*, relies on the production of stable, soluble and native mimics of Env which either exists as monomeric gp120 or trimeric gp120-gp41. However, due to the hydrophobic nature of the gp120-gp41 heterotrimer, producing soluble Env trimers *in vitro* is a challenge. To address this issue, the gp120-gp41 heterotrimer is commonly designed *in vitro* as gp140. Most strategies implemented to develop such gp140 Envs entail removal of the hydrophobic transmembrane region of the gp41 subunit to yield soluble gp140 proteins consisting of three gp120 subunits and equivalent gp41 ectodomain (gp41_{ecto}) subunits (Earl et al., 1994).

Regardless of improved solubility, gp140 trimers are highly unstable due to removal of the transmembrane region and weak non-covalent interactions between gp120 and gp41_{ecto}, therefore the trimer loses its conformational integrity and readily

dissociates into separate gp120 and gp41_{ecto} subunits (Sanders et al., 2013). In an attempt to improve the stability and maintain the trimeric conformation of soluble gp140 trimers, several studies have removed the cleavage site between gp120 and gp41 or introduced stabilizing motifs such as trimeric GCN4 and mutations such as SOSIP into Env sequences (Binley et al., 2000, Julien et al., 2015, Sanders et al., 2002, Sanders et al., 2013, Yang et al., 2000a, Yang et al., 2000b). The GCN4 motif in gp140 trimers (gp140_{GCN4}) is a leucine zipper protein added to the C-terminal end of gp41_{ecto} to stabilize gp120-gp41_{ecto} interactions through formation of α -helices and coiled coil structures (Yang et al., 2000b, Yang et al., 2000a).

Although gp140_{GCN4} trimers are stable, a majority of them do not have a cleavage site between gp120 and gp41_{ecto} while the minority with this site show partial cleavage (Binley et al., 2000, Forsell et al., 2005, Kothe et al., 2006, Kothe et al., 2007, Yang et al., 2000a). Hence such trimers do not quite resemble native Envs which require complete proteolytic cleavage to form fully functional Envs. Therefore SOSIP mutations are introduced on gp140 trimers with intact protease cleavage sites to form fully cleaved soluble native-like Envs (Binley et al., 2000, Schülke et al., 2002, Sanders et al., 2002). These mutations include introduction of a disulphide bond (SOS) between gp120 and gp41 to stabilize their interaction, a substitution of Isoleucine to Proline at position 559 within the N terminus of gp41 to stabilize gp41 subunits (Sanders et al., 2002). Since then, more studies have developed interest in developing different versions of SOSIP trimers for structural and functional studies of Env (Julien et al., 2013, Lyumkis et al., 2013, Pancera et al., 2014, Ozorowski et al., 2017). Env trimers with such mutations are referred to as SOSIP gp140 (gp140_{SOSIP}). Accordingly, a previous study by (Sanders et al., 2013) produced a modified version of the gp140_{SOSIP} with increased stability and solubility due to removal of the membrane proximal external region (MPER) within the gp41 subunit (Khayat et al., 2013, Klasse et al., 2013). This protein is called BG505 SOSIP.664 gp140 derived from a subtype A BG505 founder virus and consists of a sequence of up to residue 664 that encodes for gp120 and gp41 (Sanders et al., 2013). Since the discovery of BG505 SOSIP.664 gp140 was specific for HIV subtype A, a SOSIP form of gp140 comprised of HIV-1 subtype C sequences called ZM197M SOSIP.664 (Julien et al., 2015) was produced and characterized. Our laboratory developed another HIV-1 subtype C gp140_{SOSIP} based on a consensus founder virus subtype C

sequence (FVC). This sequence was generated from extensive bioinformatic analysis of Env sequences isolated from newly infected 80 African patients, i.e. the transmitted founder viruses (Killick et al., 2014). The availability of such stable and immunogenic forms of trimeric Env with conformations similar to native Env could be of great use in *in vitro* Env functional and structural studies such as HIV-1 mediated apoptosis.

1.4 Research motivation

Membrane bound and soluble HIV-1 Env exists in monomeric and trimeric conformations. However, despite advances in the role of soluble shed HIV-1 Env in bystander apoptosis of uninfected CD4⁺ T cells, there is still limited and contradicting research on the contribution of each Env conformation in mediating this process. Accordingly, a previous unpublished study from our laboratory evaluated the apoptosis-inducing ability of monomeric gp120 from two different subtypes (subtype C gp120ZM651 and subtype B gp120BaL) and trimeric subtype C gp140 (gp140AncC) in Jurkat T and activated CD4⁺ T cells (Pillay, 2011).

Apoptosis was measured through detection of biomarkers such as translocation of a membrane phospholipid called phosphatidylserine (PS) to the outer surface of the membrane and DNA fragmentation. PS translocation was in turn monitored by Annexin V/7-aminoactinomycin D (7-AAD) analysis, which indicated that all three conformations of gp120 induced low levels of apoptosis in Jurkat T cells but significantly high levels in activated CD4⁺ T cells. This was attributed to the presence of CD4/CCR5 signalling in CD4⁺ activated T cells. The trimeric gp140 AncC demonstrated higher levels of apoptosis than the two monomeric conformations in CD4⁺ T cells, suggesting that trimeric conformation of gp120 effectively induces apoptosis. However, DNA fragmentation detected by Terminal deoxynucleotidyl transferase dUTP nick end labelling (TUNEL) assay indicated contrasting findings; monomeric subtype C gp120 induced higher levels of apoptosis than the subtype B counterpart and subtype C trimeric form. These results further emphasized the controversy around the Env conformation that is responsible for apoptosis of bystander CD4⁺ T cells during HIV infection and raises the need for further studies. Moreover, the recombinant Env proteins used in this previous study were only

purified using lectin affinity chromatography and contaminating proteins likely impacted on the results. Purification methodologies have subsequently improved in our laboratory and worldwide since this study. Therefore, since there is limited and contrasting research in HIV-1 subtype C Env-mediated bystander apoptosis; a predominant subtype in South Africa, there is renewed interest in the current study to delineate the role of CD4 signalling via different Env conformations in bystander apoptosis of uninfected CD4⁺ T cells.

1.5 Research aim and objectives

The overall aim of the study was to evaluate the ability of different HIV-1 subtype C Env conformations to induce apoptosis of HIV-1-uninfected bystander CD4⁺ T cells via CD4 signalling. These Env conformations were based on a matched FVC sequence and included monomeric gp120_{FVC}, trimeric gp140_{GCN4} and gp140_{SOSIP}.

The aim was achieved by the following specific objectives:

- To optimally express and purify matched HIV-1 subtype C monomeric gp120_{FVC}, trimeric gp140_{GCN4} and the gp140_{SOSIP} in human embryonic kidney 293T (HEK 293T) adherent cell lines.
- To confirm the structural integrity and functionality of the purified recombinant Envs using SDS PAGE, Western blot analysis and ELISAs.
- To evaluate and compare the ability of the different Env conformations to induce apoptosis of CD4-expressing HIV-1 uninfected Jurkat T cells using flow cytometry.

2. Materials and Methods

2.1 Reagents used in this study

2.1.1 Recombinant plasmids

In this study, pCDNA 3.1 (Invitrogen, Grand Island, NY) and pUC19 (New England BioLabs, USA) were used for the propagation of CH505 Env sequence as positive controls for transformation of *Escherichia coli* (*E.coli*) DH5 α cells (ThermoFisher Scientific, Rockford, IL, USA). pCDNA 3.3 (Invitrogen, Grand Island, NY) was used for transient expression of Furin in mammalian cells. VRC 3831 and pET15 plasmids available in our laboratory were respectively used for transient expression of recombinant FVC gp140_{SOSIP} Env in mammalian cells and bacterial expression of soluble wild type two domain CD4 (2dCD4 WT). The pCI-neo (Promega, Corporation, Madison, USA) was used for transient expression of Green Fluorescence Protein (GFP) positive transfection control.

2.1.2 Bacterial strains

E.coli DH5 α cells and BL21 star competent cells (ThermoFisher Scientific, Rockford, IL, USA) were respectively selected for the propagation of recombinant plasmids through transformation and batch expression of 2dCD4 WT.

2.1.3 Mammalian cell lines

The HEK 293T and stably transfected HEK 293F cell lines were both available in our laboratory. HEK 293T cells were used for transient expression of the recombinant gp140_{SOSIP} while the HEK 293F cell line was used for continual expression of the gp120_{FVC} and gp140_{GCN4}. Jurkat T cells were kindly provided by Dr Jaclyn Mann at the HIV Pathogenesis Programme, Hasso Plattner Research Laboratory, Nelson R. Mandela School of Medicine and used in the evaluation of recombinant HIV-1 Env protein mediated apoptosis via CD4 binding.

2.1.4 Antibodies used in the Indirect ELISAs and Western blot analyses

CAP256-VRC26.25, Anti-HIV-1 gp120 Monoclonal (VRC01) and Anti-HIV-1 gp41 Monoclonal (10E8) antibodies were previously produced in our laboratory. Anti-HIV-1 gp120 Monoclonal (IgG1b12) and Anti-HIV-1 gp120 Monoclonal (17b) were obtained from the National Institute of Health (NIH) AIDS Research and Reference Program, Division of AIDS, NIAID. These antibodies bind to different conformations of HIV-1 Env. CAP256-VRC26.25 is an Env quaternary structure-specific antibody which binds gp140_{SOSIP}, VRC01 binds the CD4 binding site of gp120_{FVC} and 10E8 is specific for the MPER of gp140_{GCN4}. All antibodies with the exception of 17b were used as primary antibodies for confirmation of conformational integrity of the respective Env conformations in the indirect enzyme-linked immunosorbent assays (ELISAs). A CD4 induced (CD4i) epitope specific antibody (17b) was used to confirm functionality of the respective Env conformations in an Indirect ELISA. Anti-human IgG-Horse Radish Peroxidase (HRP) linked antibody (GE Healthcare, New York, USA) was used as a secondary antibody in all ELISAs for specifically binding fragment crystallization (F_C) regions of the previously mentioned primary antibodies.

Rabbit sera 38 which was originally terminally isolated from a New Zealand White Rabbit (*Oryctolagus cuniculus*) post immunization with gp120_{FVC} by (Killick et al., 2015) was available in our laboratory. The serum was used as a primary antibody for detection of HIV-1 Env expression in western blots. Anti-rabbit-HRP linked antibody (GE Healthcare, New York, USA) was used as a secondary antibody in the western blots. The latter is a polyclonal gamma immunoglobulin specific antibody raised in goat.

2.1.5 Recombinant proteins

The following recombinant HIV-1 Env proteins: gp140_{SOSIP}, gp140_{GCN4} and gp120_{FVC} were produced in this study from HEK 293T cells and a HEK 293F stable cell line. The Envs were used for inducing apoptosis in Jurkat T cells for the evaluation of Env-mediated bystander apoptosis. The 2dCD4 WT recombinant protein was also produced in this study and used to confirm functionality of purified Env proteins. HIV-1 BaL gp120 (gp120_{BaL}) was obtained from the NIH AIDS Research and Reference

Reagent Programme and used as a positive control for the Indirect ELISAs and western blot analysis.

2.2 Plasmid DNA propagation and maintenance

2.2.1 Preparation of chemically competent cells

E.coli DH5 α cells (5 μ l) were cultured overnight shaking at 250 revolution per minute (rpm), 37 °C in 5 ml sterile Luria Bertani (LB) broth composed of 5 g Sodium chloride (NaCl, Sigma-Aldrich, Steinheim, Germany), 5 g Yeast extract (Biolab, Wadeville, Gauteng, South Africa) and 10 g Tryptone (Oxoid, Hampshire, England). The overnight starter culture was upscaled into a 40 ml LB broth and incubated with shaking (250 rpm) at 37 °C to an exponential growth phase where cells are metabolically active and maximally competent (optical density of 0.4-0.6). Thereafter, cells were centrifuged at 1500 rpm for 10 minutes at 4 °C using the Eppendorf® Centrifuge 5804/5804R (Sigma-Aldrich, Steinheim, Germany). The resulting pellet was then re-suspended in 10 ml chilled transformation buffer (Appendix A.1, Table 1) and incubated on ice for 20 minutes. After incubation on ice, the cells were further centrifuged at 15000 rpm for 10 minutes at 4 °C. The pellet was then re-suspended in 1 ml transformation buffer and aliquoted into 100 μ l volumes for storage at -80 °C.

2.2.2 Transformation of chemically competent cells

To confirm that the *E.coli* DH5 α cells were chemically competent, 0.04 pg/ml of control plasmids pUC19 and 636.17 ng/ μ l CH505 pCDNA 3.1 were added separately into 30 μ l of cells and incubated for 20-30 minutes on ice. The latter was then heat shocked at 42 °C for 45 seconds to increase permeability of the bacterial cell membrane and allow entry of the respective plasmids. Subsequently, the two reactions were placed on ice for five minutes for recovery of the cell membrane. Positive transformants containing either of the two plasmids were selected for by plating on LB agar supplemented with 100 μ g/ml Ampicillin (Appendix A.1, Table 1). The plates were then incubated for 12-20 hours at 37 °C and colonies enumerated after the incubation period. A cells only control was included as a negative control for

detection of contamination. The competency of *E.coli* DH5 α cells was confirmed by the presence of two or more colonies.

The recombinant Furin pCDNA 3.3 (592.5 ng/ μ l) and gp140_{SOSIP} VRC 3831 (530.2 ng/ μ l) plasmids were used at respective final concentrations of 11.85 ng/ μ l and 10.6 ng/ μ l for transformation into the chemically competent *E.coli* DH5 α cells. Ampicillin (100 μ g/ml) and 50 μ g/ml Kanamycin (Appendix A.1, Table 1) were used for antibiotic selection of positive Furin pCDNA 3.3 and gp140_{SOSIP} VRC 3831 transformants, respectively.

2.3 Plasmid DNA isolation

2.3.1 Qiagen maxi prep

Propagated Furin pCDNA 3.3 and gp140_{SOSIP} VRC 3831 plasmids were isolated from transformed *E.coli* DH5 α cells using the QIAGENTM plasmid kit (Qiagen, Maryland, USA) as per manufacturer's instructions. Briefly, a 5 ml LB broth was inoculated with a single colony from transformed *E.coli* DH5 α cells for production of a starter culture supplemented with 100 μ g/ml Ampicillin or 50 μ g/ml Kanamycin (Appendix A.1, Table 1) where necessary.

The starter culture was incubated for eight hours at 37 °C with shaking at 250 rpm to allow transition from lag phase to exponential phase of bacterial growth. After the specified incubation period, the starter culture was upscaled to a 200 ml culture at the same temperature and incubated for 12-16 hours. This allowed transition from exponential phase to stationary phase which is optimal for replication of the plasmids. The bacterial cells were harvested from the large scale culture by centrifugation at 6000 \times g (7400 rpm) and a temperature of 4 °C for 15 minutes using an Avanti J-E Series centrifuge (Beckman Coulter Life Sciences, Indianapolis, USA).

Harvested cells were re-suspended in 10 ml re-suspension Buffer P1 supplemented with RNase to degrade RNA (Appendix A.1, Table 2). Thereafter, 10 ml lysis Buffer P2 (Appendix A.1, Table 2) was added followed by vigorous inverting and incubation at room temperature (RT) for five minutes to lyse the cell membrane and denature DNA under alkaline conditions. This was followed by addition of 10 ml chilled

neutralization Buffer P3 (Appendix A.1, Table 2), vigorous mixing and incubation on ice for 20 minutes to reduce alkalinity and re-nature single stranded DNA. The reaction mixture was centrifuged at 20 000 x *g* (14 099 rpm) at 4 °C for 30 minutes and the supernatant containing plasmid DNA was re-centrifuged under the same conditions for 15 minutes. During the second centrifugation step, a QIAGEN-tip 500 affinity chromatography column was equilibrated with 10 ml Buffer QBT (Appendix A.1, Table 2) by gravity flow. The resulting supernatant was removed promptly and applied to the column for adherence of DNA to the resin and elution of impurities.

The column was washed twice with 30 ml Buffer QC and DNA was eluted from the resin with 15 ml Buffer QF (Appendix A.1, Table 2). Eluted DNA was then precipitated with 10 ml isopropanol (Sigma-Aldrich, Steinheim, Germany) and centrifuged at 20 000 x *g* (14 099 rpm) at 4 °C for 30 minutes. Following centrifugation, the pellet was washed with 5 ml RT 70 % ethanol and centrifugation at 15 000 x *g* (12 210 rpm) at the same temperature for 10 minutes. The pellet was air-dried for 10 minutes and the purified plasmid DNA dissolved in dH₂O.

2.3.2 Quantification of isolated plasmid DNA

Concentrations of the purified Furin pCDNA 3.3 and gp140_{SOSIP} VRC 3831 plasmids were quantified by the Nano drop ND-1000 spectrophotometer (Nano drop Technologies, Inc, Wilmington, USA). The ratio of absorbance at 260 nm and 280 nm ($A_{260:280}$) was measured for evaluation of DNA purity.

2.3.3 Analysis of plasmid DNA isolation

Aliquots of 100 µl were taken at several steps of the QIAGEN maxi kit protocol for analysis of the plasmid isolation procedure. Each aliquot was mixed with a 2x loading dye (Appendix A.1, Table 3) at an equal ratio to a 1x final concentration and loaded together with the O'GeneRuler DNA ladder mix (Thermo Scientific, Rockford, IL, USA) on a 0.8 % agarose gel (Appendix A.1, Table 3) prepared in 1x TAE electrophoresis buffer (Thermo Scientific, Rockford, IL, USA). Ethidium bromide solution (Promega, Wisconsin, Dane, USA) was added at 3 µl to the 0.8 % agarose gel for fluorescent labelling of the DNA before the gel was left to solidify. The gel was

then electrophoresed at 100 V for 90 minutes in 1× TAE electrophoresis buffer and visualized under a White/ 2UV transilluminator (Analytik Jena, Upland, Canada, USA).

2.4 Mammalian and bacterial protein expression

2.4.1 General mammalian cell culture

2.4.1.1 Maintenance of HEK 293T, HEK 293F and Jurkat T cells

HEK 293T adherent cells were grown in Dulbecco's Modified Eagle Medium (DMEM, Sigma-Aldrich, Steinheim, Germany) supplemented with 10 % Fetal Calf Serum (FCS, Gibco, Grand Island, USA), 2 mM Glutamine, 100 µg/ml Penicillin and 100 µg/ml Streptomycin (Gibco, Grand Island, USA). The stable suspension cell line HEK 293F was grown in FreeStyle™ 293 Expression Medium (ThermoFisher Scientific, Rockford, IL, USA) supplemented with 0.35 mg/ml Geneticin (G418, Sigma-Aldrich, Steinheim, Germany). Jurkat T cells were grown in Roswell Park Memorial Institute medium (RPMI 1640, Sigma-Aldrich, Steinheim, Germany) supplemented with 10 mM HEPES, 2 mM L-Glutamine, 50 U/ml Penicillin-Streptomycin (PSA, Gibco, Grand Island, USA) and 10 % FCS. All cell types were maintained at 37 °C, 5 % CO₂ within a humid Forma series II water jacketed CO₂ incubator (ThermoFisher Scientific, Rockford, IL, USA) for 24-48 hours until 80 % confluency was reached.

Once an optimal confluency was established, the adherent HEK 293T cells were rinsed with 1× phosphate buffered saline (PBS), the monolayer detached from the surface of a 75 cm² Corning cell culture flask (Sigma-Aldrich, Steinheim, Germany) using trypsin (ThermoFisher Scientific, Rockford, IL, USA). Thereafter, HEK 293T cells, HEK 293F cell line and Jurkat T cells were respectively stained with 20 µl Trypan blue stain (ThermoFisher Scientific, Rockford, IL, USA) at a 1:1 volume ratio of cells to Trypan blue stain. Subsequently, all the cells were counted and cell viability was checked using the Countess II FL automated cell counter (Life Technologies, Johannesburg, South Africa).

Following cell enumeration and viability analysis, each cell type was passaged. HEK 293T cells and HEK 293F cell line were passaged every two days at a concentration

of 3×10^6 cells/ml in 15 ml DMEM and 15 ml FreeStyle™ 293 Expression Medium (ThermoFisher Scientific, Rockford, IL, USA) per 75 cm^2 culture flask respectively. Jurkat T cells were passaged every two to three days by discarding 50-90 % of the cell culture and replacing it with the remaining cells in 15 ml fresh RPMI 1640 medium per 75 cm^2 culture flask. A fresh vial of each cell type was thawed after 30 passages and excess cells from the passaging were used in preparation of frozen stocks for short or long term storage.

2.4.1.2 Preparation of HEK 293T, HEK 293F and Jurkat T cells stocks

To prepare the HEK 293T, HEK 293F and Jurkat T cells stocks for short and long term storage, the cells were grown as previously mentioned in section 2.4.1.1 to 80 % confluency and counted using the Countess II FL automated cell counter. Post enumeration, 5×10^6 cells/ml HEK 293T cells, 10×10^6 cells/ml HEK 293F and 6×10^6 cells/ml Jurkat T cells were pelleted by centrifugation at $4 \text{ }^\circ\text{C}$, 1500 rpm for 10 minutes using the Eppendorf centrifuge 5804R (ThermoFisher Scientific, Rockford, IL, USA). The pellets from each cell type were then re-suspended in 1 ml freeze medium (10 % DMSO and 90 % FCS). Thereafter, the re-suspended cells were immediately transferred into Cryogenic vials (Sigma-Aldrich, Steinheim, Germany), placed in the NALGENE™ cryo $1 \text{ }^\circ\text{C}$ freezing container (ThermoFisher Scientific, Rockford, IL, USA) and left overnight at $-80 \text{ }^\circ\text{C}$ for slow freezing at $-1 \text{ }^\circ\text{C}/\text{min}$ rate. The frozen cryogenic vials were transferred into freezer boxes at $-80 \text{ }^\circ\text{C}$ for short term storage and transferred into liquid nitrogen for long term storage. Isopropanol in the freezing container was changed after every two to three uses.

2.4.2 Optimization of transient transfection of HEK 293T cells for recombinant gp140_{SOSIP} expression

HEK 293T cells were co-transfected with the gp140_{SOSIP} VRC 3831 and Furin pCDNA 3.3 plasmid vectors for the transient expression of recombinant gp140_{SOSIP} Env protein. The transient transfection was initially optimized in a 12 well plate by seeding 1×10^5 cells in 2 ml DMEM and overnight incubation in a $37 \text{ }^\circ\text{C}$, 5 % CO_2 Forma series II water jacketed CO_2 incubator to a confluency of 70-80 %.

Following optimal confluency, recombinant plasmid DNA was prepared. This included optimization of total plasmid DNA with amounts ranging from 1 µg to 4 µg and ratios of gp140_{SOSIP} VRC 3831 to Furin pCDNA 3.3 (1:1, 2:1 and 4:1) required for efficient cleavage and trimerization of expressed gp140_{SOSIP}. The amount of 1 mg/ml Polyethylenimine pH 7 (PEI, Sigma-Aldrich, Steinheim, Germany) transfection reagent relative to total amount of DNA was optimized using DNA: PEI ratios of 1:3 and 1:6. Polyfect (Qiagen, Hilden, Germany) was added as a positive transfection reagent control as per manufacturer's instructions. Briefly, 640 ng (7.4 ng/µl) of gp120_{BaL} pCDNA 3.3 plasmid was complexed with 6.4 µl of 2 mg/ml Polyfect, added to 80 µl Opti-MEM reduced serum media (ThermoFisher Scientific, Rockford, IL, USA), incubated for 5 minutes at RT and transferred to the cells. The latter were incubated at 37 °C, 5 % CO₂ in a Forma series II water jacketed CO₂ incubator for expression.

Post the optimizations, the transient transfections were upscaled. Briefly, HEK 293T cells were cultured as previously mention in section 2.4.1.1 to 7×10⁶ cells in 35 ml DMEM per 175 cm² culture flask and incubated at 37 °C, 5 % CO₂ in a Forma series II water jacketed CO₂ incubator overnight to a confluency of 70-80 %. Thereafter, the transfection solution was prepared by adding 70 µg total plasmid DNA i.e. gp140_{SOSIP} VRC 3831 to Furin pCDNA 3.3 ratio of 2:1, 1:3 total DNA to 1 mg/ml PEI transfection reagent (Sigma-Aldrich, Steinheim, Germany) and Opti-MEM reduced serum media (ThermoFisher Scientific, Rockford, IL, USA) to a final volume of 5 ml transfection solution per 175 cm² culture flask. The solution was mixed briefly and gently by vortexing and left at RT for 10-15 minutes to allow complex formation between the DNA and transfection reagent. Subsequently, the DMEM was discarded and 5 ml transfection solution was added to the seeded cells in a drop-wise manner.

The recombinant gp120_{BaL} pCDNA 3.3 and pCI neo expressing GFP were used at 70 µg as positive controls for transfection. The transfection solution in each flask was mixed gently for thorough distribution and placed in a 37 °C, 5 % CO₂ Forma series II water jacketed CO₂ incubator for eight hours. Post the incubation period, the transfection solution was replaced with 30 ml of FreeStyle™ 293 Expression Medium (ThermoFisher Scientific, Rockford, IL, USA) and further incubated at 37 °C, 5 % CO₂ for 48 hours.

The cell culture supernatant with expressed gp140_{SOSIP} was harvested after 48 hours by collecting the medium from the flask using a pipette and 30 ml fresh media was added. The harvests were conducted two to three times until the cell monolayer began to detach from the flask's surface. To remove cell debris from the harvested supernatants, the harvests were centrifuged at 2000 rpm for 10 minutes and filtered with a 0.45 micron filter (Sigma-Aldrich, Steinheim, Germany). The filtered supernatants were stored at -20 °C and only thawed for purification.

2.4.3 Expression of gp120_{FVC} and gp140_{GCN4} from stable HEK 293F cell line

Stably transfected HEK 293F cell line was used for continuous expression gp120_{FVC} and gp140_{GCN4}, respectively. The cell line was maintained as previously mentioned in section 2.4.1.1 and 6×10^6 cells/ml were seeded in a 175 cm² culture flasks after every two to three days in 35 ml FreeStyle™ 293 Expression Medium. The expressed gp120_{FVC} and gp140_{GCN4} were harvested as supernatants and 35 ml FreeStyle™ 293 Expression Medium was replaced every two to three days. Cell debris was removed from supernatant as described in section 2.4.2.

2.4.4 Expression of 2dCD4 WT

BL21 star *E.coli* competent cells (ThermoFisher Scientific, Rockford, IL, USA) were transformed with 2dCD4 WT pET15 recombinant plasmid following the protocol previously mentioned in section 2.2.2, using 100 µg/ml Ampicillin (Appendix A.1, Table 1) as a selection marker for positive clones. Following successful transformation, a single colony was picked and added into 100 ml LB broth (Appendix A.1, Table 1) and incubated at 37 °C overnight with shaking to form a starter culture. The starter cell culture was upscaled to 1 litre through 50 times dilution i.e. 20 ml starter culture was added to 1 litre LB broth and incubated at 37 °C with shaking at 250 rpm until an optical density at 600 nm (OD₆₀₀) of 0.6-0.8 (mid log phase) was reached. A total of 4 litres culture was prepared as separate 1 litre cultures. Following establishment of the desired OD₆₀₀, each culture was further incubated at 20 °C with shaking overnight for expression of insoluble 2dCD4 WT.

2.5 Confirmation of protein expression

To confirm expression of recombinant gp140_{SOSIP}, gp140_{GCN4}, gp120_{FVC} Env proteins and 2dCD4 WT, sodium dodecyl sulphate polyacrylamide gel electrophoresis (SDS-PAGE) and western blot analysis were conducted using supernatants harvested during protein expression.

2.5.1 SDS-PAGE

Two SDS-polyacrylamide gels consisting of an 8 % separating gel and 4 % stacking gel (Appendix A.1, Table 4) were prepared to 1.5 mm thickness and left to polymerize for 30-45 minutes. During the polymerization period, 30 µl aliquots of protein supernatants (gp140_{SOSIP}, gp140_{GCN4}, gp120_{FVC} and 2dCD4 WT) were added to 2x reducing buffer composition detailed in (Appendix A.1, Table 4) to a final 1x buffer concentration and boiled for five minutes. The polymerized gels were added to a tank system and 500 ml 1x tank running buffer (Appendix A.1, Table 4) was added into the tank and in each well. The prepared protein samples were loaded into the wells with a 100 µl Hamilton syringe (Sigma-Aldrich, Steinheim, Germany) at final volumes of 30 µl. Additionally, 10 µl of Colour Prestained Protein Standard, broad range (11-245 kDa, New England BioLabs, USA) was added as a molecular weight marker to determine the molecular weight of separated proteins.

The protein samples were then separated based on size through electrophoresis at constant 150 V for 30-45 minutes until the dye front reached the bottom of the gels. Following electrophoresis, one gel was stained with 100 ml of 0.025 % Coomassie Blue R250 stain (Appendix A.1, Table 4) overnight and destained with 7 % ethanol, 5 % acetic acid destain solution (Appendix A.1, Table 4) by shaking at RT until the Coomassie blue was completely removed and stained proteins were visible. The gel was then visualized under white light in the Gel DocumentationTM system (Bio-Rad, Hercules, CA). The second gel was used for western blot analysis of the Env proteins only.

2.5.2 Western blot analysis

The second gel with Env protein samples separated by SDS-PAGE was equilibrated in transfer buffer (Appendix A.1, Table 5) for 20 minutes. The transfer cassette was prepared by cutting six Whatman™ 3MM chromatography blotting papers (GE Healthcare Life Sciences, New York, USA) and the Nitrocellulose membrane (ThermoFisher Scientific, Rockford, IL, USA) to the size of the gel. The latter were soaked in transfer buffer (Appendix A.1, Table 5) for 20 minutes by shaking at RT. Following the gel equilibration and soaking period, the transfer cassette was assembled as a sandwich on the Transblot SD semi-dry transfer cell (Bio-Rad, Hercules, CA) by stacking three layers of blotting paper at the bottom, Nitrocellulose membrane and the separated gel in the middle and three blotting paper on top.

The proteins were then transferred onto the membrane at 20 V for 30 minutes. To remove non-specific binding, the membrane was blocked with 5 % skimmed milk (Appendix A.1, Table 5) for one hour by shaking at RT. The blocked membrane was then washed five times for five minutes by shaking at RT with 1× 0.1 % Tween-Tris Buffered Saline (T-TBS, Appendix A.1, Table 5) and incubated with 1:2000 diluted Rabbit serum 38 primary antibody for one hour in the dark. Post the one hour incubation period, the membrane was washed three times for five minutes by shaking at RT with T-TBS and incubated for one hour with HRP linked Anti-rabbit IgG (GE Healthcare, New York, USA) secondary antibody diluted 2000 times. The antibodies were prepared in 1× T-TBS. The membrane was then washed three times for five minutes with 1× T-TBS and incubated for five minutes with SuperSignal™ West Pico PLUS Chemiluminescent Substrate (ThermoFisher Scientific, Rockford, IL, USA) prepared at a 1:1 ratio of enhancer solution and stable solution. Post development with the substrate, excess substrate was dabbed off and the proteins on the membrane were visualized via chemiluminescence using the Gel Documentation™ system (Bio-Rad, Hercules, CA).

Following confirmation of recombinant Env protein (gp140_{SOSIP}, gp140_{GCN4}, gp120_{FVC}) and 2dCD4 WT expression by SDS-PAGE and western blot analysis, the proteins were purified.

2.6 Protein purification

2.6.1 Purification of recombinant gp140_{SOSIP}, gp140_{GCN4} and gp120_{FVC} Env proteins

2.6.1.1 Lectin affinity chromatography

Following confirmation of optimal expression of gp140_{SOSIP}, gp140_{GCN4} and gp120_{FVC} Env proteins, the harvested supernatants were then purified by *Galanthus nivalis* lectin (Sigma-Aldrich, Steinheim, Germany) affinity chromatography. The technique separates the respective Env proteins from contaminating non-Env impurities based on their binding affinity for lectin. This is possible because HIV-1 Env is extensively glycosylated and has a high affinity for sugar residues on the lectin. The harvested supernatants were incubated with 2 ml *Galanthus nivalis* lectin at 4 °C with stirring overnight to facilitate Env binding to lectin.

The column was washed and equilibrated with 20 ml 1× PBS (Sigma-Aldrich, Steinheim, Germany). Post the column wash and Env-lectin incubation period, the supernatants were passed through the lectin column. This process was repeated and the column was then washed with 100 ml of 1 M and 0.5 M NaCl solutions (Appendix A.1, Table 6) in 1× PBS followed by a 100 ml 1× PBS wash. The proteins were then eluted from the column with 40 ml 1 M methyl- α -D-manno-pyranoside (MMP, Sigma-Aldrich, Steinheim, Germany) in 1× PBS after 30 minutes of incubation. Following elution, the column was washed with 20 ml of 1× PBS and stored in 20 % ethanol (Appendix A.4) at 4 °C. The eluted proteins were concentrated in an Amicon Ultra-50 (Sigma-Aldrich, Steinheim, Germany) concentrator by centrifugation at 5000 rpm and washed with 1× PBS to remove the MMP. The concentrated proteins were stored at -20 °C for long term storage and at 4 °C for short term storage. Aliquots (40 μ l) at each purification step were collected for analysis of the purification procedure by SDS-PAGE and western blot analysis.

2.6.1.2 Size exclusion chromatography (SEC)

SEC was used to isolate gp140_{SOSIP}, gp140_{GCN4} trimer from contaminating monomers and dimers and gp120_{FVC} monomer from contaminating dimers post lectin purification. The Env proteins were separated based on size and hydrodynamic radius using a HiPrepTM 16/60 Sephacryl S-300 HR gel filtration column (Sigma-Aldrich, Steinheim, Germany) with a stationary phase that has defined pore sizes (separates 10-1500 kDa globular proteins).

The column was pump washed with 10 ml 0.5 M NaOH (Appendix A.1, Table 7) and 50 ml NaOH was passed through the column. This was followed by a second pump wash with 70 % ethanol which allowed 50 ml 70 % ethanol (Appendix A.1, Table 7) to be passed through the column. The wash was repeated with 20 % ethanol at the same volumes. Since the respective proteins were solubilised in 1× PBS, the column was equilibrated with 1× PBS through a 50 ml pump wash and 140 ml 1× PBS was passed through the column.

In preparation of the 1 mg/ml protein sample, 1× PBS was added to the protein in a final volume of 1 ml and spun at 5000 rpm for 10 minutes in the Eppendorf 5415R benchtop microcentrifuge (Merck, Darmstadt, Germany). The protein samples were each introduced into the column through loading into the sample port of the AKTA_{FPLC} SEC system (GE Healthcare Life Sciences, New York, USA) for separation of the monomer, dimer and trimer fractions. The different conformations (monomer, dimer, and trimer) differ in shape, size and molecular weights. As such, they were eluted at different volumes within different time points and 2 ml fractions of each elution volume were collected for further analysis. Ultra-violet (UV) light absorbance at 280 nm wavelength was measured for each eluted protein as a marker of protein intensity or concentration. The UV absorbance value from the 1× PBS was blanked (UV-autozero) and used as a reference point.

2.6.2 Nickel affinity chromatography purification of 2dCD4 WT

To purify the expressed 2dCD4 WT recombinant protein, the BL21 star *E.coli* bacterial culture was centrifuged at 5000 rpm at 4 °C for 20 minutes using the Eppendorf centrifuge 5804R. The pellet was re-suspended in 50 ml/litre 1× PBS (Sigma-Aldrich, Steinheim, Germany) and 0.5 mg/ml chicken lysozyme (Sigma-Aldrich, Steinheim, Germany) and incubated at 4 °C with shaking for an hour to hydrolyse the bacterial cell wall. The sample was then placed at -80 °C until frozen and immediately thawed at 65 °C. This freeze-thaw cycle was repeated three times and the cell suspension was further lysed through sonication; sonicated for three to six times for one minute cycles at an amplitude of 80 %, pulse on for one second and pulse off for half a second.

Once the bacterial cell membrane was disrupted by sonication, the sample containing 2dCD4 WT in insoluble inclusion bodies and other insoluble cell debris was retrieved by centrifugation at 16 000 rpm for 45 minutes at 4 °C. The resulting supernatant was discarded and the pellet re-suspended in 50 ml wash buffer 1 (WB1, Appendix A.1, Table 8) to solubilize the proteins and incubated at RT with shaking for an hour. The suspension was further centrifuged at 16 000 rpm for 30 minutes at 4 °C, the resulting supernatant was collected and incubated with equilibrated Nickel (Ni) beads at 4 °C (Appendix A.1, Table 8) for selective purification of denatured soluble 2dCD4 WT by Ni affinity chromatography. This was possible because the sequence encoding for 2dCD4 WT protein was codon optimized for *E.coli* expression and a 6× polyhistidine (His) tag encoding sequence was introduced in frame at the 3' terminus within the pET15 recombinant expression vector (Cerutti et al., 2010). The expressed His tag has high affinity for Ni.

The Ni resin was prepared by adding 2 ml of Ni slurry to 3 ml recharge buffer (Appendix A.1, Table 8) and shaking at RT for 30 minutes. The recharged resin was poured into 50 ml Falcon tubes (Sigma-Aldrich, Steinheim, Germany) and washed five times with 50 ml WB1 by centrifugation at 5000 rpm at 4 °C for five minutes. The washes were repeated five times with WB2 (Appendix A.1, Table 8) and the denatured soluble 2dCD4 WT was eluted in 10 ml of wash buffer containing 500 mM Imidazole (Appendix A.1, Table 8).

Following Ni affinity purification of soluble denatured 2dCD4 WT, the protein was refolded using decreasing Urea concentrations and dialysis. The eluted 2dCD4 WT was transferred into SnakeSkin® Pleated Dialysis Tubing (Pierce; Rockford, IL) and dialysed overnight at 4 °C with stirring in 1 litre folding buffer A (Appendix A.1, Table 9). The dialysis buffer was then changed to folding buffer B (Appendix A.1, Table 9) and the protein was incubated overnight at 4 °C. The refolded protein was then dialysed against 1× PBS (Sigma-Aldrich, Steinheim, and Germany) three times for two hours per dialysis for the first two times at 4 °C with PBS replacement after each dialysis and the last change was left overnight. The dialysed protein was then centrifuged at 4000 rpm for 10 minutes at 4 °C to remove the precipitate and the supernatant was further filtered through 0.45 micron filters (Sigma-Aldrich, Steinheim, Germany). The filtered protein was concentrated in a 10 000 Da cut off Amicon Ultra-50 (Sigma-Aldrich, Steinheim, Germany) concentrator and quantified through calorimetry using the Pierce BCA protein assay kit (ThermoFisher Scientific, Rockford, IL, USA), as per manufacturer's instructions. To confirm expression, SDS-PAGE was conducted from the quantified protein.

2.7 Concentration and quantification of purified proteins

2.7.1 Bicinchoninic acid assay (BCA)

Purified gp140_{SOSIP}, gp140_{GCN4}, gp120_{FVC} Env and 2dCD4 WT recombinant proteins were quantified using the Pierce BCA Protein Assay Kit (ThermoFisher Scientific, Rockford, IL, USA) as per manufacturer's instructions. Briefly, bovine serum albumin (BSA, Roche; Mannheim, Germany) protein standards at concentrations ranging from 0 µg/ml to 2000 µg/ml were prepared in 1× PBS (Appendix A.1, Table 10). BCA reagent A was added to reagent B in a 50:1 ratio to form a working reaction (Appendix A.7), 25 µl of each protein standard and the purified proteins (gp140_{SOSIP}, gp140_{GCN4}, gp120_{FVC}) were added into Polysorp 96 well plate (ThermoFisher Scientific, Rockford, IL, USA). This was followed by addition of 200 µl of the working reaction into each well and the plate was thoroughly mixed by shaking at 37 °C and 1500 rpm for 30 minutes in the dark. Once the plate cooled to RT, the absorbance was measured at 562 nm on the iMark Microplate reader (Bio-Rad, Hercules, CA).

The protein concentrations were then determined by plotting a standard curve from absorbance values of blank corrected protein standards.

2.8 Biochemical characterization of purified Env; confirmation of correct structural orientation and functionality

2.8.1 Blue native-PAGE

To differentiate and isolate SEC fractions containing the trimeric Env conformation from the monomeric or dimeric form in three different Env proteins (gp140_{SOSIP}, gp140_{GCN4}, gp120_{FVC}), blue native PAGE was conducted according to a protocol previously described by (Wittig et al., 2006). Briefly, a 1× NativePAGE Anode buffer was prepared by adding 50 ml of 20× NativePAGE running buffer (Life Technologies, Rockford, IL, USA) to 950 ml of deionized water (DI) and a 1× NativePAGE dark blue cathode buffer was prepared by adding 50 ml 20× NativePAGE running buffer (Life Technologies, Rockford, IL, USA) and 50 ml 20× NativePAGE cathode to a final volume of 900 ml deionized water. A 3-13 % precast gradient gel was assembled into a mini-gel running tank system and the wells were rinsed three times with 1× NativePAGE dark blue cathode buffer. Following the washes, the wells were filled with 1× NativePAGE dark blue cathode buffer and protein fractions eluted and isolated from the same SEC peak were pooled or concentrated together using an Ultra-50 concentrator (Sigma-Aldrich, Steinheim, Germany).

To prepare concentrated protein samples, a 4× blue native loading dye was added to a final 1× concentration in a total volume of 20 µl pooled/concentrated post SEC protein fractions. BSA was included in the same manner as a positive control to determine the molecular weight of the proteins. Each prepared sample was loaded onto the gel and NativeMark™ Unstained Protein Standard (ThermoFisher Scientific, Rockford, IL, USA) was also loaded as a reference for measurements of molecular weights. Once all samples were loaded, the upper cathode buffer chamber in the mini-gel running system was filled with 200 ml 1× NativePAGE dark blue cathode buffer while the lower anode buffer chamber was filled with 550 ml NativePAGE Anode buffer. The gel was then electrophoresed at 150 V constant voltage for 90-115 minutes to separate the proteins based on their native molecular weight.

To stain the gradient gel post electrophoresis, the gel was placed in 100 ml fix solution (40 % methanol, 10 % acetic acid) and heated in a microwave on 950-1100 watts for 45 seconds. The gel was shaken on the Heidolph Unimax 1010 orbital shaker (Labotec, Midrand, South Africa) for 15-30 minutes at RT and post this period the fix solution was decanted. The fixing was repeated to ensure that the proteins were effectively fixed onto the gel. The gel was then stained with 100 ml Coomassie R-250 stain (0.02 % Coomassie R-250 in 30 % methanol and 10 % acetic acid), heated on high (950-1100 watts) in a microwave for 45 seconds and was shaken on an orbital shaker for 15-30 minutes prior decanting the stain. To destain the gel, 100 ml destaining solution (8 % acetic acid) was added and heated on 950-1100 watts in a microwave for 45 seconds. For an optimal destaining result, the gel was left on an orbital shaker at RT overnight for visualization with UV light on the Gel Documentation™ system (Bio-Rad, Hercules, CA).

2.8.2 Indirect ELISA: confirmation of Env conformation integrity and functionality

An indirect ELISA was conducted to confirm the conformational integrity of the respective SEC purified Env conformations (gp140_{SOSIP}, gp140_{GCN4}, gp120_{FVC}) as indicated in Figure 2.1. Their functionality was assessed based on their ability to bind soluble CD4 as indicated in Figure 2.2. Two Nunc MaxiSorp™ high protein-binding capacity 96 well ELISA plates (ThermoFisher Scientific, Rockford, IL, USA) were coated with 2 µg/ml *Galanthus nivalis* lectin in 1× PBS (Sigma-Aldrich, Steinheim, Germany), 100 µl per well and incubated overnight at 4 °C to facilitate effective binding of the Env to the plate. The plates were washed three times with 0.05 % Tween-20 (T) (Sigma-Aldrich, Steinheim, Germany) in PBS. The plates were then blocked with 250 µl/well of 1 % BSA in 0.05 % PBS-T for an hour at RT to prevent non-specific binding of protein antigens and antibodies.

Once blocked, the plates were washed three times with 0.05 % PBS-T. Subsequently, the first plate was incubated at RT for an hour with three fold dilutions of each 2 µg/ml Env protein which were added as a 100 µl protein/well for confirmation of conformational integrity. In the second plate, three fold dilutions of each 2 µg/ml Env protein were incubated at RT for an hour with an equal volume

(100 µl) of non-diluted 2 µg/ml 2dCD4 WT to allow interaction and complex formation between CD4 and the Env proteins. This was necessary for confirmation of functionality of the respective Env proteins based on their ability to bind CD4.

Following incubation with the Envs on the first plate and Env-CD4 complex formation on the second plate, the plates were washed five times with 0.05 % PBS-T and different antibodies were added to either confirm correct structural integrity or functionality. The first plate coated with the Envs was incubated with 100 µl/well of 1 µg/ml gp140_{SOSIP} trimer specific primary antibody CAP256-VRC26.25 (Doria-Rose et al., 2015), gp120 CD4 binding site primary antibody IgG1b12 for gp120_{FVC} and MPER binding primary antibody 10E8 (Huang et al., 2012) for gp140_{GCN4} at RT for one hour. The second plate with Env-CD4 complexes was incubated with 100 µl/well of 1 µg/ml CD4 induced epitopes binding primary antibody 17b for an hour at RT.

The five times washes with 0.05 % PBS-T were repeated and the plates were incubated with 100 µl/well of a 1:1000 diluted Anti-human HRP-linked IgG (GE Healthcare, New York, USA) secondary antibody at RT for an hour. Lastly, the plates were washed five times with 0.05 % PBS-T and the colour was developed by using 100 µl/well 3,3', 5,5'-tetramethylbenzidine (TMB, Life Technologies, Johannesburg, South Africa) as a substrate and incubated at RT in the dark for 20 minutes without shaking.

TMB is a substrate for HRP conjugated on the secondary antibody; this reagent converts the colour of the reaction product (positive binding of primary antibody to the Env or Env-CD4 complexes) to blue in the presence of HRP. The reaction was stopped by adding 100 µl/well 2 M sulphuric acid (Sigma-Aldrich, Steinheim, Germany) in each plate and absorbance at 450 nm was recorded on the iMark Microplate reader (Bio-Rad, Hercules, CA) within 30 minutes of stopping the reaction. Addition of sulphuric acid changes the colour of the reaction product from blue to yellow which has an absorbance peak at 450 nm.

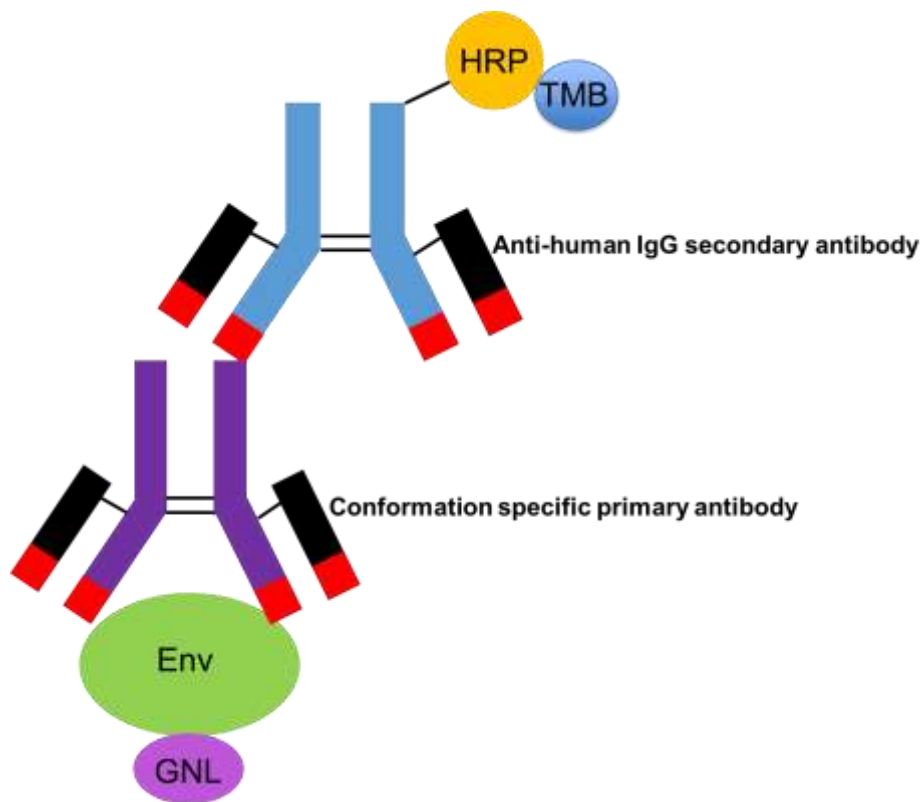


Figure 2.1: Schematic representation of an Indirect ELISA experimental set up for confirmation of Env structural/conformational integrity. A 96 well Nun-Maxisorp plate was coated with *Galanthus nivalis* (GNL) to enhance binding of different Env conformations (gp140_{SOSIP}, gp140_{GCN4}, gp120_{FVC}) to the plate. Subsequently, conformation specific antibodies; CAP256–VRC26.25, 10E8 and IgG1b12 were added to confirm conformational integrity of the respective Envs. HRP-linked anti-human IgG secondary antibody and its substrate TMB were then added to confirm binding. Colour change and increase in absorbance intensity of substrate served as an indication of correct structural integrity of the Env conformations. The diagram was adapted from (Gan and Patel, 2013).

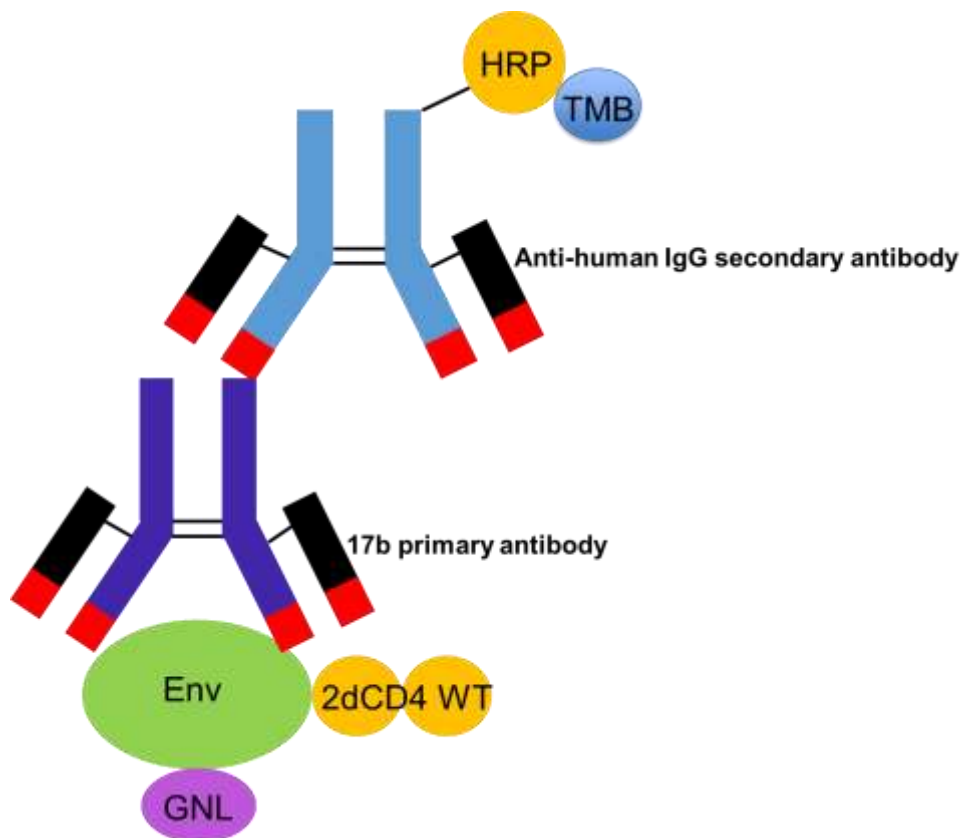


Figure 2.2: Schematic representation of an Indirect ELISA experimental set up for confirmation of Env functionality. GNL coating on a 96 well Nunc-Maxisorp plate was used to enhance binding of gp140_{SOSIP}, gp140_{GCN4} and gp120_{FVC} to the plate. Functionality of each Env was measured based on their ability to bind 2dCD4 WT which resulted with exposure of CD4 induced epitopes (CD4i). The latter were then detected by CD4i specific antibody 17b which was further validated by adding an HRP-linked anti-human IgG secondary and its TMB substrate. Colour change and increase in absorbance intensity of substrate served as an indication of functional Env conformations. The diagram was adapted from (Gan and Patel, 2013).

2.9 Flow cytometry detection of apoptosis by the Muse Cell analyser

Env-mediated bystander apoptosis of Jurkat T cells was measured through detection of different biomarkers of apoptosis. The latter included use of assay kits to detect early biomarkers of apoptosis such as exposure of a membrane phospholipid PS and mitopotential depolarization. Late biomarkers such as caspase 3/7 activation and DNA damage were also detected.

During early stages of apoptosis, PS is translocated from the inner to outer leaflet of the cell membrane (Rysavy et al., 2014). Moreover, there is an independent shift in the distribution of electrons across the mitochondrial membrane which results in a decrease of the negative charge (depolarization) inside the mitochondria (Gyulkhandanyan et al., 2015). This is an early biomarker of apoptosis indicative of apoptosis initiation through the intrinsic/mitochondrial pathway. To detect PS translocation, an Annexin V assay kit was used. Annexin V is a calcium dependent cellular protein with high binding affinity for phospholipids such as PS (Audo et al., 2017). To detect mitopotential depolarization a mitopotential dye assay kit was used. The assay includes a positively charged, lipophilic fluorescent dye with an ability to pass through intact cellular and mitochondrial membrane subsequently binding negative charges within the mitochondria.

Late stages of apoptosis are associated with caspase 3/7 activation and DNA damage. Caspase 3 cysteine-aspartic acid protease exists as an inactive proenzyme that undergoes proteolytic processing at conserved aspartic residues to produce an active caspase 3 dimer (Choudhary et al., 2015). The latter is involved in the sequential activation of caspase 6 and 7 leading to apoptosis via Fas ligand mediated pathway (extrinsic). To detect caspase 3/7 activation, a Caspase 3/7 kit (Merck KGaA, Darmstadt, Germany) was used. This contains a Caspase 3/7 reagent which is a non-toxic membrane permeable reagent with a DNA binding dye linked to a fluorescent DEVD peptide substrate (caspase substrate).

DNA damage entails formation of double stranded breaks (DSB) in the DNA i.e. simultaneous damage of two complementary strands of DNA double helix (Podhorecka et al., 2010). This was measured by detecting activation of two DNA repair proteins recruited to DSB; Ataxia telangiectasia mutated kinase (ATM) and Histone variant H2A.X. ATM is a serine threonine protein kinase whose role is to

activate (by phosphorylation on Serine 139) key proteins (Alvarez-Quilón et al., 2014) such as H2A.X (Ji et al., 2017, Rogakou et al., 1998) to initiate DNA repair or induce apoptosis if the DNA damage is beyond repair. Dual detection of phosphorylated ATM and H2A.X is indicative of the presence of DSB in the DNA. Activated ATM was detected using a phospho-specific ATM antibody conjugated with a fluorescent dye PE (phospho-specific ATM-PE, Merck KGaA, Darmstadt, Germany) while activated H2A.X was detected by a phospho-specific H2A.X antibody conjugated with a fluorescent dye PECy5 (phospho-specific histone H2AX-PECy5, Merck KGaA, Darmstadt, Germany) as per manufacturer's instructions.

2.9.1 Flow cytometer set up and maintenance

The Muse cell analyser (Merck KGaA, Darmstadt, Germany) was used for detection of apoptotic cells for all assays. Prior to and post each assay, a system clean procedure was conducted to ensure system runs smoothly and possible cell debris was removed from the tubing system as per manufacturer's instructions. Briefly, 1 ml of Guava instrument cleaning fluid i.e. ICF (Merck KGaA, Darmstadt, Germany) was loaded onto the system for thorough cleaning of capillary tubing and the tubing was rinsed with 1 ml DI water. Following the system clean, a system check procedure was conducted to evaluate and confirm performance by the Muse system i.e. confirm accuracy in counting and fluorescence detection. Briefly, a 1 in 20 dilution of the System check beads (Merck KGaA, Darmstadt, Germany) was prepared by adding 20 µl of System check beads into 380 µl of diluent. The beads lot number, expiration date and check codes were added onto the Muse system software as a reference point for accuracy evaluation for each system check. The prepared System check beads were loaded onto the system and analysed in three replicates. Acquired fluorescence and beads counts for all three replicates were averaged to determine whether they were within the expected range as prescribed by the manufacturer.

2.9.2 Set up of assays for apoptosis induction and detection

HIV-1 Env-mediated bystander apoptosis of Jurkat T cells via CD4 signalling was initiated by pre-seeding various concentrations of Jurkat T cells per assay overnight in a 96 well plate as described in sections 2.9.2.1 to 2.9.2.4 below. The same plate layout was used for all assays as illustrated in Figure 2.3. Concentrations of gp140_{SOSIP}, gp140_{GCN4} and gp120_{FVC} ranging from 50 nM, 250 nM and 500 nM (6 µg/ml, 30 µg/ml and 60 µg/ml) were added in replicates of two to induce apoptosis through interaction with the CD4 receptor on Jurkat T cells for varying incubation periods i.e. 24, 48 and 72 hours at 37 °C and 5 % CO₂. The replicates were necessary to ensure consistency in the results while different time points were necessary for detection of both early and late apoptotic cells. In addition, the varied concentrations were added to determine whether apoptosis induction occurred in a dose dependent manner.

Untreated or cells only control was included as a negative control i.e. baseline for comparison with Env treated samples. An additional negative control for Env functionality (ability to bind to CD4 receptor on Jurkat T cells)/ apoptosis induction through CD4 signaling was added. Here 500 nM of gp140_{SOSIP}, gp140_{GCN4} and gp120_{FVC} were denatured at 80 °C and added to Jurkat T cells. Heat denaturation alters the conformational integrity of the respective Env, therefore a non-functional CD4 binding site and subsequent inability to induce apoptosis was expected. Treatment with 4 µM (1.392 µg/ml) Camptothecin (Sigma-Aldrich; Steinheim, Germany) was included as a positive control for apoptosis induction. Camptothecin is a cytotoxic alkaloid which induces apoptosis through inhibition of DNA topoisomerase I during DNA synthesis which results in irreversible DNA damage and ultimately apoptosis (Liu et al., 2015).

Following each incubation period; the counting and fluorescence accuracy of the MUSE mini flow cytometer was evaluated as previously described in section 2.9.1. Thereafter, various amounts of Jurkat T cells were harvested as illustrated in Figure 2.3 for detection of PS translocation, mitopotential depolarization, caspase 3/7 activation and DNA damage using Annexin V, Mitopotential dye, Caspase 3/7 reagent and Multicolor DNA damage assays (Merck KGaA, Darmstadt, Germany) on the Muse mini flow cytometer as per manufacturer's instructions.

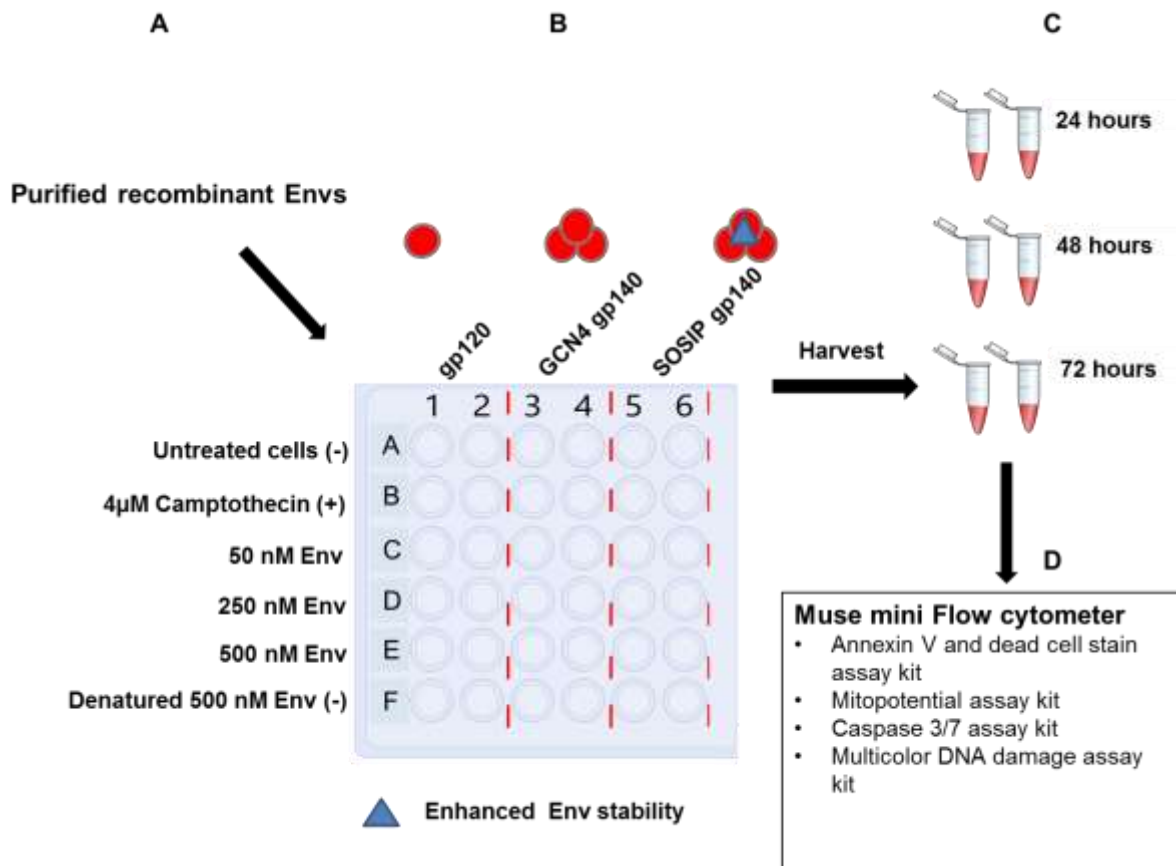


Figure 2.3: Schematic representation of apoptosis induction experiment set-up in Jurkat T cells and detection of apoptotic hall marks using flow cytometry. A and B. Jurkat T cells were co-incubated with various concentrations of purified and functional recombinant FVC Env (gp140_{SOSIP}, gp140_{GCN4} and gp120_{FVC}) including positive and negative controls in replicates of two for 24, 48 and 72 hours for apoptosis induction. **C.** Following each incubation period, the cells were harvested. **D.** Detection of apoptosis; PS translocation, mitopotential depolarization, caspase 3/7 activation and DNA damage using Muse assay kits and Muse mini flow cytometer.

2.9.2.1 Annexin V assay

Jurkat T cells were pre-seeded overnight at 2×10^6 cells/ml in a 96 well plate; 600 000 cells per well in 300 μ l of supplemented RPMI medium as previously described in section 2.4.1.1 at 37 °C and 5 % CO₂. Post-apoptosis induction as described in section 2.9.2, 100 μ l of Jurkat T cells were harvested and Annexin V (Merck KGaA, Darmstadt, Germany) was used to detect PS translocation.

PS translocation is not only limited to apoptosis, it is also observed in necrotic cells. However, during early stages of apoptosis the cell membrane remains intact while in necrotic cells membrane integrity is immediately lost, making the cell more permeable or leaky. Therefore to distinguish between live, necrotic, early and late apoptotic cells based on PS exposure, Annexin V binding was coupled with a dead cell stain 7-AAD (Merck KGaA, Darmstadt, Germany) as per manufacturer's instructions. 7-AAD is a fluorochrome with an ability to pass through cell membranes of dead cells and stain their DNA with preferential binding to Guanine-Cytosine (GC) rich regions (Adan et al., 2017).

Briefly, 100 μ l of the Jurkat T suspension cells isolated from the apoptosis assay were added into different tubes. This was followed by addition of 100 μ l of the Muse Annexin V dead cell stain and 7-AAD dead cell stain into each tube. The solution was then mixed thoroughly by pipetting up and down or vortexing at medium speed for 3 to 5 seconds. The samples were left to stain for 20 minutes at RT in the dark and analyzed by flow cytometry for Annexin V and 7-AAD fluorescence.

The data was shown as flow cytometry scatter dot plots with x and y axes representative of forward and side scatter showing size and complexity respectively were dots represent individual cells. Annexin V staining was illustrated on the x axis and viability based on 7-AAD staining on the y axis. Additionally, the plots consist of 4 quadrants which separate cell populations as percentages based on positive or negative staining of Annexin V and 7-AAD as illustrated in Figure 2.4 below. Quadrant 3 shows live Jurkat T cells that stain negative for both Annexin V and 7-AAD. An anticlockwise shift of this cell population into quadrant 4 is indicative of early apoptotic cells that stain positive for only Annexin V. Similarly, a shift from

quadrant 4 to 2 represents late apoptotic cells that stain positive for both Annexin and 7-AAD and possibly early necrotic cells in quadrant 1.

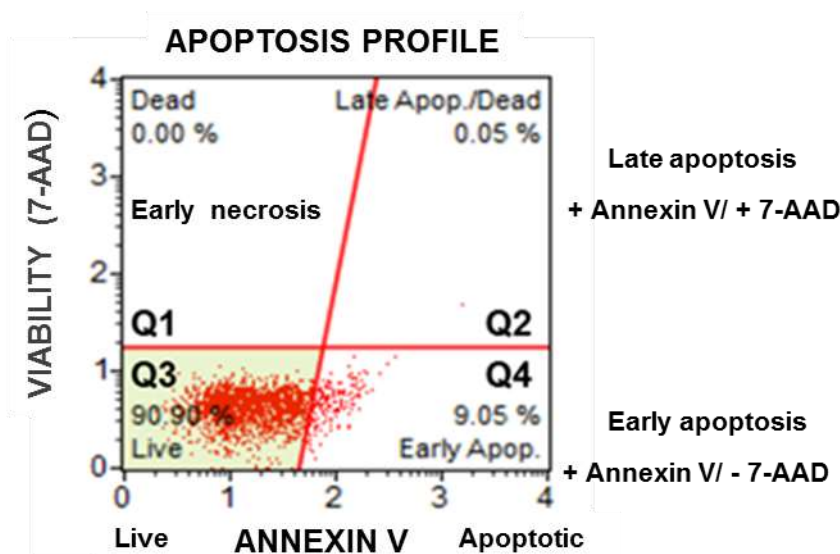


Figure 2.4: Representative scatter dot plot acquired from Muse mini flow cytometer for Annexin V assay analysis. Different cell populations are shown in quadrants (Q) 1 to 4 as percentage number of cells staining either positive or negative for Annexin V (X-axis) and 7-AAD viability stain (Y-axis). Q1 = Early necrotic cells with negative staining for both Annexin V and 7-AAD, Q2 = late apoptotic cells with positive staining for both stains, Q3 = Live cells with negative staining for both stains and Q4 = early apoptotic cells with positive staining for Annexin V only.

2.9.2.2 Mitopotential assay

Jurkat T cells were pre-seeded at 2×10^6 cells/ml in a 96 well plate in 150 μ l RPMI medium per well (300 000 cells/well) overnight. Apoptosis induction was conducted as described in section 2.9.2. Post -apoptosis induction at each incubation period, 50 μ l of cells were harvested for detection of mitopotential depolarization using a Mitopotential dye (Merck KGaA, Darmstadt, Germany). Since live cells also have the ability to uptake positively charged ions, they can also be subjected to a decrease in negative charge i.e., depolarization. To distinguish between early apoptotic and live

cells which have depolarized membrane potential, 7-AAD stain (Merck KGaA, Darmstadt, Germany) was coupled with the mitopotential dye.

Briefly, a mitopotential reagent was thawed from -20 °C in the dark and a working solution was prepared by diluting the Muse™ mitopotential dye 1000 times in 1× assay buffer (1:1000 dilution). The working solution was left to warm up at RT, the harvested 50 µl of Jurkat T cells treated with Env and controls were centrifuged at 300 x g for 5 minutes using the Eppendorf 5415R benchtop microcentrifuge (Merck, Darmstadt, Germany). The cells in each tube were then re-suspended to concentrations of 1×10^5 to 5×10^5 cells/ml in 100 µl of 1× assay buffer. Following Jurkat T cells preparation, 95 µl of mitopotential working solution was added to each tube and mixed thoroughly by pipetting up and down or vortexing for 3 to 5 seconds. The stained Jurkat T cells were then incubated at 37 °C and 5 % CO₂ for 20 minutes. Following the incubation period, 5 µl of Muse mitopotential 7-AAD reagent was added into each tube and mixed thoroughly by pipetting up and down or vortexing for three to 5 seconds. The Jurkat T cells were then incubated for 5 minutes at RT to allow intracellular staining of the DNA by 7-AAD. Thereafter, each tube/treatment was analysed for mitopotential dye and 7-AAD fluorescence using flow cytometry.

Similarly to Annexin V assay analysis, the data was shown as 4 quadrants scatter dot plots with mitopotential dye staining on x axis and 7-AAD staining (viability) on the y axis as illustrated on Figure 2.5. Quadrant 4 shows live non-depolarized cells which stain negative for both mitopotential dye and 7-AAD. A clockwise shift of this cell population into quadrant 3 shows depolarized live cells which stain positive for only mitopotential dye. An additional shift from quadrant 3 to 1 shows depolarized apoptotic cells which stain positive for both mitopotential dye and 7-AAD. Quadrant 2 shows dead non depolarized cell population.

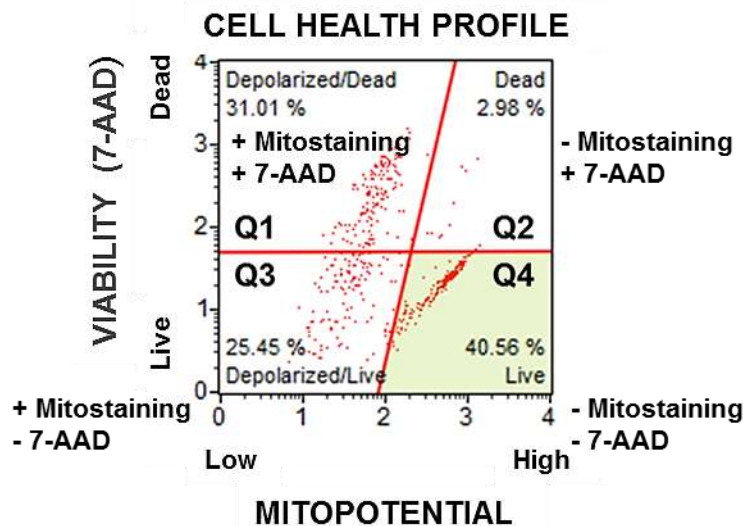


Figure 2.5: Representative scatter dot plot acquired from Muse mini flow cytometer for Mitopotential depolarization assay analysis. Different cell populations are shown in quadrants (Q) 1 to 4 as percentage number of cells with differential Mitopotential dye (X-axis) / 7-AAD viability staining (Y-axis). Q1 = Dead depolarized cells with positive Mitostaining and 7-AAD staining. Q2 = Dead non-depolarized cells with positive staining for only 7-AAD. Q3 = Depolarized live cells with positive staining for the Mitopotential dye only. Q4 = Live non depolarized cells with negative staining for both dyes.

2.9.2.3 Caspase 3/7 assay

Jurkat T cells were pre-seeded at 2×10^6 cells/ml of RPMI in a 96 well plate to a final volume of 150 μ l per well (300 000 cells/ml). Apoptosis was induced as previously described in section 2.9.2. Similar to the protocol established for the mitopotential assay, 50 μ l of the Jurkat T cells were harvested at each time point for detection of caspase 3/7 activation. Caspase 3/7 activation was detected using a kit with DNA binding dye conjugated to a fluorescent DEVD caspase 3/7 substrate. When bound to DEVD the dye is unable to bind DNA. Cleavage by active caspase 3/7 in the cell results in release of the dye, translocation to the nucleus, binding of the dye to DNA and high fluorescence. This is an indication of caspase 3/7 activation in the cells. 7-AAD intracellular dead cell marker (Merck KGaA, Darmstadt, Germany) was coupled with the caspase 3/7 reagent to distinguish between live, early and late apoptotic cells based on membrane structural integrity as per manufacturer's instructions.

Briefly, the Muse™ caspase 3/7 reagent stored at 2-8 °C protected from light was left to warm up to RT and a working solution was prepared by diluting the stock solution 1:8 in 1× PBS (18.9 µl reagent into 131.1 µl 1× PBS). The Muse™ caspase 7-AAD working solution was then prepared by adding 60 µl of Muse™ caspase 7-AAD stock solution to 4440 µl of 1× assay buffer BA (Merck KGaA, Darmstadt, Germany). Both working solutions were prepared on the day of the experiment and stored in the dark until use.

The harvested Jurkat T cells for each treatment were added into different tubes and 50 µl of these cells were spun down at 300 x g for 5 minutes using the Eppendorf 5415R benchtop microcentrifuge to remove the apoptosis-inducing agents. Thereafter, 5 µl of Muse™ caspase 3/7 reagent working solution was added to the pelleted cells and the cells were re-suspended by pipetting up and down or vortexing at a medium speed for 3 to 5 seconds. Following thorough mixing, the tubes were capped loosely and incubated for 30 minutes at 37 °C and 5 % CO₂. After the incubation period, 150 µl of Muse™ caspase 7-AAD working solution was added to the cells in each tube and mixed thoroughly by either pipetting up and down or vortexing at a medium speed for 3 to 5 seconds. The tubes were then incubated in the dark at RT for 5 minutes. Following the incubation, each Jurkat T cell treatment was analysed for caspase 3/7 activation (DEVD dye fluorescence) by flow cytometry.

Similarly to Annexin V assay analysis, the data was shown as 4 quadrants scatter dot plots with caspase 3/7 staining on x axis and viability based on 7-AAD on the y axis as illustrated on Figure 2.6. Quadrant 3 shows live Jurkat T cells which stain negative for caspase 3/7 reagent and 7-AAD. An anticlockwise shift of this population to quadrant 4 and 2 shows early and late apoptotic cells. Early apoptotic cells stain positive for caspase 3/7 only (quadrant 4) while late apoptotic cells stain positive for both reagents (quadrant 2). Quadrant 1 shows dead cells which undergo other forms of cell death without caspase 3/7 activation.

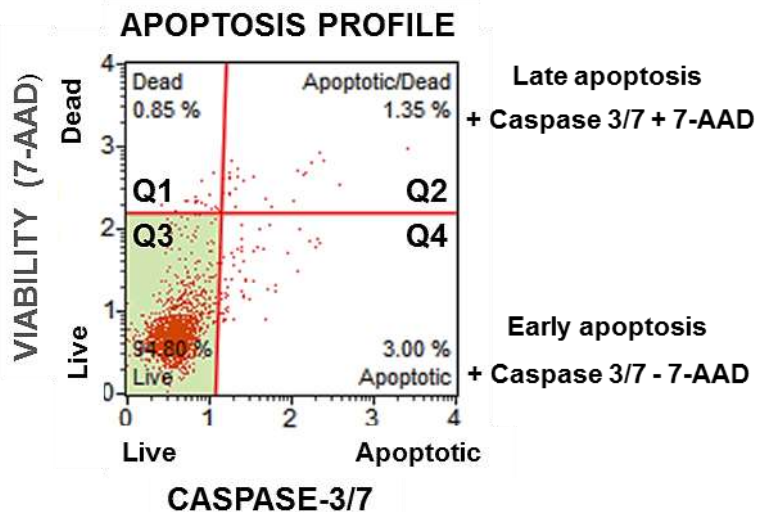


Figure 2.6: Representative scatter dot plot acquired from Muse mini flow cytometer for caspase 3/7 activation analysis. Different cell populations are shown in quadrants (Q) 1 to 4 as percentage number of cells based on Caspase 3/7 (X-axis) and 7-AAD staining (Y-axis). Q1 = dead cells with negative Caspase 3/7 staining but positive 7-AAD staining. Q2 = Late apoptotic cells which stain positive for both Caspase 3/7 and 7-AAD dye. Q3 = Live cells with negative staining for both dyes. Q4 = Early apoptotic cells with positive staining for only Caspase 3/7 dye.

2.9.2.4 Multicolor DNA damage assay

Jurkat T cells (2×10^6 cells/ml) were seeded in RPMI in a 96 well plate to a final volume of 150 μ l per well i.e. 300 000 cells per well. Following apoptosis induction as described in section 2.9.2, 50 μ l of the Jurkat T cells were harvested at each time point for detection of DNA damage measured as DSB. Dual detection of phosphorylated ATM and H2A.X is indicative of the presence of DSB in the DNA. Phosphorylated (activated) ATM was detected using a phospho-specific ATM antibody conjugated with a fluorescent dye PE (phospho-specific ATM-PE, Merck KGaA, Darmstadt, Germany) while phosphorylated (activated) H2A.X was detected by a phospho-specific H2A.X antibody conjugated with a fluorescent dye PECy5 (phospho-specific histone H2AX-PECy5, Merck KGaA, Darmstadt, Germany) as per manufacturer's instructions.

Briefly, 5× assay buffer (Merck KGaA, Darmstadt, Germany) stored at 2-8 °C was left to warm up to RT and diluted to a 1× concentration with DI water. The antibody working cocktail solution was prepared by adding phospho-specific ATM-PE and phospho-specific histone H2AX-PECy5 antibodies in a 1:1 ratio i.e. 150 µl of each antibody for 30 reactions. Following reagent preparation, the harvested 50 µl of the controls and Env treated Jurkat T cells at each time point were spun down at 300 x g for 5 minutes using the Eppendorf 5415R benchtop microcentrifuge to remove apoptosis-inducing agents in treated cells. The pelleted cells were then re-suspended in 50 µl of 1× assay buffer.

The cell suspension in each tube was fixed in a 1:1 ratio of fixation buffer (Merck KGaA, Darmstadt, Germany) to cell suspension i.e. for every 50 µl of cells 50 µl of fixation buffer was added. Thereafter, the cells were incubated on ice for 10 minutes. Since some phosphorylation or activation states are transient, the fixation of Jurkat T cells was necessary to ensure that the phosphorylation/activation state of ATM and H2A.X is captured at the right time by the phospho activation specific antibodies.

Following fixation, Jurkat T cells in each tube were spun down at 300 x g for five minutes using the Eppendorf 5415R benchtop microcentrifuge and the supernatant was discarded. The cells in each tube were then treated with 100 µl of ice cold 1× Permeabilization buffer for 10 minutes on ice to make the cells permeable to detection antibodies (phospho-specific H2A.X -PECy5 and phospho-specific ATM-PE). Thereafter, the cells in each tube were spun down at 300 x g for 5 minutes using previously mentioned microcentrifuge to remove remaining cell debris in the supernatant. The pellets were then re-suspended in 90 µl 1× assay buffer and 10 µl of previously prepared antibody working cocktail was added into each cell suspension. The latter were incubated in the dark at RT for 30 minutes to allow antibody interaction with phosphorylated ATM and H2A.X. Following the incubation period, 100 µl of 1× assay buffer was added to each tube and centrifuged at 300 x g for 5 minutes.

The supernatants were discarded and the cells in the pellets were re-suspended in 200 µl of 1× assay buffer. Subsequently, phosphorylated/activated ATM and H2A.X were detected from the cells by flow cytometry based on fluorescence intensity of PE

conjugated phospho-specific ATM and PEcy5 conjugated phospho-specific Histone H2A.X antibodies.

The data was represented as 4 quadrant scatter dot plots showing population of cells with phosphorylated H2A.X on x axis and those with phosphorylated ATM on the y axis. Jurkat T cells that stain negative for both phospho-specific ATM and PEcy5 conjugated phospho-specific H2A.X antibodies are live cells with no DNA damage as shown in quadrant 3. A clockwise shift of this cell population to quadrant 1 and an anticlockwise shift from quadrant 3 to 4 respectively show positive staining for only ATM activation and activated H2A.X. A shift from quadrant three to two show positive staining for both antibodies which is indicative of apoptotic cells with DSB i.e. DNA damage.

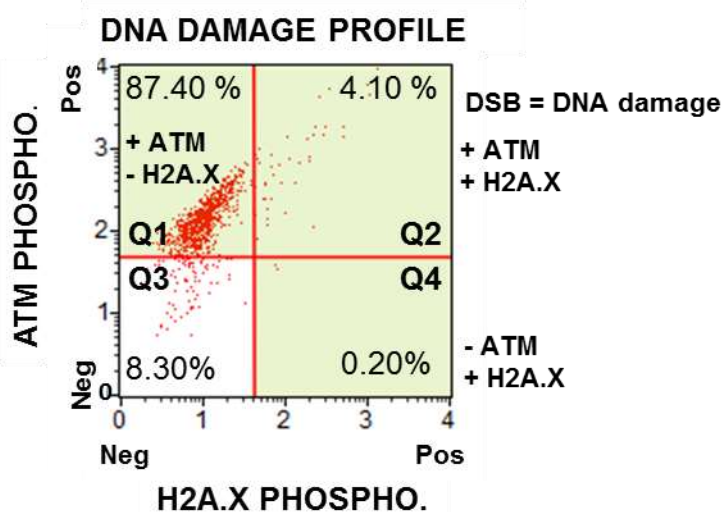


Figure 2.7: Representative scatter dot plot acquired from Muse mini flow cytometer for DNA damage analysis. Different cell populations are shown as quadrants (Q) 1 to 4 as percentage number of cells with differential staining for phosphorylated H2A.X (X-axis) and phosphorylated ATM (Y-axis). Q1 = Cells with a single stranded break showing positive staining for ATM phosphorylation. Q2 = Cells with double stranded breaks (DSB) showing positive staining for both ATM and H2A.X phosphorylation. Q3 = Cells with intact DNA (no damage) staining negative for both DNA repair proteins. Q4 = Cells with a single stranded DNA break

2.9.2.5 Data analysis

Apoptosis induction assays were conducted in replicates of two for each Env conformation per concentration tested. Untreated cells were then used as a baseline for apoptosis induction for each replicate and a percentage change in apoptosis relative to untreated cells was calculated. The mean percentage change in apoptosis relative to untreated cells control was then determined from these replicates and represented in bar graphs. In addition, the variation of each replicate from the mean change in apoptosis was represented as a standard deviation which was shown as error bars on the graphs.

Furthermore, data obtained from all flow cytometry apoptosis assays was analysed by an unpaired student T test using GraphPad prism software. This test compares the mean of two separate sets of independent samples to determine statistical significance or difference. In simple terms, the unpaired T test simply means that the both samples consist of distinct test subjects. Although the current study used the same cell line to test apoptosis in untreated and Env treated cells, apoptosis was measured in untreated Jurkat T cells and then measured in Env treated cells. These two samples consisted of distinct test subjects because they differed in experimental conditions (one was treated while the other was not), hence an unpaired T test was deemed suitable to determine statistical significance between the two. Since untreated cells and Env (gp140_{SOSIP}, gp140_{GCN4} and gp120_{FVC}) treated cells were prepared separately and collected independently, this test assessed whether there was a statistical significance in levels of apoptosis between untreated and Env treated Jurkat T cells, respectively. The comparison was conducted between untreated cells and varied concentrations (50-500 nM) of each Env conformation. Moreover, Camptothecin and heat denatured 500 nM version of each Env conformation were also compared to the untreated cells as positive and negative controls, respectively. The statistical significance in apoptosis induction relative to untreated cells was measured as a probability value (p-value). A p-value of less than or equivalent to 0.05 ($p \leq 0.05$) was considered statistically significant i.e. a significant increase in apoptosis post exposure to Env or positive control.

3. Results

3.1 Expression and purification of recombinant gp140_{SOSIP}, gp120_{FVC}, gp140_{GCN4} and 2dCD4 WT

3.1.1 Large scale propagation of recombinant gp140_{SOSIP} VRC 3831 and Furin pCDNA 3.3 plasmids

In preparation for the large scale propagation of gp140_{SOSIP} VRC 3831 and Furin pCDNA 3.3, the recombinant plasmids were successfully transformed into chemical competent *E. coli* DH5 α cells (Figure 3.1).

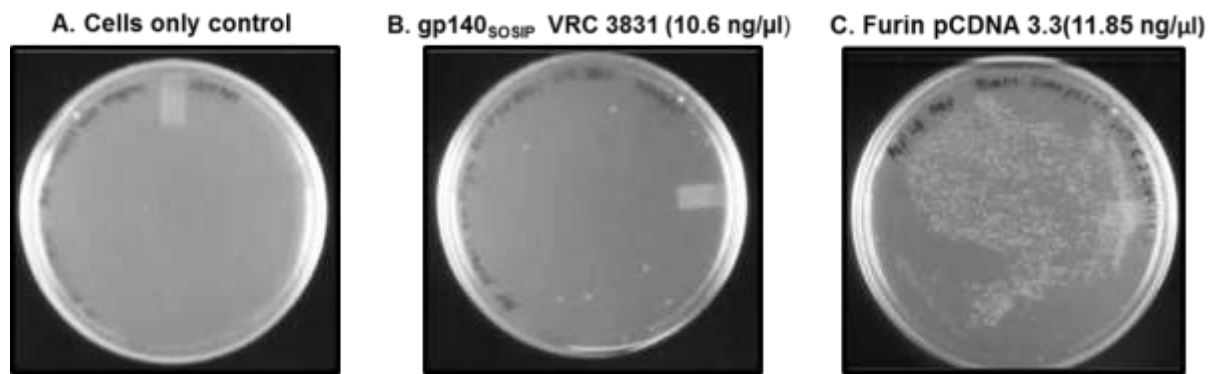


Figure 3.1: Transformation of chemically competent *E.coli* DH5 α cells with gp140_{SOSIP} VRC 3831 and Furin pCDNA 3.3. Chemically competent *E.coli* DH5 α cells were transformed with varying concentrations of the mentioned plasmids. Ampicillin and Kanamycin were respectively used for an overnight selection of positive transformants at 37 °C which were counted as colonies. **A.** Cells only negative control for detecting contamination. Transformation with **B.** gp140_{SOSIP} VRC 3831 and **C.** Furin pCDNA 3.3.

3.1.2 Purification of propagated gp140_{SOSIP} VRC 3831 and Furin pCDNA 3.3 plasmids

Single colonies from *E. coli* DH5 α cells transformed with recombinant gp140_{SOSIP} VRC 3831 and Furin pCDNA 3.3 plasmids were grown overnight and used for extraction/purification of the respective plasmids. The isolated plasmid DNA was quantified (Appendix B, Figure 3B1). Aliquots were collected at several steps of the procedure and analysed by agarose gel electrophoresis to determine the purity of the DNA and any potential decrease in yield during the purification (Figure 3.2).

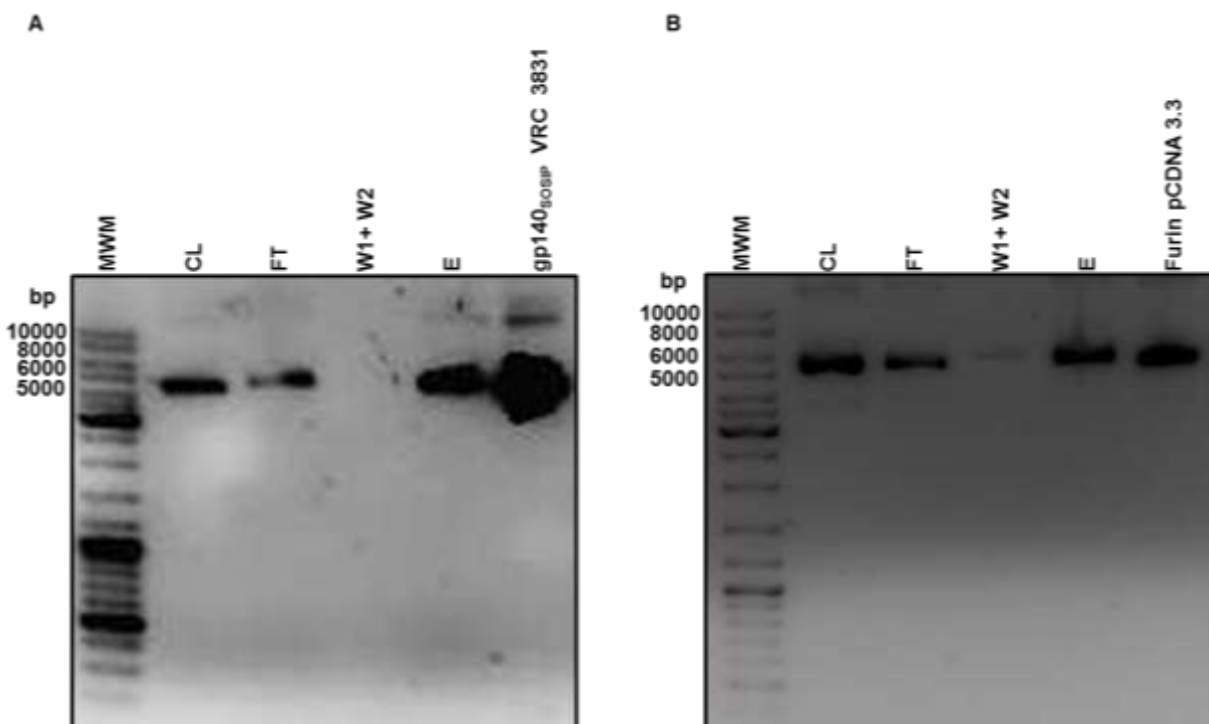


Figure 3.2: Agarose gel analysis of Qiagen maxi kit DNA purification procedure used for extraction of gp140_{SOSIP} VRC 3831 and Furin pCDNA 3.3 recombinant plasmids. Aliquots of several steps of the purification procedure were collected for **A.** gp140_{SOSIP} VRC 3831 and **B.** Furin pCDNA 3.3. Each aliquot was loaded on a 0.8 % agarose gel which was electrophoresed at 100 V and visualized with UV light for analysis. MWM-molecular weight marker O'GeneRuler™ Mix (ThermoFisher Scientific, Rockford, IL, USA), CL-cleared lysate, FT-flow through from column, W1+W2-combined wash fractions, E-eluted Furin pCDNA 3.3 and gp140_{SOSIP} VRC 3831 plasmids which were later precipitated out of solution with isopropanol.

The aliquots were isolated from cleared lysate containing respective supercoiled plasmid DNA and degraded RNA, flow through solution from the extraction column, wash fractions, eluted DNA and final isopropanol precipitated DNA. Purification analysis of both gp140_{SOSIP} VRC 3831 and Furin pCDNA 3.3 demonstrated well defined DNA bands on the agarose gel for the cleared lysate, flow through from the column, eluted DNA and precipitated DNA (Figure 3.2A and B). In addition, the band intensity of the flow through sample was lower compared to the cleared lysate and no bands were observed in the wash fractions as expected (Figure 3.2A and B).

Presence of a single DNA band on the gel from the cleared lysate was validation that the growth and lysis conditions were optimal for the transformed *E.coli* DH5 α competent cells. Gel analysis of the flow through sample determines DNA binding efficiency to the Qiagen resin. Therefore, the reduction of band intensity compared to the cleared lysate sample is indicative of efficient binding of DNA to the resin while the observed band still suggested that not all the DNA was bound to the purification resin. Absence of a DNA band in the wash fractions was an indication that no DNA was lost during the column washes. A well-defined band in the eluted DNA sample confirmed that the DNA was efficiently removed from the resin and eluted from the column while an increase in band intensity of the precipitated DNA compared to the eluate, suggested that the isolated plasmid DNA was highly concentrated.

The purified of gp140_{SOSIP} VRC 3831 and Furin pCDNA 3.3 plasmids were then used for expression of recombinant gp140_{SOSIP} Env proteins in transient transfections of HEK 293T cells.

3.1.3 Optimization of transient transfections of HEK 293T cells for gp140_{SOSIP} expression, and expression of gp120_{FVC}, gp140_{GCN4} from stably transfected HEK 293F cell lines

Recombinant gp140_{SOSIP} VRC 3831 and Furin pCDNA 3.3 plasmids were successfully co-transfected for transient expression of trimeric gp140_{SOSIP} Env in HEK 293T cells using PEI in a 12 well plate (Figure 3.3). Co-transfection with Furin plasmid DNA was necessary to increase the amount of Furin protease being expressed by the cells to enhance cleavage of the expressed gp140_{SOSIP} into gp120-

gp41 heterotrimers required for a fully functional gp140_{SOSIP} Env. This required optimization of the total amount of plasmid DNA and amount of the transfection reagent relative to the amount of DNA added into the transfection mix. The protein was harvested from the supernatant and expression was confirmed by SDS-PAGE and western blot analysis under reducing conditions. The gp120_{BaL} pCDNA 3.3 and GFP pCI-neo were transfected with Polyfect transfection reagent as positive transfection controls and Polyfect as a positive transfection reagent control. The total DNA amounts ranged from 1 µg to 4 µg with 1:3 and 1:6 respective DNA: PEI transfection reagent ratio.

The western blots demonstrated successful expression of gp140_{SOSIP} at all DNA amounts with the highest expression at 2 µg and 4 µg total DNA (Figure 3.3A). The latter showed equal amounts of expression. Two protein bands of varying sizes; the 120 kDa and 140 kDa bands were observed under reducing conditions. The gp120-gp41 heterotrimer is linked by disulfide bonds, thus under reducing conditions 120 kDa bands and 41 kDa bands were expected. However the observed 120 kDa and 140 kDa protein bands suggested partial cleavage of the gp140_{SOSIP} by Furin protease resulting in an uncleaved gp140 trimer and gp120 monomer. Therefore, the ratio of gp140_{SOSIP} VRC 3831 to Furin pCDNA 3.3 plasmid constructs was optimized to enhance cleavage of expressed gp140_{SOSIP} into a gp120-gp41 heterotrimer (Figure 3.3B). This resulted in the effective expression of cleaved gp140_{SOSIP} when HEK 293T cells were transfected with 2 µg and 4 µg total plasmid DNA amount (gp140_{SOSIP} VRC 3831 and Furin pCDNA 3.3 plasmids), 2:1 gp140_{SOSIP} VRC 3831 to Furin pCDNA 3.3 ratio and 1:3 plasmid DNA:PEI ratio (Figure 3.3A and B). These conditions were upscaled for large scale expression of gp140_{SOSIP} and since there was no distinction in expression between 2 µg and 4 µg total DNA amounts, 2 µg DNA was upscaled.

Recombinant gp120_{FVC} and gp140_{GCN4} were harvested from the supernatant of stably transfected HEK 293F cell lines and western blot analysis confirmed the successful expression of these recombinant Envs (Figure 3.4C and D).

Collectively, the above results confirmed optimal expression of the recombinant Envs which were further purified to homogeneity.

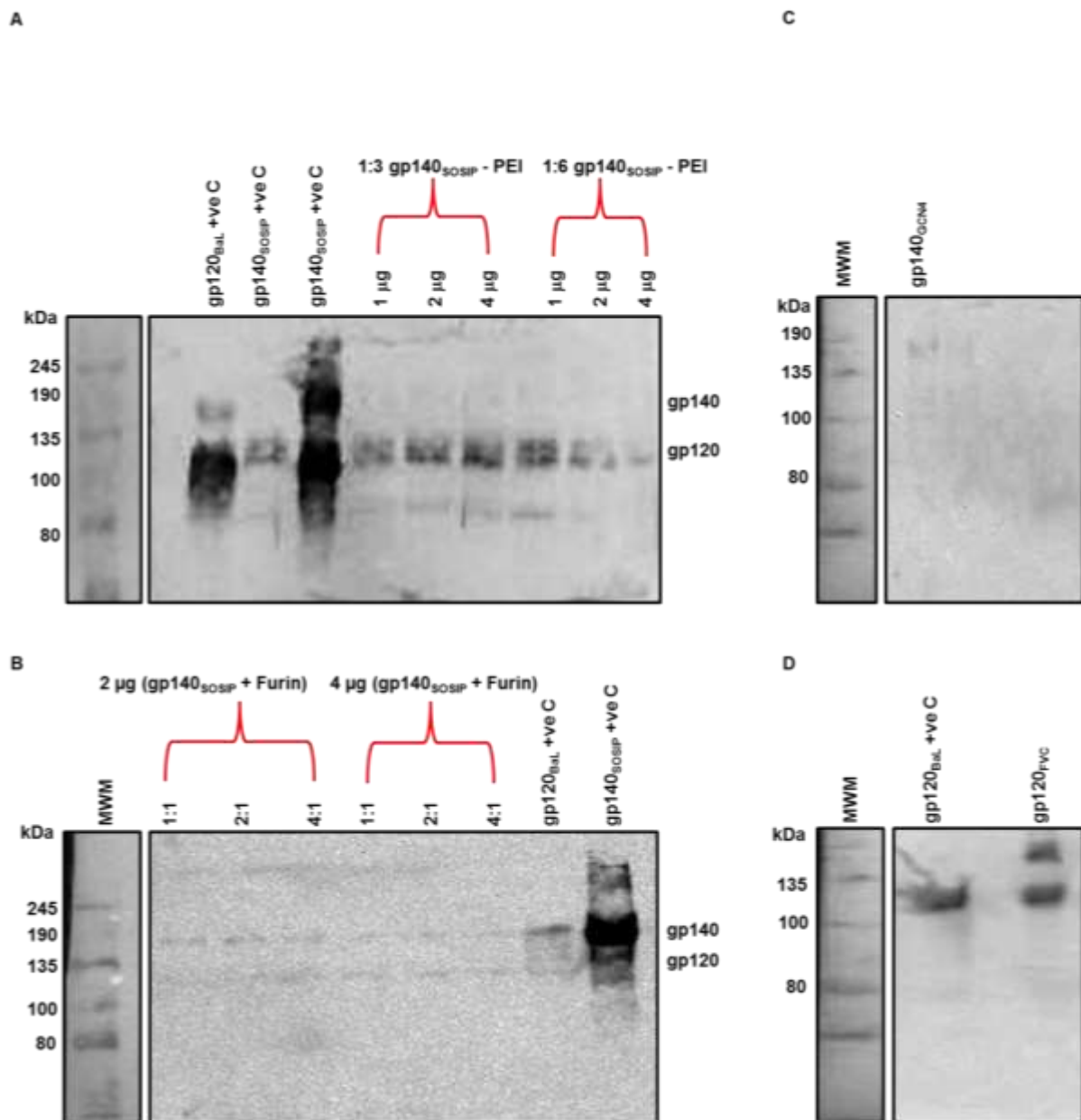


Figure 3.3: Western blot validation of recombinant Env (gp140_{SOSIP}, gp140_{GCN4} and gp120_{FVC}) expression. **A.** Total amount of gp140_{SOSIP} VRC 3831 plasmid DNA, amount of PEI relative to DNA (DNA: PEI ratio) and **B.** ratio of gp140_{SOSIP} VRC 3831: Furin pCDNA 3.3 constructs were optimized for transient expression of gp140_{SOSIP} in HEK 293T cells. **C.** gp140_{GCN4} and **D.** gp120_{FVC} were harvested continuously from stable HEK 293F cell lines. The gp120_{BaL} and previously expressed gp140_{SOSIP} were included as positive controls for the western blots. A rabbit serum and anti-rabbit IgG were respectively used as a primary and secondary antibody for detection of all Env. MWM- molecular weight marker of broad range i.e.11-245 kDa (NEB, Ipswich, England).

3.1.4 Purification of expressed gp140_{SOSIP}, gp140_{GCN4} and gp120_{FVC} by lectin affinity and size exclusion chromatography

Following optimal expression of the respective FVC Env conformations (gp140_{SOSIP}, gp140_{GCN4} and gp120_{FVC}), the harvested Env proteins were purified by lectin affinity chromatography. Expression of each Env conformation and purification procedure were confirmed and analysed by SDS-PAGE and western blot. To analyse the purification procedure with the latter techniques, samples of each purification step were collected.

Western blot analysis of gp140_{SOSIP} lectin affinity chromatography purification showed no protein bands on the column flow through (FT) and the washes (W) with 0.5 M, 1 M NaCl and PBS (Figure 3.4A). The SDS-PAGE analysis for gp140_{GCN4} and gp120_{FVC} showed the same observation (Figure 3.4B and C). This was an indication that no Env conformation was lost during the purification process. All the recombinant Env conformations were detected at the expected band sizes, with an approximately 140 kDa band for gp140_{GCN4} and approximately 120 kDa for gp140_{SOSIP} and gp120_{FVC} under reducing conditions (Figure 3.4A-C). The observed 120 kDa band instead of 140 kDa band for gp140_{SOSIP} under reducing conditions is indicative of efficient cleavage by the Furin protease. Additionally, detection of the Env conformations at the expected sizes was a confirmation that all the Envs were not degraded, they were still intact.

Since lectin affinity chromatography is not conformationally selective i.e. does not differentiate between Env trimer, monomer or dimer, each lectin purified Env conformation was brought to homogeneity using size exclusion chromatography (Figure 3.5). The latter separated gp140_{SOSIP} and gp140_{GCN4} trimers from the contaminating monomers and dimers using a HiPrep 16/60 Sephacryl S-300 HR gel filtration column. Lectin purified gp120_{FVC} monomer was also separated from contaminating dimers. All the desired Env conformations were isolated from the contaminants through fractionation.

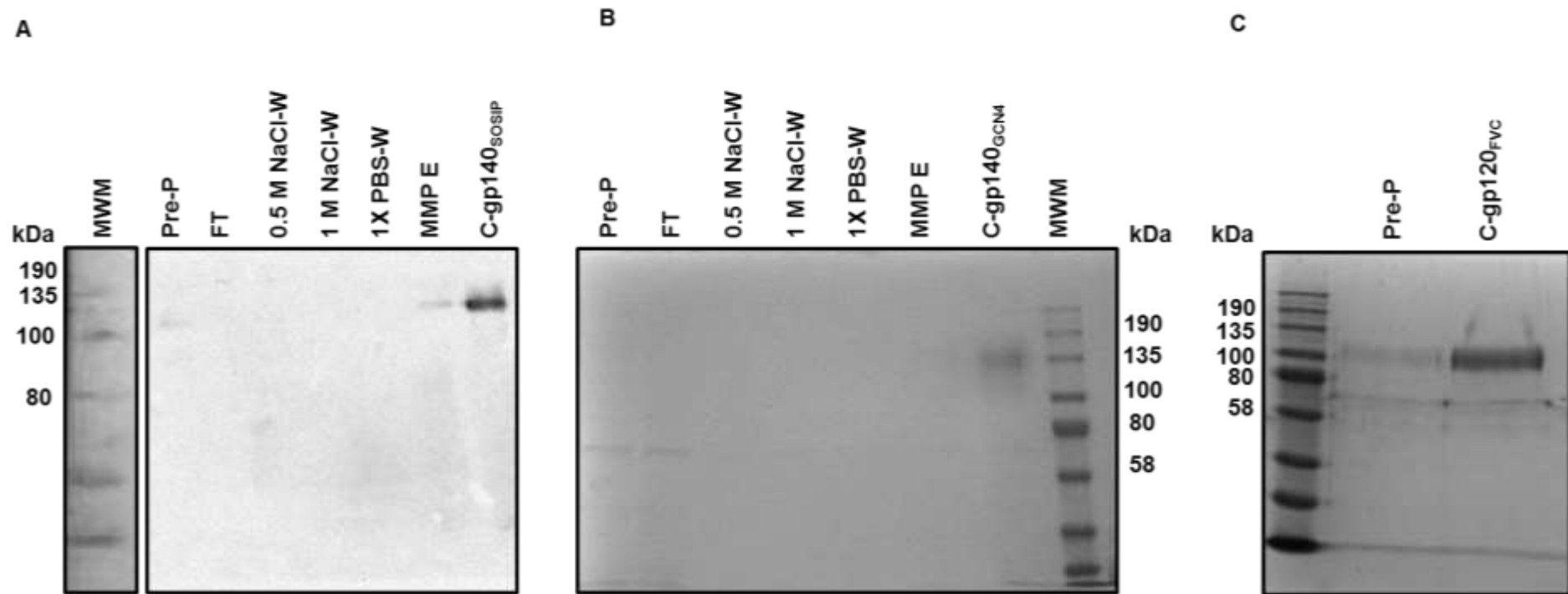


Figure 3.4: Western blot and SDS-PAGE analysis of lectin affinity chromatography purification of FVC Env conformations (gp140_{SOSIP}, gp140_{GC4} and gp120_{FVC}). Recombinant gp140_{SOSIP} was transiently expressed from HEK 293T cells while gp140_{GC4} and gp120_{FVC} were expressed from stably transfected HEK 293F cell lines. The Envs were harvested, filter sterilized with a 0.45 micron filter, clarified by centrifugation and purified using a lectin column. **A.** Samples of each purification step were isolated and analysed by western blot for gp140_{SOSIP}. **B.** SDS-PAGE for gp140_{GC4} and **C.** gp120_{FVC}. MWM- molecular weight marker of broad range i.e.11-245 kDa (NEB, Ipswich, England), Pre-P- pre purification supernatant of each Env conformation, FT- flow through, W-wash, MMP E- elution with Methyl α -d-mannopyranoside and C- concentrated Env post elution.

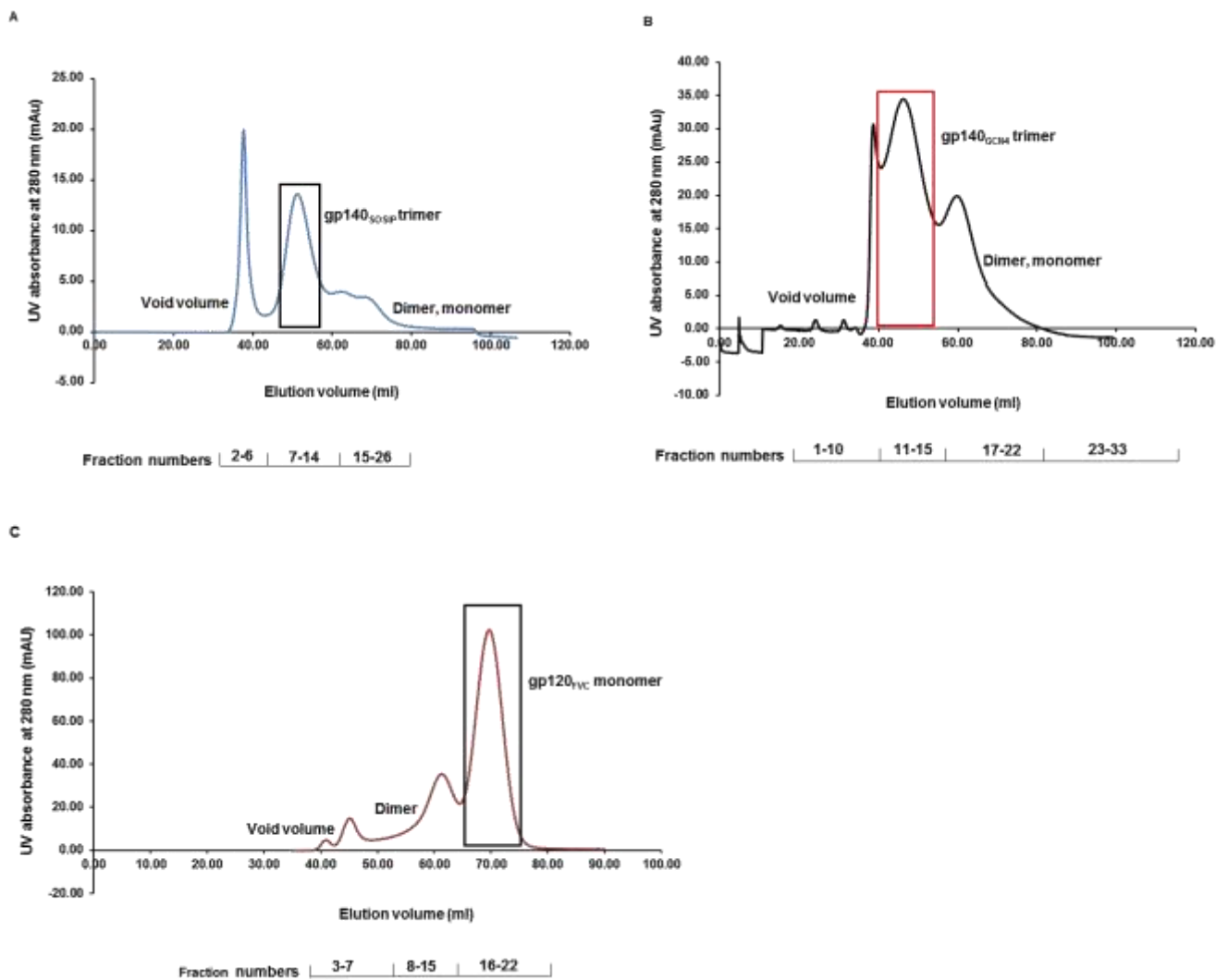


Figure 3.5: SEC profiles of Envs post purification by lectin affinity chromatography. The lectin purified Envs were each purified by SEC to isolate monomeric and trimeric conformations using a HiPrep 16/60 Sephacryl S-300 HR gel filtration column. Fractions from which the desired conformation for each Env was collected are highlighted as a box area **A**. SEC profile for gp140_{SOSIP}, **B**. gp140_{GCN4} and **C**. gp120_{FVC}.

The SEC elution profiles of the fractionated Env conformations display the absorbance units (at 280 nm) at different elution volumes (Figure 3.5). The absorbance units were indicative of the amount of each purified Env conformation. During SEC purification, each Env was separated based on molecular weight and hydrodynamic radius e i.e. size and shape, with smaller Env conformations (monomer) being eluted last at larger volumes than the larger Env conformations (dimers and trimers). The SEC elution profile for gp140_{SOSIP} and gp140_{GCN4} respectively demonstrated a high absorbance intensity trimer peak than a monomer peak which served as a validation that the trimeric populations were dominant, as expected (Figure 3.5A and B, boxed areas). In contrast, SEC purification of gp120_{FVC} displayed a high absorbance intensity monomer peak than the contaminating dimers (Figure 3.5C, boxed area). This was also an indication that the correct monomeric gp120 conformation was successfully isolated from contaminating dimeric conformations.

To confirm correct isolation of monomer, dimer and trimer conformations of the Envs post SEC, fractions collected during the SEC purification were analysed by Blue native PAGE (Figure 3.6). This was necessary for assessing the purity and homogeneity of the SEC purified Envs based on their native molecular weights. The fractions collected under the same SEC profile peak were pooled; concentrated and 1 µg of the pooled fractions was loaded on a precast Blue native gel.

The Blue native PAGE analysis confirmed enrichment of the desired trimeric gp140_{SOSIP} and gp140_{GCN4}, and monomeric gp120_{FVC} Env conformations (Figure 3.6). The trimeric gp140_{SOSIP} and gp140_{GCN4} protein bands respectively migrated at approximately 600 kDa and 720 kDa (Figure 3.6A and B) while the monomeric gp120_{FVC} migrated at approximately 200 kDa (Figure 3.6C). Moreover, the trimeric conformations of gp140_{SOSIP} and gp140_{GCN4} were identified at higher band intensities than the contaminating gp120 monomer and dimer (Figure 3.6A and B). Similarly, the gp120_{FVC} Env consisted of monomeric and dimeric conformations, with the monomer showing high band intensity (Figure 3.6C). Collectively, these Blue native PAGE results validated that the desired trimeric and monomeric Env conformations predominate and each conformation was close to homogeneity.

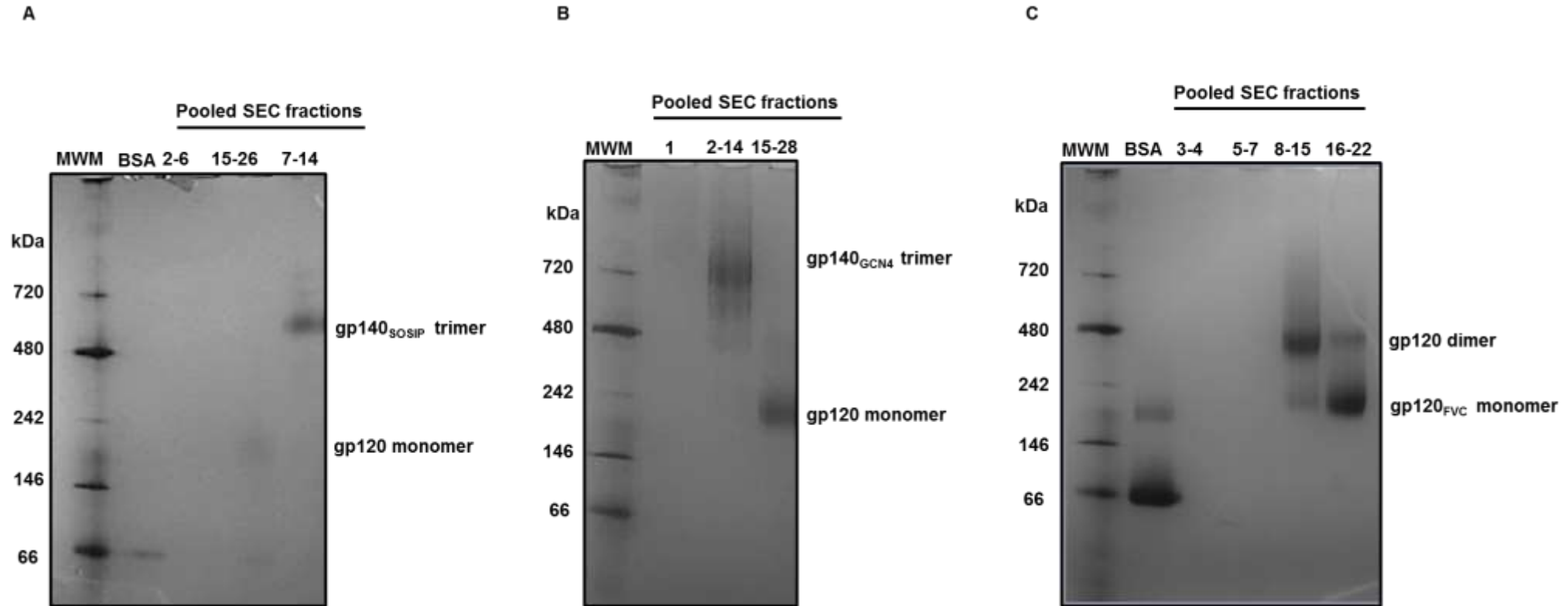


Figure 3.6: Blue native PAGE analysis of SEC purified Envs. Fractions collected from the same SEC profile peak were pooled; concentrated and 1 μ g of each fraction pool was loaded and electrophoresed on a 3-13 % precast gradient Blue native PAGE gel. **A.** Pooled SEC fractions for gp140_{SOSIP}, **B.** gp140_{GCIN4} and **C.** gp120_{FVC}. MWM- molecular weight marker called NativeMark™ (Novex, Life Technologies, Carlsbad, CA, USA) with a size range of 20- 720 kDa.

Following successful Env expression from mammalian cell lines and purification, bacterial expression and purification of recombinant 2dCD4 WT was verified.

3.1.5 Bacterial expression and purification of 2dCD4 WT

Recombinant 2dCD4 WT was harvested from chemically competent *E.coli* BL21 star cells, purified by Ni affinity chromatography and eluted. SDS-PAGE analysis of the eluted protein confirmed successful expression and purity with a band size of 25 kDa, as expected under reducing conditions (Figure 3.7). A 32 kDa band which is usually found under non-reducing conditions was also observed, suggesting partial reduction 2dCD4 WT during the SDS-PAGE analysis.

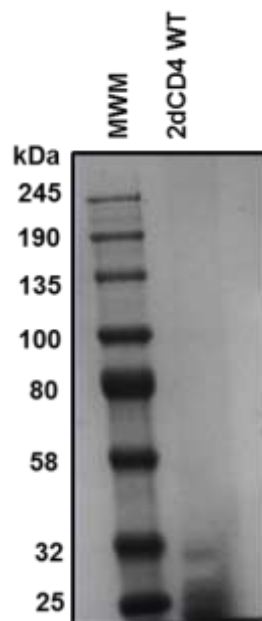


Figure 3.7: SDS-PAGE analysis confirming expression of 2dCD4 WT post Ni affinity purification. Following expression of 2dCD4 WT from *E.coli* BL21 star cells, the protein was purified by Ni affinity chromatography and analyzed by SDS-PAGE under reducing conditions. Lane 1; MWM- molecular weight marker of broad range i.e.11- 245 kDa (NEB, Ipswich, England). Lane 2; 25 kDa band shows reduced 2dCD4 WT confirming its expression and purification, 32 kDa band shows a non-reduced 2dCD4 WT.

The recombinant 2dCD4 WT protein (Figure 3.7) was expressed and purified as required for functional analysis of recombinant Envs in ELISAs.

3.2 Characterization of purified Env for conformational integrity and functionality assessment

Indirect ELISAs confirmed the conformational integrity and functionality of the SEC purified gp140_{SOSIP}, gp140_{GCN4} trimers and gp120_{FVC} monomer (Figure 3.8 and Figure 3.9). The conformational integrity was evaluated in two replicates using antibodies specific for each Env conformation and the results are represented as mean OD readings. CAP256-VRC26.25 antibody which binds exclusively to variable regions one and two (V1V2) of an intact quaternary trimeric Env structure confirmed correct structural/conformational integrity of the gp140_{SOSIP}. The 10E8 antibody which binds to the MPER region of gp140_{GCN4} and IgG1b12 which binds CD4 binding site of gp120 monomer validated the correct structural integrity of the respective Envs.

The results showed that CAP256-VRC26.25, 10E8 and IgG1b12 successfully bound to gp140_{SOSIP}, gp140_{GCN4} and gp120_{FVC}, respectively (Figure 3.8A-C). In addition, the binding of each antibody to the respective Env conformation increased with increasing concentrations of Env. These findings confirmed that the purified gp120_{FVC} monomer, gp140_{SOSIP} and gp140_{GCN4} trimers were isolated in desired intact conformations. The gp120_{BaL} (added as negative control for CAP256-VRC26.25 and 10E8 binding) showed no binding (Figure 3.8A and B), which confirmed that CAP256-VRC26.25 binds exclusively to an intact gp140_{SOSIP} trimer and 10E8 to MPER region of gp140_{GCN4} trimer. Additionally, binding of IgG1b12 to gp120_{BaL} validated that this antibody binds to the CD4-binding sites on monomeric Env conformations.

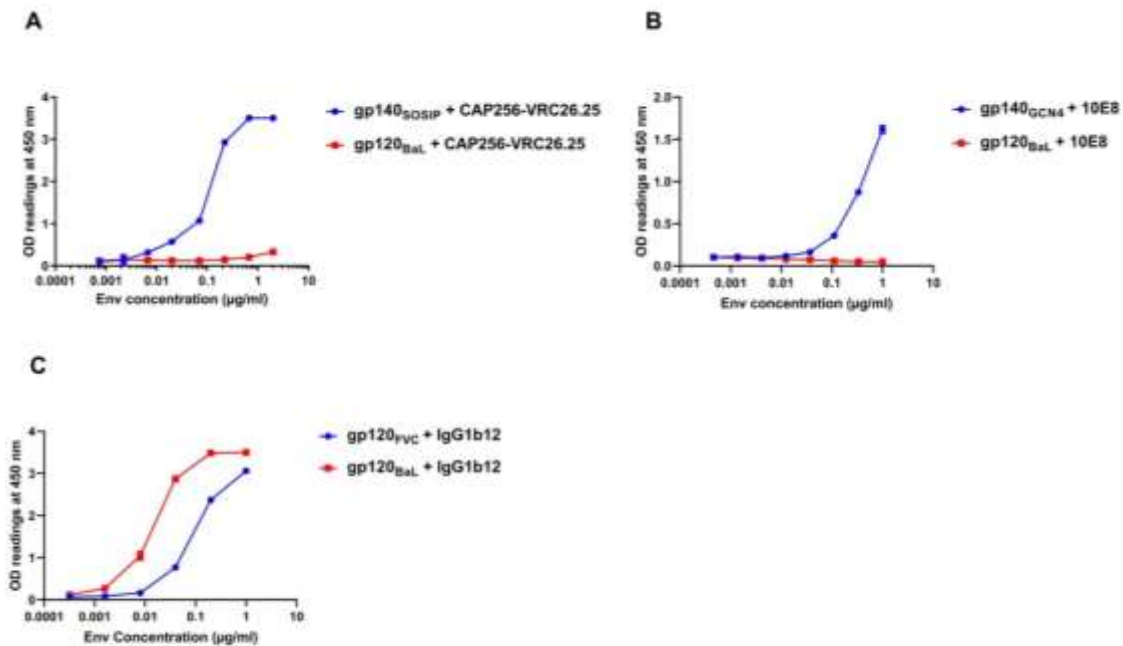


Figure 3.8: Confirmation of conformational integrity of purified Envs. Each Env protein was serially diluted in two replicates, immobilized on ELISA plates and conformational integrity was confirmed through binding to 1 µg/ml conformation specific antibodies CAP256-VRC26.25, 10E8, IgG1b12 and 1 in 2000 anti-human IgG HRP conjugated secondary antibody. The results are represented as a mean OD reading for each serial dilution **A.** gp140_{SOSIP}, **B.** gp140_{GCNA4} and **C.** gp120_{FVC}. The gp120_{BaL} was added as a negative control for the antibody binding specificity to the trimers and positive control for binding to the monomer.

Post confirmation of Env conformational integrity, the functionality of the Envs was assessed based on their ability to bind 2dCD4 WT and induce exposure of CD4i epitopes in two replicates (Figure 3.9). The latter epitopes were detected by antibody 17b binding and the results are represented as mean OD readings for each serial dilution.

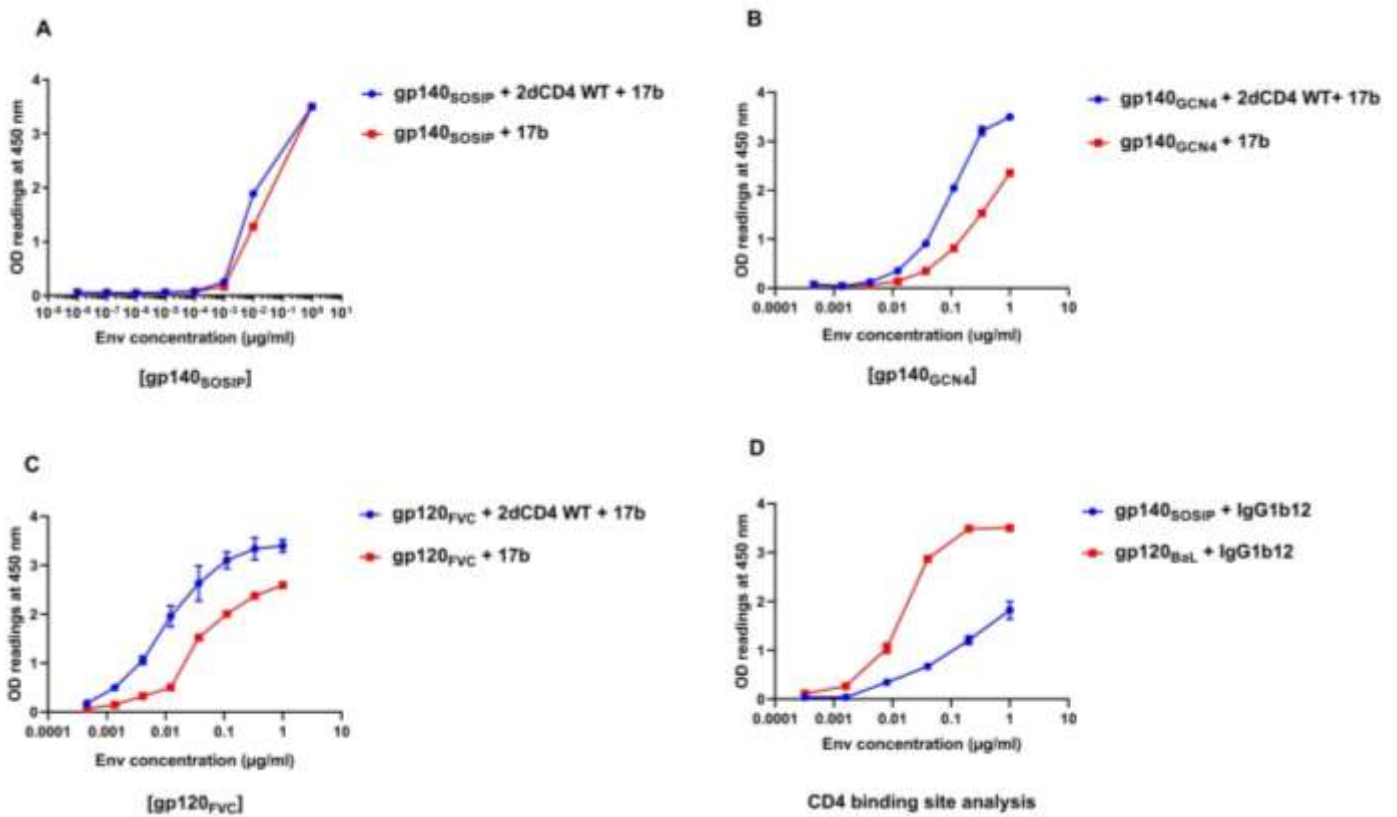


Figure 3.9: Functionality assessment of purified Envs. Equivalent concentrations (2 µg/ml) of each Env conformation were serially diluted in replicates of two and complexed with 2 µg/ml 2dCD4 WT for exposure of CD4i epitopes which were subsequently detected by 1 µg/ml antibody 17b and 1 in 200 HRP conjugated secondary antibody. The results are represented as a mean OD reading from the replicates for each serial dilution **A.** gp140_{SOSIP}, **B.** gp140_{GCN4} **and C.** gp120_{FVC}. A no CD4 control (Env + 17b, red graphs) was included as a reference point for measuring enhancement of 17b binding in the presence of 2dCD4 WT. **D.** Assessment of CD4 binding site integrity of gp140_{SOSIP} using IgG1b12 with gp120_{BaL} as a positive control.

Results from the functionality ELISAs show that antibody 17b bound to each Env conformation (gp140_{SOSIP}, gp140_{GCN4} and gp120_{FVC}) in the absence of 2dCD4 WT i.e. No CD4 control (Figure 3.9A-C, red graphs), suggesting that CD4i epitopes were already exposed to some extent. However, 17b binding to the Envs was generally enhanced in the presence of 2dCD4 WT (Figure 3.9 A-C, blue curve) as indicated by shifting of the curves to higher OD readings. This was confirmation that the binding of 2dCD4 WT induced further Env conformational changes that exposed CD4i epitopes on the Envs which were detected by CD4i binding antibody 17b, hence a validation that the Envs were functional i.e. able to bind CD4.

Although 17b demonstrated increased binding to the gp140_{SOSIP} trimer in the presence of 2dCD4 WT, the increase in binding was not as high as the other Env conformations (Figure 3.9A). Hypothetically, this observation suggested reduced structural integrity of the gp140_{SOSIP} CD4 binding site. Therefore, IgG1b12 was used to detect whether the CD4 binding site of gp140_{SOSIP} trimer was intact or not. The results show that IgG1b12 successfully bound to gp120_{BaL} positive control and gp140_{SOSIP} trimer (Figure 3.9D) confirming that the CD4 binding site was intact and the gp140_{SOSIP} trimer was indeed functional.

3.3 Flow cytometry assessment of Env-mediated bystander apoptosis of uninfected Jurkat T cells

3.3.1 Annexin V detection of apoptotic uninfected Jurkat T cells post treatment with varying concentrations of gp140_{SOSIP}, gp140_{GCN4} and gp120_{FVC}

Env concentrations ranging from 50 nM to 500 nM were used in two replicates to induce apoptosis of CD4-expressing Jurkat T cells for varying incubation periods i.e. 24, 48 and 72 hours. The different time points were necessary for detection of both early and late apoptotic events in the treated Jurkat T cells. Post-apoptosis induction, the ability of each Env conformation to induce bystander apoptosis was evaluated by Annexin V and 7-AAD dead cell staining (Appendix C) for detection of PS translocation to the surface of the membrane as a measure of apoptosis at each time point. Camptothecin was used as an apoptosis control, and the results were acquired as scatter dot plots showing percentage of early (Figure 3.10A and B, Q4) and late apoptotic cells (Figure 3.10A and B, Q2) which were combined to a total

percentage of apoptotic cells for each treatment including controls. Untreated cells control was then used a baseline for each replicate and the results are represented as a mean % change in apoptosis relative to untreated cells in a bar graph (Figure 3.11) for each Env concentration and time point. The variation of each replicate from the mean % change in apoptosis is indicated as a standard deviation which is represented as error bars on the bar graph (Figure 3.11). Results for all flow cytometry assays throughout this dissertation are represented in the same manner, and detailed scatter plots for each assay are available in the relevant appendices.

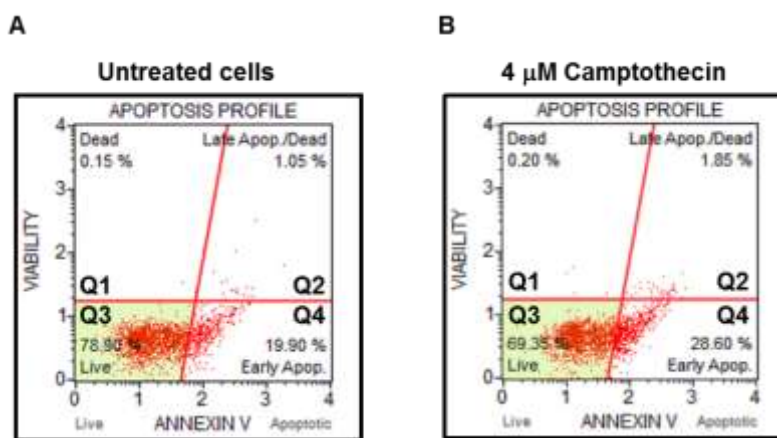


Figure 3.10: Representative scatter plots of Annexin V and 7- AAD staining results post 24 hours of Jurkat T cells treatment. A. Untreated cells and B. 4 μM Camptothecin treated Jurkat T cells. Q- quadrant.

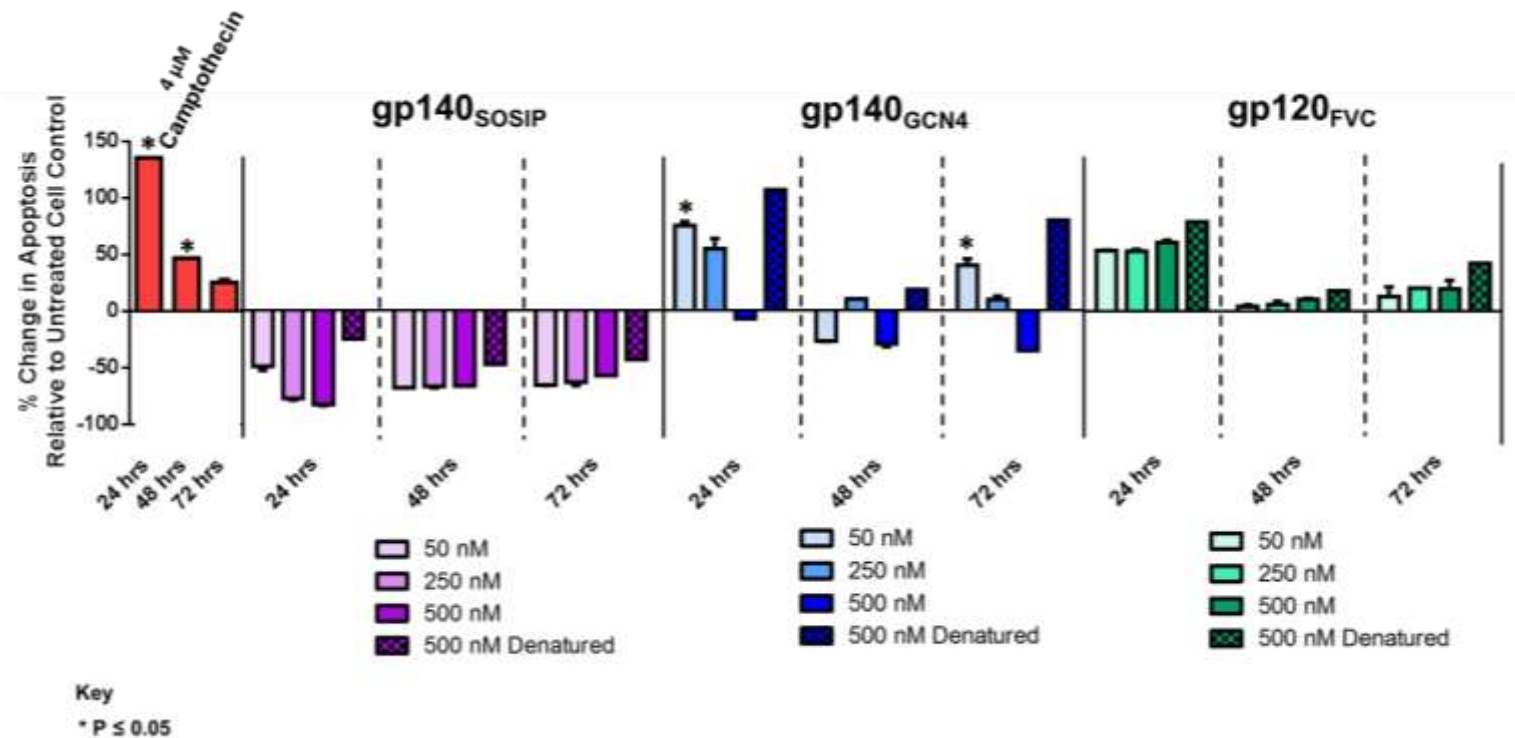


Figure 3.11: Apoptosis detection by Annexin V and 7- AAD analysis. Jurkat T cells were treated with varying concentrations (50 nM to 500 nM) of gp140_{SOSIP}, gp140_{GC4} and gp120_{FVC} over time (24, 48 and 72 hours) in two replicates to induce apoptosis. Post each incubation period, Annexin V and 7- AAD staining were used to detect PS translocation as a measure of apoptosis and results were represented as a mean % change in apoptosis relative to untreated cells control over time for each Env concentration. Red- Camptothecin, Purple- gp140_{SOSIP}, Blue- gp140_{GC4} and Green- gp120_{FVC}. Darker shades of each colour- higher Env concentration and shaded graphs- denatured Env. Statistical significance is shown as an asterisk and was calculated from an unpaired student T test.

The Annexin V results show that treatment of the Jurkat T cells with Camptothecin (positive control) induced the highest levels of apoptosis, with a statistically significant mean increase of approximately 140 % relative to the untreated cells control at 24 hours post treatment (Figure 3.11, red graphs). This was an indication that PS was sufficiently externalized for detection by Annexin V and confirmation that apoptosis is inducible in Jurkat T cells. Although, an increase in levels of apoptosis was observed with the Camptothecin positive control treatment at 48 and 72 hours relative to untreated cells (Figure 3.11, red graphs), the levels were lower compared to the same treatment at 24 hours.

Treatment with 50 nM to 500 nM gp140_{SOSIP} showed no PS translocation suggesting no apoptotic effect, with lower levels of apoptosis relative to the untreated cells control at 24, 48 and 72 hours (Figure 3.11, purple graphs). In contrast, addition of 50 nM and 250 nM gp140_{GCN4} trimer induced higher levels of apoptosis with an approximately 78 % and 50 % increase in Jurkat T cells expressing the apoptotic marker PS on their membrane surface at 24 hours. Interestingly, the highest gp140_{GCN4} concentration of 500 nM showed no apoptotic effect at all-time points. Treatment with 50 nM, 250 nM and 500 nM gp120_{FVC} monomer induced average levels of apoptosis with comparable percentage increases of approximately 50 % relative to untreated cells at 24 hours (Figure 3.11, green graphs). Similarly to treatment with gp140_{GCN4}, the levels of apoptosis at these concentrations decreased over 48 and 72 hours relative to the same concentrations at 24 hours' time point.

Addition of the heat denatured 500 nM gp140_{GCN4} and gp120_{FVC} showed increases in apoptosis at 24 hours which decreased over time (Figure 3.11, shaded graphs). This suggests that heat denaturation does not inhibit the ability of the Envs to bind to Jurkat T cells and induce bystander apoptosis.

Collectively the results from Annexin V analysis showed that only the monomeric gp120_{FVC} and gp140_{GCN4} trimeric Env conformations were able to induce bystander apoptosis of Jurkat T cells through exposure of PS.

Since PS translocation or exposure is not pathway specific, other apoptosis biomarkers were explored to determine whether Env-mediated bystander apoptosis occurred via the intrinsic/extrinsic pathways of apoptosis.

3.3.2 Mitopotential assay detection of apoptosis via intrinsic pathway post treatment of uninfected Jurkat T cells with varying concentrations of gp140_{SOSIP}, gp140_{GCN4} and gp120_{FVC}

Jurkat T cells were treated in two replicates with varying concentrations (50 nM to 500 nM) of gp140_{SOSIP}, gp140_{GCN4} and gp120_{FVC}, including positive and negative controls over time (24, 48 and 72 hours). Post each time point, Mitopotential dye was used to detect mitopotential depolarization as a measure of apoptosis via the intrinsic pathway (Appendix D). Mitopotential depolarization was measured as a total percentage of depolarized dead and live cells (Figure 3.12, Q1 and Q3). The results are represented as a mean % change in apoptosis (mitopotential depolarization) relative to untreated cells control as a baseline (Figure 3.13)

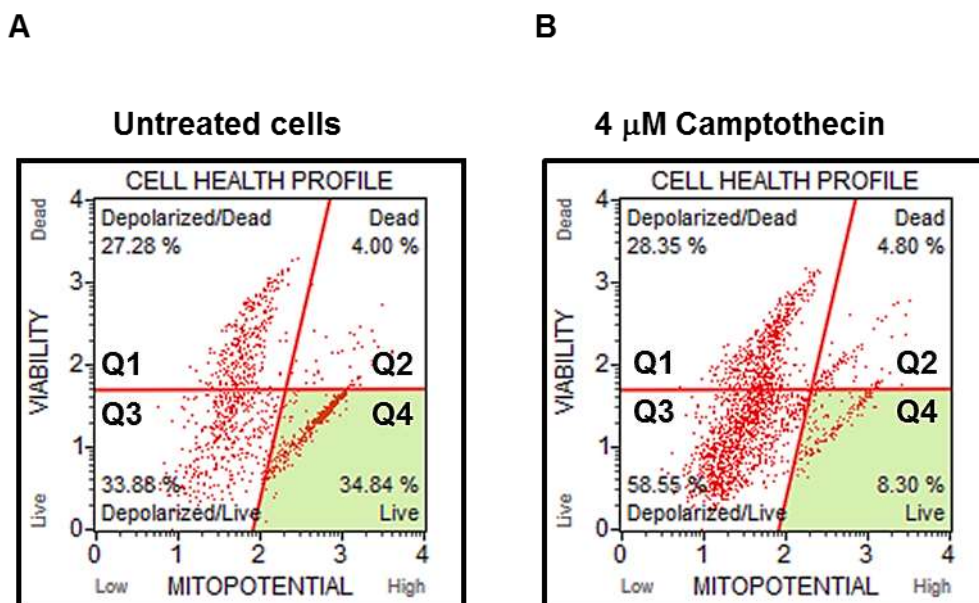


Figure 3.12: Representative scatter dot plot results from Mitopotential assay. A. Untreated cells control and **B.** Camptothecin treated Jurkat T cells at 24 hours post treatment. Q- quadrant.

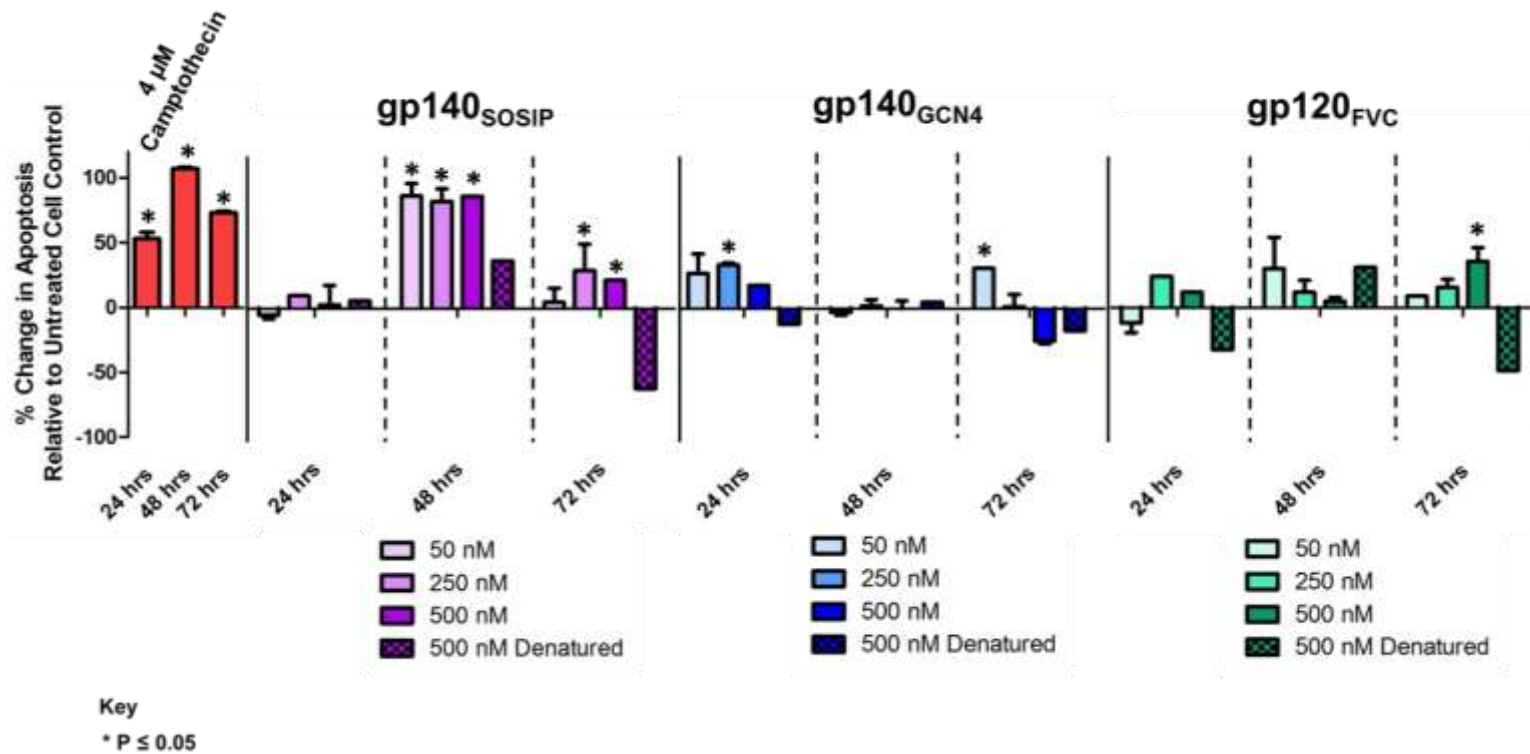


Figure 3.13: Apoptosis induced via the intrinsic pathway, as detected by mitopotential assay analysis. Concentrations (50 nM to 500 nM) of gp140_{SOSIP}, gp140_{GCN4} and gp120_{FVC} were used in two replicates to induce bystander apoptosis of Jurkat T cells over time (24, 48 and 72 hours). Subsequently, Mitopotential dye was used to detect mitopotential depolarization as a measure of apoptosis via the intrinsic pathway at each time point. Results are represented as a mean % change in apoptosis (mitopotential depolarization) relative to the untreated cells control for each Env concentration over time. Red- Camptothecin, Purple- gp140_{SOSIP}, Blue- gp140_{GCN4} and Green- gp120_{FVC}. Darker shades of each colour- higher Env concentration and shaded graphs- denatured Env. Statistical significance is shown as an asterisk and was calculated from an unpaired student T test.

Mitopotential assay analysis demonstrated that treatment with 4 μ M Camptothecin (positive control) resulted in significantly higher proportions (50 %, 100 % and 75 % mean % change in apoptosis) of Jurkat T cells with depolarized mitopotential at 24, 48 and 72 hours relative to the untreated cells control (Figure 3.13, red graphs). This was an indication that addition of Camptothecin shifted the membrane potential resulting in less negative charge within the inner mitochondrial membrane, as detectable by the mitopotential dye. Additionally, this observation also confirmed that early apoptosis via the intrinsic pathway is inducible in Jurkat T cells.

Treatment with 50 nM, 250 nM to 500 nM gp140_{SOSIP} induced significantly high levels of apoptosis via mitopotential depolarization at 48 and 72 hours relative to untreated cells (Figure 3.13, purple graphs). This finding contrasts with previously mentioned Annexin V staining results (Figure 3.11, purple graphs) where the gp140_{SOSIP} did not show any PS translocation. Overall, these results suggest that gp140_{SOSIP} trimer was able to induce bystander apoptosis of Jurkat T cells via the intrinsic pathway without translocating PS to the surface of the cell membrane.

Similarly to the gp140_{SOSIP} trimer and consistent with the Annexin V findings, treatment with 50 nM and 250 nM gp140_{GCN4} also resulted in increased apoptosis compared to the untreated cells control at 24 and 72 hours (Figure 3.13, blue graphs). However, analysis at 48 hours showed no apoptotic effect compared to the same concentrations at 24 hours. Addition of 50 nM and 250 nM of gp120_{FVC} induced low levels of apoptosis at 48 hours, while 500 nM showed significantly higher levels of mitopotential depolarized Jurkat T cells at 72 hours (Figure 3.13, green graphs).

Exposure of the Jurkat T cells to the heat denatured 500 nM gp140_{SOSIP}, gp140_{GCN4} and gp120_{FVC} showed no apoptotic effects with lower levels of mitopotential depolarization detected relative to the untreated cells control (Figure 3.13, shaded graphs).

Taken together, mitopotential assay results show that both the monomeric and trimeric Env conformations were able to induce bystander apoptosis via CD4 signalling and the intrinsic pathway.

To determine whether Env-mediated bystander apoptosis also occurred via the extrinsic pathway, caspase 3/7 activation was assessed as a biomarker of late apoptosis in this pathway.

3.3.3 Caspase 3/7 activation in uninfected Jurkat T cells post treatment with varying concentrations of gp140_{SOSIP}, gp140_{GCN4} and gp120_{FVC}

Post treatment of Jurkat T cells with varying concentrations of gp140_{SOSIP}, gp140_{GCN4} and gp120_{FVC} in two replicates, caspase 3 substrate DEVD peptide conjugated to a fluorescent DNA binding dye was used for detection of apoptosis via the extrinsic pathway (Appendix E). The percentage early and late apoptotic (Figure 3.14, Q2 and Q4) Jurkat T cells with active caspase 3/7 were combined and results are represented as a mean percentage change in apoptosis relative to untreated cells control (Figure 3.15).

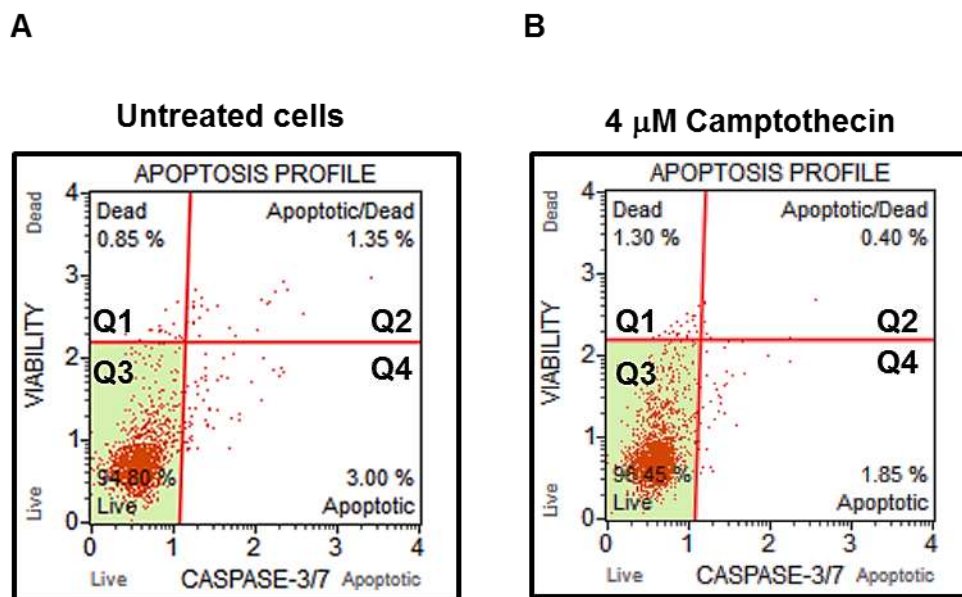


Figure 3.14: Representative caspase 3/7 activation analysis in Jurkat T cells. A. Untreated cells control. **B.** Treatment with 4 μM Camptothecin positive control post 24 hours of treatment. Q- quadrant.

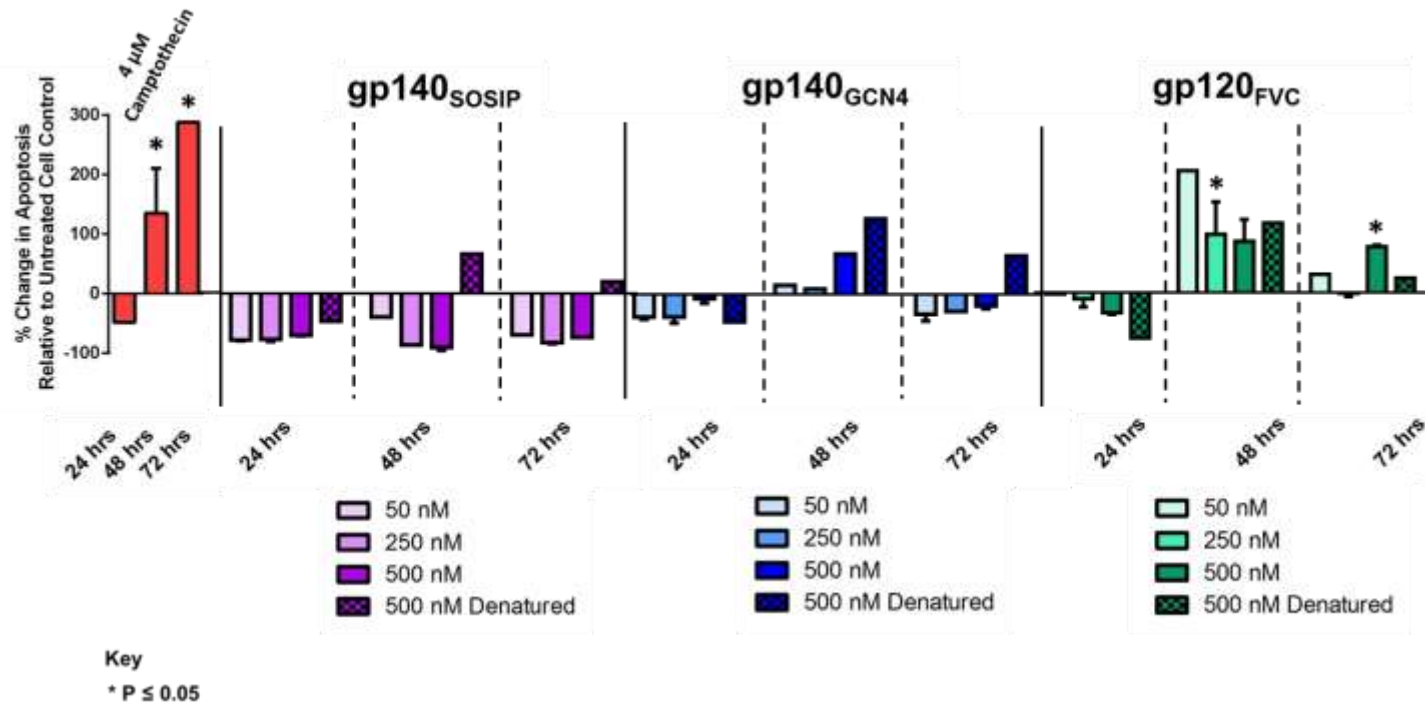


Figure 3.15: Apoptosis via caspase 3/7 activation in Env treated Jurkat T cells. Concentrations (50 nM, 250 nM and 500 nM) of gp140_{SOSIP}, gp140_{GCIN4} and gp120_{FVC} were used in two replicates to induce bystander apoptosis of uninfected Jurkat T cells over time (24, 48 and 72 hours). At each time point, caspase 3/7 DEVD substrate conjugated to a fluorescent DNA binding dye was used to assess the ability of the Envs to induce bystander apoptosis via caspase 3/7 activation i.e. the extrinsic pathway. Results are represented as a mean % change in apoptosis relative to the untreated cells control for each Env concentration and time point, with statistical significance shown in asterisks. Unpaired student T test was used to determine the statistical significance. Red-Camptothecin, shades of Purple- gp140_{SOSIP}, Blue- gp140_{GCIN4}, Green- gp120_{FVC}. Env concentrations increase with darker shades of each colour.

Assessment of caspase 3/7 activation in Jurkat T cells treated with 4 μ M Camptothecin showed no apoptotic effect at 24 hours with low levels of Jurkat T cells showing active caspase 3/7 relative to untreated cells (Figure 3.15). This was expected as caspase 3/7 activation is a late biomarker of apoptosis. The latter results suggest that during early apoptosis, Camptothecin uses alternative pathways other than Fas ligand mediated caspase 3/7 activation to induce apoptosis. This finding is similar to the observations made in mitopotential assay, which showed high proportion of depolarized mitopotential during 24 hours of apoptosis induction (Figure 3.13, red graphs), suggesting the role of Camptothecin in inducing apoptosis via the intrinsic pathway during early apoptosis. However, levels of apoptosis increased significantly at 48 and 72 hours post treatment with Camptothecin as expected.

Relative to the untreated cells control, addition of varying concentrations of gp140_{SOSIP} showed no caspase 3/7 activation hence no apoptotic effect, implying that this Env conformation does not induce apoptosis via the extrinsic pathway (Figure 3.15, purple graphs). However, treatment with gp140_{GCN4} trimer showed an approximately 50 % mean increase in Jurkat T cells with active caspase 3/7 only at the highest concentration of 500 nM, at 48 hours post treatment (Figure 3.15, blue graphs). Interestingly, no apoptosis via caspase 3/7 activation was observed at the same concentration at 72 hours.

Similarly to the Camptothecin positive control and gp140_{GCN4}, addition of 50nM, 250 nM and 500 nM gp120_{FVC} increased apoptosis at 48 hours which seemed reversible for lower concentrations (50 nM and 250 nM) at 72 hours (Figure 3.15, green graphs).

Low levels of apoptosis via the extrinsic pathway were detected when cells were treated with the respective heat denatured Env conformations, suggesting apoptosis induction via mechanisms other than CD4 signalling (Figure 3.15, shaded graphs).

Collectively, caspase 3/7 activation analysis showed that only the gp140_{GCN4} trimer and gp120_{FVC} monomer induced apoptosis via the extrinsic pathway.

To further determine whether Env-mediated bystander apoptosis resulted in DNA fragmentation i.e. DSB, which is a very late biomarker of apoptosis, Multicolour DNA damage assay was conducted.

3.3.4 DNA fragmentation in uninfected Jurkat T cells treated with varying concentrations of gp140_{SOSIP}, gp140_{GCN4} and gp120_{FVC}

Jurkat T cells treated with two replicates of 50 nM to 500 nM gp140_{SOSIP}, gp140_{GCN4} and gp120_{FVC} including controls were subjected to phospho-specific H2A.X-PECy5 and phospho-specific ATM-PE antibodies for detection of DSB as a measure of apoptosis (Appendix F). The DSB were detected at 24, 48 and 72 hours post treatment from Env treated cells and untreated cells control as a percentage of Jurkat T cells with dual activated ATM and H2A.X DNA repair proteins (Figure 3.16, Q2). The results were then represented as a mean percentage change in apoptosis (DSB- DNA damage) relative to untreated cells control as a baseline (Figure 3.17).

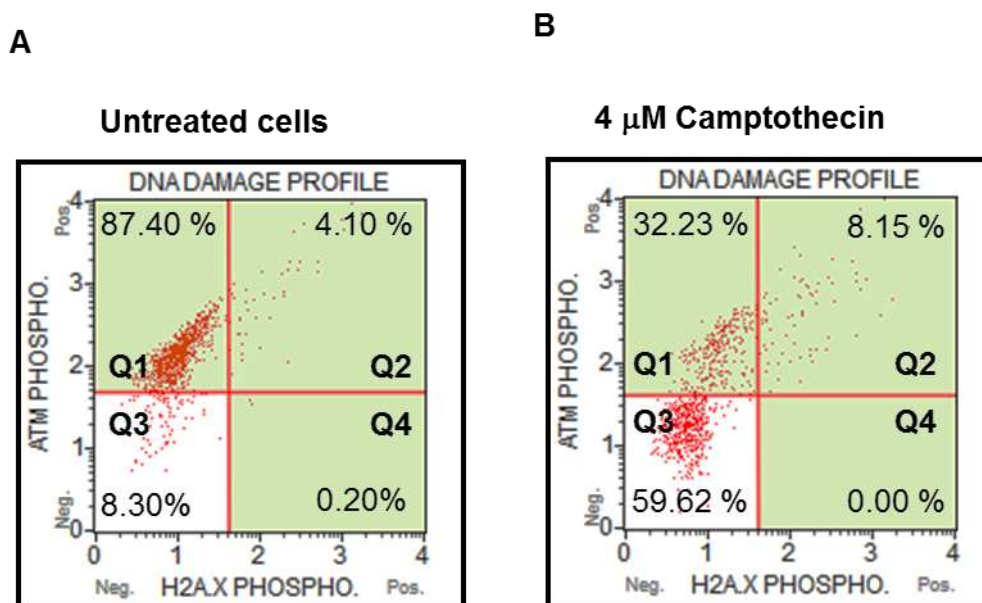


Figure 3.16: Representative DNA fragmentation results post 24 hours of Jurkat T cells treatment. A. Untreated cells control and **B.** Treatment with 4 μM Camptothecin. Q- quadrant.

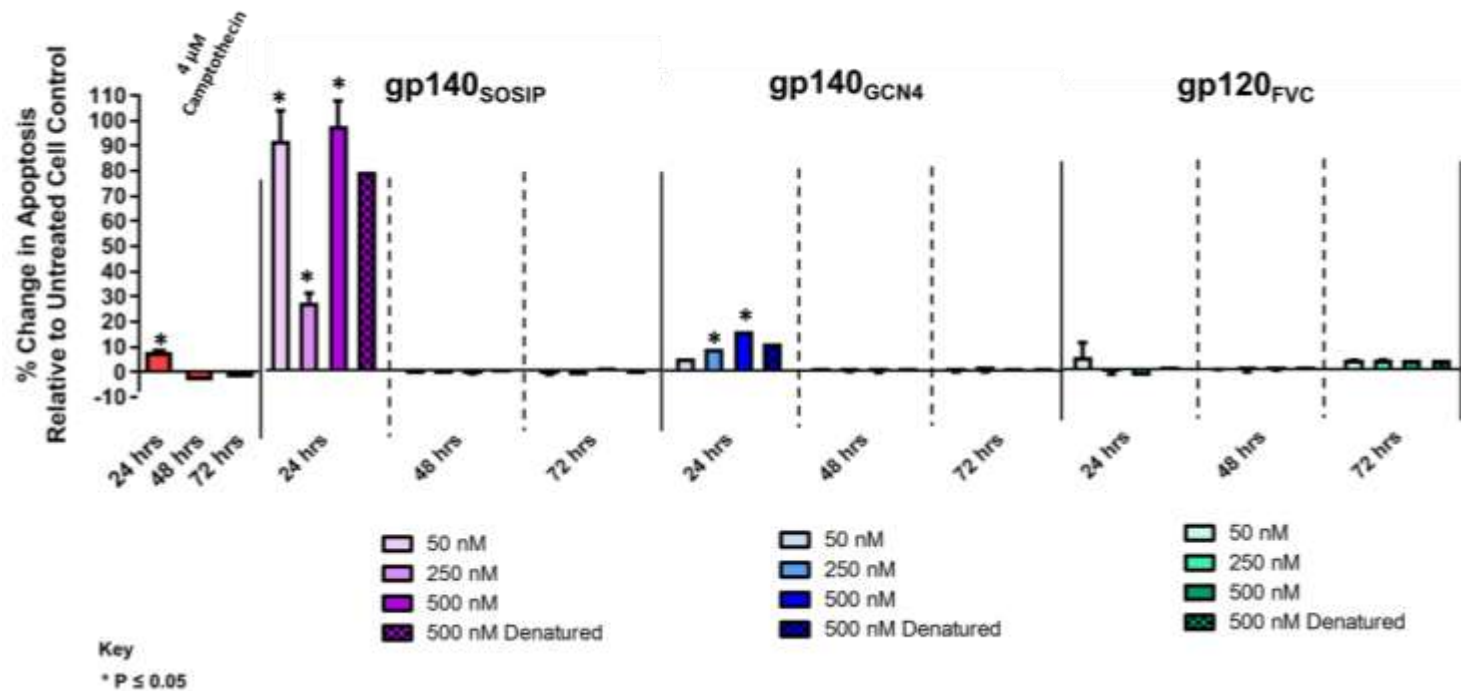


Figure 3.17: DNA fragmentation analysis in Env treated uninfected Jurkat T cells. Varying concentrations (50 nM, 250 nM and 500 nM) of gp140_{SOSIP}, gp140_{GC4} and gp120_{FVC} were added to Jurkat T cells in two replicates to induce bystander apoptosis over time (24, 48 and 72 hours). Post each time point, the ability of each Env to induce apoptosis via DNA fragmentation was evaluated by subjecting treated cells to phospho-specific H2A.X-PECy5 and phospho-specific ATM-PE antibodies. Results are represented as a mean % change in apoptosis (presence of DSB- dual activation of ATM and H2A.X) relative to the untreated cells control for each Env concentration and time point. Statistical significance is shown in asterisks and was determined using an unpaired student T test. Red- Camptothecin, Purple- gp140_{SOSIP}, Blue- gp140_{GC4} and Green- gp120_{FVC}. Increase in darkness of each colour is indicative of increasing Env concentrations. Shaded graph- heat denatured Envs.

Analysis of apoptosis via DNA fragmentation measured as DSB in Camptothecin treated Jurkat T cells showed a mean 10 % increase in levels of apoptosis relative to untreated cells post 24 hours of treatment (Figure 3.17, red graphs). This was confirmation that the positive control does induce DNA damage as expected. However, apoptosis decreased to levels comparable to untreated cells control over 48 and 72 hours.

Treatment with 50 nM, 250 nM and 500 nM gp140_{SOSIP} induced significantly high levels of apoptosis with mean 90 %, 30 % and 100 % increases of DNA fragmentation relative to untreated cells respectively at 24 hours (Figure 3.17, purple graphs). However, these levels of apoptosis dropped to levels comparable to untreated cells after 48 and 72 hours. Similarly to the gp140_{SOSIP} trimer, addition of 50 nM and 250 nM gp140_{GCN4} resulted in increased levels of apoptosis only at 24 hours with respective mean 10 % and 20 % increases in DNA fragmentation relative to the untreated cells (Figure 3.17, blue graphs). In contrast to the two trimeric conformations, treatment with gp120_{FVC} showed negligible levels of DNA fragmentation over time suggesting the inability of the monomer to induce apoptosis via DNA fragmentation (Figure 3.17, green graphs).

Unexpectedly, treatment with 500 nM heat denatured gp140_{SOSIP} and gp140_{GCN4} showed increased levels of DNA fragmentation i.e. apoptosis relative to untreated cells (Figure 3.17, shaded graphs). To confirm that the Env proteins had been denatured sufficiently, reversibility of heat denaturation was evaluated through monitoring heat denaturation curves (Figure 3.18). The results showed that the unfolding or denaturation of the gp140_{SOSIP} and gp140_{GCN4} as a result of increasing temperature was irreversible with refolding patterns (Figure 3.18 A and B line 1, right side of the graph) being completely different from the unfolding patterns (Figure 3.18 A and B, line 1, left side of the graph). Light scattering was measured concurrently with unfolding and refolding patterns of the Envs as a measure of protein aggregation (precipitation) and showed that increasing temperature increased light scatter by the gp140_{SOSIP} and not gp140_{GCN4} (Figure 3.18A and B, line 2). This confirmed that the gp140_{SOSIP} formed precipitates which plausibly induced apoptosis. However, lack of precipitation of gp140_{GCN4} heat denaturation, suggested that the heat denatured version of this Env plausibly used alternative pathways other than CD4 signalling or precipitates to induce bystander apoptosis via DNA fragmentation.

In summary, results from flow cytometry analysis demonstrated that all three HIV-1 Env conformations tested induce varying levels of apoptosis in Jurkat T cells via different mechanisms. The trimeric gp140_{SOSIP} and gp140_{GCN4} induced bystander apoptosis via the intrinsic pathway with onset reversible DNA fragmentation. However apoptosis induction by gp140_{SOSIP} was not associated with PS translocation while the gp140_{GCN4} trimer showed PS translocation. The monomeric gp120_{FVC} induced bystander apoptosis via both the intrinsic and extrinsic pathways with low levels PS translocation.

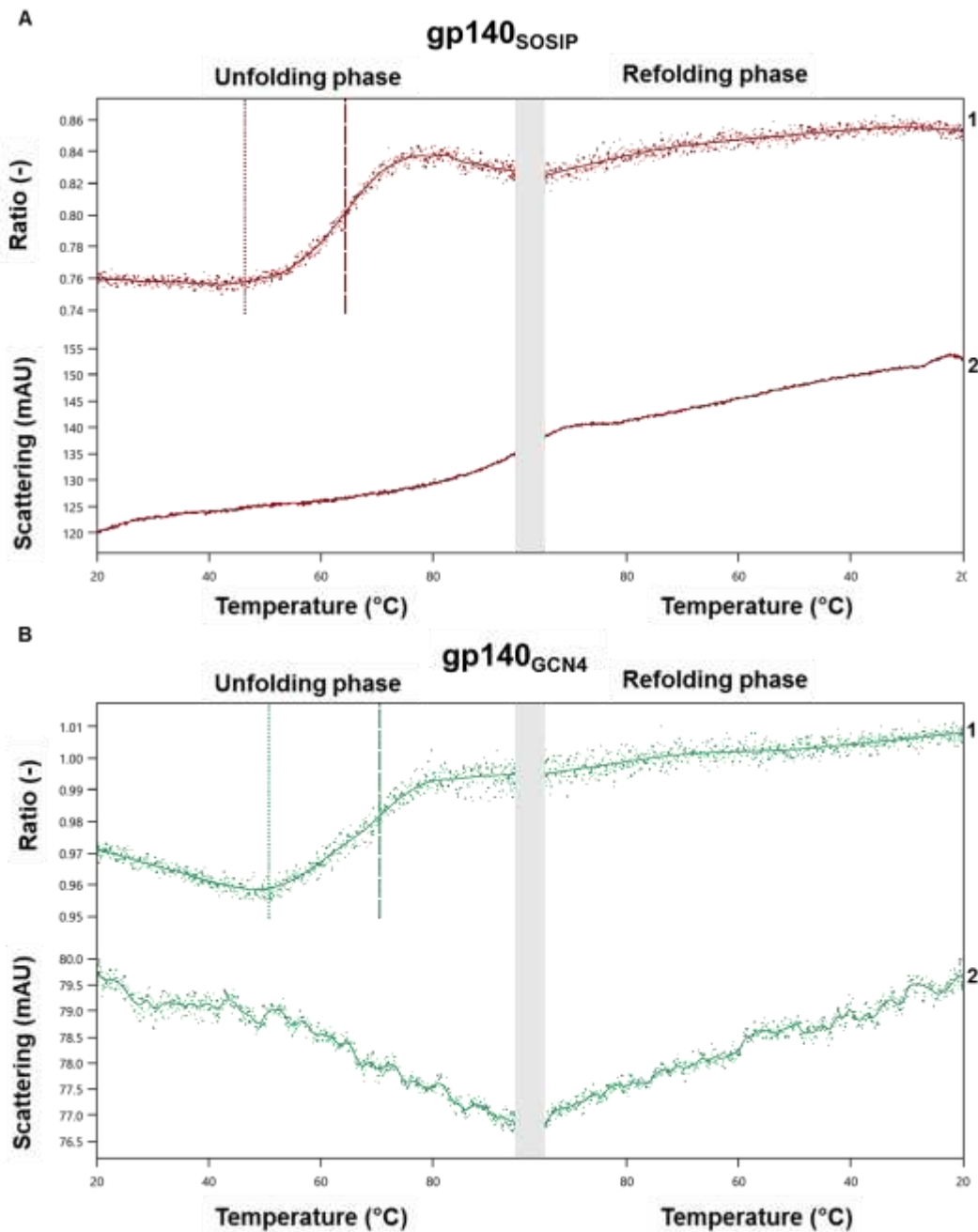


Figure 3.18: Env protein stability analysis through heat denaturation curves. Three μg amounts of each gp140_{SOSIP} and gp140_{GC4} were loaded onto the Prometheus NanoTemper.48 machine (NanoTemper Technologies, Munchen, Germany) for exposure of the Envs to increasing temperature and monitoring of the denaturation process. Denaturation is represented as protein unfolding phase measured as an intrinsic fluorescence ratio of Tyrosine and Tryptophan (-) (left side of line 1). The refolding pattern is indicated on the right (line 1). Protein precipitation is shown as light scattering (line 2). **A.** Unfolding and refolding pattern for gp140_{SOSIP} and **B.** gp140_{GC4}.

4. Discussion

The depletion of uninfected CD4⁺ T cells as a result of shed HIV-1 gp120-mediated apoptosis has been extensively studied (Chen et al., 2013, Février et al., 2011, Green et al., 2013, Vashistha et al., 2009). However, HIV-1 Env exists in monomeric and trimeric conformations, and the contribution of each conformation to bystander apoptosis remains controversial. Therefore this study sought to evaluate the contribution of HIV-1 subtype C matched monomeric (gp120_{FVC}) and trimeric (gp140_{GCN4} and gp140_{SOSIP}) Env conformations to bystander apoptosis, specifically via interaction with CD4 receptors on target Jurkat T cells. Comprehension of the latter interaction could give insight into the pathogenesis of HIV-1 infection, and novel therapeutic strategies.

To evaluate the role of the different Env conformations in bystander apoptosis, the first objective was to transiently and stably express the respective recombinant Envs in mammalian cell lines.

4.1 Transient and stable expression and purification of recombinant HIV-1 Env conformations (gp140_{SOSIP}, gp140_{GCN4}, gp120_{FVC})

Recombinant plasmids with the gp140_{SOSIP} Env sequence were propagated through chemical transformation of competent *E.coli* DH5 α cells (Figure 3.1) and effectively purified (Figure 3.2). Other than chemical transformation, electroporation i.e. the use of an electrical field to increase membrane permeability has also been used as an alternative way of transforming bacterial cells (Morrison, 1997, Sambrook and Russell, 2006, Yan et al., 2016). However, this process of electroporation requires high cell density compared to chemical methods, making it less advantageous, hence calcium chloride (Cohen, 1972, Chan et al., 2013) chemical transformation was used in this study. Interestingly, the transformation efficiency of chemically competent *E.coli* cells was poor at very low plasmid concentrations (0.04 $\mu\text{g}/\mu\text{l}$, data not shown) and improved when concentrations were increased to nanogram amounts (10.85 $\text{ng}/\mu\text{l}$, 11.85 $\text{ng}/\mu\text{l}$, Figure 3.1). This is different from previous studies which have shown that transformation efficiency of *E.coli* DH5 α , B21 star and JM109 strains decreased with increasing plasmid concentrations and was optimal at

maximum concentrations of 100 ng/ml i.e. 0.1 ng/ μ l (Liu et al., 2014). The contradiction of the observed results with the latter studies could be attributed to the smaller sizes of the recombinant plasmids used in this study (4000- 6000 bp), which resulted in improved passive diffusion into the *E.coli* DH5 α cells during transformation. In agreement with this hypothesis, a study by (Hanahan, 1983) has proven that compact supercoiled form of plasmids transformed various strains of *E.coli* more efficiently than their extended open circular relaxed forms, with the relaxed form transforming optimally at size ranges of 2000- 6600 bp.

The HIV-1 Env is expressed as a gp160 precursor glycoprotein which is cleaved by an endopeptidase called Furin protease into a non-covalently linked gp120-gp41 heterotrimer (Checkley et al., 2011, Liu et al., 2008, Sharma et al., 2015). The proteolytic cleavage of gp160 into the gp120-gp41 heterotrimer is essential for correct folding of the trimer into a functional quaternary structured Env (Pugach et al., 2015). To produce the latter functional and stable Env trimers, gp140 oligomers which are generally soluble versions of Envs with full length gp120 but truncated cytoplasmic tail and transmembrane regions of gp41 were previously designed (Forsell et al., 2009, Killick et al., 2014, Sanders et al., 2002, Sanders et al., 2013) Therefore, in an attempt to produce fully functional Envs in this study, the successfully propagated and purified recombinant Furin and gp140_{SOSIP} plasmids were co-transfected (Binley et al., 2000) for transient expression of the gp140_{SOSIP} trimer in HEK 293T cells while gp120_{FVC} monomer and gp140_{GCN4} trimer were each stably expressed in mammalian HEK 293F cell lines.

Evaluation of both the transient and stable mammalian cell line expression of the Envs demonstrated production of the desired gp140_{SOSIP}, gp140_{GCN4} trimers at the expected sizes of approximately 120 kDa and 140 kDa (Figure 3.3A-C) respectively under reducing conditions while gp120_{FVC} was also detected at 120 kDa (Figure 3.3D). The gp140_{GCN4} trimer with an intact Furin cleavage site was detected as a 140 kDa band even under reducing conditions, thus suggesting inefficient proteolytic cleavage into a gp120-gp41 heterotrimer with potential to dissociate into respective subunits (Figure 3.3C). This result complies with those of (Binley et al., 2000, Forsell et al., 2005, Kothe et al., 2006, Kothe et al., 2007, Yang et al., 2000a) who attributed the inefficient cleavage to inadequate amounts of inherently expressed Furin and suggested co-transfection with a Furin expressing plasmid as an effective strategy to

enhance full proteolytic cleavage of the trimer. Therefore future studies could utilize this strategy to enhance proteolytic cleavage of the gp140_{GCN4} trimer. Similarly to gp140_{GCN4}, the gp140_{SOSIP} trimer consists of an intact Furin protease cleavage site however with disulphide bonds linking the gp120 and truncated ectodomain of gp41 (Klasse et al., 2013, Sanders et al., 2002, Sanders et al., 2013), therefore under reducing conditions, bands at approximately 120 kDa and 41 kDa were expected. Conversely, transient expression of gp140_{SOSIP} also showed inefficient proteolytic cleavage of expressed gp140_{SOSIP} (Figure 3.3A), as shown by the presence of both cleaved 120 kDa and uncleaved 140 kDa states. Although co-transfection with a Furin protease enhanced the proteolytic cleavage of the gp140_{SOSIP} trimer (Figure 3.3B) with a decrease in the 140 kDa band intensity noted under reducing conditions, the cleavage was still not 100 % complete. This finding is consistent with those of (Binley et al., 2000, Morikawa et al., 1993, Moulard and Decroly, 2000) who showed that cleavage of some gp140 Env trimers was still not complete even with Furin co-expression. Other studies attributed this incomplete cleavage to high concentration levels of Env trimers saturating the Furin protease (Binley et al., 2000, Kothe et al., 2007, Zhang et al., 2001b) which reduces its cleavage efficiency. To circumvent the partial proteolytic cleavage of Env trimers, previous studies (Sanders et al., 2002, Sharma et al., 2015) suggested generation of cleavage independent native like Env trimers by substituting the Furin cleavage site (REKR) at the carboxyl terminus of gp120 subunit with a longer 2xG₄S peptide that covalently links gp120 to gp41. The latter strategy has been recently applied successfully in BG505 Env trimers which exhibited quaternary and carbohydrate structures similar to the native Envs (Sarkar et al., 2018) and an enhanced I559P mutation in what are termed SOSIP trimers, increasing trimerization (Sanders et al., 2002). Therefore, future studies could investigate the effect of a 2xG₄S peptide introduction on the quaternary structure of recombinant gp140_{SOSIP}.

Transient expressions produce proteins for the limited life of the transfected cells, while stable cell lines produce proteins continuously (Khan, 2013). As a result thereof, stable cell lines are more likely to produce higher protein yields than the transiently transfected cell lines. Consistent with this prediction, the transient expressions of gp140_{SOSIP} in this study, showed low yields (500 µg/ml per 500 ml expression medium) post purification relative to respective continuously expressed

gp120_{FVC} and gp140_{GCN4} (1 mg/ml per 500 ml expression medium, data not shown). In agreement with these findings, a previous study has proven that gp140_{BG505 SOSIP} trimer purified from stable HEK 293T and Chinese hamster ovary (CHO) cell lines had yields 10 and 32 fold greater than transiently transfected HEK 293T and CHO cells, respectively (Chung et al., 2014). Despite the challenges with Env yields, the gp140_{SOSIP} was expressed frequently to reach sufficient concentration levels required for subsequent experiments in this study. To improve the Env protein yields, future studies could involve generation of a stable gp140_{SOSIP} expressing cell line.

Mammalian cell lines were preferentially used in this study for the Env expression other than bacterial cell lines. This is mainly because mammalian expression systems are able to introduce correct protein folding and essential post-translational modifications such as glycosylation which results in the attachment of large and complex glycans to the expressed protein (Khan, 2013, Lasky et al., 1986). The glycosylation is of significance for ensuring correct assembly of expressed Env into a functional Env (Khan, 2013, Pritchard et al., 2015), and masking of immunologically important epitopes. Since glycan residues on mammalian cell line expressed Envs have high binding affinities for lectin, the glycosylated state allowed for successful purification of the Envs by *Galanthus nivalis* lectin affinity chromatography (Figure 3.4A-C). However, lectin purified Envs have been previously shown to contain a mixture of conformations i.e. aggregates, trimers, dimers and monomers (Ringe et al., 2017), suggesting that lectin affinity chromatography is not conformation selective. Therefore to select for desired homogeneous trimeric (gp140_{SOSIP} and gp140_{GCN4}) and monomeric (gp120_{FVC}) Env conformations, SEC was subsequently used post lectin purification of the Envs (Figure 3.5A-C). SEC profiles and Blue native PAGE analysis of SEC purified Envs confirmed that the Env conformations were homogeneous with desired trimeric gp140_{SOSIP} and gp140_{GCN4} and monomeric gp120_{FVC} predominating relative to contaminating conformations (Figure 3.5A-C and Figure 3.6A-C). The latter findings are consistent with those of (Pugach et al., 2015, Ringe et al., 2017, Sanders et al., 2013) who demonstrated an increase in the desired Env conformation purity post SEC. Therefore this suggested that expressed recombinant Envs in the present study were purified to correct trimeric and monomeric conformations in their most pure forms.

4.2 Purified recombinant FVC gp140_{SOSIP}, gp140_{GCN4} and gp120_{FVC} are conformationally intact and functional

To examine whether the expressed and purified Envs were arranged in intact and correct monomeric and trimeric conformations, antibodies (CAP256-VRC26.25, 10E8 and IgG1b12) specific for the respective Env conformations were used in Indirect ELISAs (Figure 3.8A-C). CAP256-VRC26.25 broadly neutralizing antibody (bnAb) was previously isolated from an HIV-1 subtype C infected donor (Doria-Rose et al., 2014, Moore et al., 2011). This bnAb binds preferentially to the apex variable regions one and two (V1V2) of an intact HIV-1 subtype C trimer (Bhiman et al., 2015, Doria-Rose et al., 2016), hence was selected in the present study for integrity analysis of subtype C gp140_{SOSIP}. Since the gp140_{GCN4} trimer consists of a gp120 subunit and an uncleaved gp41 ectodomain, it includes bnAb epitopes within the MPER of gp41 which allowed for confirmation of structural integrity using an MPER binding bnAb 10E8 (Huang et al., 2012, Kwon et al., 2016, Lee et al., 2016). The gp120_{FVC} monomer exists as a single unit without the gp41 subunit and lacks quaternary structure, therefore to test for conformational integrity, the CD4-binding site antibody IgG1b12 (Burton et al., 1994, Tran et al., 2012, Zhou et al., 2007) was used.

Analysis of the conformational integrity of the Envs with the abovementioned antibodies confirmed successful binding of CAP256-VRC26.25, 10E8 and IgG1b12 to gp140_{SOSIP}, gp140_{GCN4} and gp120_{FVC} respectively, in a concentration dependent manner (Figure 3.8A-C). This suggests that the purified FVC Envs were correctly folded into monomeric and quaternary trimers. In addition, effective binding of gp120_{FVC} to IgG1b12 was confirmation that the native CD4 binding site conformation was intact (Ozorowski et al., 2017, Sapphire et al., 2001). Moreover, the ability of the Envs to bind to the bnAbs suggested the presence of intact bnAb epitopes, and the potential of the FVC Envs to elicit appropriate antibody responses if used as vaccine immunogens. Additionally, subtype A founder virus strain BG505 based gp140_{SOSIP} trimers were highly reactive with bnAbs including quaternary structure specific antibodies CH01, PG9, PG16 and PGT145 (Dosenovic et al., 2015, Sanders et al., 2013, Sanders et al., 2015). This is further confirmation that founder virus Envs have promising immunogenic characteristics. Although outside the scope of the present

study, future studies could look into evaluating the immunogenicity of the FVC sequence based gp140_{SOSIP} trimer in animal models.

Having proven that the expressed and purified Envs were conformationally intact, the next step was to assess their functionality based on their ability to bind soluble CD4 (2dCD4 WT) and antibody 17b in ELISAs (Figure 3.9A-C). Antibody 17b binds CD4i epitopes which are exposed as a result of conformational changes in gp120 following binding to CD4 (Dalglish et al., 1984, Gardner et al., 2016, Tran et al., 2012). Evaluation of the Env functionality ELISAs confirmed enhancement of 17b binding to the Envs following binding to 2dCD4 WT compared to a no CD4 control (Env + 17b only, Figure 3.9A-C). These results validated that the Envs effectively interacted with CD4 which resulted in conformational changes that exposed CD4i epitopes to 17b, hence providing proof that the purified Envs were indeed functional. Moreover, the tertiary and quaternary conformational changes associated with CD4 binding to gp120 are essential for promoting the subsequent interaction of the gp120 subunit with co-receptors CCR5 or CXCR4 allowing for gp41-mediated viral entry into the target cells (Choe et al., 1996, Feng et al., 1996, Guttman et al., 2014, Mistry et al., 2016). Therefore, successful recognition of 17b by the Envs in the current study was also a further demonstration that each Env conformation was able to induce conformational changes relevant for co-receptor binding during HIV-1 infection. The latter observation also reaffirms the native like nature of the recombinant Envs in the present study.

Interestingly, 17b also exhibited binding to the respective Envs even in the absence of CD4 (Figure 3.9A-C), with the gp140_{SOSIP} trimer illustrating less 17b enhancement relative to the no CD4 control (Figure 3.9A). This suggested pre-exposure of some CD4i epitopes prior to interaction with CD4 and complies with the findings of (Thali et al., 1993, Tran et al., 2012) who revealed that binding of HIV-1 BaL Env to 17b alone was sufficient to induce formation of an open quaternary Env conformation which exposed CD4i epitopes. Moreover, (Ahmed et al., 2017, Kaplan et al., 2016) suggested that due to structural flexibility, soluble forms of Env frequently adopt a relatively open conformation exposing epitopes for CD4i antibodies. Therefore the latter studies explain why 17b bound to the Envs in the absence of CD4 (no CD4 control) in the present study (Figure 3.9A-C).

The observation made with the gp140_{SOSIP} trimer illustrating the least enhancement in 17b binding relative to the no CD4 control suggested low binding efficiency of the trimer to CD4 or reduced structural integrity of the CD4 binding site. To confirm the latter hypothesis, the conformational integrity of the gp140_{SOSIP} CD4 binding site was tested with a CD4 binding site antibody IgG1b12 in an Indirect ELISA. The ELISA confirmed successful binding of IgG1b12 to gp140_{SOSIP} in a concentration dependent manner (Figure 3.9D) which confirmed that the CD4 binding site of the trimer was intact. Future studies could evaluate the CD4 binding affinity of gp140_{SOSIP} using surface plasmon resonance. However, to explain the observed unexpected finding with gp140_{SOSIP} trimer, several studies have investigated the effects of SOSIP mutations on Env quaternary structure, its ability to bind various antibodies and CD4 engagement. Studies by (Julien et al., 2013, Lyumkis et al., 2013, Pancera et al., 2014) demonstrated that as a result of the introduced SOSIP mutations, the gp120 core of the SOSIP trimers resembles a CD4 bound conformation even in the absence of CD4, suggesting that CD4i epitopes are extensively exposed prior CD4 engagement and thus 17b binding does not enhance their exposure extensively. Moreover, SOSIP changes in HIV-1 BG505 Env reduced recognition or interaction of the trimer to soluble CD4 and other open conformation preferring antibodies such as 17b (Alsaifi et al., 2018). Collectively, these findings suggest that although SOSIP mutations stabilize the HIV Envs into correctly cleaved and folded quaternary trimeric proteins, their interaction with CD4 requires further investigations.

Having confirmed that the purified Envs were conformationally intact and functional, their ability to induce bystander apoptosis via binding to CD4 receptors on target uninfected Jurkat T cells was tested.

4.3 Apoptosis-inducing ability of monomeric and trimeric FVC Envs in uninfected Jurkat T cells

As previously stated and reiterated here, the role of shed soluble HIV Env in bystander apoptosis contributing to CD4⁺ T cells depletion during HIV infection has been well investigated based on varied observations. Cell death of uninfected CD4⁺ T cells outnumbered that of the HIV-infected cell population (Finkel et al., 1995) proposing bystander apoptosis as a contributor to HIV pathogenesis. Also, the

depletion of immune cells is largely limited to CD4⁺ T cells (Garg et al., 2011, Holm et al., 2004, Holm and Gabuzda, 2005) suggesting an essential role of the CD4 receptor in this phenomenon. Therefore, the current study evaluated the ability of soluble monomeric and trimeric Env conformations to induce bystander apoptosis of uninfected Jurkat T cells exclusively via CD4 interactions. Although several studies have implicated CCR5 and CXCR4 co-receptors interaction with Env in bystander apoptosis (Biard-Piechaczyk et al., 2000, Garg and Joshi, 2017, Joshi et al., 2011, Joshi et al., 2017, Li and Pauza, 2011, Tsao et al., 2016), CD4 signalling plays the most essential role in Env-mediated bystander apoptosis.

To initiate bystander apoptosis, concentrations of each Env conformation ranging from 50 nM to 500 nM were added to Jurkat T cells for 24, 48 and 72 hours. Thereafter, the treated cells were analysed by flow cytometry for detection of various biomarkers of apoptosis such as PS translocation, mitopotential depolarization, caspase 3 activation and DNA fragmentation.

PS translocation is an early biomarker of apoptosis and was detected through binding to Annexin V and 7-AAD stain, which showed the ability of 50 nM, 250 nM gp140_{G_{CN4}} trimer and 50 nM, 250 nM, 500 nM gp120_{F_{VC}} monomer to initiate bystander apoptosis through exposure of membrane lipid PS at 24 hours (Figure 3.11, blue and green graphs). Since Jurkat T cells in the current have been previously shown to only express the CD4 receptor, these findings served as proof that the apoptosis induction occurred solely due to Env-CD4 interaction. In agreement with the latter observation, inhibition of gp120–sCD4 interactions also inhibited Env-mediated bystander apoptosis (Biard-Piechaczyk et al., 2000) further reiterating the essentiality of CD4 receptor binding in Env-mediated bystander apoptosis.

Although both gp140_{G_{CN4}} and gp120_{F_{VC}} induced apoptosis (PS translocation) in a concentration dependent response, the gp140_{G_{CN4}} trimer showed increased apoptosis at lower concentrations with the gp120_{F_{VC}} monomer illustrating the opposite (Figure 3.11, blue and green graphs). In contrast, interaction of the gp140_{S_{OSIP}} trimer with the Jurkat T cells did not induce any PS translocation (Figure 3.11, purple graphs) suggesting lack of apoptosis or initiation of apoptosis via other mechanisms. Additionally, the inability of the gp140_{S_{OSIP}} trimer to initiate apoptosis

via PS translocation corroborates with the observation made in functionality ELISAs where this trimer showed inefficient binding to CD4 (Figure 3.9A). Therefore this also suggests that due to reduced binding to CD4, gp140_{SOSIP} binding to the target Jurkat T cells was not sufficient to sustain CD4 signalling required for initiation of PS translocation i.e. apoptosis. The variations in concentration dependent apoptosis induction by gp140_{GCN4} and gp120_{FVC} assume negative and positive correlation between concentrations of monomeric and trimeric Envs and their apoptosis-inducing potential, respectively. Additionally, these results also suggest differences in fusogenic properties between monomeric and trimeric Env conformations to CD4, contributing to differences in apoptosis induction at varied concentrations. In support of this hypothesis, previous studies by (Holm et al., 2004, Meissner et al., 2005, Meissner et al., 2006) have suggested phenotypic properties of gp120 such as CD4 and co-receptor binding affinities can influence fusion of the Envs to T cells as well as apoptosis-inducing capability. Therefore to fully understand the role of Env-CD4 binding affinities to bystander apoptosis, future studies could determine CD4 binding kinetics of each Env conformation at concentrations of 50-500 nM used in the present study.

Interestingly, levels of apoptosis induction by gp140_{GCN4} and gp120_{FVC} over 48 and 72 hours were lower than those observed at 24 hours, suggesting reversibility of apoptosis. Since PS translocation is an early biomarker of apoptosis, the low levels of apoptosis could be a result of many cells having undergone necrosis over 48 and 72 hours hence reduced Annexin V staining. Alternatively, Env-CD4 interactions could be plausibly unstable and short lived, resulting in dissociation of Env from target Jurkat T cells over time, which then reduces CD4 signalling relevant for further enhancement of bystander apoptosis. Our results and hypothesis comply with the findings of (Dobrowsky et al., 2008, Myszka et al., 2000) who showed destabilization of gp120-CD4 interaction over time.

Having shown the ability of gp140_{GCN4} and gp120_{FVC} to initiate bystander apoptosis via PS exposure, the next step was to determine whether the initiated apoptosis occurred via activation of the intrinsic and/or extrinsic pathways. Since the gp140_{SOSIP} trimer failed to induce PS translocation, it was also essential to find out whether this Env could induce bystander apoptosis via other mechanisms.

Apoptosis induction via the intrinsic pathway was measured as the ability of the Envs to depolarize the mitopotential. All Env conformations were able to induce bystander apoptosis via mitopotential depolarization i.e. the intrinsic pathway up to 72 hours post Env exposure, at 50-500 nM concentrations (Figure 3.13 purple, blue and green graphs). In accordance with the latter findings, (Ferri et al., 2000b, Joshi et al., 2011, Roggero et al., 2001) showed the ability of membrane expressed Envs to mediate bystander apoptosis in cell lines such as SupT1 cells and PBMCs through depolarizing their mitopotential and releasing the pro-apoptotic protein cytochrome C. Future studies could also monitor cytochrome C secretion in Env treated T cells by conducting immunoprecipitation with anti-cytochrome C antibodies as an alternative measure of apoptosis via the intrinsic pathway.

Interestingly, the gp140_{SOSIP} trimer induced low levels of apoptosis via mitopotential depolarization relative to gp140_{GCN4} and gp120_{FVC} at 24 hours which later increased to significant levels at 48 hours (Figure 3.13 purple, blue and green graphs at 24 hours). This observation suggests that gp140_{SOSIP} trimer binding to CD4 is a slow process which requires prolonged periods of time to initiate pro-apoptotic signals. To decipher whether this suggestion is valid, forthcoming experiments could determine the rate at which CD4 associates with gp140_{SOSIP}. Moreover, this finding could also be attributed to the observation made with functionality ELISAs where the gp140_{GCN4} trimer and gp120_{FVC} monomer showed higher binding to CD4 relative to the gp140_{SOSIP} trimer (Figure 3.9A-C).

Consistent with Annexin V results, levels of apoptosis for all Env conformations were lower at 72 hours relative to 48 hours further emphasizing the possibility of Env-mediated apoptosis through the intrinsic pathway being a reversible pathway. Similar to Annexin V data, apoptosis induction by the gp140_{GCN4} and gp120_{FVC} Envs also showed opposite dose dependent responses, further reiterating differences in fusogenic properties as previously mentioned. However, no dose dependent response was observed with gp140_{SOSIP} mediated apoptosis induction via the intrinsic pathway, with 50 nM, 250 nM and 500 nM concentrations showing relatively equivalent levels of bystander apoptosis at 24 hours. This finding suggests that, at concentrations of 50 nM Env, the CD4 receptor was already saturated, resulting in no increase in levels of apoptosis at higher Env concentrations. In contrast, previous *in vitro* studies showed a dose response of soluble gp120 at concentrations as low

as 500 ng/ml (Vlahakis et al., 2001) were able to induce sufficient levels of T cell death while the current study used 50 nM (7 µg/ml), 250 nM (35 µg/ml), 500 nM (70 µg/ml) of Envs and failed to induce a dose response. Additionally, gp120 concentrations as low as 100 ng/ml, 10 nM (1.4 µg/ml) and 10 µg/ml were sufficient to induce bystander apoptosis of Jurkat JE.61, PBMCs, HeLa and Human umbilical vein endothelial (HUVEC) cells (Anand and Ganju, 2006, Green et al., 2013, Li and Pauza, 2011). Moreover, concentration ranges of 300 pg/ml-960 ng/ml of soluble gp120 were detected in lymph nodes and spleen from *ex vivo* examinations of HIV-infected individuals (Cummins et al., 2010, Pantaleo et al., 1993a, Rychert et al., 2010, Sunila et al., 1997). Therefore, to be able to evaluate a dose dependent response and add clinical relevance to our findings, forthcoming experiments could utilize lower clinically relevant Env concentrations in bystander apoptosis assays.

Since the intrinsic and extrinsic pathways of apoptosis can either occur concurrently or independently, the current study determined whether Env-CD4 interactions on Jurkat T cells resulted in caspase 3/7 activation as a measure of apoptosis via the extrinsic pathway. In contrast to the findings from the mitopotential assays, 50-500 nM gp140_{G_{CN4}} interactions with Jurkat T cells resulted in caspase 3/7 activation only after 48 hours which seemed to be completely reversible at 72 hours post Env exposure (Figure 3.15 blue graphs). The gp140_{SOSIP} did not induce caspase 3/7 activation (Figure 3.15 purple graphs). These findings imply that both gp140_{SOSIP} and gp140_{G_{CN4}} trimeric conformations did not mediate apoptosis via the extrinsic pathway, their apoptosis induction mechanism was solely via the intrinsic pathway as previously observed in the mitopotential assays (Figure 3.13 purple and blue graphs). Unlike the trimeric Env conformations, the gp120_{FVC} monomer was able to mediate bystander apoptosis via caspase 3/7 activation i.e. the extrinsic pathway from 48 up to 72 hours post Env exposure (Figure 3.15 green graph). However, caspase activation seemed to be completely reversible only for the lower gp120_{FVC} concentrations (50-250 nM) at 72 hours. This suggests that higher concentrations of monomeric Env conformation were able to sustain pro-apoptotic signals required for apoptosis induction via caspase 3/7 activation. In support of the gp120_{FVC} monomer inducing apoptosis via caspase 3 activation, findings of (Ullrich et al., 2000) demonstrated that HUVEC experienced apoptosis via caspase 3 activation when the cells were treated with gp120 and gp160 HIV-1 Envs. Additionally, treatment with a

general caspase 3 enzyme inhibitor resulted in reduced levels of HUVEC apoptosis mediated by gp120 and gp160 (Ullrich et al., 2000), suggesting the essential role of caspase 3 activation i.e. the extrinsic pathway in bystander apoptosis. However, most studies have extensively investigated the role of soluble gp120 and membrane bound Env trimers (Anand and Ganju, 2006, Green et al., 2013, Joshi et al., 2011, Joshi et al., 2016, Li and Pauza, 2011) with limited research being conducted on the role of soluble gp140 trimers in bystander apoptosis. This raises the need for further investigations and comparisons of bystander apoptosis mediated by gp120 monomers and gp140 trimers, in order to fully understand the mechanisms of Env-mediated bystander apoptosis during HIV-1 infection.

Although the caspase 3/7 activation was a measure of bystander apoptosis via the extrinsic pathway in the current study, there are limitations associated with using this assay as a deciding factor for apoptosis induction via either the intrinsic or extrinsic pathways. Caspase 3/7 is an executioner enzyme activated by upstream caspases such as caspase 9 in the intrinsic pathway and caspase 8 in the extrinsic pathway (Rampal et al., 2012, Walczak and Krammer, 2000). This implies that activation of this caspase 3/7 can either be due to intrinsic or extrinsic pro-apoptotic signals mediated by the respective Envs. Therefore to clearly delineate the role of Env-mediated bystander apoptosis via the extrinsic pathway, activation of upstream extrinsic pathway specific enzymes such as caspase 8 can be detected in future. In addition, the Fas receptor initiates stimulus necessary for apoptosis induction via the extrinsic pathway upon binding of Fas ligand and previous studies suggest overexpression of this receptor and its ligand in HIV-infected individuals (Ipp et al., 2014, Mitra et al., 1996, York et al., 2013). Findings of (Nardacci et al., 2015) have also shown the contribution of overexpressed Fas ligand to bystander apoptosis of uninfected CD4⁺ T cells. Therefore, forthcoming studies could also monitor the expression of Fas as a measure of apoptosis via the extrinsic pathway.

Overall, the current study has thus far shown that trimeric Env conformations preferentially induced bystander apoptosis via the intrinsic pathway while the monomer activated both the intrinsic and extrinsic pathways. The discrepancies observed in apoptosis-inducing potential of trimeric versus monomeric conformations could be attributed to differences in quaternary structures which influenced Env- CD4 interactions and ultimately their ability to induce apoptosis. For instance, the

gp120_{FVC} monomer is made up of a single gp120 subunit while the trimeric conformations consist of a gp120-gp41 complex, with the gp140_{SOSIP} trimer having a truncated gp41 subunit compared to gp140_{GCN4}. Since the gp41 is essential for promoting fusion of the Envs to membranes on target T cells (Wyatt and Sodroski, 1998), absence and truncation of this subunit could imply differences in fusion properties between the Env conformations which might have influenced their ability to induce apoptosis. In agreement with this suggestion, previous studies have argued that although gp120 is required for induction of bystander apoptosis through binding to CD4 receptors, the gp41 subunit mediates membrane fusion, hence to an extent plays a critical role in bystander apoptosis (Blanco et al., 2003, Garg and Blumenthal, 2006a). Evidence of this essentiality was shown in HIV-infected individuals who illustrated a reduction in CD4 decline when treated with Enfuvirtide as a gp41 inhibitor (Barretina et al., 2004). In addition, changes (V38E mutation) in gp41 which reduces functionality of this Env subunit resulted in inhibition of bystander apoptosis *in vitro* (Garg et al., 2009) and a slower CD4 decline in humanized mice (Garg et al., 2011). Therefore to distinguish between contributions of monomeric and trimeric Env conformations to bystander apoptosis, it is necessary to determine the effects of their structural differences on their ability to interact with target T cells.

The ultimate goal of apoptosis through either the intrinsic or extrinsic pathways is to induce DNA damage in the apoptotic cells which results in complete cell death if not repaired. To detect whether gp140_{SOSIP}, gp140_{GCN4}, gp120_{FVC} mediated bystander apoptosis resulted in DNA damage, the Multicolour DNA damage assay was used to detect DSB as a measure of DNA damage and apoptosis. As previously shown, a single DSB is sufficient to induce cell death if not repaired properly (Papamichos-Chronakis and Peterson, 2013), hence it is a good measure of apoptosis. This is mainly because DSB results in chromosomal aberrations such as translocations and deletions which ultimately lead to cell death (Varga and Aplan, 2005). From the DNA damage analysis, treatment with the gp140_{SOSIP} and gp140_{GCN4} trimers showed significant levels of DSB i.e. apoptosis at 24 hours (Figure 3.17 purple and blue graphs). These findings comply with the observation made in mitopotential assays where the gp140_{SOSIP} and gp140_{GCN4} trimers induced significant levels of mitopotential depolarization at 24 hours (Figure 3.13 purple and blue graphs),

suggesting apoptosis induction via the intrinsic pathway. The intrinsic pathway is triggered by changes in the internal cell environment such as growth factor withdrawal, biochemical stress and DNA damage (Jorgensen et al., 2017, Loreto et al., 2014). Therefore, the observed ability of the Env trimers to induce DNA damage and initiate mitopotential depolarization, suggests that interaction of the Jurkat T cells with the gp140_{SOSIP} and gp140_{GCN4} trimers via the CD4 receptor, initiated DNA damage which then triggered pro-apoptotic signals to induce bystander apoptosis via the intrinsic pathway. However, no DSB were observed at 48 and 72 hours for treatment with each trimer, suggesting reversibility of the DNA damage and apoptosis. This also assumes that the Env-mediated DNA damage was completely repaired. In addition, these findings further suggests that the reduced mitopotential depolarization observed after 48 and 72 hours of treatment with gp140_{SOSIP} and gp140_{GCN4} relative to 24 hours (Figure 3.13 purple and blue graphs), was a result of repaired DNA damage which plausibly reduced pro-apoptotic signals in the intrinsic pathway.

In contrast to the trimeric conformations, the gp120_{FVC} monomer did not induce any DNA damage post 24, 48 and 72 hours of Env addition to the Jurkat T cells (Figure 3.17 green graphs). This suggests that bystander apoptosis mediated by this monomer did not result in any DNA damage necessary to completely kill the cells and plausibly resorted to other mechanisms to finalise the bystander apoptosis. In support of this hypothesis, previous studies have proven soluble gp120-CD4 interactions in conformational changes that expose CD4i epitopes (Richard et al., 2016). The exposed CD4i epitopes generate an antibody response against the uninfected cells increasing their susceptibility to antibody dependent cellular cytotoxicity (ADCC) which results in cell death (Richard et al., 2018). ADCC is a mechanism implemented by the immune system to target and eradicate virally infected cells by recruiting natural killer cells. These cells lyse and kill target cells by releasing proteases and granzyme B (Pollara et al., 2011). Interestingly, HIV-1 infected cells were protected from ADCC while bystander uninfected T cells (from PBMCs) were highly sensitive to CD4i mediated ADCC as a result of soluble gp120 binding to the CD4 receptors (Richard et al., 2016). Therefore to determine whether gp120_{FVC} mediated bystander cell death co-functions with immune responses such as ADCC, forthcoming studies could evaluate whether the gp120_{FVC} treated T cells

are recognizable by ADCC mediating antibodies such as A32 in the presence of natural killer cells.

Contrary to the findings in this study, soluble gp120 in previous studies was able to mediate DNA fragmentation after 12-48 hours of treatment (Anand and Ganju, 2006, Green et al., 2013, Joshi et al., 2014, Ullrich et al., 2000). The discrepancies between the findings in the current study and previous literature can be attributed to differences in cell lines, target receptor, gp120 sequences and concentrations, as well as the DSB detection method. In the current study, concentrations of 50-500 nM of a FVC based gp120_{FVC} were used to mediate apoptosis of Jurkat T cells via CD4 receptor signalling and DSB were detected using a Multicolour DNA damage assay which measured co-phosphorylation and recruitment of DNA repair proteins such as ATM and H2A.X. However, the previous studies it was compared to have used cell lines such as HUVEC, HeLa, CHO, PBMCs, measured apoptosis via both CD4 and co-receptor binding to 10-100 ng/ml Envs and detected DSB using TUNEL assay based on the ability of terminal deoxynucleotidyl transferase (TdT) to label blunt ends (3'OH) of DSB. Although a study by Anand and Ganju, 2006 also used a Jurkat T cell line (JE6.1) to test gp120-mediated apoptosis, the apoptosis induction was based on gp120 concurrent interactions with CD4, CD45 and CXCR4 co-receptors on the surface of the Jurkat T cells. In contrast, the Jurkat T cell line used in the current study expressed only the CD4 receptor without expression of any co-receptor and was previously tested with antibodies to confirm the lack of this co-receptor expression. Therefore, apoptosis induction in the Anand and Ganju, 2006 study was possibly attributed to the presence of the CD45 and CXCR4 co-receptor. Also the differences in previously used Env sequences such as the HIV-1 subtype B IIB gp120 strain (Anand and Ganju, 2006, Ullrich et al., 2000), primary Envs (Joshi et al., 2014) and the FVC sequence used in the current study could imply differences in phenotypes contributing to differences in CD4 engagement and the observed discrepancies in DNA fragmentation.

To prove without reasonable doubt that the bystander apoptosis mediated by gp140_{SOSIP}, gp140_{GCN4} and gp120_{FVC} occurred exclusively via CD4 signalling, a heat denatured control of each Env conformation was included in all apoptosis assays. The heat denaturation was expected to induce loss of conformation integrity, distort the conformation of the CD4 binding site and perturb functionality of each Env.

Overall and as expected, low to negligible levels of apoptosis were observed when the Jurkat T cells were treated with this heat denatured control proving exclusive mediation of bystander apoptosis by the trimeric and monomeric Env conformations via CD4 signalling. However, in instances where some levels of apoptosis were observed in the heat denatured Envs, we assumed heat driven precipitation of the Envs out of solution, which was proven by evaluation of protein folding and unfolding patterns (Figure 3.18). Therefore these precipitates plausibly induced apoptosis via mechanisms other than CD4 signalling. Although the heat denatured Envs were able to prove bystander apoptosis through CD4 signalling, the low levels of apoptosis observed in some instances suggests that the Envs were not completely inactive. Heat denaturation was likely incomplete, or partial refolding of the protein occurred following denaturation, with reconstitution of the CD4 binding sites, albeit to a small amount. Therefore, future studies could involve either blocking the CD4 receptor on Jurkat T cells with anti-CD4 antibodies or completely depleting the receptor with small interfering RNAs and monitoring Env-mediated bystander apoptosis in this context. An additional hypothesis to test is whether different Env conformations bind to different epitopes on the CD4 molecule, thereby accounting for the different apoptotic signalling pathways initiated following Env exposure.

In conclusion, the current study has proven the ability of monomeric and trimeric Env conformations to induce bystander apoptosis of Jurkat T cells exclusively via CD4 signalling, albeit using different mechanisms. The trimeric gp140_{SOSIP} and gp140_{GCN4} preferentially induced bystander apoptosis via the intrinsic pathway with onset reversible DNA fragmentation. However apoptosis induction by the gp140_{SOSIP} was not associated with PS translocation while the gp140_{GCN4} trimer showed PS translocation. The monomeric gp120_{FVC} induced bystander apoptosis via intrinsic and extrinsic pathways with low levels PS translocation and no DNA fragmentation. These findings give insight into the pathogenesis of HIV infection. This study has also shown that shed soluble gp120 monomers cause bystander apoptosis via CD4 signalling, which contributes to CD4⁺ T cell depletion in HIV-1 infected individuals, a hallmark of AIDS. Moreover, different conformations of gp140 trimers can induce bystander apoptosis, but the variable results imply differences in CD4 binding affinities and signal activation. To delineate the differences in CD4 binding affinities, future studies will involve determination of Env-CD4 binding kinetics using surface

plasmon resonance. Therapies that could block Env-mediated bystander apoptosis may be beneficial for reduction of CD4⁺ T cell depletion and prolong progression from HIV infection to AIDS.

Appendix A: Composition of solutions used in this study

The compositions of all reagents and buffer solutions used in this study are represented in Tables 1-10 below.

Table 1: Solutions for bacterial cell culture and transformation

| Solution | Composition |
|------------------------------|---|
| LB broth | 5 g NaCl (Sigma-Aldrich, Steinheim, Germany), 5 g yeast extract (Biolab, Wadeville, Gauteng, South Africa), 10 g Tryptone (Oxoid, Hampshire, England) and dH ₂ O was added to a final 1 litre volume. The media was autoclaved at 121 °C for 20 minutes, left to cool at RT and stored at 4 °C until use. |
| LB agar plates | 12 g of LB agar powder (Biolab, Wadeville, Gauteng, South Africa) was added 1 litre of LB broth. The agar was autoclaved at 121 °C for 20 minutes, left to cool at RT and appropriate antibiotic was added at final concentration of 100 µg/ml (Ampicillin) or 50 µg/ml (Kanamycin). Once cool, the 25 ml agar was poured into each 90 mm petri dish, left to set at RT and stored at 4 °C until use. |
| Transformation buffer | 1.4702 g of 100 mM CaCl ₂ (Sigma-Aldrich, Steinheim, Germany), 0.3024 g of 10 mM PIPES HCl (Boehringer Mannheim, GmbH, Germany), 15 ml of 15 % glycerol (Merck, Hohenbrunn, Germany) were mixed with dH ₂ O to a final 1 L volume. The buffer pH was adjusted to 7.0 with 10 M NaOH (Merck KGaA, Darmstadt, Germany). |
| Ampicillin stock (100 mg/ml) | 1 g of Ampicillin (Roche, Basel, Switzerland) was dissolved in a final 10 ml volume of dH ₂ O and stored at -20 °C until use. |
| Kanamycin stock (50 mg/ml) | 0.5 g of Kanamycin (Gibco Life Technologies, USA) was dissolved in a final 10 ml volume of dH ₂ O and stored at -20 °C until use. |

Table 2: Buffer solutions used during plasmid DNA isolation.

| Buffer solution | Composition |
|--|---|
| Re-suspension buffer P1 (50 mM Tris-Cl, pH 8.0, 10 mM EDTA, 100 µg/ml RNase A) | 6.06 g Tris base, 3.72 g EDTA-2H ₂ O were dissolved in 800 ml dH ₂ O. The pH was adjusted to 8.0 with HCl before making up solution to 1 litre with dH ₂ O. A 100 mg of RNase A was added per 1 litre buffer P1 and buffer was stored at 4 °C. |
| Lysis buffer P2 (200 mM NaOH, 1 % SDS) | 8.09 g of NaOH pellets were dissolved in 950 ml dH ₂ O and 50 ml 20 % SDS solution to a final volume of 1 litre. Buffer was stored at RT. |
| Neutralization buffer P3 (3.0 M potassium acetate, pH 5.5) | 294.5 g Potassium Acetate was dissolved in 500 ml dH ₂ O and pH was adjusted to 5.5 with glacial acid before making up the buffer to 1 litre with dH ₂ O. The buffer was stored at 4 °C. |
| Equilibration buffer QBT (750 mM NaCl, 50 mM MOPS, pH 7.0, 15 % isopropanol, 0.15 % Triton X-100) | 43.83 g NaCl, 10.46 g MOPS (free acid) were dissolved in 800 ml dH ₂ O and the pH was adjusted to 7.0 with NaOH. Following pH adjustment, 150 ml pure isopropanol and 15 ml 10 % Triton X-100 solution were added. The buffer volume was made up to 1 litre with dH ₂ O and stored at RT. |
| Wash buffer QC (1.0 M NaCl, 50 mM MOPS, pH 7.0, 15 % isopropanol) | 8.44 g NaCl and 10.46 g MOPS (free acid) were dissolved in 800 ml dH ₂ O. The pH was adjusted to 7.0 with NaOH prior addition of 150 ml pure isopropanol. The buffer was made to a final volume of 1 litre with dH ₂ O and stored at RT. |
| Elution buffer QF (1.25 M NaCl, 50 mM Tris-Cl, pH 8.5, 15 % isopropanol) | 73.05 g NaCl and 6.06 g Tris base were dissolved in 800 ml dH ₂ O and the pH was adjusted to 8.5 with HCl. Following pH adjustment, 150 ml pure isopropanol was added, the buffer volume was adjusted to 1 litre and stored at RT. |

The solutions were adapted from the (Qiagen Maxi kit manual, Qiagen, Maryland, USA).

Table 3: Solutions and buffers used for agarose gel electrophoresis

| Agarose gel electrophoresis reagent | Composition |
|--|---|
| 2x loading dye (LD) | 2x loading dye was prepared per sample by diluting 7 µl of 6x Orange LD (ThermoFisher Scientific, Rockford, IL, USA) with 13 µl dH ₂ O. The diluted 2x LD was then mixed with each DNA sample in equal volumes prior loading to the gel. |
| 0.8 % agarose gel | 0.8 g of SeaKem LE Agarose (Lonza Biosciences, Singapore, Asia) was dissolved in 100 ml 1x TAE buffer through heating in the microwave. The dissolved solution was left to cool for 10 minutes and 3 µl of Ethidium bromide solution was added as a fluorescent tag for DNA. The gel was left to set in a gel casting system until use. The gel was prepared before each use. |

Table 4: SDS-PAGE reagents

| Solution | Composition |
|---|--|
| Monomer solution (30.8 % acrylamide, 2.7 % bisacrylamide) | 60 g acrylamide and 1.6 g bisacrylamide (Sigma-Aldrich, Steinheim, Germany) were dissolved in 200 ml dH ₂ O; container was covered with foil to avoid exposure to light and stored at 4 °C until use. |
| 10 % Sodium Dodecyl Sulphate (SDS) | 10 g SDS (Merck, Darmstadt, Germany) was dissolved in 100 ml and stored at RT. |
| 10 % Ammonium persulfate (APS) | 0.1 g APS (Sigma-Aldrich, Steinheim, Germany) was dissolved in 1 ml dH ₂ O. This solution was prepared fresh for each use. |
| 2x loading buffer (0.125 M Tris-HCl, 4 % SDS, 20 % glycerol) | 2.5 ml 4x stacking gel, 4 ml 10 % SDS, 2 ml Glycerol (Merck, Darmstadt, Germany), 1 mg Bromophenol blue (Saarchem, Midrand, South Africa), 500 µl β-Mercaptoethanol (Sigma-Aldrich; Steinheim, Germany) were mixed to a final volume of 10 ml with dH ₂ O. The buffer was stored at -20 °C until use. |
| 4x running/separating gel buffer (1.5 M Tris-HCl, pH 8.8) | 36.3 g Tris (Sigma-Aldrich, Steinheim, Germany) was dissolved in 150 ml dH ₂ O and the pH was adjusted to 8.8 with HCl prior addition of dH ₂ O to a final volume of 200 ml. The buffer was stored at 4 °C in the dark. |
| 4x stacking gel buffer (0.5 M Tris-HCl pH 6.8) | 3 g Tris (Sigma-Aldrich, Steinheim, Germany) was dissolved in 40 ml dH ₂ O and the pH was adjusted to 6.8 with HCl prior addition of dH ₂ O to a final volume of 50 ml. The buffer was stored at 4 °C in the dark. |
| 10x tank buffer (0.025 M Tris, 0.192 M glycine, 0.1 % SDS, pH 8.3) | 30.28 g Tris (Sigma-Aldrich, Steinheim, Germany), 144.13 g Glycine (Merck, Darmstadt, Germany) and 10 g SDS (Merck, Darmstadt, Germany) were dissolved in 1 litre dH ₂ O. The solution was stored at RT and diluted 10 times before use. |
| 8 % separating gel | 4 ml of 30.8 % acrylamide, 2.7 % bisacrylamide monomer solution, 3.75 ml 4x separating gel buffer, 150 µl 10 % |

| | |
|------------------|---|
| | SDS and 7.05 ml dH ₂ O were mixed together. The solution was polymerized with 75 µl of 10 % APS and 15 µl Tetramethylethylenediamine (TEMED, Sigma-Aldrich; Steinheim, Germany). |
| 4 % stacking gel | 940 µl of 30.8 % acrylamide, 2.7 % bisacrylamide monomer solution, 1.75 ml 4x stacking gel buffer, 10 % SDS and 4.3ml dH ₂ O were mixed together. The solution was polymerized with 35 µl of 10 % APS and 15 µl TEMED (Sigma-Aldrich; Steinheim, Germany). |

Table 5: Western blot buffers

| Solution | Composition |
|--|--|
| 10x Tris-buffered saline (TBS, pH 7.4) | 30 g Tris, 144.1 g Glycine, 2 g KCl and 10 g NaCl (Sigma-Aldrich; Steinheim, Germany) were dissolved in 950 ml dH ₂ O and pH was adjusted to 7.4 using HCl. The solution was made up to 1 litre with dH ₂ O, autoclaved at 121 °C for 20 minutes and stored at RT until use. |
| Transfer buffer (20 % methanol, 80 % 1x tank buffer, pH 9.2) | 200 ml Methanol (Merck Chemicals, Saarchem, Wadeville, South Africa), 100 ml 10x tank buffer and 700 ml dH ₂ O were mixed together and stored until use. |
| 5 % Skimmed milk blocking solution | 5 g Skimmed milk (Pick n Pay, South Africa) was dissolved in 100 ml 1x T-TBS. The blocking solution was prepared fresh for each use. |
| 0.1 % Tween 20-Trisma Buffered Saline (T-TBS) | 100 ml 10x TBS was added to 900 ml dH ₂ O and 1 ml Tween-20 (Saarchem, Midrand, South Africa) was added to the solution with gentle mixing. The solution was prepared fresh when required. |

Table 6: Lectin affinity chromatography buffers

| Solution | Composition |
|------------------------------------|---|
| 0.5 M NaCl | 29.22 g NaCl was dissolved in 1 litre 1× PBS (Sigma-Aldrich, Steinheim, Germany) and stored at RT until use. |
| 1 M NaCl | 58.44 g NaCl was dissolved in 1 litre 1× PBS (Sigma-Aldrich, Steinheim, Germany) and stored at RT until use. |
| 1 M methyl -manno-pyranoside (MMP) | 9.709 g MMP was dissolved in 50 ml 1× PBS (Sigma-Aldrich, Steinheim, Germany). This solution was prepared fresh for each use. |
| 20 % Ethanol | 200 ml 100 % Ethanol was added to 800 ml dH ₂ O and stored at RT until required. |

Table 7: Size exclusion chromatography buffers

| Solution | Composition |
|-----------------|--|
| 0.5 M NaOH | 500 ml 1 M NaOH (Sigma-Aldrich, Steinheim, Germany) was added to 500 ml SEC water and autoclaved at 121 °C for 20 minutes. The solution was left to cool and stored at RT until required. |
| 20 % Ethanol | 200 ml 100 % Ethanol (Sigma-Aldrich, Steinheim, Germany) was added to 800 ml SEC water and autoclaved at 121 °C for 20 minutes. The solution was left to cool and stored at RT until required |
| 70 % Ethanol | 700 ml 100 % Ethanol (Sigma-Aldrich, Steinheim, Germany) was added to 300 ml SEC water and autoclaved at 121 °C for 20 minutes. The solution was left to cool and stored at RT until required. |
| 1× PBS | 100 ml 10× PBS (Sigma-Aldrich, Steinheim, Germany) was diluted was diluted in 900 ml SEC water and autoclaved at 121 °C for 20 minutes. The solution was left to cool and stored at RT until required. |

Table 8: CD4 purification buffers

| Buffer solution | Composition |
|---|--|
| Wash buffer 1 (50 mM Glycine, 0.5 M, NaCl, 2 mM β -Mercaptoethanol, 8 M Urea, 20 mM Imidazole) | 3.75 g Glycine, 21.33 g NaCl, 480 g Urea and 1.36 g Imidazole (Sigma-Aldrich, Steinheim, Germany) were dissolved in 1 litre dH ₂ O and buffer was stored at RT until use. |
| Wash buffer 2 (50 mM Glycine, 0.5 M, NaCl, 2 mM β -Mercaptoethanol, 8 M Urea, 50 mM Imidazole) | 3.75 g Glycine, 21.33 g NaCl, 480 g Urea and 3.40 g Imidazole were dissolved in 1 litre dH ₂ O and the buffer was stored at RT until use. |
| Elution buffer (50 mM Glycine, 0.5 M, NaCl, 2 mM β -Mercaptoethanol, 8 M Urea, 500 mM Imidazole) | 3.75 g Glycine, 21.33 g NaCl, 480 g Urea and 34 g Imidazole were dissolved in 1 litre ml dH ₂ O and the buffer was stored at RT until use. |
| Nickel sulphate recharge buffer (NiSO ₄) | 5.257 g NiSO ₄ (Sigma-Aldrich, Steinheim, Germany) was dissolved in 200 ml dH ₂ O and stored at RT until use. |

Table 9: CD4 refolding buffers

| Buffer solution | Composition |
|--|---|
| 0.5 M Ethylenediaminetetraacetic acid, pH 8 (EDTA) | 186.1 g Disodium EDTA (Sigma-Aldrich, Steinheim, Germany) was dissolved in 800 ml dH ₂ O and pH was adjusted to 8 with NaOH. The solution volume was adjusted to 1 litre and stored at RT until required. |
| 2 M NaOH | 8 g NaOH (Sigma-Aldrich, Steinheim, Germany) was dissolved in 100 ml dH ₂ O and autoclaved at 121 °C for 20 minutes. The solution was left to cool and stored at RT until use. |
| Folding buffer A (50 mM Glycine, 10 % Sucrose, 1 mM EDTA, 1 mM oxidised Glutathione synthetase (GSSG), 0.1 mM | 3.75 g Glycine, 100 g Sucrose, 240 g Urea, 0.31 g GSH and 0.06 g GSSG (Sigma-Aldrich, Steinheim, Germany) were dissolved in 900 ml dH ₂ O. 2 ml of 0.5 M EDTA stock and 7.8 ml of 2 M NaOH stock were added into the solution and pH was adjusted to 9.6 with NaOH. The solution |

| | |
|--|---|
| Glutathione (GSH), 4 M Urea, 15.6 mM NaOH, pH 9.6) | volume was adjusted to 1 litre with dH ₂ O and was prepared fresh prior each use. |
| Folding buffer B (15 mM Na ₂ CO ₃ , 35 mM NaHCO ₃ , 10 % Sucrose, 1 mM EDTA, 0.1 mM GSH, 0.01mM GSSG, pH 9.6) | 1.59 g Na ₂ CO ₃ , 2.93 g NaHCO ₃ , 100 g Sucrose, 0.031 g GSH and 0.006 g GSSG (Sigma-Aldrich, Steinheim, Germany) were dissolved in 900 ml dH ₂ O. 2 ml of 0.5 M NaOH stock was added to the solution and pH was adjusted to 9.6 with NaOH. The buffer volume was adjusted to 1 litre with dH ₂ O and prepared fresh for each use. |

Table 10: BCA protein standards

| Tube label | Volume of diluting agent (1× PBS) (μl) | Volume of BSA stock (μl) | Final BSA concentration (μg/ml) |
|-------------------|---|---------------------------------|--|
| A | 0 | 300 of stock | 2000 |
| B | 125 | 375 of stock | 1500 |
| C | 325 | 325 of stock | 1000 |
| D | 175 | 175 of tube B dilution | 750 |
| E | 325 | 325 of tube C dilution | 500 |
| F | 325 | 325 of tube E dilution | 250 |
| G | 325 | 325 of tube F dilution | 125 |
| H | 400 | 100 of tube G dilution | 25 |
| I | 400 | 0 | 0 (Blank) |

The standards were adapted from (Pierce™ BCA Protein Assay Kit, ThermoFisher Scientific, Rockford, IL, USA)

Appendix B- Quantification of purified plasmid DNA

All purified plasmid DNA were quantified by the Nanodrop and results were represented as follows

Quantification of purified plasmid DNA

The recombinant gp140_{SOSIP} VRC 3831 and Furin pcDNA 3.3 plasmid DNA were isolated from an overnight large scale culture of transformed *E.coli* DH5 α cells using a QIAGEN plasmid isolation kit. The isolated plasmid DNA was quantified by the Nano drop through absorbance spectra analysis.

Absorbance spectra analysis was conducted as measure of DNA purity through comparison of absorbance at 260 and 280 nm wavelengths (A_{260} / A_{280} ratio). DNA absorbs light at 260 nm while proteins absorb at 280 nm and the standard A_{260} / A_{280} ratio of 1.8 is indicative of pure DNA while a ratio less than 1.8 suggests contamination of the DNA by proteins. The gp140_{SOSIP} VRC 3831 and Furin pcDNA 3.3 demonstrated A_{260} / A_{280} ratio of 1.97 and 1.96 respectively, indicating that the isolated plasmid DNA was pure (Figure 3B1). Presence of potential contaminants other than proteins such as phenol, residual guanidine from the purification column were accounted for by comparing absorbance at 230 nm and 260 nm for DNA i.e. A_{260} / A_{230} ratio. A standard A_{260} / A_{230} ratio ranging from 2 to 2.2 is acceptable for pure DNA without residual guanidine and phenol. Analysis of gp140_{SOSIP} VRC 3831 and Furin pcDNA 3.3 isolated plasmids demonstrated A_{260} / A_{230} ratios of 2.44 and 2.14 respectively (Figure 3B1). This was confirmation that the isolated plasmids DNA were of sufficient purity.

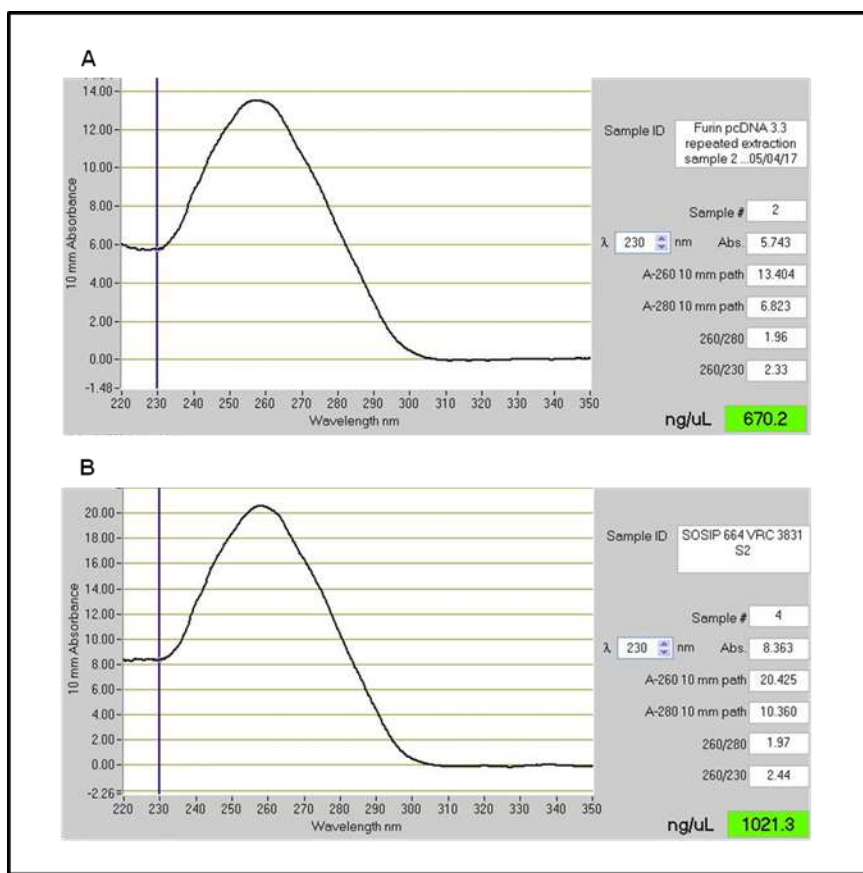


Figure 3B1: Spectra analysis and quantification of QIAGEN maxi kit isolated plasmid DNA. A. Absorbance spectra was measured at 260 nm using the Nano drop for detection and confirmation of isolated Furin pcDNA 3.3, 280 nm for detection of contaminating proteins, $A_{260} / 280$ of 1.96 and $A_{260} / 230$ of 2.33 for evaluation of purity and a concentration of 670.2 ng/μl was quantified. **B.** Absorbance spectra of gp140_{SOSIP} VRC 3831 isolated plasmid DNA demonstrated $A_{260} / 280$ of 1.97 and $A_{260} / 230$ of 2.44 as indicators of DNA purity and a concentration of 1021.3 ng/μl was quantified.

Appendix C- Annexin V data

Post treatment of the Jurkat T cells with controls and varying concentrations of gp140_{SOSIP}, gp140_{GCN4} and gp120_{FVC} over 24, 48 and 72 hours, Annexin V and 7-AAD detected apoptosis via PS translocation using flow cytometry. The results are represented as scatter plots for each time point including replicates (Figure 3C1-6).

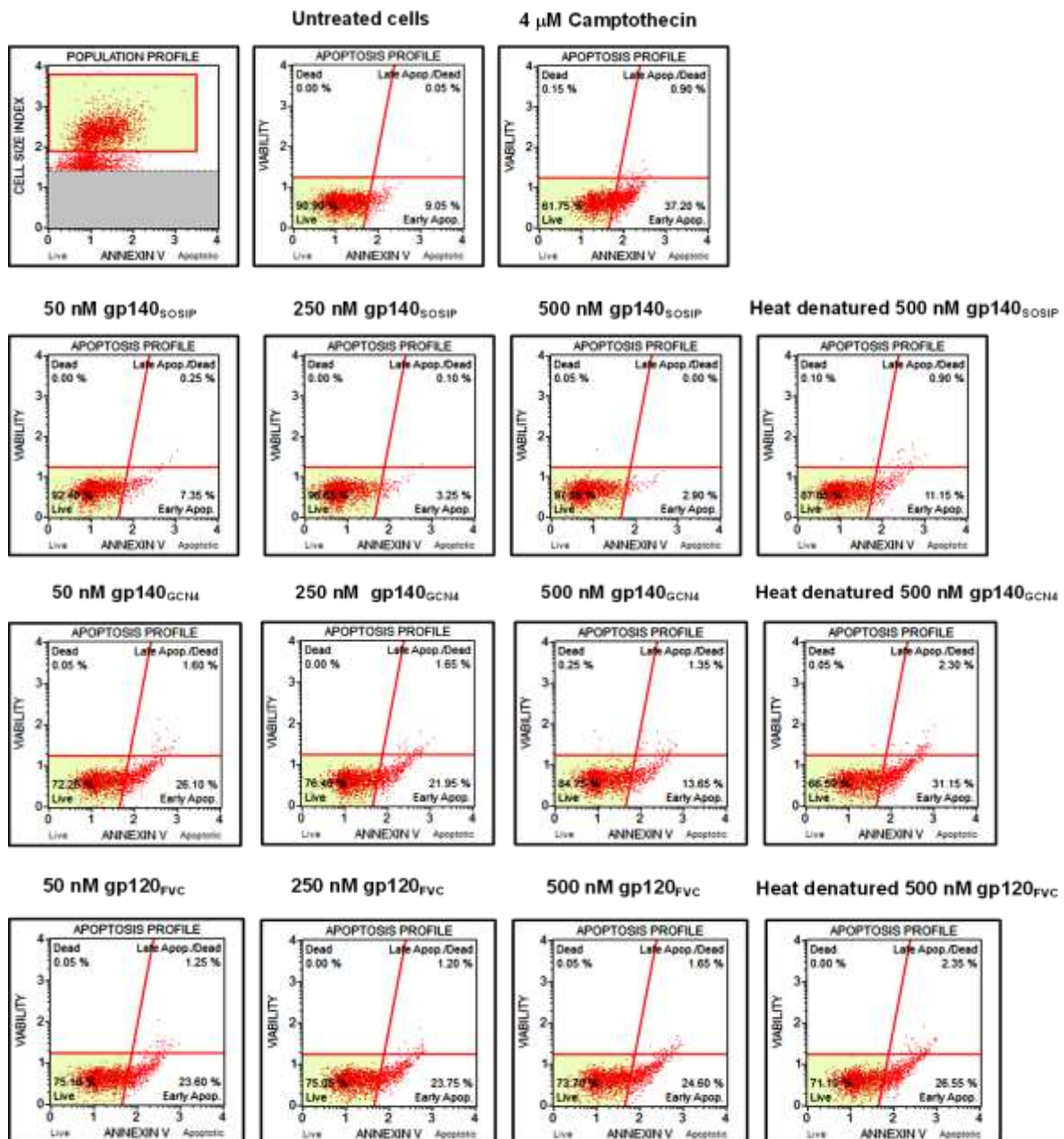


Figure 3C1: Annexin V flow cytometry scatter plots post 24 hours of Jurkat T cells treatment with 50 to 500 nM concentrations of gp140_{SOSIP}, gp140_{GCN4} and gp120_{FVC}. Each plot is a representative of first replicate at this time point.

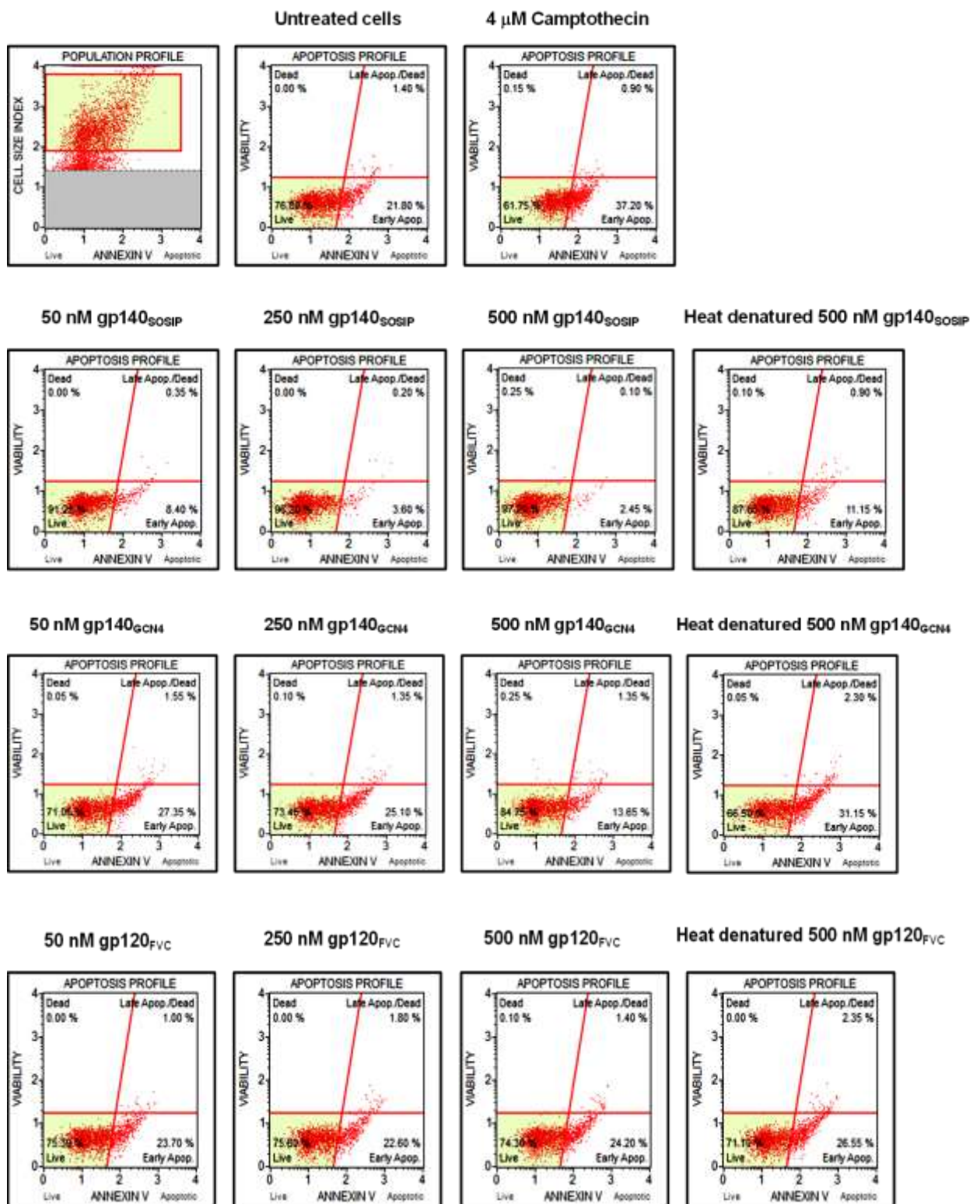


Figure 3C2: Annexin V flow cytometry scatter plots post 24 hours of Jurkat T cells treatment with 50 to 500 nM of gp140_{SOSIP}, gp140_{GCN4} and gp120_{FVC}. Each plot is a representative of the second replicate at this time point.

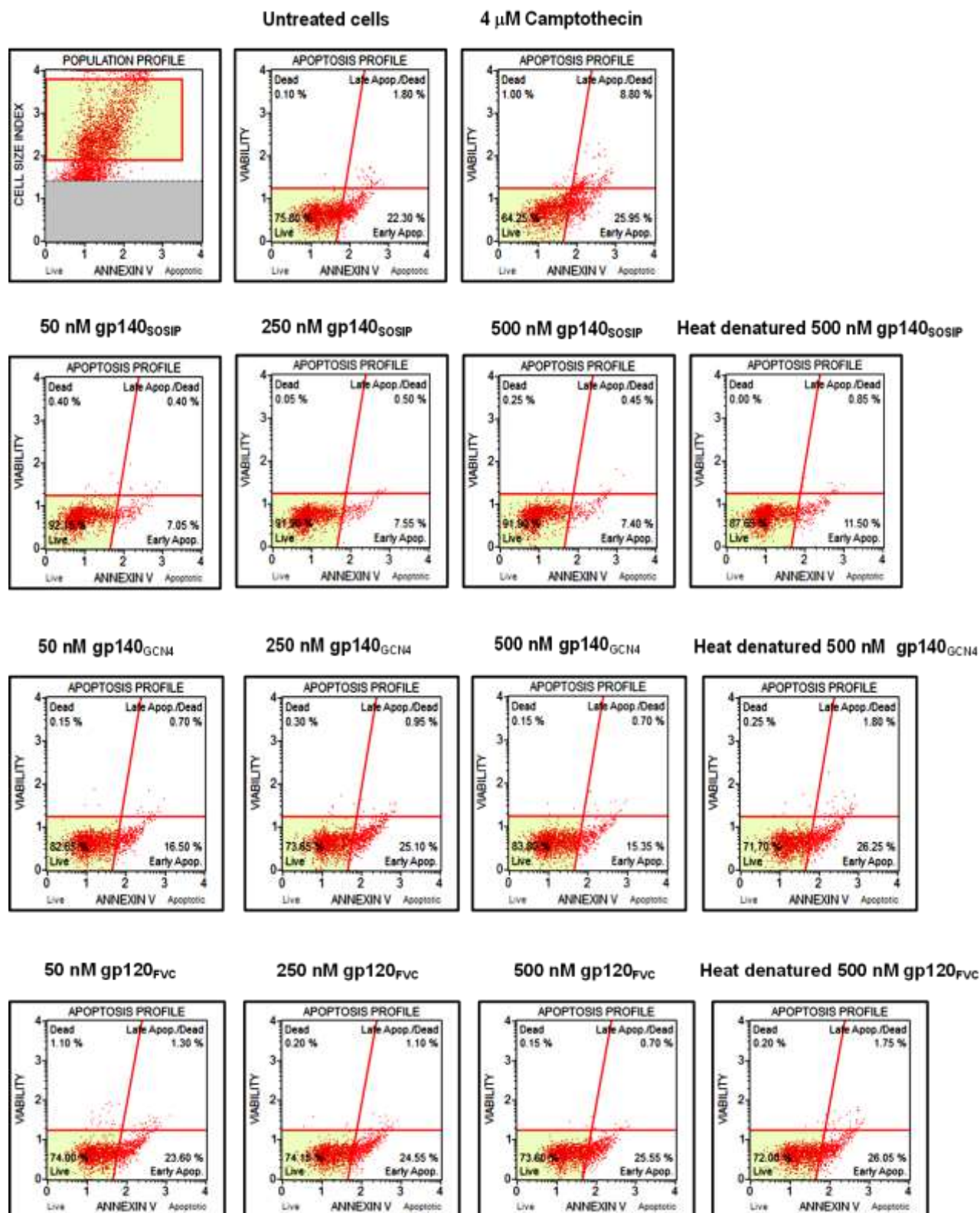


Figure 3C3: Annexin V flow cytometry scatter plots post 48 hours of Jurkat T cells treatment with 50 to 500 nM of gp140_{SOSIP}, gp140_{GCN4} and gp120_{FVC}. Each plot is a representative of the first replicate at this time point.

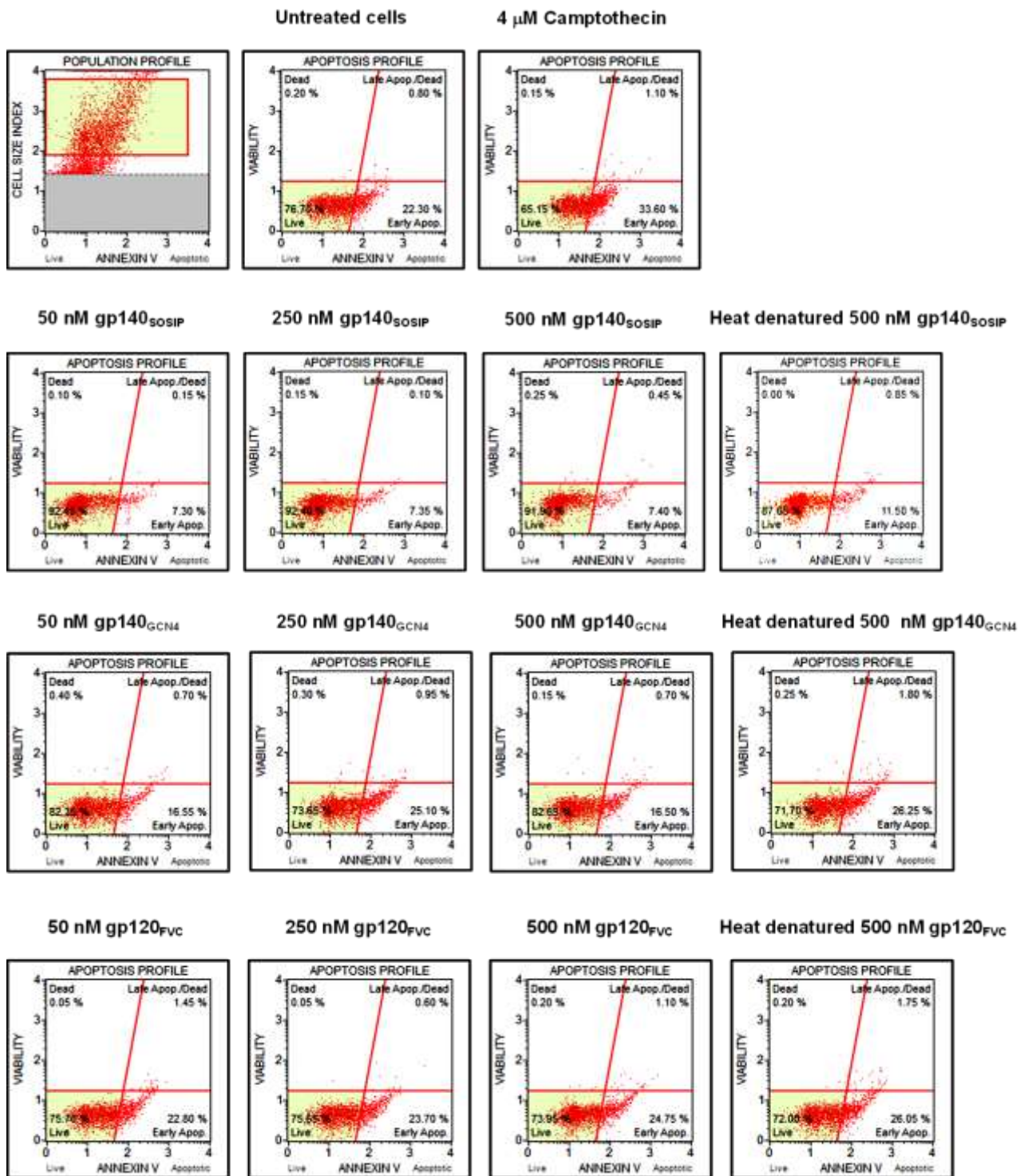


Figure 3C4: Annexin V flow cytometry scatter plots post 48 hours of Jurkat T cells treatment with 50 to 500 nM of gp140_{SOSIP}, gp140_{GCN4} and gp120_{FVC}. Each plot is a representative of the second replicate at this time point.

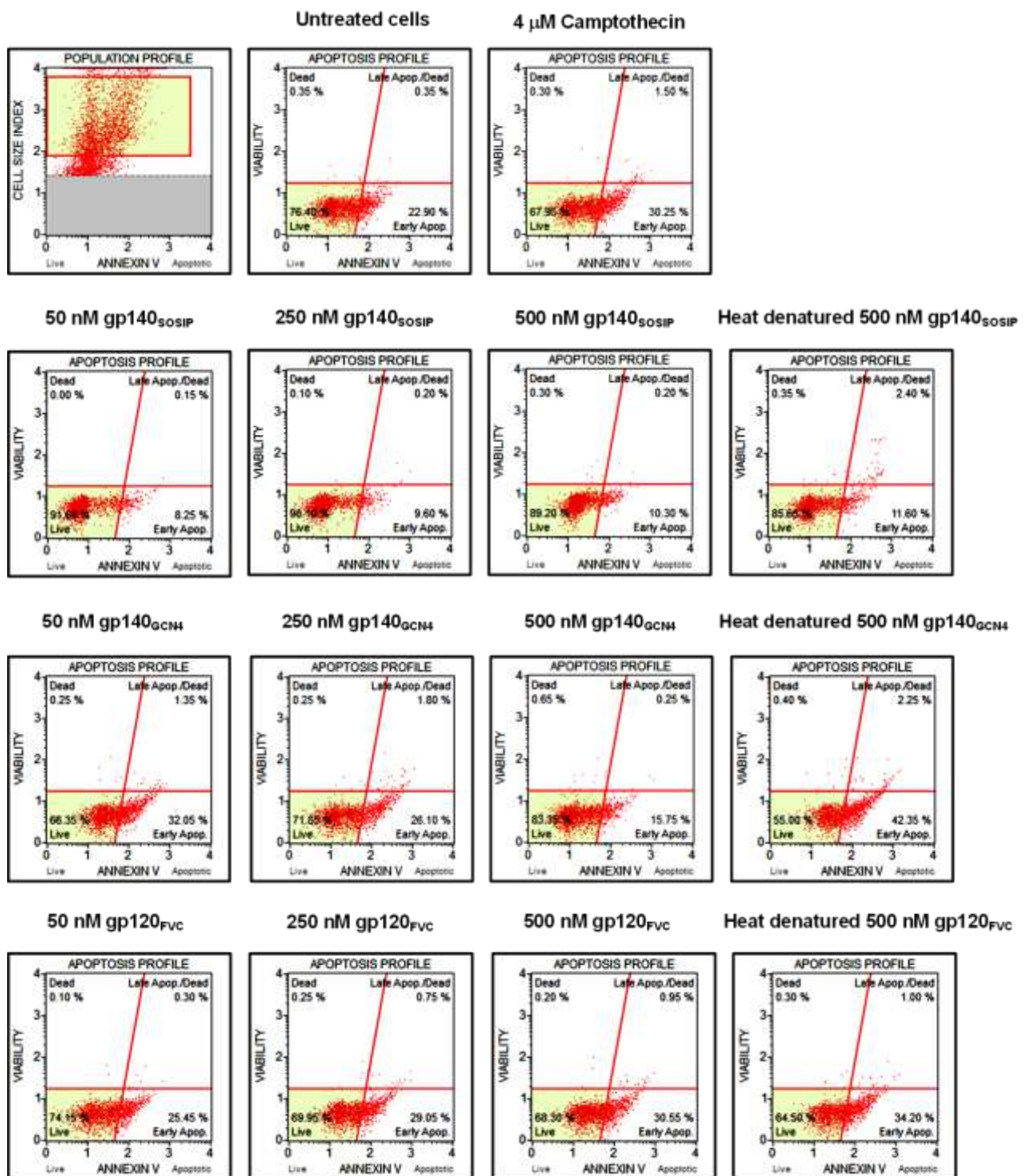


Figure 3C5: Annexin V flow cytometry scatter plots post 72 hours of Jurkat T cells treatment with 50 to 500 nM of gp140_{SOSIP}, gp140_{GCN4} and gp120_{FVC}. Each plot is a representative of the first replicate at this time point.

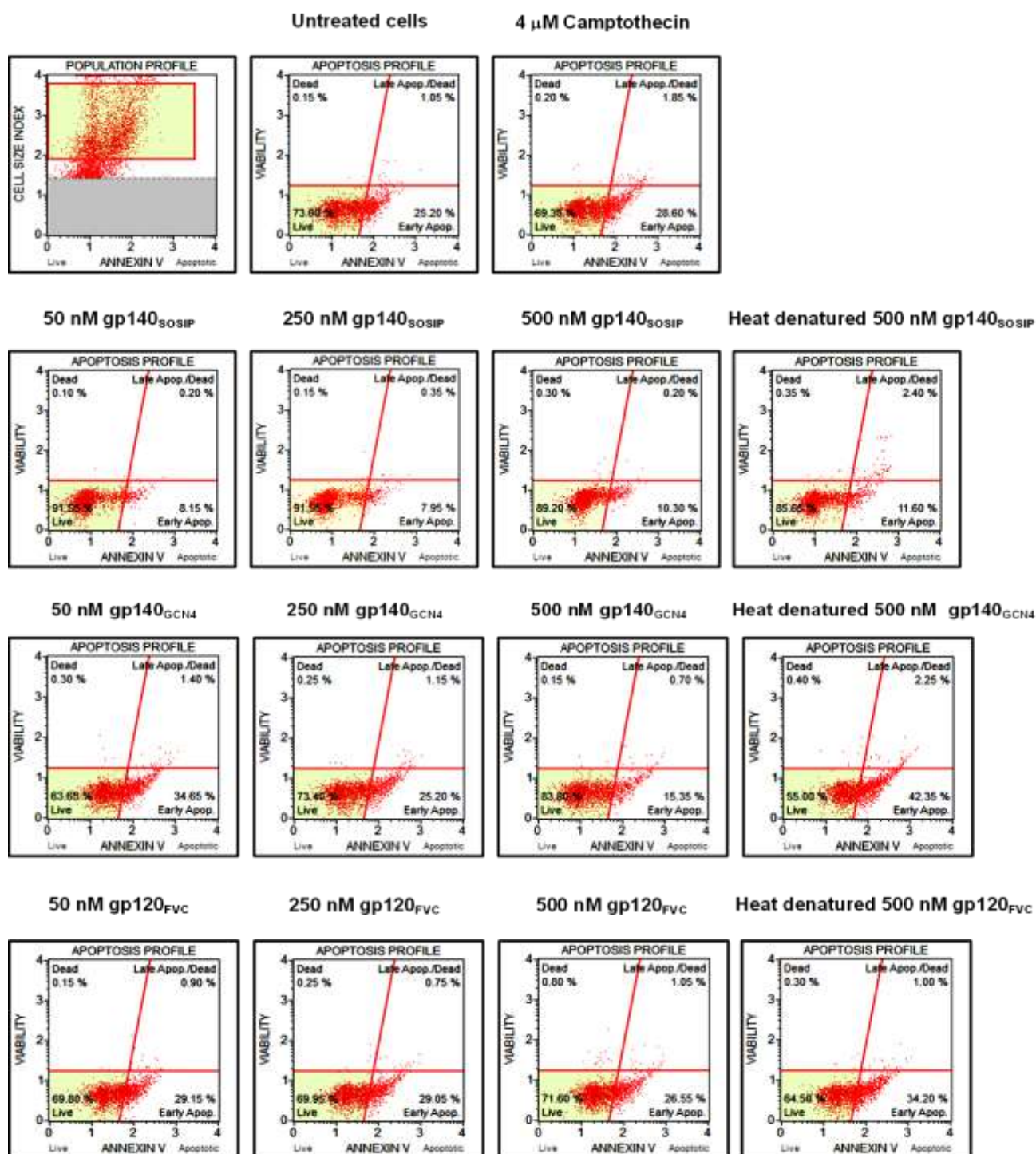


Figure 3C6: Annexin V flow cytometry scatter plots post 72 hours of Jurkat T cells treatment with 50 to 500 nM of gp140_{SOSIP}, gp140_{GCN4} and gp120_{FVC}. Each plot is a representative of the second replicate at this time point.

Appendix D- Mitopotential data

Jurkat T cells were treated with varying concentrations of gp140_{SOSIP}, gp140_{GCN4} and gp120_{FVC} to induce apoptosis over 24, 48 and 72 hours. At each time point, the treated cells including controls were analysed by mitopotential assay using flow cytometry to detect intrinsic apoptosis. Results are represented as scatter plots for each time point including replicates (Figure 3D1- 6).

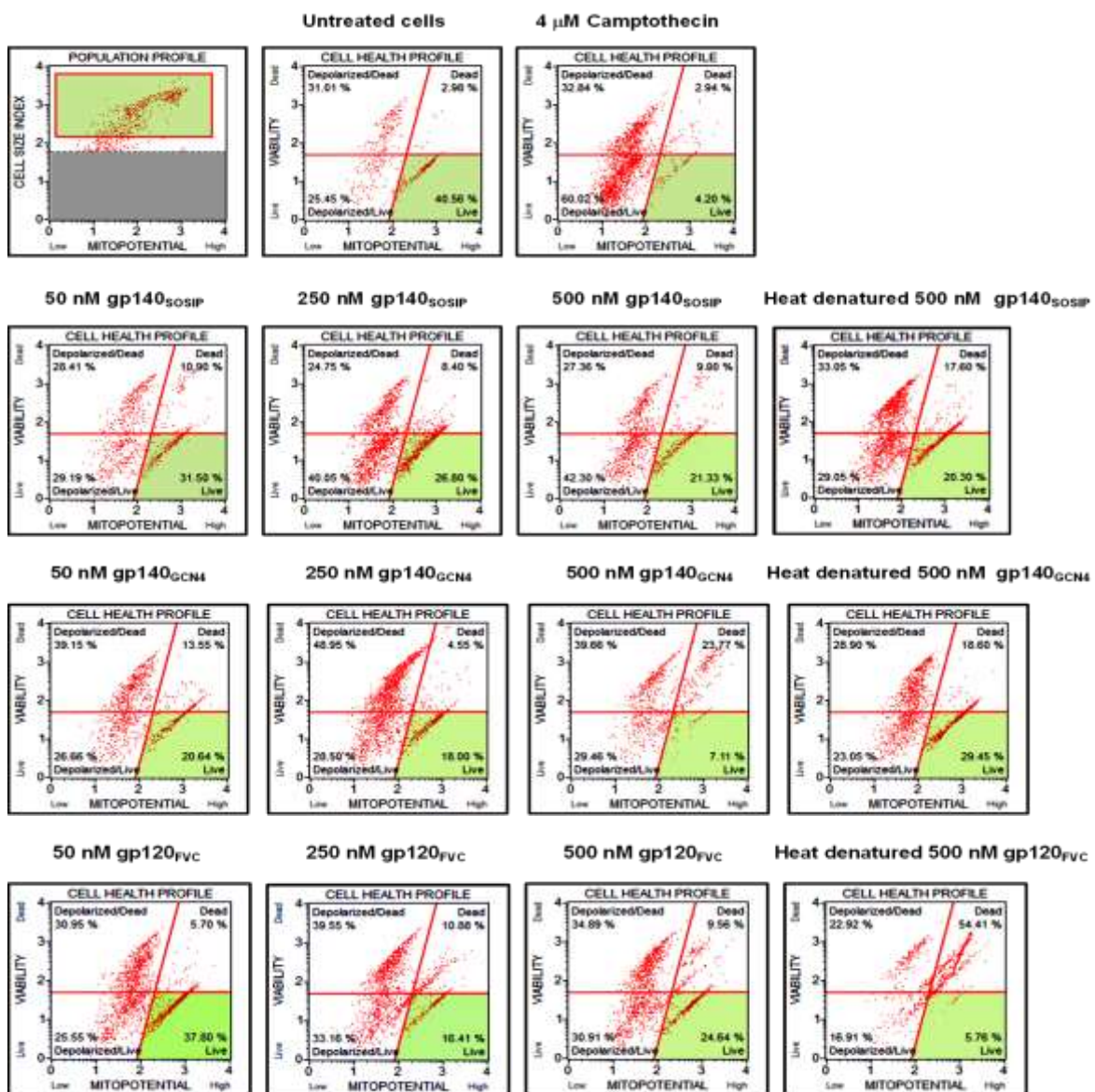


Figure 3D1: Mitopotential assay flow cytometry scatter plots post 24 hours of Jurkat T cells treatment with 50 to 500 nM of gp140_{SOSIP}, gp140_{GCN4} and gp120_{FVC}. Each plot is a representative of first replicate at this time point.

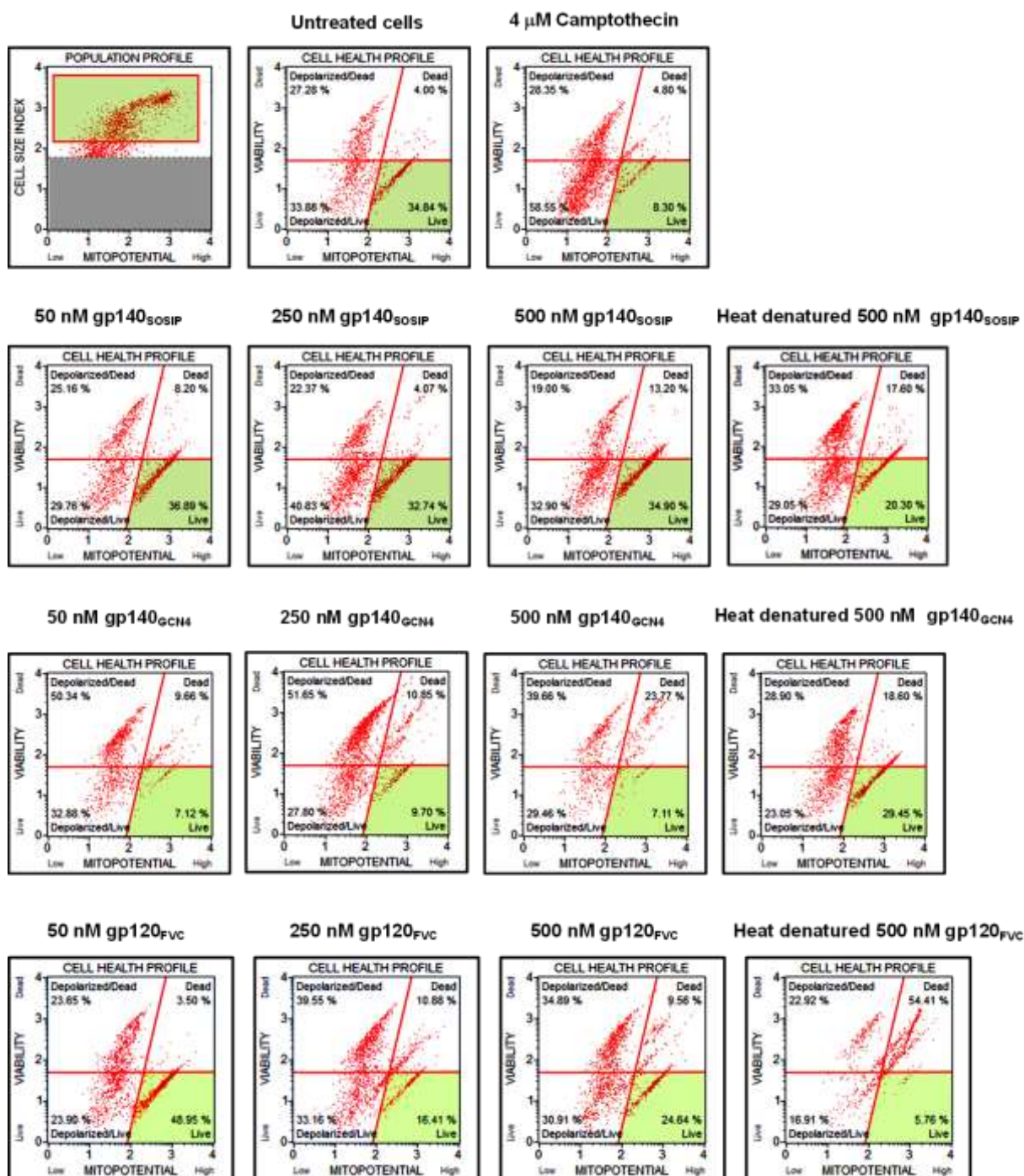


Figure 3D2: Mitopotential assay flow cytometry scatter plots post 24 hours of Jurkat T cells treatment with 50 to 500 nM of gp140_{SOSIP}, gp140_{GCN4} and gp120_{FVC}. Each plot is a representative of the second replicate at this time point.

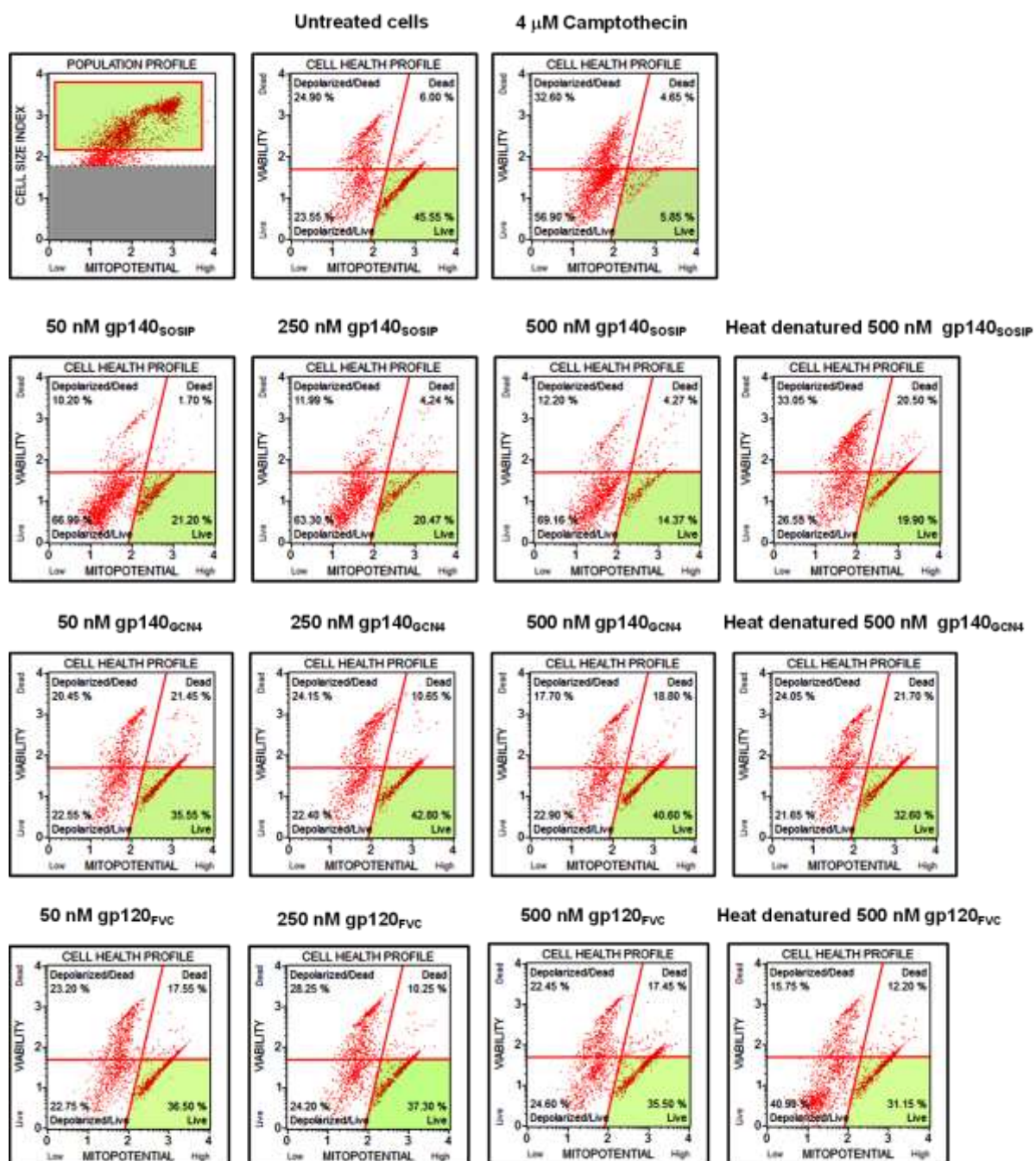


Figure 3D3: Mitopotential assay flow cytometry scatter plots post 48 hours of Jurkat T cells treatment with 50 to 500 nM of gp140_{SOSIP}, gp140_{GCN4} and gp120_{FVC}. Each plot is a representative of the first replicate at this time point.

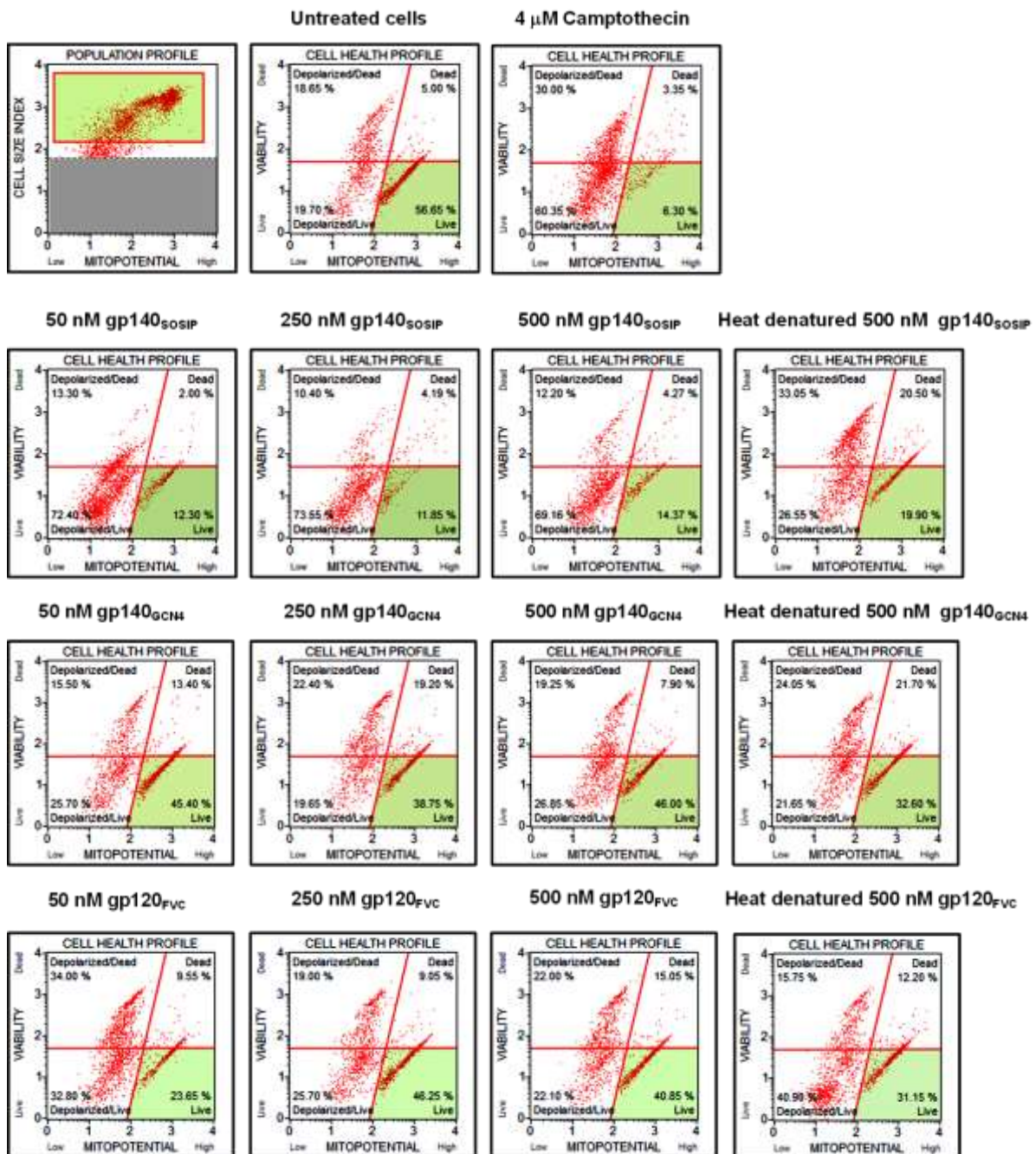


Figure 3D4: Mitopotential assay flow cytometry scatter plots post 48 hours of Jurkat T cells treatment with 50 to 500 nM of gp140_{SOSIP}, gp140_{GC14} and gp120_{FVC}. Each plot is a representative of the second replicate at this time point.

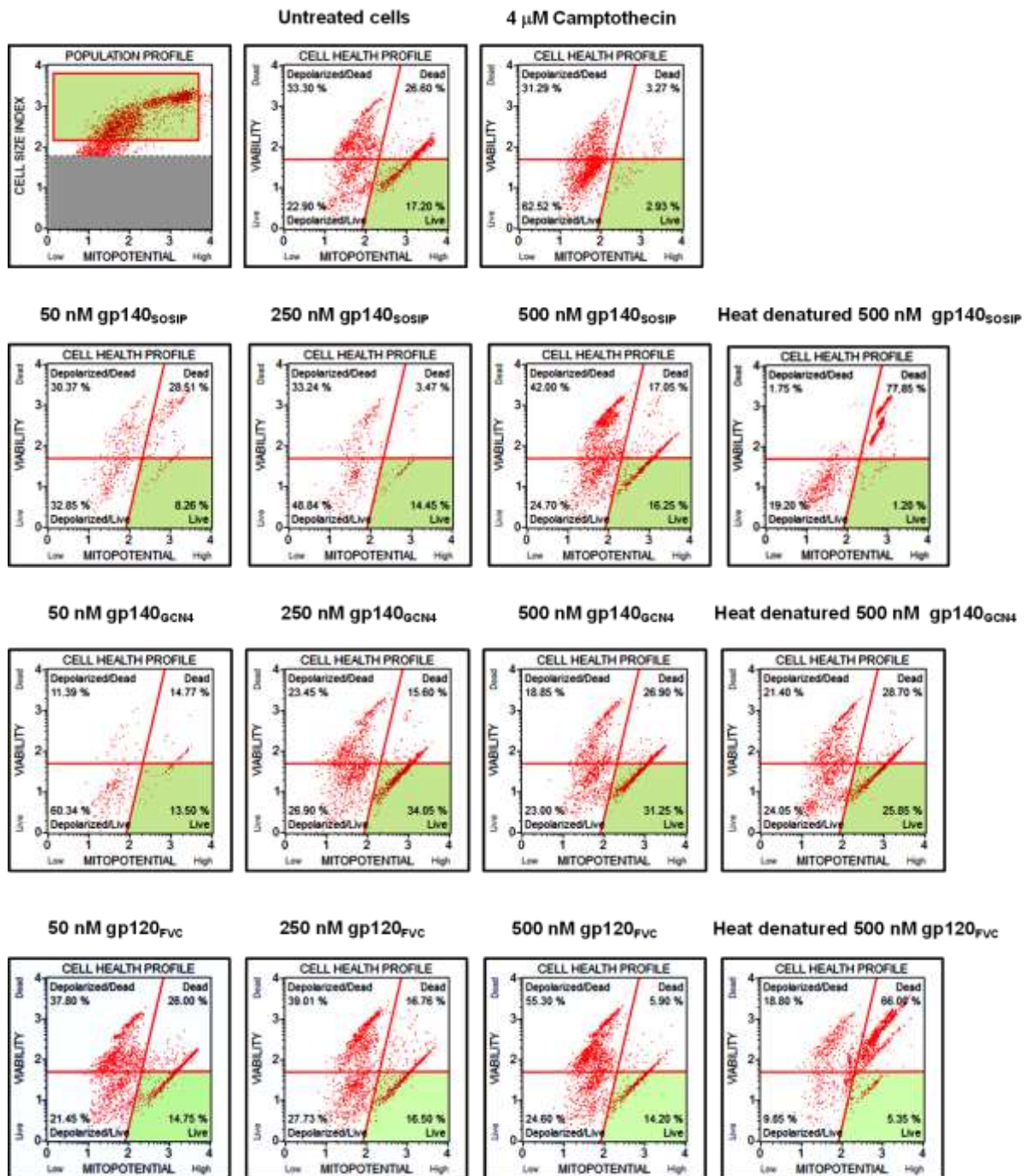


Figure 3D5: Mitopotential assay flow cytometry scatter plots post 72 hours of Jurkat T cells treatment with 50 to 500 nM of gp140_{SOSIP}, gp140_{GCN4} and gp120_{FVC}. Each plot is a representative of the first replicate at this time point.

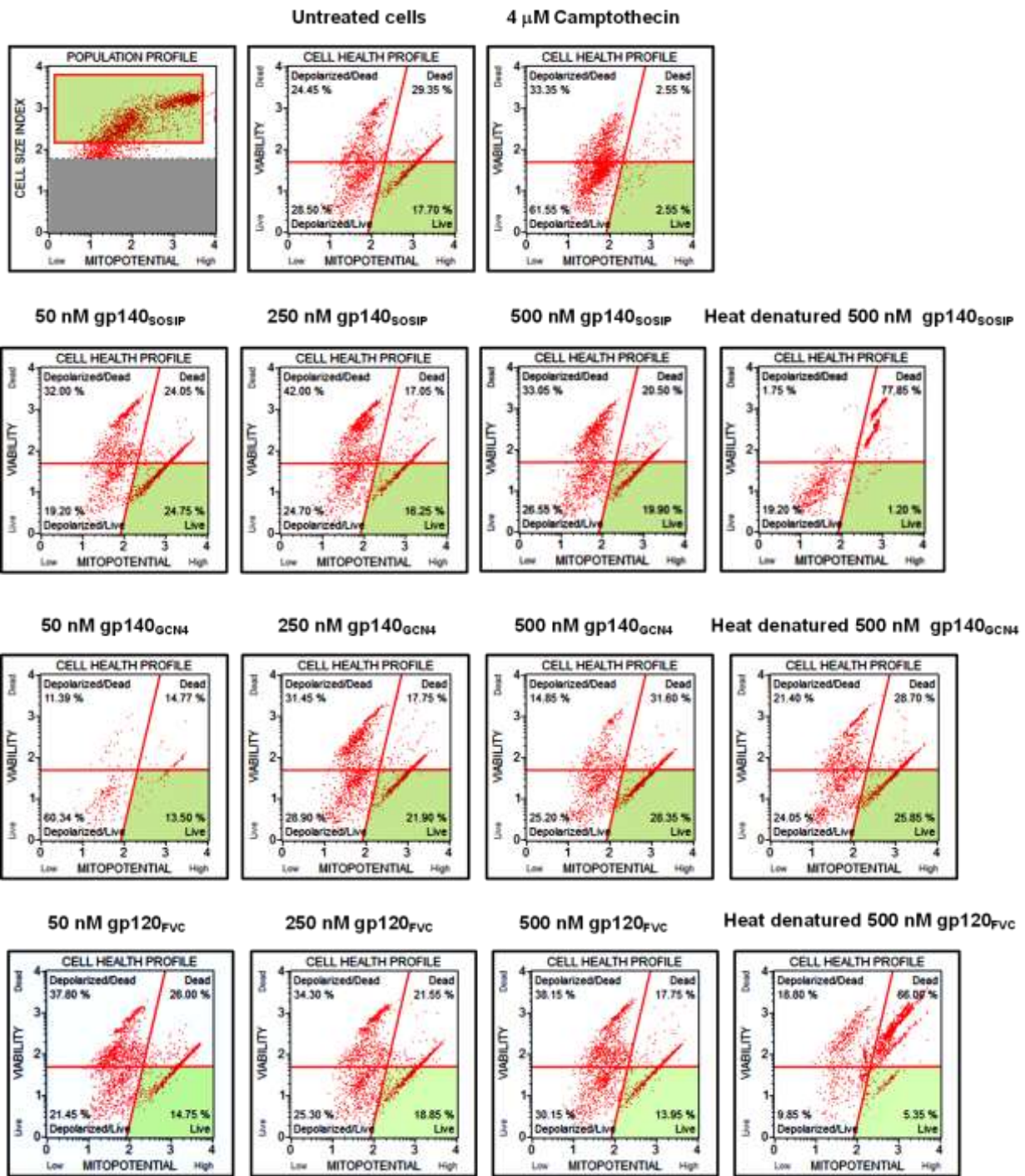


Figure 3D6: Mitopotential assay flow cytometry scatter plots post 72 hours of Jurkat T cells treatment with 50 to 500 nM of gp140_{SOSIP}, gp140_{GCN4} and gp120_{FVC}. Each plot is a representative of the second replicate at this time point.

Appendix E- Caspase 3/7 activation data

Jurkat T cells were treated with varying concentrations of gp140_{SOSIP}, gp140_{GCN4} and gp120_{FVC} including controls over 24, 48 and 72 hours. Thereafter, the cells were analysed for caspase 3/7 activation using flow cytometry to detect apoptosis via extrinsic pathway. The results at each time point are represented at scatter plots including replicates (Figure 3E1 - 6).

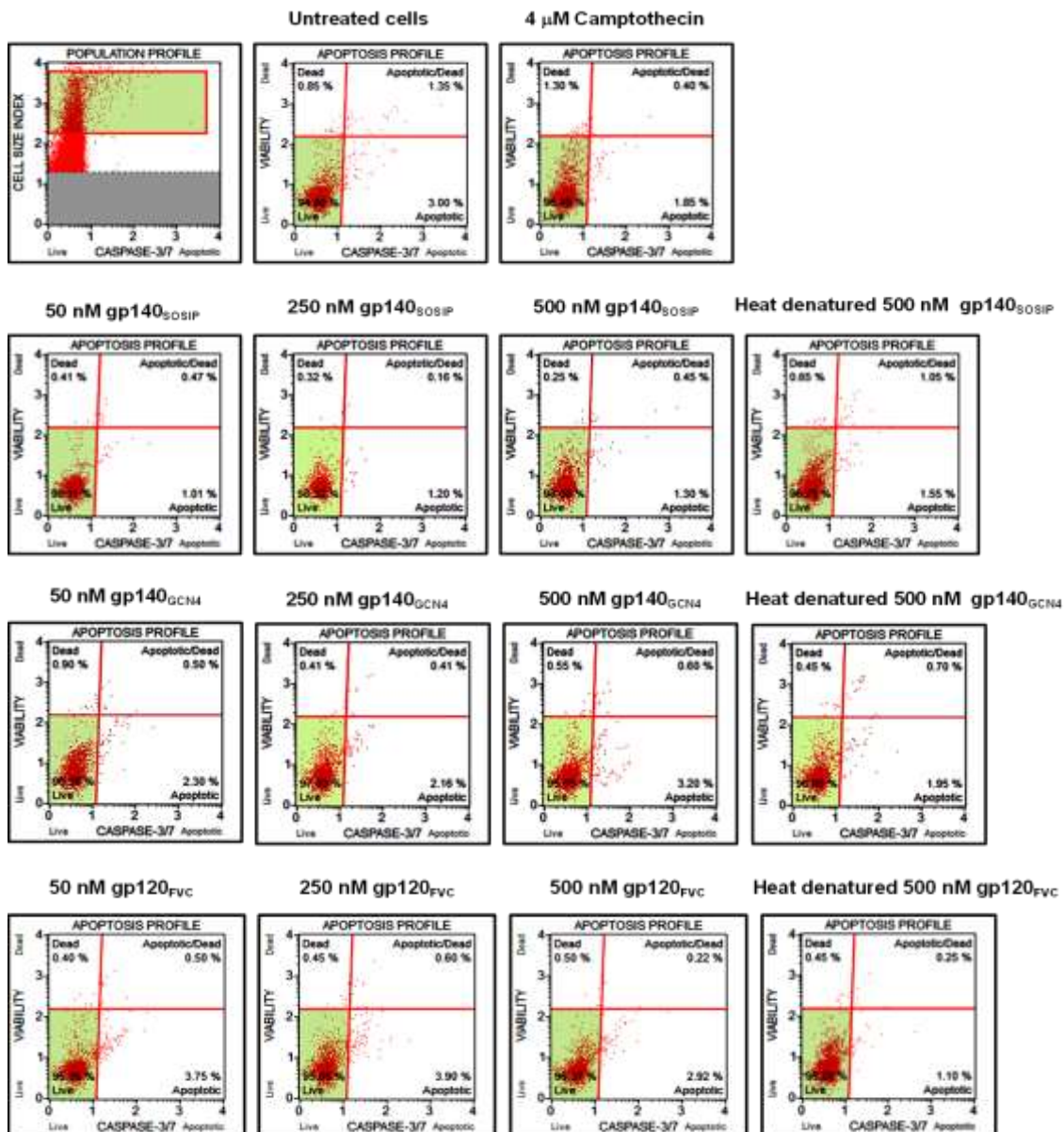


Figure 3E1: Caspase 3/7 activation flow cytometry scatter plots post 24 hours of Jurkat T cells treatment with 50 to 500 nM of gp140_{SOSIP}, gp140_{GCN4} and gp120_{FVC}. Each plot is a representative of the first replicate at this time point.

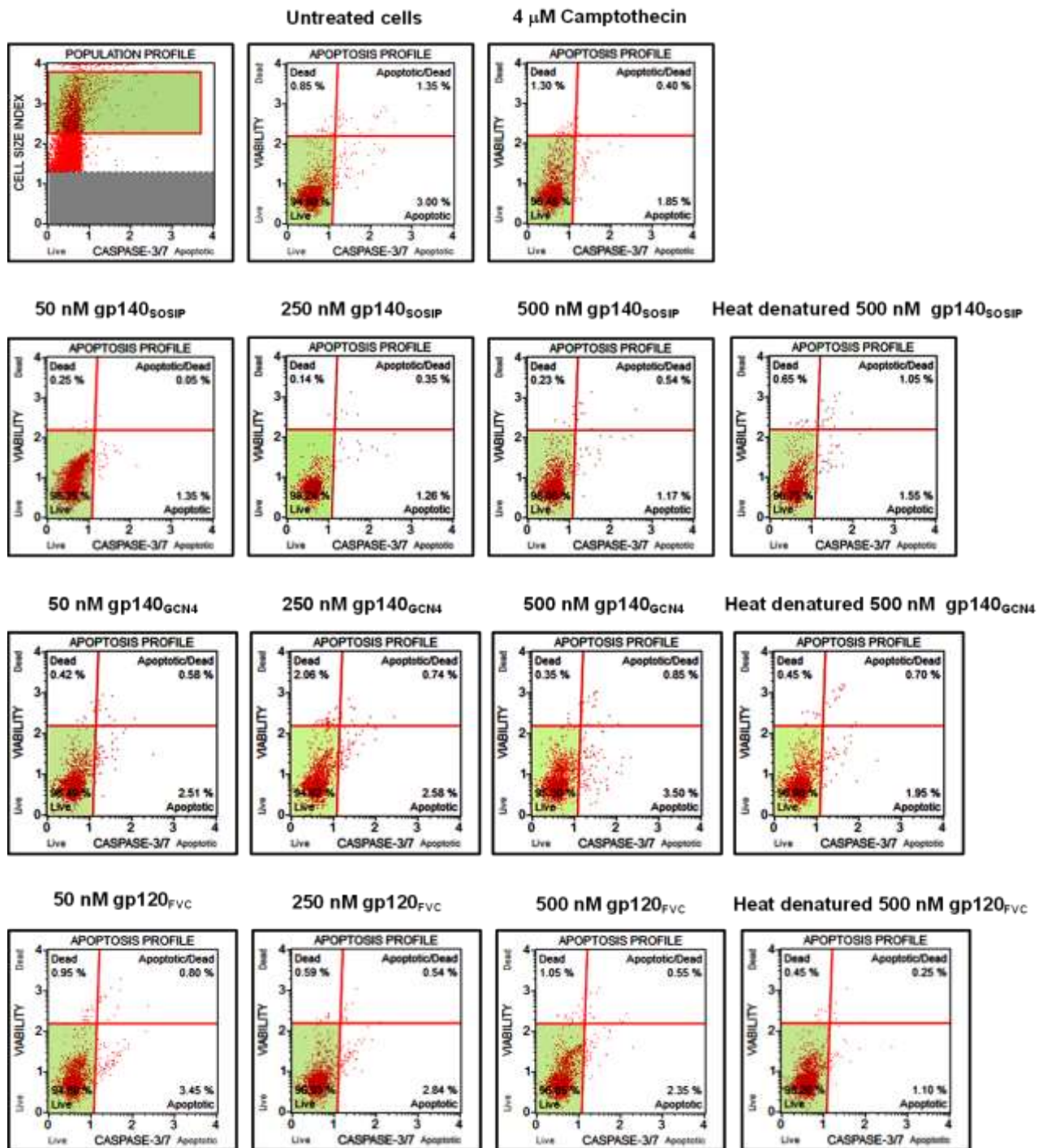


Figure 3E2: Caspase 3/7 activation flow cytometry scatter plots post 24 hours of Jurkat T cells treatment with 50 to 500 nM of gp140_{SOSIP}, gp140_{GCN4} and gp120_{FVC}. Each plot is a representative of the second replicate at this time point.

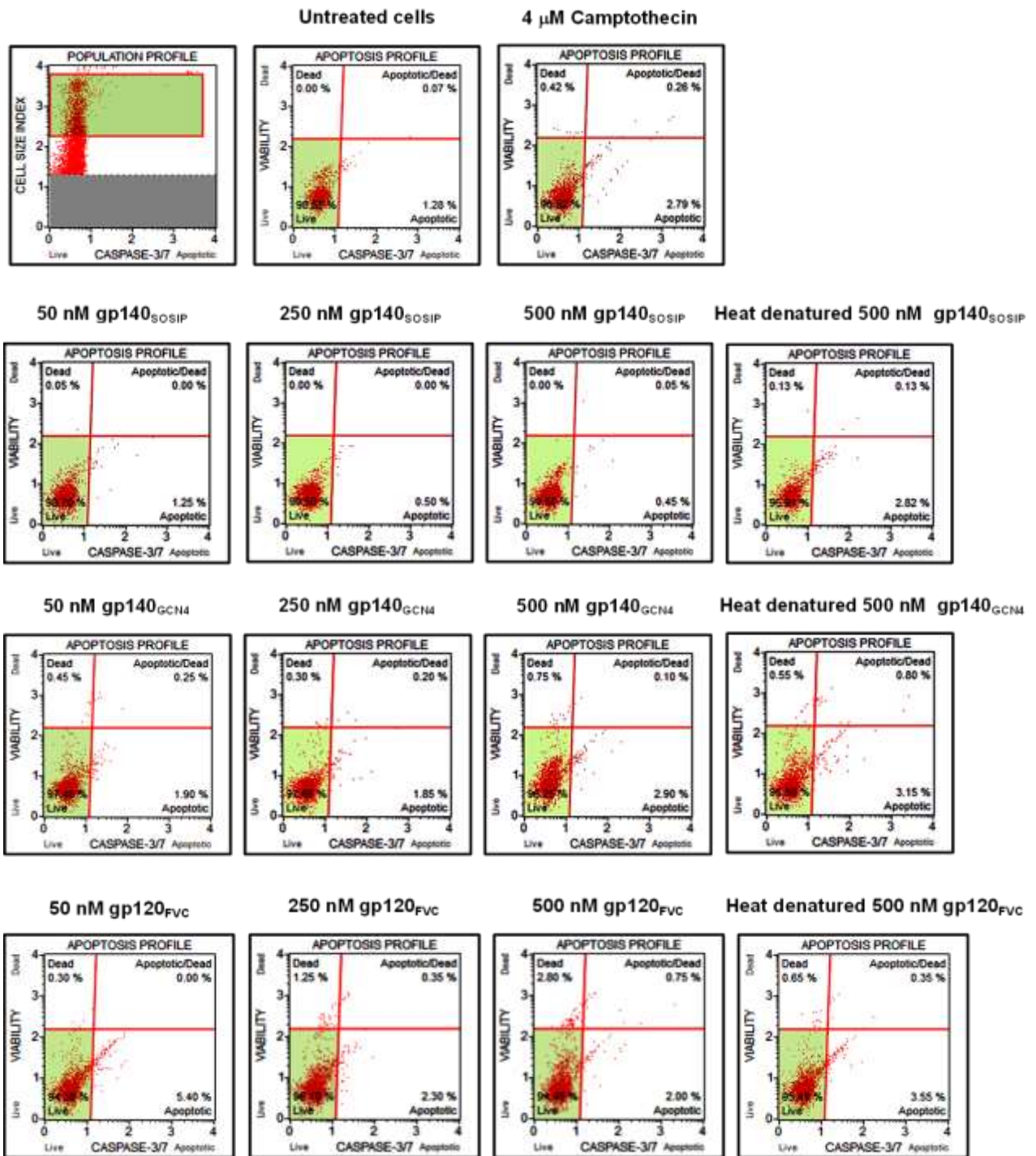


Figure 3E3: Caspase 3/7 activation flow cytometry scatter plots post 48 hours of Jurkat T cells treatment with 50 to 500 nM of gp140_{SOSIP}, gp140_{GCN4} and gp120_{FVC}. Each plot is a representative of the first replicate at this time point.

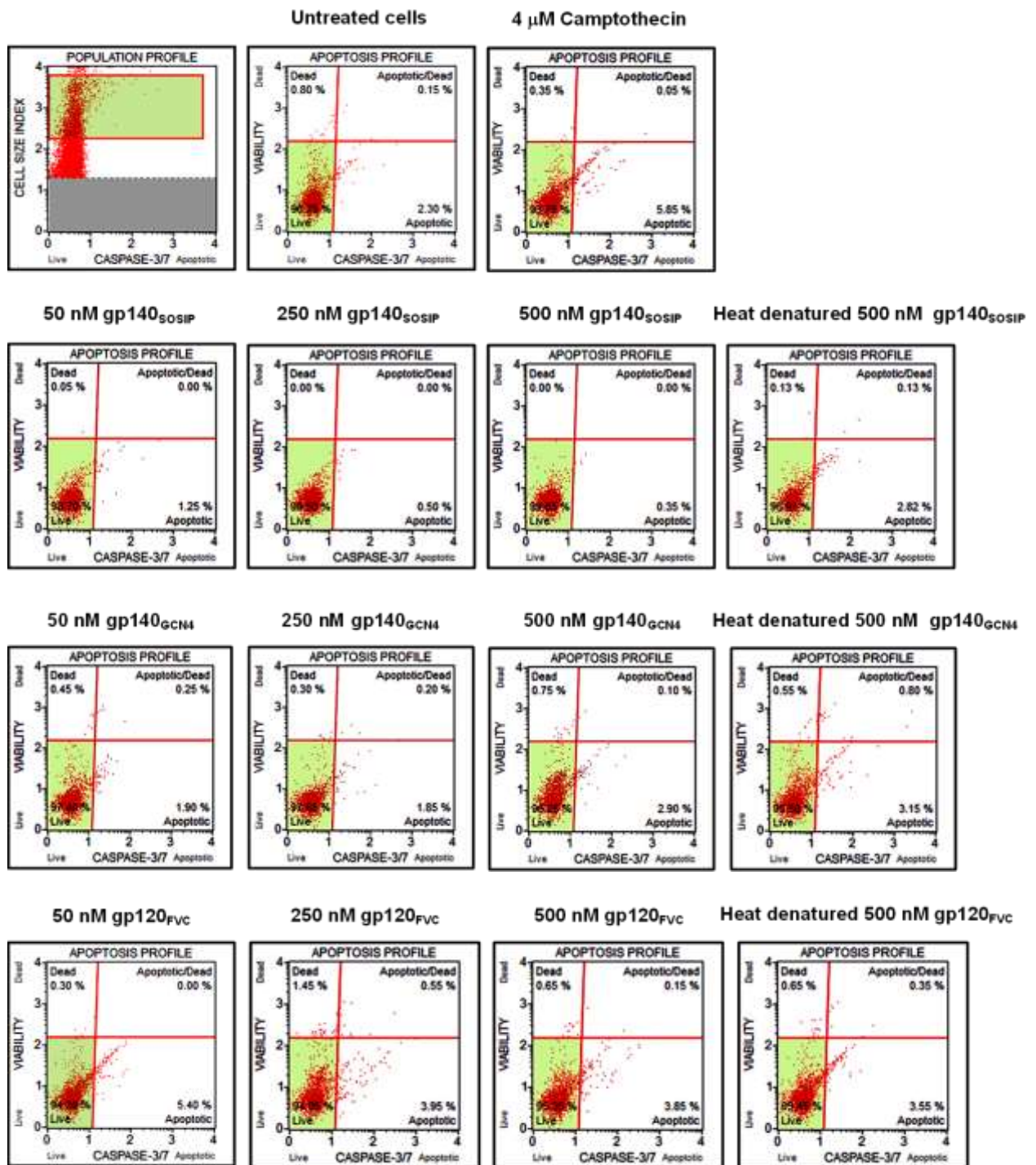


Figure 3E4: Caspase 3/7 activation flow cytometry scatter plots post 48 hours of Jurkat T cells treatment with 50 to 500 nM of gp140_{SOSIP}, gp140_{GC4} and gp120_{FVC}. Each plot is a representative of the second replicate at this time point.

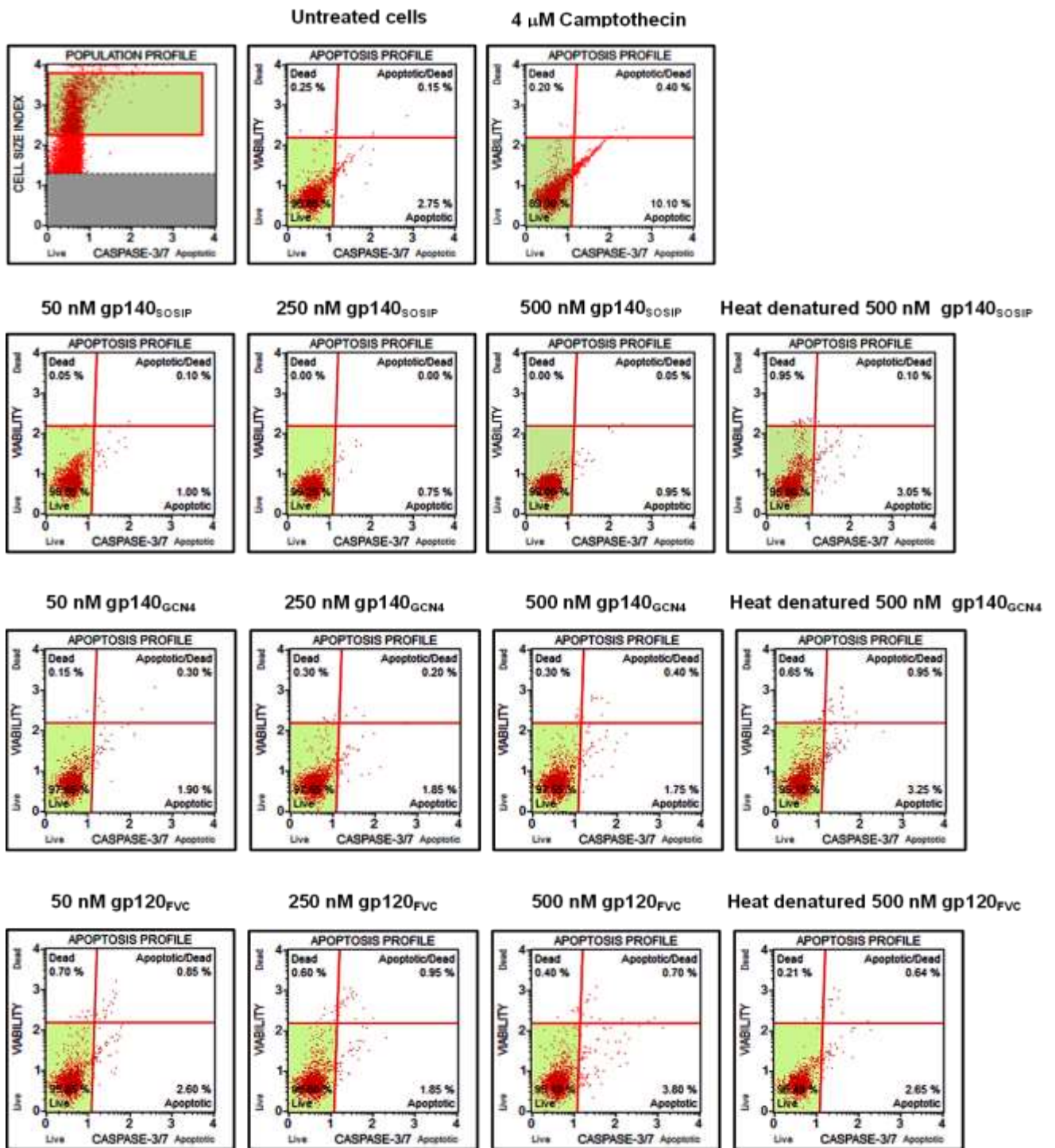


Figure 3E5: Caspase 3/7 activation flow cytometry scatter plots post 72 hours of Jurkat T cells treatment with 50 to 500 nM of gp140_{SOSIP}, gp140_{GC4} and gp120_{FVC}. Each plot is a representative of the first replicate at this time point.

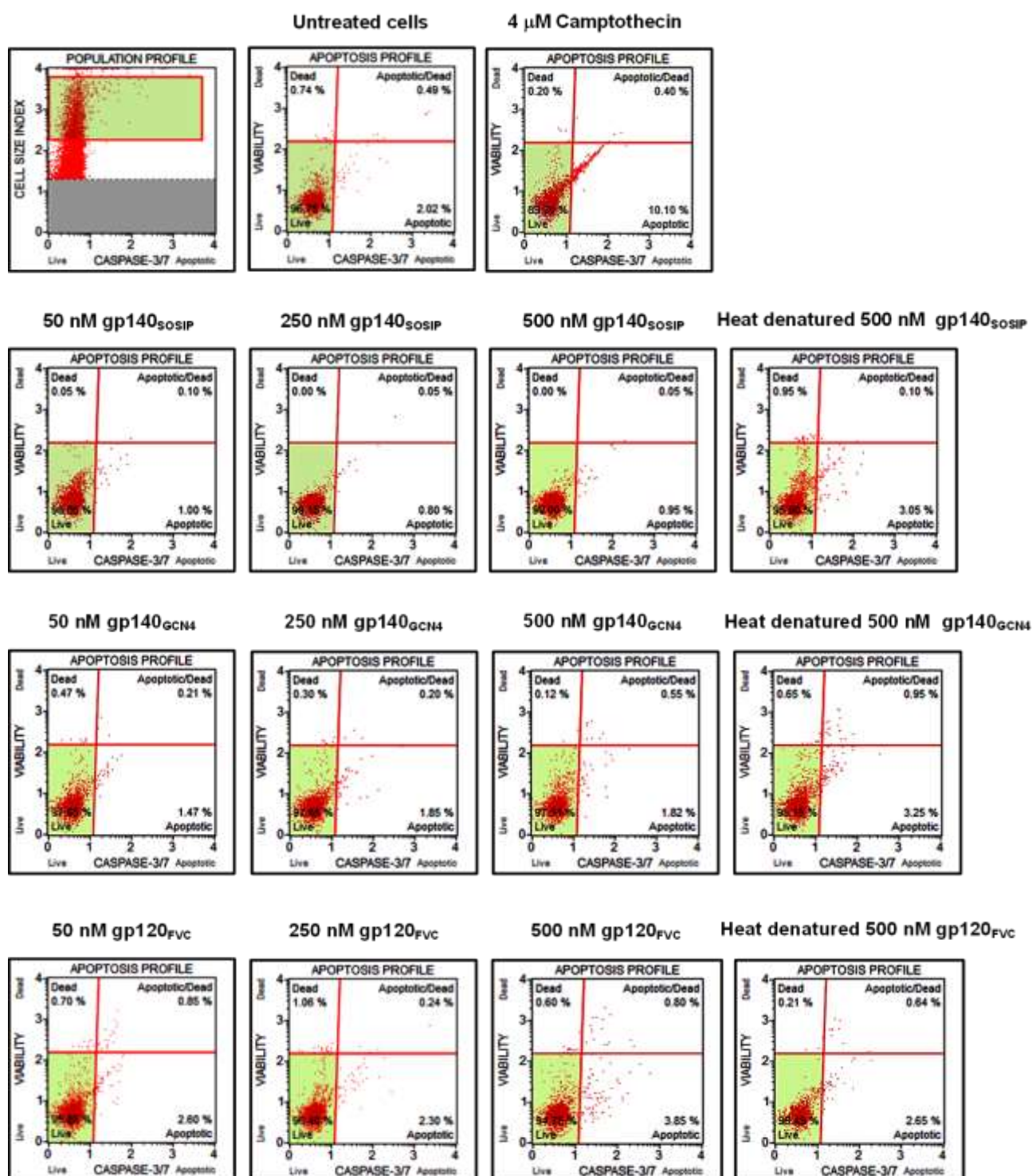


Figure 3E6: Caspase 3/7 activation flow cytometry scatter plots post 72 hours of Jurkat T cells treatment with 50 to 500 nM of gp140_{SOSIP}, gp140_{GC44} and gp120_{FVC}. Each plot is a representative of the second replicate at this time point.

Appendix F- DNA fragmentation data

Post treatment with varying concentrations of gp140_{SOSIP}, gp140_{GCN4} and gp120_{FVC} including controls over 24, 48 and 72 hours, Jurkat T cells were analysed for detection of DNA damage as a measure of apoptosis using flow cytometry. The results are represented as scatter plots at each time point including replicates (Figure 3F1 – 6).

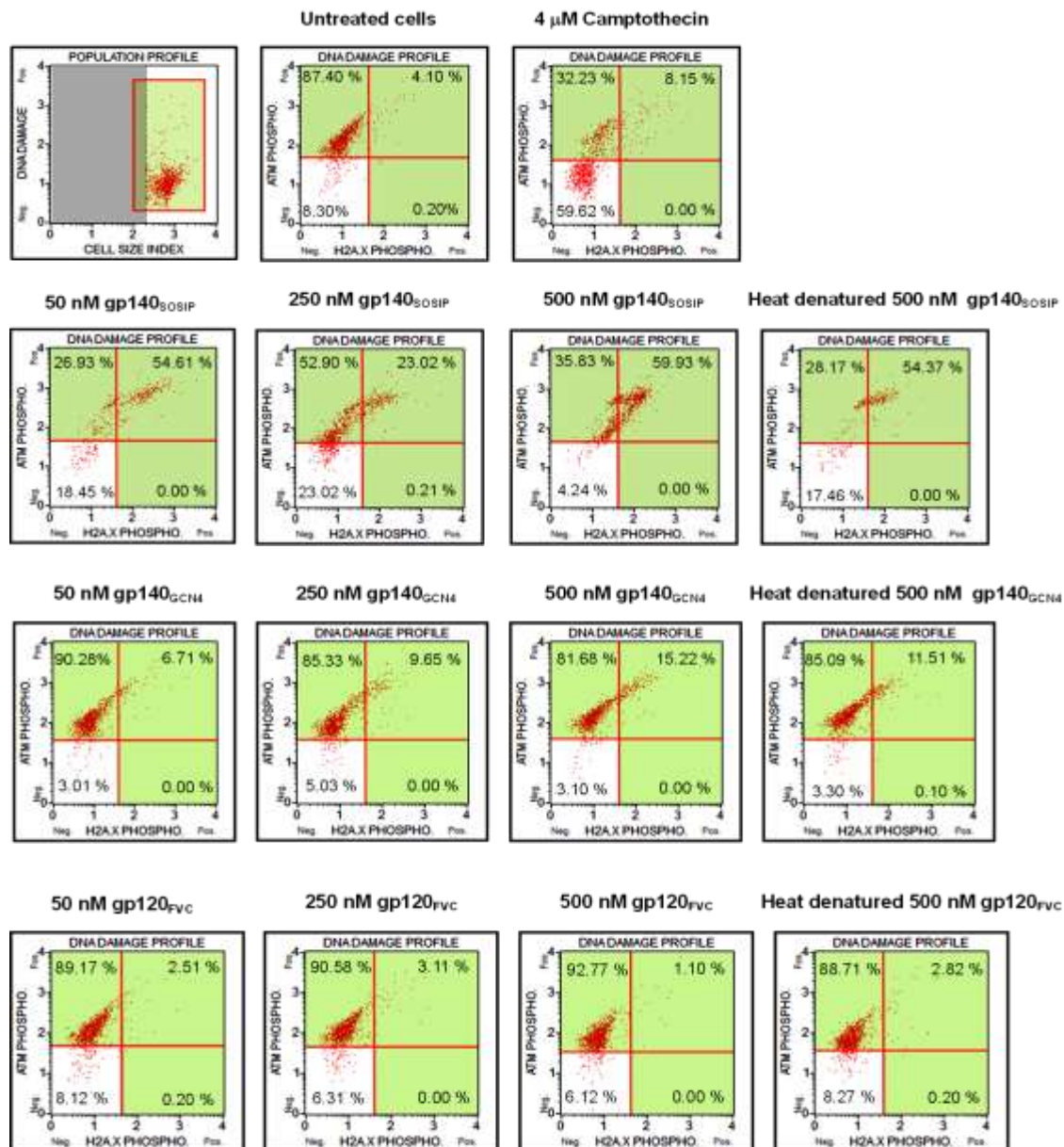


Figure 3F1: DNA fragmentation flow cytometry scatter plots post 24 hours of Jurkat T cells treatment with 50 to 500 nM of gp140_{SOSIP}, gp140_{GCN4} and gp120_{FVC}. Each plot is a representative of the first replicate at this time point.

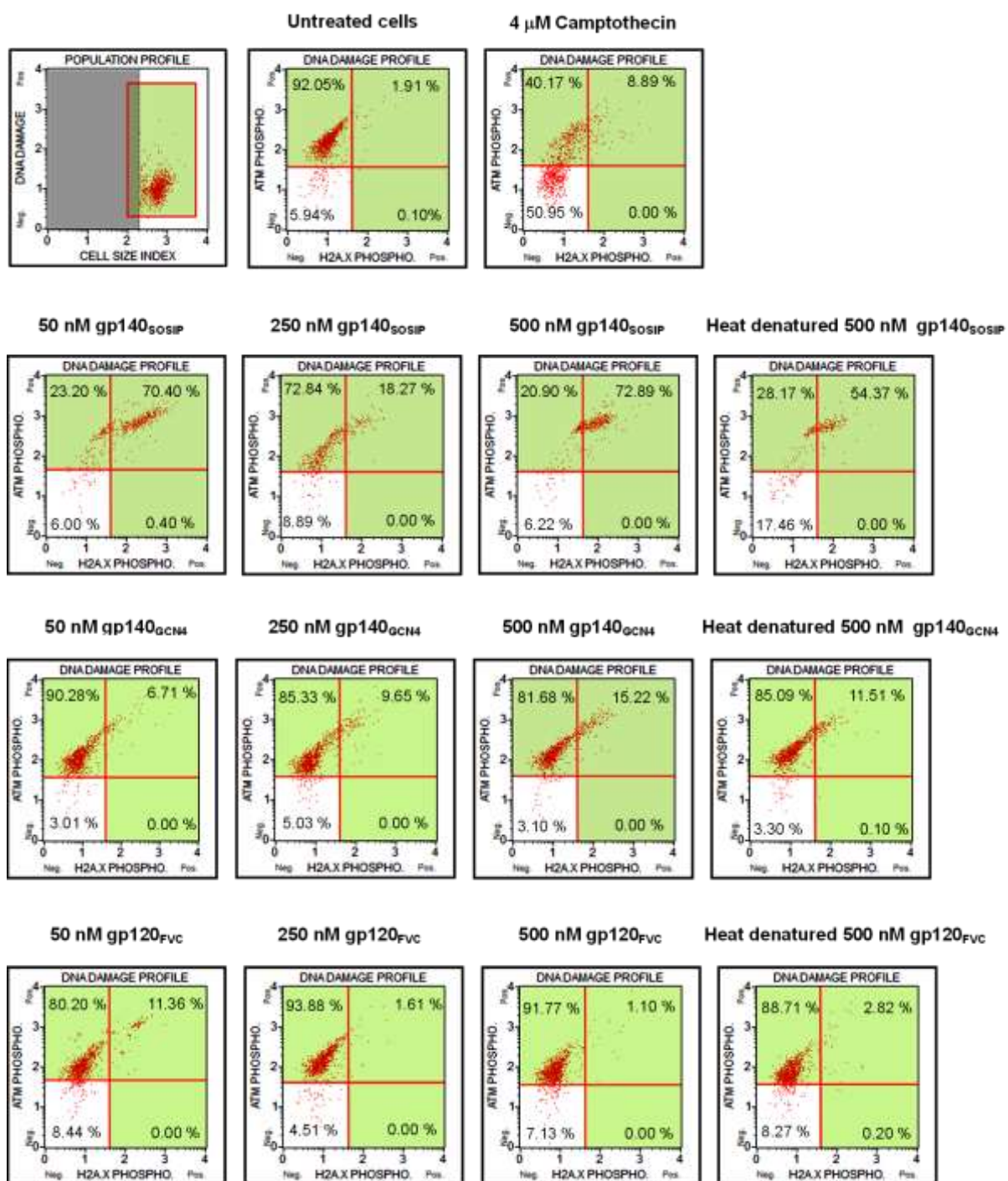


Figure 3F2: DNA fragmentation flow cytometry scatter plots post 24 hours of Jurkat T cells treatment with 50 to 500 nM of gp140_{SOSIP}, gp140_{GCN4} and gp120_{FVC}. Each plot is a representative of the second replicate at this time point.

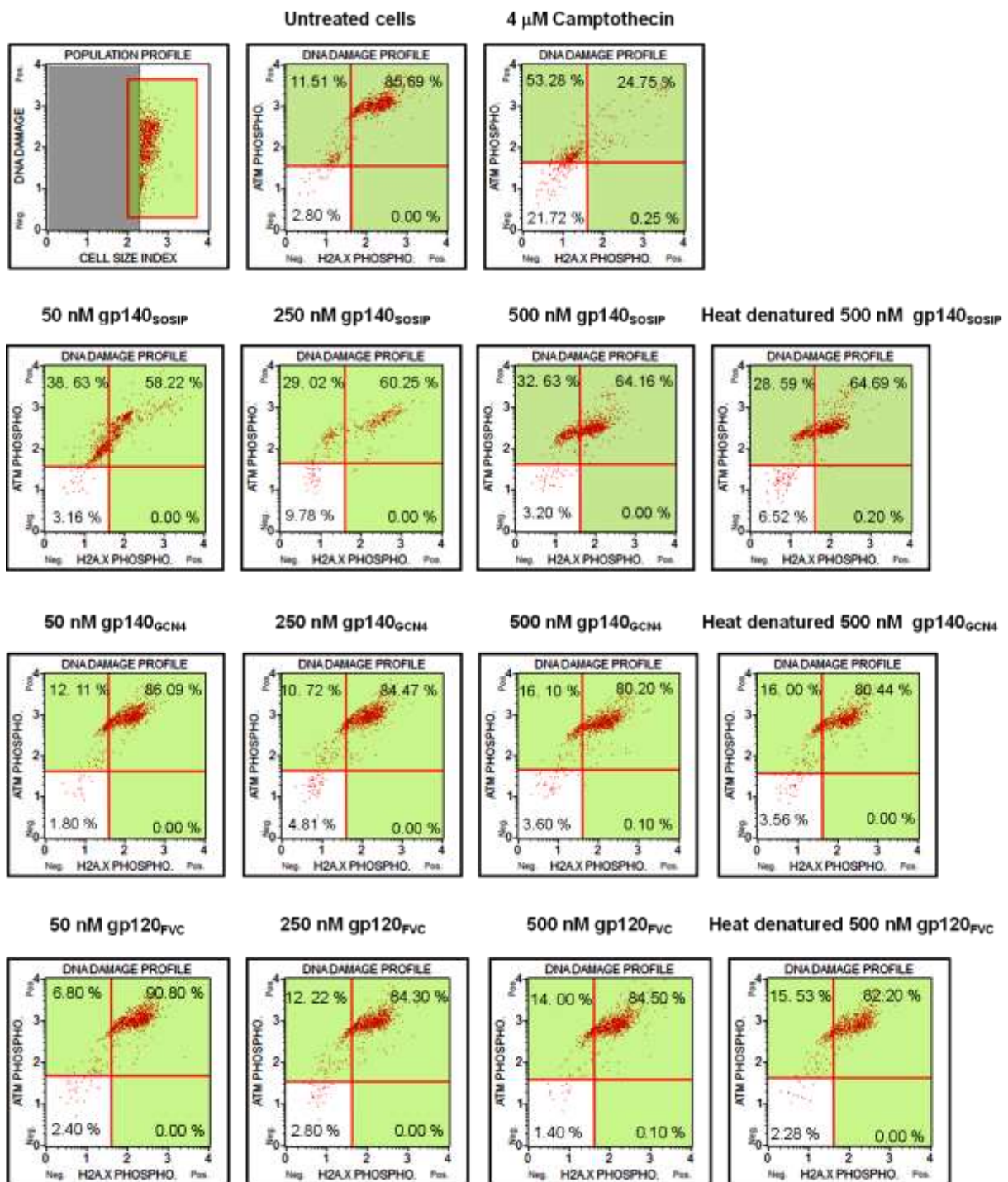


Figure 3F3: DNA fragmentation flow cytometry scatter plots post 48 hours of Jurkat T cells treatment with 50 to 500 nM of gp140_{SOSIP}, gp140_{GCN4} and gp120_{FVC}. Each plot is a representative of the first replicate at this time point.

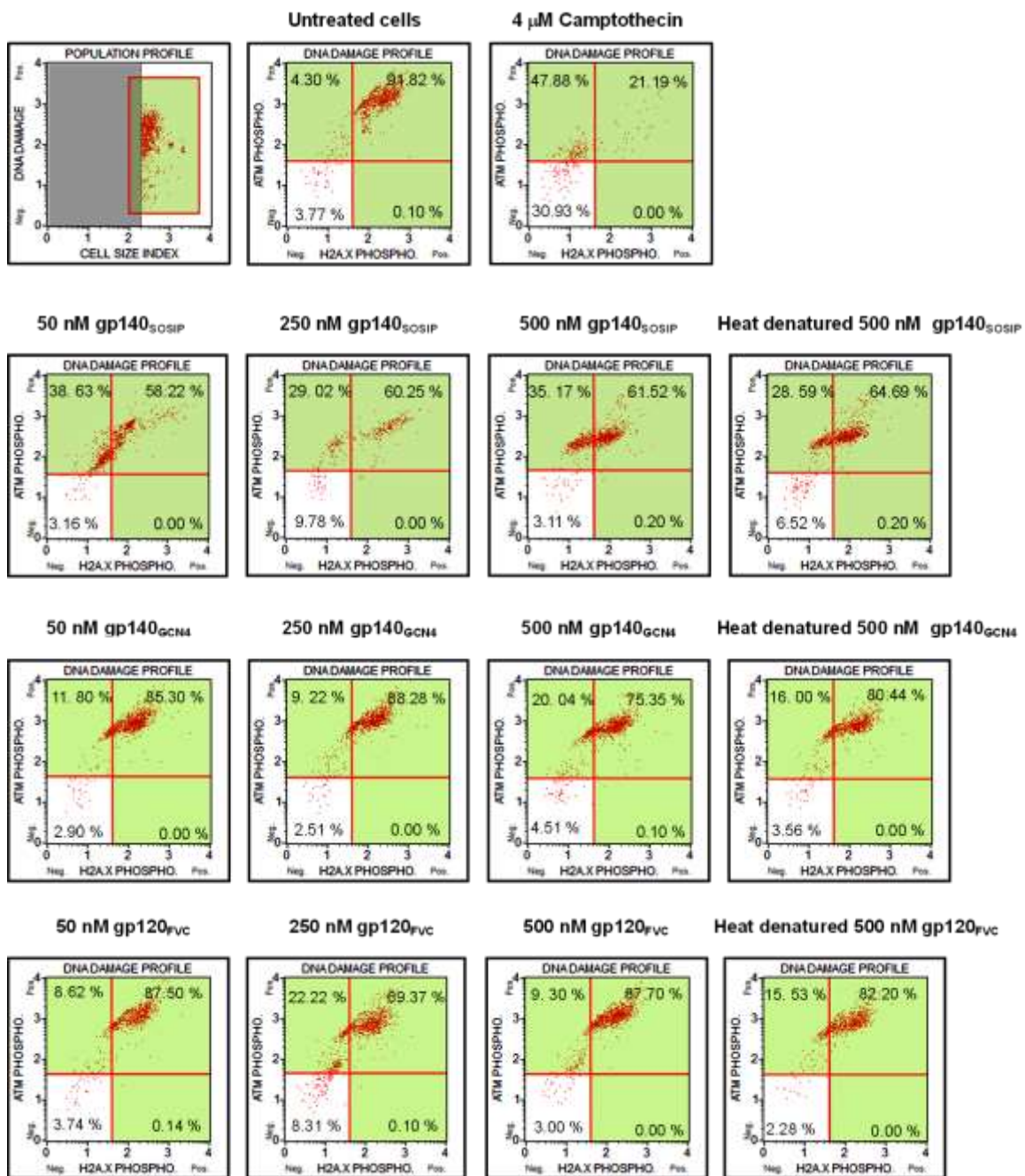


Figure 3F4: DNA fragmentation flow cytometry scatter plots post 48 hours of Jurkat T cells treatment with 50 to 500 nM of gp140_{SOSIP}, gp140_{GCIN4} and gp120_{FVC}. Each plot is a representative of the second replicate at this time point.

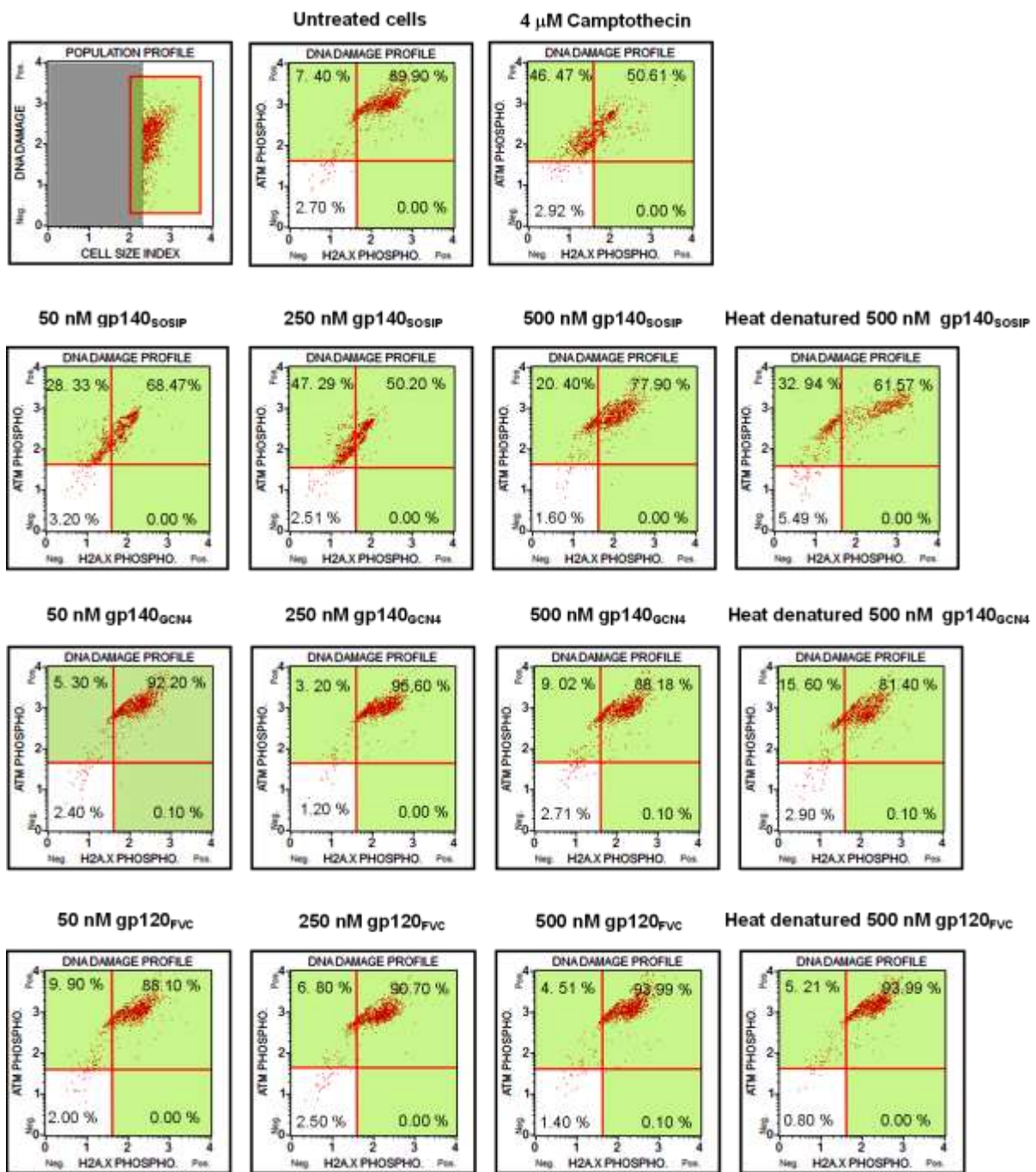


Figure 3F5: DNA fragmentation flow cytometry scatter plots post 72 hours of Jurkat T cells treatment with 50 to 500 nM of gp140_{SOSIP}, gp140_{GCN4} and gp120_{FVC}. Each plot is a representative of the first replicate at this time point.

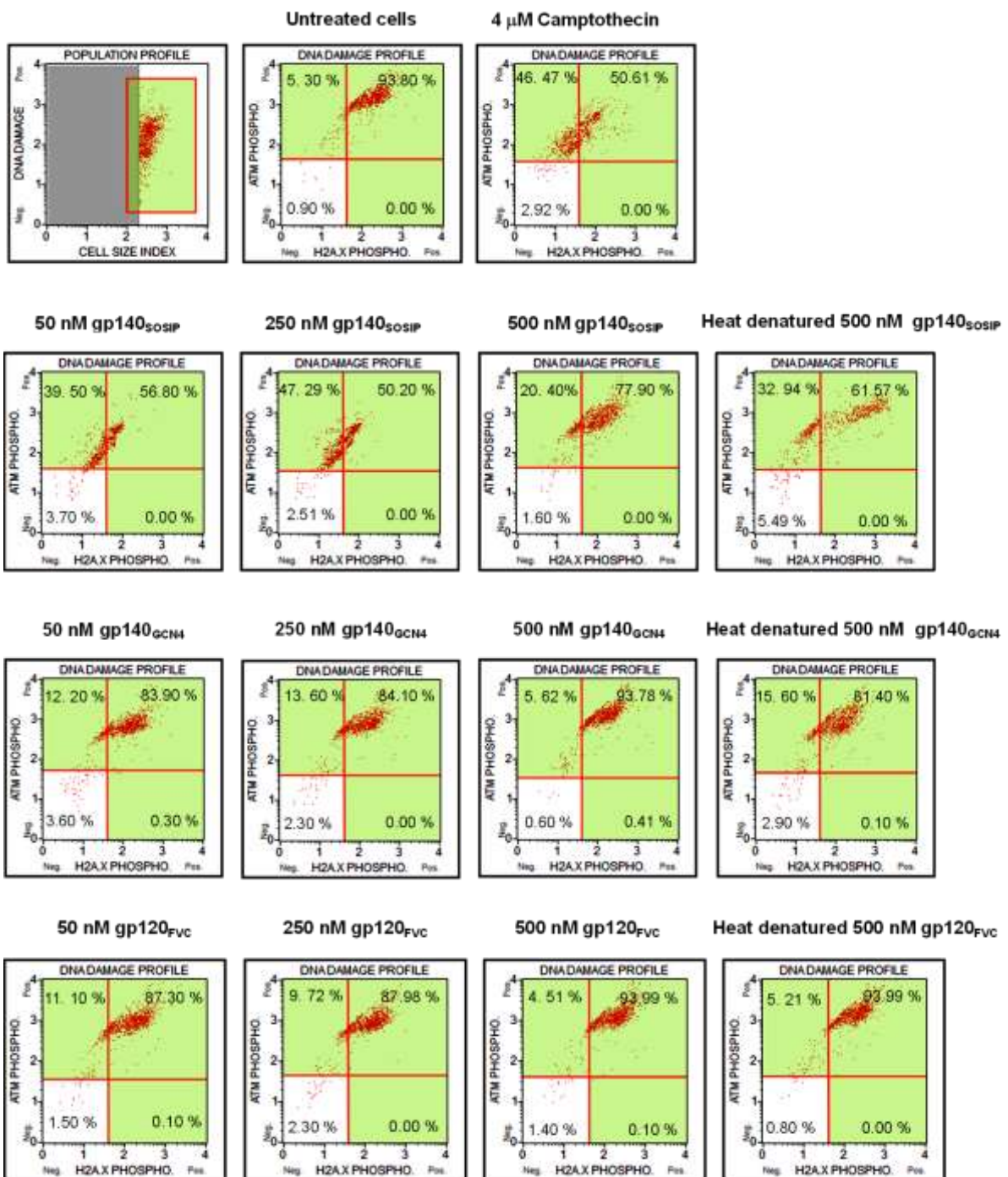


Figure 3F6: DNA fragmentation flow cytometry scatter plots post 72 hours of Jurkat T cells treatment with 50 to 500 nM of gp140_{SOSIP}, gp140_{GCN4} and gp120_{FVC}. Each plot is a representative of the second replicate at this time point.

References

1. ABBAS, W. & HERBEIN, G. 2013. T-cell signaling in HIV-1 infection. *The open virology journal*, 7, 57.
2. ADAN, A., ALIZADA, G., KIRAZ, Y., BARAN, Y. & NALBANT, A. 2017. Flow cytometry: basic principles and applications. *Critical reviews in biotechnology*, 37, 163-176.
3. AGUCHI, J. Y., DEVARE, S. G. & BRENNAN, C. A. 2000. Sequence Note: Identification of a New HIV-2 Subtype Based on Phylogenetic Analysis of Full-Length Genomic Sequence. *AIDS research and human retroviruses*, 16, 925-930.
4. AHMED, S., SHRIVASTAVA, T., KUMAR, N., OZOROWSKI, G., WARD, A. B. & CHAKRABARTI, B. K. 2017. Stabilization of a soluble, native-like trimeric form of an efficiently cleaved Indian HIV-1 clade C envelope glycoprotein. *Journal of Biological Chemistry*, jbc. M117. 776419.
5. AHR, B., ROBERT-HEBMANN, V., DEVAUX, C. & BIARD-PIECHACZYK, M. 2004. Apoptosis of uninfected cells induced by HIV envelope glycoproteins. *Retrovirology*, 1, 12.
6. AILLET, F., MASUTANI, H., ELBIM, C., RAOUL, H., CHÊNE, L., NUGEYRE, M.-T., PAYA, C., BARRÉ-SINOUSI, F., GOUGEROT-POCIDALO, M.-A. & ISRAËL, N. 1998. Human immunodeficiency virus induces a dual regulation of Bcl-2, resulting in persistent infection of CD4+ T-or monocytic cell lines. *Journal of virology*, 72, 9698-9705.
7. ALESSANDRI-GRADT, E., DE OLIVEIRA, F., LEOZ, M., LEMEE, V., ROBERTSON, D. L., FEYERTAG, F., NGOUPPO, P.-A., MAUCLERE, P., SIMON, F. & PLANTIER, J.-C. 2018. HIV-1 group P infection: towards a dead-end infection? *Aids*, 32, 1317-1322.
8. ALIMONTI, J. B., BALL, T. B. & FOWKE, K. R. 2003. Mechanisms of CD4+ T lymphocyte cell death in human immunodeficiency virus infection and AIDS. *Journal of general Virology*, 84, 1649-1661.
9. ALSAHAFI, N., ANAND, S. P., CASTILLO-MENENDEZ, L., VERLY, M. M., MEDJAHED, H., PRÉVOST, J., HERSCHHORN, A., RICHARD, J., SCHÖN, A. & MELILLO, B. 2018. SOSIP changes affect human immunodeficiency virus type 1 envelope glycoprotein conformation and CD4 engagement. *Journal of virology*, 92, e01080-18.
10. ALTICE, F., EVUARHERHE, O., SHINA, S., CARTER, G. & BEAUBRUN, A. C. 2019. Adherence to Hiv treatment regimens: systematic literature review and meta-analysis. *Patient preference and adherence*, 13, 475.
11. ALVAREZ-QUILÓN, A., SERRANO-BENÍTEZ, A., LIEBERMAN, J. A., QUINTERO, C., SÁNCHEZ-GUTIÉRREZ, D., ESCUDERO, L. M. & CORTÉS-LEDESMA, F. 2014. ATM specifically mediates repair of double-strand breaks with blocked DNA ends. *Nature communications*, 5, 3347.
12. AMBROSE, Z. & AIKEN, C. 2014. HIV-1 uncoating: connection to nuclear entry and regulation by host proteins. *Virology*, 454, 371-379.
13. AMEISEN, J. C. & CAPRON, A. 1991. Cell dysfunction and depletion in AIDS: the programmed cell death hypothesis. *Immunology today*, 12, 102-105.

14. ANAND, A. R. & GANJU, R. K. 2006. HIV-1 gp120-mediated apoptosis of T cells is regulated by the membrane tyrosine phosphatase CD45. *Journal of Biological Chemistry*, 281, 12289-12299.
15. ANDERSEN, J. L., DEHART, J. L., ZIMMERMAN, E. S., ARDON, O., KIM, B., JACQUOT, G., BENICHO, S. & PLANELLES, V. 2006. HIV-1 Vpr-induced apoptosis is cell cycle dependent and requires Bax but not ANT. *PLoS pathogens*, 2, e127.
16. ANDREAU, K., PERFETTINI, J.-L., CASTEDO, M., MÉTIVIER, D., SCOTT, V., PIERRON, G. & KROEMER, G. 2004. Contagious apoptosis facilitated by the HIV-1 envelope: fusion-induced cell-to-cell transmission of a lethal signal. *Journal of cell science*, 117, 5643-5653.
17. ANTON, P. A., ELLIOTT, J., POLES, M. A., MCGOWAN, I. M., MATUD, J., HULTIN, L. E., GROVIT-FERBAS, K., MACKAY, C. R., CHEN, I. S. & GIORGI, J. V. 2000. Enhanced levels of functional HIV-1 co-receptors on human mucosal T cells demonstrated using intestinal biopsy tissue. *Aids*, 14, 1761-1765.
18. APPAY, V., PAPAGNO, L., SPINA, C. A., HANSASUTA, P., KING, A., JONES, L., OGG, G. S., LITTLE, S., MCMICHAEL, A. J. & RICHMAN, D. D. 2002. Dynamics of T cell responses in HIV infection. *The Journal of Immunology*, 168, 3660-3666.
19. ARIES, S., SCHAAF, B., MÜLLER, C., DALHOFF, K. & DENNIN, R. 1995. Fas (CD95) expression on CD4+ T cells from HIV-infected patients increases with disease progression. *Journal of molecular medicine*, 73, 591-593.
20. ARNOULT, D., PETIT, F., LELIEVIE, J., LECOSSIER, D., HANCE, A., MONCEAUX, V., FANG, R. H. T., HUNTREL, B., AMEISEN, J. & ESTAQUIER, J. 2003. Caspase-dependent and-independent T-cell death pathways in pathogenic simian immunodeficiency virus infection: relationship to disease progression. *Cell death and differentiation*, 10, 1240.
21. ARNOULT, D., VIOLLET, L., PETIT, F., LELIÈVRE, J.-D. & ESTAQUIER, J. 2004. HIV-1 triggers mitochondrion death. *Mitochondrion*, 4, 255-269.
22. AROKIUM, H., KAMATA, M. & CHEN, I. 2009. Virion-associated Vpr of human immunodeficiency virus type 1 triggers activation of apoptotic events and enhances fas-induced apoptosis in human T cells. *Journal of virology*, 83, 11283-11297.
23. ASHKENAZI, A. & DIXIT, V. M. 1998. Death receptors: signaling and modulation. *science*, 281, 1305-1308.
24. AUDDO, R., HUA, C., HAHNE, M., COMBE, B., MOREL, J. & DAIEN, C. I. 2017. Phosphatidylserine outer layer translocation is implicated in IL-10 secretion by human regulatory B cells. *PloS one*, 12, e0169755.
25. AVDOSHINA, V., FIELDS, J. A., CASTELLANO, P., DEDONI, S., PALCHIK, G., TREJO, M., ADAME, A., ROCKENSTEIN, E., EUGENIN, E. & MASLIAH, E. 2016. The HIV protein gp120 alters mitochondrial dynamics in neurons. *Neurotoxicity research*, 29, 583-593.
26. AZAD, A. A. 2000. Could Nef and Vpr proteins contribute to disease progression by promoting depletion of bystander cells and prolonged survival of HIV-infected cells? *Biochemical and biophysical research communications*, 267, 677-685.
27. BACHMANN, N., VON SIEBENTHAL, C., VONGRAD, V., TURK, T., NEUMANN, K., BEERENWINKEL, N., BOGOJESKA, J., FELLAY, J., ROTH, V. & KOK, Y. L. 2019. Determinants of HIV-1 reservoir size and long-term dynamics during suppressive ART. *Nature communications*, 10, 3193.

28. BAI, L., SMITH, D. C. & WANG, S. 2014. Small-molecule SMAC mimetics as new cancer therapeutics. *Pharmacology & therapeutics*, 144, 82-95.
29. BANDERA, A., FERRARIO, G., SARESELLA, M., MARVENTANO, I., SORIA, A., ZANINI, F., SABBATINI, F., AIROLDI, M., MARCHETTI, G. & FRANZETTI, F. 2010. CD4+ T cell depletion, immune activation and increased production of regulatory T cells in the thymus of HIV-infected individuals. *PloS one*, 5, e10788.
30. BARRÉ-SINOUSI, F., CHERMANN, J.-C., REY, F., NUGEYRE, M. T., CHAMARET, S., GRUEST, J., DAUGUET, C., AXLER-BLIN, C., VÉZINET-BRUN, F. & ROUZIQUX, C. 1983. Isolation of a T-lymphotropic retrovirus from a patient at risk for acquired immune deficiency syndrome (AIDS). *Science*, 220, 868-871.
31. BARRETINA, J., BLANCO, J., BONJOCH, A., LLANO, A., CLOTET, B. & ESTÉ, J. A. 2004. Immunological and virological study of enfuvirtide-treated HIV-positive patients. *Aids*, 18, 1673-1682.
32. BARTZ, S. R. & EMERMAN, M. 1999. Human immunodeficiency virus type 1 Tat induces apoptosis and increases sensitivity to apoptotic signals by up-regulating FLICE/caspase-8. *Journal of virology*, 73, 1956-1963.
33. BAUR, A. S., SAWAI, E. T., DAZIN, P., FANTL, W. J., CHENG-MAYER, C. & PETERLIN, B. M. 1994. HIV-1 Nef leads to inhibition or activation of T cells depending on its intracellular localization. *Immunity*, 1, 373-384.
34. BENDER, A. M., SIMONETTI, F. R., KUMAR, M. R., FRAY, E. J., BRUNER, K. M., TIMMONS, A. E., TAI, K. Y., JENIKE, K. M., ANTAR, A. A. & LIU, P.-T. 2019. The Landscape of persistent viral genomes in ART-treated SIV, SHIV, and HIV-2 infections. *Cell host & microbe*, 26, 73-85. e4.
35. BENNETT, G. J., DOYLE, T. & SALVEMINI, D. 2014. Mitotoxicity in distal symmetrical sensory peripheral neuropathies. *Nature Reviews Neurology*, 10, 326.
36. BHIMAN, J. N., ANTHONY, C., DORIA-ROSE, N. A., KARIMANZIRA, O., SCHRAMM, C. A., KHOZA, T., KITCHIN, D., BOTHA, G., GORMAN, J. & GARRETT, N. J. 2015. Viral variants that initiate and drive maturation of V1V2-directed HIV-1 broadly neutralizing antibodies. *Nature medicine*, 21, 1332.
37. BIARD-PIECHACZYK, M., ROBERT-HEBMANN, V., RICHARD, V., ROLAND, J., HIPSKIND, R. A. & DEVAUX, C. 2000. Caspase-dependent apoptosis of cells expressing the chemokine receptor CXCR4 is induced by cell membrane-associated human immunodeficiency virus type 1 envelope glycoprotein (gp120). *Virology*, 268, 329-344.
38. BINLEY, J. M., SANDERS, R. W., CLAS, B., SCHUELKE, N., MASTER, A., GUO, Y., KAJUMO, F., ANSELMA, D. J., MADDON, P. J. & OLSON, W. C. 2000. A recombinant human immunodeficiency virus type 1 envelope glycoprotein complex stabilized by an intermolecular disulfide bond between the gp120 and gp41 subunits is an antigenic mimic of the trimeric virion-associated structure. *Journal of virology*, 74, 627-643.
39. BLAAK, H., VAN'T WOUT, A. B., BROUWER, M., HOOIBRINK, B., HOVENKAMP, E. & SCHUITEMAKER, H. 2000. In vivo HIV-1 infection of CD45RA+ CD4+ T cells is established primarily by syncytium-inducing variants and correlates with the rate of CD4+ T cell decline. *Proceedings of the National Academy of Sciences*, 97, 1269-1274.
40. BLANCO, J., BARRETINA, J., FERRI, K. F., JACOTOT, E., GUTIÉRREZ, A., ARMAND-UGÓN, M., CABRERA, C., KROEMER, G., CLOTET, B. & ESTÉ, J. A.

2003. Cell-surface-expressed HIV-1 envelope induces the death of CD4 T cells during GP41-mediated hemifusion-like events. *Virology*, 305, 318-329.
41. BLANCO, J., BARRETINA, J., HENSON, G., BRIDGER, G., DE CLERCQ, E., CLOTET, B. & ESTÉ, J. A. 2000. The CXCR4 antagonist AMD3100 efficiently inhibits cell-surface-expressed human immunodeficiency virus type 1 envelope-induced apoptosis. *Antimicrobial agents and chemotherapy*, 44, 51-56.
 42. BOUR, S., GELEZIUNAS, R. & WAINBERG, M. A. 1995. The human immunodeficiency virus type 1 (HIV-1) CD4 receptor and its central role in promotion of HIV-1 infection. *Microbiological reviews*, 59, 63-93.
 43. BOWEN, L. N., SMITH, B., REICH, D., QUEZADO, M. & NATH, A. 2016. HIV-associated opportunistic CNS infections: pathophysiology, diagnosis and treatment. *Nature Reviews Neurology*, 12, 662.
 44. BOYA, P., ROQUES, B. & KROEMER, G. 2001. Viral and bacterial proteins regulating apoptosis at the mitochondrial level. *The EMBO journal*, 20, 4325-4331.
 45. BRADY, R. & BARCLAY, A. 1996. The structure of CD4. *The CD4 Molecule*. Springer.
 46. BRENCHLEY, J. M., SCHACKER, T. W., RUFF, L. E., PRICE, D. A., TAYLOR, J. H., BEILMAN, G. J., NGUYEN, P. L., KHORUTS, A., LARSON, M. & HAASE, A. T. 2004. CD4+ T cell depletion during all stages of HIV disease occurs predominantly in the gastrointestinal tract. *Journal of Experimental Medicine*, 200, 749-759.
 47. BRIGGS, J. A., GRÜNEWALD, K., GLASS, B., FÖRSTER, F., KRÄUSSLICH, H.-G. & FULLER, S. D. 2006. The mechanism of HIV-1 core assembly: insights from three-dimensional reconstructions of authentic virions. *Structure*, 14, 15-20.
 48. BRODER, C. C. & BERGER, E. A. 1995. Fusogenic selectivity of the envelope glycoprotein is a major determinant of human immunodeficiency virus type 1 tropism for CD4+ T-cell lines vs. primary macrophages. *Proceedings of the National Academy of Sciences*, 92, 9004-9008.
 49. BUCCIGROSSI, V., LAUDIERO, G., NICASTRO, E., MIELE, E., ESPOSITO, F. & GUARINO, A. 2011. The HIV-1 transactivator factor (Tat) induces enterocyte apoptosis through a redox-mediated mechanism. *PLoS One*, 6, e29436.
 50. BURTON, D. R., PYATI, J., KODURI, R., SHARP, S. J., THORNTON, G. B., PARREN, P., SAWYER, L. S., HENDRY, R. M., DUNLOP, N. & NARA, P. L. 1994. Efficient neutralization of primary isolates of HIV-1 by a recombinant human monoclonal antibody. *Science*, 266, 1024-1027.
 51. CABY, M.-P., LANKAR, D., VINCENDEAU-SCHERRER, C., RAPOSO, G. & BONNEROT, C. 2005. Exosomal-like vesicles are present in human blood plasma. *International immunology*, 17, 879-887.
 52. CASTEDO, M., ROUMIER, T., BLANCO, J., FERRI, K. F., BARRETINA, J., TINTIGNAC, L. A., ANDREAU, K., PERFETTINI, J. L., AMENDOLA, A. & NARDACCI, R. 2002. Sequential involvement of Cdk1, mTOR and p53 in apoptosis induced by the HIV-1 envelope. *The EMBO journal*, 21, 4070-4080.
 53. CERUTTI, N., MENDELOW, B. V., NAPIER, G. B., PAPATHANASOPOULOS, M. A., KILLICK, M., KHATI, M., STEVENS, W. & CAPOVILLA, A. 2010. Stabilization of HIV-1 gp120-CD4 receptor complex through targeted interchain disulfide exchange. *Journal of Biological Chemistry*, jbc. M110. 144121.
 54. CHAN, D. C., FASS, D., BERGER, J. M. & KIM, P. S. 1997. Core structure of gp41 from the HIV envelope glycoprotein. *Cell*, 89, 263-273.

55. CHAN, W.-T., VERMA, C. S., LANE, D. P. & GAN, S. K.-E. 2013. A comparison and optimization of methods and factors affecting the transformation of *Escherichia coli*. *Bioscience reports*, 33, e00086.
56. CHARNAY, N., IVANYI-NAGY, R., SOTO-RIFO, R., OHLMANN, T., LÓPEZ-LASTRA, M. & DARLIX, J.-L. 2009. Mechanism of HIV-1 Tat RNA translation and its activation by the Tat protein. *Retrovirology*, 6, 74.
57. CHECKLEY, M. A., LUTTGE, B. G. & FREED, E. O. 2011. HIV-1 envelope glycoprotein biosynthesis, trafficking, and incorporation. *Journal of molecular biology*, 410, 582-608.
58. CHEN, Y., HWANG, S.-L., CHAN, V. S., CHUNG, N. P., WANG, S.-R., LI, Z., MA, J., LIN, C.-W., HSIEH, Y.-J. & CHANG, K.-P. 2013. Binding of HIV-1 gp120 to DC-SIGN promotes ASK-1-dependent activation-induced apoptosis of human dendritic cells. *PLoS pathogens*, 9, e1003100.
59. CHEN, Z., LUCKAY, A., SODORA, D. L., TELFER, P., REED, P., GETTIE, A., KANU, J. M., SADEK, R. F., YEE, J. & HO, D. D. 1997. Human immunodeficiency virus type 2 (HIV-2) seroprevalence and characterization of a distinct HIV-2 genetic subtype from the natural range of simian immunodeficiency virus-infected sooty mangabeys. *Journal of virology*, 71, 3953-3960.
60. CHERNOMORDIK, L. V. & KOZLOV, M. M. 2005. Membrane hemifusion: crossing a chasm in two leaps. *Cell*, 123, 375-382.
61. CHIKANDO, A., KAO, J. P. & LEDERER, W. 2011. Effects of Mitochondrial Membrane Depolarization on Cellular Function in Cardiac Myocytes. *Biophysical Journal*, 100, 555a.
62. CHINNAIYAN, A. M. 1999. The apoptosome: heart and soul of the cell death machine. *Neoplasia*, 1, 5-15.
63. CHINYOWA, S., PALEFSKY, J. M., CHIRENJE, Z. M., MAKUNIKE-MUTASA, R., MUNJOMA, M. & MUGUTI, G. I. 2018. Anal human papillomavirus infection in HIV-positive men and women at two opportunistic infections clinics in Harare, Zimbabwe. *BMC public health*, 18, 1260.
64. CHIODI, F. & SCARLATTI, G. 2018. HiV-induced damage of B Cells and Production of HiV Neutralizing antibodies. *Frontiers in Immunology*, 9, 297.
65. CHOE, H., FARZAN, M., SUN, Y., SULLIVAN, N., ROLLINS, B., PONATH, P. D., WU, L., MACKAY, C. R., LAROSA, G. & NEWMAN, W. 1996. The β -chemokine receptors CCR3 and CCR5 facilitate infection by primary HIV-1 isolates. *Cell*, 85, 1135-1148.
66. CHOUDHARY, G. S., AL-HARBI, S. & ALMASAN, A. 2015. Caspase-3 activation is a critical determinant of genotoxic stress-induced apoptosis. *Apoptosis and Cancer*. Springer.
67. CHUNG, N. P., MATTHEWS, K., KIM, H. J., KETAS, T. J., GOLABEK, M., DE LOS REYES, K., KORZUN, J., YASMEEN, A., SANDERS, R. W. & KLASSE, P. J. 2014. Stable 293 T and CHO cell lines expressing cleaved, stable HIV-1 envelope glycoprotein trimers for structural and vaccine studies. *Retrovirology*, 11, 33.
68. CICALA, C., ARTHOS, J., RUBBERT, A., SELIG, S., WILDT, K., COHEN, O. J. & FAUCI, A. S. 2000. HIV-1 envelope induces activation of caspase-3 and cleavage of focal adhesion kinase in primary human CD4+ T cells. *Proceedings of the National Academy of Sciences*, 97, 1178-1183.
69. CLARK, S. J., SAAG, M. S., DECKER, W. D., CAMPBELL-HILL, S., ROBERSON, J. L., VELDKAMP, P. J., KAPPES, J. C., HAHN, B. H. & SHAW, G.

- M. 1991. High titers of cytopathic virus in plasma of patients with symptomatic primary HIV-1 infection. *New England Journal of Medicine*, 324, 954-960.
70. COAKLEY, E., PETROPOULOS, C. J. & WHITCOMB, J. M. 2005. Assessing chemokine co-receptor usage in HIV. *Current opinion in infectious diseases*, 18, 9-15.
71. COFFIN, J. M., HUGHES, S. H. & VARMUS, H. E. 1997. *The interactions of retroviruses and their hosts*, Cold Spring Harbor Laboratory Press, Cold Spring Harbor (NY).
72. COHEN, F. & MELIKYAN, G. 2004. The energetics of membrane fusion from binding, through hemifusion, pore formation, and pore enlargement. *The Journal of membrane biology*, 199, 1-14.
73. COHEN, M. S., CHEN, Y. Q., MCCAULEY, M., GAMBLE, T., HOSSEINIPOUR, M. C., KUMARASAMY, N., HAKIM, J. G., KUMWENDA, J., GRINSZTEJN, B. & PILOTTO, J. H. 2011. Prevention of HIV-1 infection with early antiretroviral therapy. *New England journal of medicine*, 365, 493-505.
74. COHEN, S. N., CHANG, A. C. AND HSU, L. 1972. Nonchromosomal antibiotic resistance in bacteria: genetic transformation of *Escherichia coli* by R-factor DNA. *Proc. Natl. Acad. Sci.*, 69, 2110-2111.
75. COOPER, D. A., IMRIE, A. A. & PENNY, R. 1987. Antibody response to human immunodeficiency virus after primary infection. *Journal of Infectious Diseases*, 155, 1113-1118.
76. CULLEN, B. R. 1998. Retroviruses as model systems for the study of nuclear RNA export pathways. *Virology*, 249, 203-210.
77. CUMMINS, N. & BADLEY, A. 2010. Mechanisms of HIV-associated lymphocyte apoptosis: 2010. *Cell death & disease*, 1, e99.
78. CUMMINS, N. W. & BADLEY, A. D. 2014. Making sense of how HIV kills infected CD4 T cells: implications for HIV cure. *Molecular and cellular therapies*, 2, 20.
79. CUMMINS, N. W. & BADLEY, A. D. Can HIV Be Cured, and Should We Try? Mayo Clinic Proceedings, 2015. NIH Public Access, 705.
80. CUMMINS, N. W., RIZZA, S. A. & BADLEY, A. D. 2010. How much gp120 is there? *The Journal of infectious diseases*, 201, 1273-1273.
81. CUMONT, M.-C., DIOP, O., VASLIN, B., ELBIM, C., VIOLLET, L., MONCEAUX, V., LAY, S., SILVESTRI, G., LE GRAND, R. & MÜLLER-TRUTWIN, M. 2008. Early divergence in lymphoid tissue apoptosis between pathogenic and nonpathogenic simian immunodeficiency virus infections of nonhuman primates. *Journal of virology*, 82, 1175-1184.
82. CURLIN, M. E., ZIONI, R., HAWES, S. E., LIU, Y., DENG, W., GOTTLIEB, G. S., ZHU, T. & MULLINS, J. I. 2010. HIV-1 envelope subregion length variation during disease progression. *PLoS pathogens*, 6, e1001228.
83. CZABOTAR, P. E., LESSENE, G., STRASSER, A. & ADAMS, J. M. 2014. Control of apoptosis by the BCL-2 protein family: implications for physiology and therapy. *Nature reviews Molecular cell biology*, 15, 49.
84. DAAR, E. S., MOUDGIL, T., MEYER, R. D. & HO, D. D. 1991. Transient high levels of viremia in patients with primary human immunodeficiency virus type 1 infection. *New England Journal of Medicine*, 324, 961-964.
85. DAI, H., MENG, X. W. & KAUFMANN, S. H. 2016. BCL2 family, mitochondrial apoptosis, and beyond. *Cancer Translational Medicine*, 2, 7.

86. DALGLEISH, A. G., BEVERLEY, P. C., CLAPHAM, P. R., CRAWFORD, D. H., GREAVES, M. F. & WEISS, R. A. 1984. The CD4 (T4) antigen is an essential component of the receptor for the AIDS retrovirus. *Nature*, 312, 763.
87. DE OLIVEIRA PINTO, L. M., GARCIA, S., LECOEUR, H., RAPP, C. & GOUGEON, M.-L. 2002. Increased sensitivity of T lymphocytes to tumor necrosis factor receptor 1 (TNFR1)–and TNFR2-mediated apoptosis in HIV infection: relation to expression of Bcl-2 and active caspase-8 and caspase-3. *Blood*, 99, 1666-1675.
88. DEBATIN, K., FAHRIG-FAISSNER, A., ENENKEL-STOODT, S., KREUZ, W., BENNER, A. & KRAMMER, P. 1994. High expression of APO-1 (CD95) on T lymphocytes from human immunodeficiency virus-1-infected children. *Blood*, 83, 3101-3103.
89. DENG, H., LIU, R., ELLMEIER, W., CHOE, S., UNUTMAZ, D., BURKHART, M., MARZIO, P. D., MARMON, S., SUTTON, R. E. & HILL, C. M. 1996. Identification of a major co-receptor for primary isolates of HIV-1. *Nature*, 381, 661.
90. DOBROWSKY, T. M., ZHOU, Y., SUN, S. X., SILICIANO, R. F. & WIRTZ, D. 2008. Monitoring early fusion dynamics of human immunodeficiency virus type 1 at single-molecule resolution. *Journal of virology*, 82, 7022-7033.
91. DOCKRELL, D., BADLEY, A. D., ALGECIRAS-SCHIMNICH, A., SIMPSON, M., SCHUT, R., LYNCH, D. & PAYA, C. 1999. Activation-induced CD4+ T cell death in HIV-positive individuals correlates with Fas susceptibility, CD4+ T cell count, and HIV plasma viral copy number. *AIDS research and human retroviruses*, 15, 1509-1518.
92. DOITSH, G., GALLOWAY, N. L., GENG, X., YANG, Z., MONROE, K. M., ZEPEDA, O., HUNT, P. W., HATANO, H., SOWINSKI, S. & MUÑOZ-ARIAS, I. 2014. Cell death by pyroptosis drives CD4 T-cell depletion in HIV-1 infection. *Nature*, 505, 509.
93. DORIA-ROSE, N. A., BHIMAN, J. N., ROARK, R. S., SCHRAMM, C. A., GORMAN, J., CHUANG, G.-Y., PANCERA, M., CALE, E. M., ERNANDES, M. J. & LOUDER, M. K. 2015. A new member of the V1V2-directed CAP256-VRC26 lineage that shows increased breadth and exceptional potency. *Journal of virology*, JVI. 01791-15.
94. DORIA-ROSE, N. A., BHIMAN, J. N., ROARK, R. S., SCHRAMM, C. A., GORMAN, J., CHUANG, G.-Y., PANCERA, M., CALE, E. M., ERNANDES, M. J. & LOUDER, M. K. 2016. New member of the V1V2-directed CAP256-VRC26 lineage that shows increased breadth and exceptional potency. *Journal of virology*, 90, 76-91.
95. DORIA-ROSE, N. A., SCHRAMM, C. A., GORMAN, J., MOORE, P. L., BHIMAN, J. N., DEKOSKY, B. J., ERNANDES, M. J., GEORGIEV, I. S., KIM, H. J. & PANCERA, M. 2014. Developmental pathway for potent V1V2-directed HIV-neutralizing antibodies. *Nature*, 509, 55.
96. DOSENOVIC, P., VON BOEHMER, L., ESCOLANO, A., JARDINE, J., FREUND, N. T., GITLIN, A. D., MCGUIRE, A. T., KULP, D. W., OLIVEIRA, T. & SCHARF, L. 2015. Immunization for HIV-1 broadly neutralizing antibodies in human Ig knockin mice. *Cell*, 161, 1505-1515.
97. DOUEK, D. C., ROEDERER, M. & KOUP, R. A. 2009. Emerging concepts in the immunopathogenesis of AIDS. *Annual review of medicine*, 60, 471-484.
98. DRAGIC, T., LITWIN, V., ALLAWAY, G. P., MARTIN, S. R., HUANG, Y., NAGASHIMA, K. A., CAYANAN, C., MADDON, P. J., KOUP, R. A. & MOORE, J.

- P. 1996. HIV-1 entry into CD4+ cells is mediated by the chemokine receptor CC-CKR-5. *Nature*, 381, 667.
99. EARL, P. L., BRODER, C. C., LONG, D., LEE, S. A., PETERSON, J., CHAKRABARTI, S., DOMS, R. W. & MOSS, B. 1994. Native oligomeric human immunodeficiency virus type 1 envelope glycoprotein elicits diverse monoclonal antibody reactivities. *Journal of virology*, 68, 3015-3026.
 100. ECKERT, D. M. & KIM, P. S. 2001. Mechanisms of viral membrane fusion and its inhibition. *Annual review of biochemistry*, 70, 777-810.
 101. EDO-MATAS, D., RACHINGER, A., SETIAWAN, L. C., BOESER-NUNNINK, B. D., VAN'T WOUT, A. B., LEMEY, P. & SCHUITEMAKER, H. 2012. The evolution of human immunodeficiency virus type-1 (HIV-1) envelope molecular properties and coreceptor use at all stages of infection in an HIV-1 donor-recipient pair. *Virology*, 422, 70-80.
 102. ETEMAD-MOGHADAM, B., RHONE, D., STEENBEKE, T., SUN, Y., MANOLA, J., GELMAN, R., FANTON, J. W., RACZ, P., TENNER-RACZ, K. & AXTHELM, M. K. 2001. Membrane-fusing capacity of the human immunodeficiency virus envelope proteins determines the efficiency of CD4+ T-cell depletion in macaques infected by a simian-human immunodeficiency virus. *Journal of virology*, 75, 5646-5655.
 103. ETEMAD-MOGHADAM, B., SUN, Y., NICHOLSON, E. K., FERNANDES, M., LIOU, K., GOMILA, R., LEE, J. & SODROSKI, J. 2000. Envelope glycoprotein determinants of increased fusogenicity in a pathogenic simian-human immunodeficiency virus (SHIV-KB9) passaged in vivo. *Journal of virology*, 74, 4433-4440.
 104. FANALES-BELASIO, E., RAIMONDO, M., SULIGOI, B. & BUTTÒ, S. 2010. HIV virology and pathogenetic mechanisms of infection: a brief overview. *Annali dell'Istituto superiore di sanita*, 46, 5-14.
 105. FAVALORO, B., ALLOCATI, N., GRAZIANO, V., DI ILIO, C. & DE LAURENZI, V. 2012. Role of apoptosis in disease. *Aging (Albany NY)*, 4, 330.
 106. FELBER, B. K., DRYSDALE, C. M. & PAVLAKIS, G. N. 1990. Feedback regulation of human immunodeficiency virus type 1 expression by the Rev protein. *Journal of virology*, 64, 3734-3741.
 107. FENG, Y., BRODER, C. C., KENNEDY, P. E. & BERGER, E. A. 1996. HIV-1 entry cofactor: functional cDNA cloning of a seven-transmembrane, G protein-coupled receptor. *Science*, 272, 872-877.
 108. FERRI, K., JACOTOT, E., GEUSKENS, M. & KROEMER, G. 2000a. Apoptosis and karyogamy in syncytia induced by the HIV-1-envelope glycoprotein complex. *Cell death and differentiation*, 7, 1137.
 109. FERRI, K. F., JACOTOT, E., BLANCO, J., ESTÉ, J. A. & KROEMER, G. 2000b. Mitochondrial Control of Cell Death Induced by HIV-1-Encoded Proteins. *Annals of the New York Academy of Sciences*, 926, 149-164.
 110. FÉVRIER, M., DORGHAM, K. & REBOLLO, A. 2011. CD4+ T cell depletion in human immunodeficiency virus (HIV) infection: role of apoptosis. *Viruses*, 3, 586-612.
 111. FIELDS, B. N., KNIPE, D. M. & HOWLEY, P. M. 1996. *Fields virology*, Philadelphia, Lippincott-Raven Publishers.
 112. FIELDS, J. A., SERGER, E., CAMPOS, S., DIVAKARUNI, A. S., KIM, C., SMITH, K., TREJO, M., ADAME, A., SPENCER, B. & ROCKENSTEIN, E. 2016. HIV alters neuronal mitochondrial fission/fusion in the brain during HIV-associated neurocognitive disorders. *Neurobiology of disease*, 86, 154-169.

113. FINKEL, T., TUDOR-WILLIAMS, G., BANDA, N., COTTON, M., CURIEL, T., MONKS, C., BABA, T., RUPRECHT, R. & KUPFER, A. 1995. Apoptosis occurs predominantly in bystander cells and not in productively infected cells of HIV-and SIV-infected lymph nodes. *Nature medicine*, 1, 129-134.
114. FINZI, A., PACHECO, B., ZENG, X., DO KWON, Y., KWONG, P. D. & SODROSKI, J. 2010. Conformational characterization of aberrant disulfide-linked HIV-1 gp120 dimers secreted from overexpressing cells. *Journal of virological methods*, 168, 155-161.
115. FITZON, T., LESCHONSKY, B., BIELER, K., PAULUS, C., SCHRÖDER, J., WOLF, H. & WAGNER, R. 2000. Proline residues in the HIV-1 NH2-terminal capsid domain: structure determinants for proper core assembly and subsequent steps of early replication. *Virology*, 268, 294-307.
116. FORSELL, M. N., LI, Y., SUNDBÄCK, M., SVEHLA, K., LILJESTRÖM, P., MASCOLA, J. R., WYATT, R. & HEDESTAM, G. B. K. 2005. Biochemical and immunogenic characterization of soluble human immunodeficiency virus type 1 envelope glycoprotein trimers expressed by semliki forest virus. *Journal of virology*, 79, 10902-10914.
117. FORSELL, M. N., SCHIEF, W. R. & WYATT, R. T. 2009. Immunogenicity of HIV-1 envelope glycoprotein oligomers. *Current opinion in HIV and AIDS*, 4, 380-387.
118. FORSHEY, B. M., VON SCHWEDLER, U., SUNDQUIST, W. I. & AIKEN, C. 2002. Formation of a human immunodeficiency virus type 1 core of optimal stability is crucial for viral replication. *Journal of virology*, 76, 5667-5677.
119. FRAIETTA, J. A., MUELLER, Y. M., YANG, G., BOESTEANU, A. C., GRACIAS, D. T., DO, D. H., HOPE, J. L., KATHURIA, N., MCGETTIGAN, S. E. & LEWIS, M. G. 2013. Type I interferon upregulates Bak and contributes to T cell loss during human immunodeficiency virus (HIV) infection. *PLoS pathogens*, 9, e1003658.
120. FRANKEL, A. D. & PABO, C. O. 1988. Cellular uptake of the tat protein from human immunodeficiency virus. *Cell*, 55, 1189-1193.
121. FREED, E. O. 2001. HIV-1 replication. *Somatic cell and molecular genetics*, 26, 13-33.
122. FUJII, Y., OTAKE, K., TASHIRO, M. & ADACHI, A. 1996a. Human immunodeficiency virus type 1 Nef protein on the cell surface is cytotoxic for human CD4+ T cells. *FEBS letters*, 393, 105-108.
123. FUJII, Y., OTAKE, K., TASHIRO, M. & ADACHI, A. 1996b. Soluble Nef antigen of HIV-1 is cytotoxic for human CD4+ T cells. *FEBS letters*, 393, 93-96.
124. GAARDBO, J. C., HARTLING, H. J., GERSTOFT, J. & NIELSEN, S. D. 2012. Incomplete immune recovery in HIV infection: mechanisms, relevance for clinical care, and possible solutions. *Clinical and Developmental Immunology*, 2012.
125. GAINES, H., BIBERFELD, G., BÖTTIGER, B., HANSSON, L., LUNDBERGH, P., SÖNNERBORG, A., WASSERMAN, J. & STRANNEGÅRD, O. 1990. Immunological changes in primary HIV-1 infection. *AIDS (London, England)*, 4, 995-999.
126. GAINES, H., SÖNNERBORG, A., CZAJKOWSKI, J., CHIODI, F., FENYÖ, E., SYDOW, M., ALBERT, J., PEHRSON, P., MOBERG, L. & ÅSJÖ, B. 1987. Antibody response in primary human immunodeficiency virus infection. *The Lancet*, 329, 1249-1253.
127. GALLO, S. A., FINNEGAN, C. M., VIARD, M., RAVIV, Y., DIMITROV, A., RAWAT, S. S., PURI, A., DURELL, S. & BLUMENTHAL, R. 2003. The HIV Env-

- mediated fusion reaction. *Biochimica et Biophysica Acta (BBA)-Biomembranes*, 1614, 36-50.
128. GALLOWAY, N. L., DOITSH, G., MONROE, K. M., YANG, Z., MUÑOZ-ARIAS, I., LEVY, D. N. & GREENE, W. C. 2015. Cell-to-cell transmission of HIV-1 is required to trigger pyroptotic death of lymphoid-tissue-derived CD4 T cells. *Cell reports*, 12, 1555-1563.
 129. GALLUZZI, L., VITALE, I., ABRAMS, J., ALNEMRI, E., BAEHRECKE, E., BLAGOSKLONNY, M., DAWSON, T., DAWSON, V., EL-DEIRY, W. & FULDA, S. 2012. Molecular definitions of cell death subroutines: recommendations of the Nomenclature Committee on Cell Death 2012. *Cell death and differentiation*, 19, 107.
 130. GAN, S. D. & PATEL, K. R. 2013. Enzyme immunoassay and enzyme-linked immunosorbent assay. *J Invest Dermatol*, 133, e12.
 131. GANDHI, T., NAGAPPAN, V., CINTI, S., WEI, W. & KAZANJIAN, P. 2007. Long-term immunologic and virologic responses in patients with highly resistant HIV infection who are treated with an incompletely suppressive antiretroviral regimen. *Clinical infectious diseases*, 45, 1085-1092.
 132. GANSER-PORNILLOS, B. K., CHENG, A. & YEAGER, M. 2007. Structure of full-length HIV-1 CA: a model for the mature capsid lattice. *Cell*, 131, 70-79.
 133. GANSER, B. K., LI, S., KLISHKO, V. Y., FINCH, J. T. & SUNDQUIST, W. I. 1999. Assembly and analysis of conical models for the HIV-1 core. *Science*, 283, 80-83.
 134. GAO, F., BAILES, E., ROBERTSON, D. L., CHEN, Y., RODENBURG, C. M., MICHAEL, S. F., CUMMINS, L. B., ARTHUR, L. O., PEETERS, M. & SHAW, G. M. 1999. Origin of HIV-1 in the chimpanzee *Pan troglodytes troglodytes*. *Nature*, 397, 436.
 135. GAO, F., YUE, L., ROBERTSON, D. L., HILL, S. C., HUI, H., BIGGAR, R. J., NEEQUAYE, A. E., WHELAN, T. M., HO, D. D. & SHAW, G. M. 1994. Genetic diversity of human immunodeficiency virus type 2: evidence for distinct sequence subtypes with differences in virus biology. *Journal of virology*, 68, 7433-7447.
 136. GARDNER, M. R., FELLINGER, C. H., PRASAD, N. R., ZHOU, A. S., KONDIR, H. R., JOSHI, V. R., QUINLAN, B. D. & FARZAN, M. 2016. CD4-induced antibodies promote association of the HIV-1 envelope glycoprotein with CD4-binding site antibodies. *Journal of virology*, JVI. 00803-16.
 137. GARG, H. & BLUMENTHAL, R. 2006a. HIV gp41-induced apoptosis is mediated by caspase-3-dependent mitochondrial depolarization, which is inhibited by HIV protease inhibitor nelfinavir. *Journal of leukocyte biology*, 79, 351-362.
 138. GARG, H. & BLUMENTHAL, R. 2006b. HIV gp41-induced apoptosis is mediated by caspase-3-dependent mitochondrial depolarization, which is inhibited by HIV protease inhibitor nelfinavir. *Journal of leukocyte biology*, 79, 351-362.
 139. GARG, H. & BLUMENTHAL, R. 2008. Role of HIV Gp41-mediated fusion/hemifusion in bystander apoptosis. *Cellular and molecular life sciences*, 65, 3134.
 140. GARG, H. & JOSHI, A. 2017. Host and viral factors in HIV-mediated bystander apoptosis. *Viruses*, 9, 237.
 141. GARG, H., JOSHI, A. & BLUMENTHAL, R. 2009. Altered bystander apoptosis induction and pathogenesis of enfuvirtide-resistant HIV type 1 Env mutants. *AIDS research and human retroviruses*, 25, 811-817.

142. GARG, H., JOSHI, A., FREED, E. O. & BLUMENTHAL, R. 2007. Site-specific mutations in HIV-1 gp41 reveal a correlation between HIV-1-mediated bystander apoptosis and fusion/hemifusion. *Journal of Biological Chemistry*, 282, 16899-16906.
143. GARG, H., JOSHI, A., YE, C., SHANKAR, P. & MANJUNATH, N. 2011. Single amino acid change in gp41 region of HIV-1 alters bystander apoptosis and CD4 decline in humanized mice. *Virology journal*, 8, 34.
144. GARG, H., MOHL, J. & JOSHI, A. 2012. HIV-1 induced bystander apoptosis. *Viruses*, 4, 3020-3043.
145. GARNIER, L., PARENT, L. J., ROVINSKI, B., CAO, S.-X. & WILLS, J. W. 1999. Identification of retroviral late domains as determinants of particle size. *Journal of virology*, 73, 2309-2320.
146. GELEZIUNAS, R., XU, W., TAKEDA, K., ICHIJO, H. & GREENE, W. C. 2001. HIV-1 Nef inhibits ASK1-dependent death signalling providing a potential mechanism for protecting the infected host cell. *Nature*, 410, 834.
147. GERN, J. E. 1997. Cc Ckr5: A Rantes, Mip-1alpha, Mip-1beta Receptor As A Fusion Co-factor For Macrophage-tropic Human Immunodeficiency Virus (hiv-1). *Pediatrics*, 100, 311.
148. GOUGEON, M.-L. 2003. Cell death and immunity: apoptosis as an HIV strategy to escape immune attack. *Nature Reviews Immunology*, 3, 392.
149. GRAY, L., STERJOVSKI, J., CHURCHILL, M., ELLERY, P., NASR, N., LEWIN, S. R., CROWE, S. M., WESSELINGH, S. L., CUNNINGHAM, A. L. & GORRY, P. R. 2005. Uncoupling coreceptor usage of human immunodeficiency virus type 1 (HIV-1) from macrophage tropism reveals biological properties of CCR5-restricted HIV-1 isolates from patients with acquired immunodeficiency syndrome. *Virology*, 337, 384-398.
150. GREEN, D. R. & LLAMBI, F. 2015. Cell death signaling. *Cold Spring Harbor perspectives in biology*, 7, a006080.
151. GREEN, L. A., YI, R., PETRUSCA, D., WANG, T., ELGHOUCHE, A., GUPTA, S. K., PETRACHE, I. & CLAUSS, M. 2013. HIV envelope protein gp120-induced apoptosis in lung microvascular endothelial cells by concerted upregulation of EMAP II and its receptor, CXCR3. *American Journal of Physiology-Lung Cellular and Molecular Physiology*, 306, L372-L382.
152. GREENWAY, A. L., MCPHEE, D. A., ALLEN, K., JOHNSTONE, R., HOLLOWAY, G., MILLS, J., AZAD, A., SANKOVICH, S. & LAMBERT, P. 2002. Human immunodeficiency virus type 1 Nef binds to tumor suppressor p53 and protects cells against p53-mediated apoptosis. *Journal of virology*, 76, 2692-2702.
153. GUILLERM, C., COUDRONNIÈRE, N., ROBERT-HEBMANN, V. & DEVAUX, C. 1998. Delayed human immunodeficiency virus type 1-induced apoptosis in cells expressing truncated forms of CD4. *Journal of virology*, 72, 1754-1761.
154. GUTTMAN, M., GARCIA, N. K., CUPO, A., MATSUI, T., JULIEN, J.-P., SANDERS, R. W., WILSON, I. A., MOORE, J. P. & LEE, K. K. 2014. CD4-induced activation in a soluble HIV-1 Env trimer. *Structure*, 22, 974-984.
155. GYULKHANDANYAN, A. V., MUTLU, A., FREEDMAN, J. & LEYTIN, V. 2015. Mitochondrial permeability transition pore (MPTP)-dependent and-independent pathways of mitochondrial membrane depolarization, cell shrinkage and microparticle formation during platelet apoptosis. *British journal of haematology*, 169, 142-145.

156. HALLENBERGER, S., BOSCH, V., ANGLIKER, H., SHAW, E., KLENK, H.-D. & GARTEN, W. 1992. Inhibition of furin-mediated cleavage activation of HIV-1 glycoprotein gp160. *Nature*, 360, 358.
157. HANAHAH, D. 1983. Studies on transformation of *Escherichia coli* with plasmids. *Journal of molecular biology*, 166, 557-580.
158. HENDRIKS, J. C., SATTEN, G. A., VAN AMEIJDEN, E. J., VAN DRUTEN, H. A., COUTINHO, R. A. & VAN GRIENSVEN, G. J. 1998. The incubation period to AIDS in injecting drug users estimated from prevalent cohort data, accounting for death prior to an AIDS diagnosis. *Aids*, 12, 1537-1544.
159. HERBEIN, G. & KHAN, K. A. 2008. Is HIV infection a TNF receptor signalling-driven disease? *Trends in immunology*, 29, 61-67.
160. HERBEUVAL, J.-P., BOASSO, A., GRIVEL, J.-C., HARDY, A. W., ANDERSON, S. A., DOLAN, M. J., CHOUGNET, C., LIFSON, J. D. & SHEARER, G. M. 2005. TNF-related apoptosis-inducing ligand (TRAIL) in HIV-1-infected patients and its in vitro production by antigen-presenting cells. *Blood*, 105, 2458-2464.
161. HERBEUVAL, J.-P., NILSSON, J., BOASSO, A., HARDY, A. W., KRUHLAK, M. J., ANDERSON, S. A., DOLAN, M. J., DY, M., ANDERSSON, J. & SHEARER, G. M. 2006. Differential expression of IFN- α and TRAIL/DR5 in lymphoid tissue of progressor versus nonprogressor HIV-1-infected patients. *Proceedings of the National Academy of Sciences*, 103, 7000-7005.
162. HILL, M. M., ADRAIN, C., DURIEZ, P. J., CREAGH, E. M. & MARTIN, S. J. 2004. Analysis of the composition, assembly kinetics and activity of native Apaf-1 apoptosomes. *The EMBO journal*, 23, 2134-2145.
163. HINDMARSH, P. & LEIS, J. 1999. Retroviral DNA integration. *Microbiology and Molecular Biology Reviews*, 63, 836-843.
164. HO, D. D., SARNGADHARAN, M., RESNICK, L., DIMARZOVERONESE, F., ROTA, T. R. & HIRSCH, M. S. 1985. Primary human T-lymphotropic virus type III infection. *Annals of internal medicine*, 103, 880-883.
165. HOLM, G. H. & GABUZDA, D. 2005. Distinct mechanisms of CD4+ and CD8+ T-cell activation and bystander apoptosis induced by human immunodeficiency virus type 1 virions. *Journal of virology*, 79, 6299-6311.
166. HOLM, G. H., ZHANG, C., GORRY, P. R., PEDEN, K., SCHOLS, D., DE CLERCQ, E. & GABUZDA, D. 2004. Apoptosis of bystander T cells induced by human immunodeficiency virus type 1 with increased envelope/receptor affinity and coreceptor binding site exposure. *Journal of virology*, 78, 4541-4551.
167. HSU, H., XIONG, J. & GOEDDEL, D. V. 1995. The TNF receptor 1-associated protein TRADD signals cell death and NF- κ B activation. *Cell*, 81, 495-504.
168. HUANG, J., OFEK, G., LAUB, L., LOUDER, M. K., DORIA-ROSE, N. A., LONGO, N. S., IMAMICHI, H., BAILER, R. T., CHAKRABARTI, B. & SHARMA, S. K. 2012. Broad and potent neutralization of HIV-1 by a gp41-specific human antibody. *Nature*, 491, 406.
169. HUANG, Y., ERDMANN, N., PENG, H., HEREK, S., DAVIS, J. S., LUO, X., IKEZU, T. & ZHENG, J. 2006. TRAIL-mediated apoptosis in HIV-1-infected macrophages is dependent on the inhibition of Akt-1 phosphorylation. *The Journal of Immunology*, 177, 2304-2313.
170. IIDA, T., ICHIMURA, H., SHIMADA, T., IBUKI, K., UI, M., TAMARU, K., KUWATA, T., YONEHARA, S., IMANISHI, J. & HAYAMI, M. 2000. Role of apoptosis induction in both peripheral lymph nodes and thymus in progressive

- loss of CD4+ cells in SHIV-infected macaques. *AIDS research and human retroviruses*, 16, 9-18.
171. IPP, H., NKAMBULE, B. B., REID, T. D., DE SWARDT, D., BEKKER, L.-G. & GLASHOFF, R. H. 2014. CD4+ T cells in HIV infection show increased levels of expression of a receptor for vasoactive intestinal peptide, VPAC2. *Immunologic research*, 60, 11-15.
 172. JACOB, R. A., JOHNSON, A. L., PAWLAK, E. N., DIRK, B. S., VAN NYNATTEN, L. R., HAERYFAR, S. M. & DIKEAKOS, J. D. 2017. The interaction between HIV-1 Nef and adaptor protein-2 reduces Nef-mediated CD4+ T cell apoptosis. *Virology*, 509, 1-10.
 173. JACOBSON, M. D., WEIL, M. & RAFF, M. C. 1997. Programmed cell death in animal development. *Cell*, 88, 347-354.
 174. JACOTOT, E., FERRI, K. F., EL HAMEL, C., BRENNER, C., DRUILLENNEC, S., HOEBEKE, J., RUSTIN, P., MÉTIVIER, D., LENOIR, C. & GEUSKENS, M. 2001. Control of mitochondrial membrane permeabilization by adenine nucleotide translocator interacting with HIV-1 viral protein R and Bcl-2. *Journal of Experimental Medicine*, 193, 509-520.
 175. JAMES, C. O., HUANG, M.-B., KHAN, M., GARCIA-BARRIO, M., POWELL, M. D. & BOND, V. C. 2004. Extracellular Nef protein targets CD4+ T cells for apoptosis by interacting with CXCR4 surface receptors. *Journal of virology*, 78, 3099-3109.
 176. JEKLE, A., KEPPLER, O. T., DE CLERCQ, E., SCHOLS, D., WEINSTEIN, M. & GOLDSMITH, M. A. 2003. In vivo evolution of human immunodeficiency virus type 1 toward increased pathogenicity through CXCR4-mediated killing of uninfected CD4 T cells. *Journal of virology*, 77, 5846-5854.
 177. JI, J., ZHANG, Y., REDON, C. E., REINHOLD, W. C., CHEN, A. P., FOGLI, L. K., HOLBECK, S. L., PARCHMENT, R. E., HOLLINGSHEAD, M. & TOMASZEWSKI, J. E. 2017. Phosphorylated fraction of H2AX as a measurement for DNA damage in cancer cells and potential applications of a novel assay. *PloS one*, 12, e0171582.
 178. JORGENSEN, I., RAYAMAJHI, M. & MIAO, E. A. 2017. Programmed cell death as a defence against infection. *Nature reviews immunology*, 17, 151.
 179. JOSHI, A., LEE, R. T., MOHL, J., SEDANO, M., KHONG, W. X., NG, O. T., MAURER-STROH, S. & GARG, H. 2014. Genetic signatures of HIV-1 envelope-mediated bystander apoptosis. *Journal of Biological Chemistry*, 289, 2497-2514.
 180. JOSHI, A., NYAKERIGA, A. M., RAVI, R. & GARG, H. 2011. HIV ENV glycoprotein-mediated bystander apoptosis depends on expression of the CCR5 co-receptor at the cell surface and ENV fusogenic activity. *Journal of Biological Chemistry*, 286, 36404-36413.
 181. JOSHI, A., PUNKE, E. B., SEDANO, M., BEAUCHAMP, B., PATEL, R., HOSSENLOPP, C., ALOZIE, O. K., GUPTA, J., MUKHERJEE, D. & GARG, H. 2017. CCR5 promoter activity correlates with HIV disease progression by regulating CCR5 cell surface expression and CD4 T cell apoptosis. *Scientific reports*, 7, 232.
 182. JOSHI, A., SEDANO, M., BEAUCHAMP, B., PUNKE, E. B., MULLA, Z. D., MEZA, A., ALOZIE, O. K., MUKHERJEE, D. & GARG, H. 2016. HIV-1 Env glycoprotein phenotype along with immune activation determines CD4 T cell loss in HIV patients. *The Journal of Immunology*, 1501588.
 183. JOZA, N., SUSIN, S. A., DAUGAS, E., STANFORD, W. L., CHO, S. K., LI, C. Y., SASAKI, T., ELIA, A. J., CHENG, H.-Y. M. & RAVAGNAN, L. 2001. Essential

- role of the mitochondrial apoptosis-inducing factor in programmed cell death. *Nature*, 410, 549-554.
184. JUBAULT, V., BURGARD, M., LE CORFEC, E., COSTAGLIOLA, D., ROUZIOUX, C. & VIARD, J. 1998. High rebound of plasma and cellular HIV load after discontinuation of triple combination therapy. *AIDS (London, England)*, 12, 2358.
 185. JULIEN, J.-P., CUPO, A., SOK, D., STANFIELD, R. L., LYUMKIS, D., DELLER, M. C., KLASSE, P.-J., BURTON, D. R., SANDERS, R. W. & MOORE, J. P. 2013. Crystal structure of a soluble cleaved HIV-1 envelope trimer. *Science*, 1245625.
 186. JULIEN, J.-P., LEE, J. H., OZOROWSKI, G., HUA, Y., DE LA PEÑA, A. T., DE TAEYE, S. W., NIEUSMA, T., CUPO, A., YASMEEN, A. & GOLABEK, M. 2015. Design and structure of two HIV-1 clade C SOSIP. 664 trimers that increase the arsenal of native-like Env immunogens. *Proceedings of the National Academy of Sciences*, 112, 11947-11952.
 187. KAPLAN, G., ROITBURD-BERMAN, A., LEWIS, G. K. & GERSHONI, J. M. 2016. The range of CD4-bound conformations of HIV-1 gp120, as defined using conditional CD4-induced antibodies. *Journal of virology*, JVI. 03206-15.
 188. KHAN, K. H. 2013. Gene expression in mammalian cells and its applications. *Advanced pharmaceutical bulletin*, 3, 257.
 189. KHAYAT, R., LEE, J. H., JULIEN, J.-P., CUPO, A., KLASSE, P. J., SANDERS, R. W., MOORE, J. P., WILSON, I. A. & WARD, A. B. 2013. Structural characterization of cleaved, soluble human immunodeficiency virus type-1 envelope glycoprotein trimers. *Journal of virology*, JVI. 01222-13.
 190. KILLICK, M., CAPOVILLA, A. & PAPATHANASOPOULOS, M. A. 2014. Generation and characterization of an HIV-1 subtype C transmitted and early founder virus consensus sequence. *AIDS research and human retroviruses*, 30, 1001-1005.
 191. KILLICK, M. A., GRANT, M. L., CERUTTI, N. M., CAPOVILLA, A. & PAPATHANASOPOULOS, M. A. 2015. Env-2dCD4S60C complexes act as super immunogens and elicit potent, broadly neutralizing antibodies against clinically relevant human immunodeficiency virus type 1 (HIV-1). *Vaccine*, 33, 6298-6306.
 192. KIM, N., DABROWSKA, A., JENNER, R. G. & ALDOVINI, A. 2007. Human and simian immunodeficiency virus-mediated upregulation of the apoptotic factor TRAIL occurs in antigen-presenting cells from AIDS-susceptible but not from AIDS-resistant species. *Journal of virology*, 81, 7584-7597.
 193. KISCHKEL, F., HELLBARDT, S., BEHRMANN, I., GERMER, M., PAWLITA, M., KRAMMER, P. & PETER, M. 1995. Cytotoxicity-dependent APO-1 (Fas/CD95)-associated proteins form a death-inducing signaling complex (DISC) with the receptor. *The EMBO journal*, 14, 5579.
 194. KLASSE, P. J. 2012. The molecular basis of HIV entry. *Cellular microbiology*, 14, 1183-1192.
 195. KLASSE, P. J., DEPETRIS, R. S., PEJCHAL, R., JULIEN, J.-P., KHAYAT, R., LEE, J. H., MAROZSAN, A. J., CUPO, A., COCCO, N. & KORZUN, J. 2013. Influences on trimerization and aggregation of soluble, cleaved HIV-1 SOSIP envelope glycoprotein. *Journal of virology*, JVI. 01226-13.
 196. KLATZMANN, D., BARRE-SINOUSSE, F., NUGEYRE, M. T., DANQUET, C., VILMER, E., GRISCELLI, C., BRUN-VEZIRET, F., ROUZIOUX, C., GLUCKMAN,

- J. C. & CHERMANN, J.-C. 1984. Selective tropism of lymphadenopathy associated virus (LAV) for helper-inducer T lymphocytes. *Science*, 225, 59-63.
197. KORBER, B., GASCHEN, B., YUSIM, K., THAKALLAPALLY, R., KESMIR, C. & DETOURS, V. 2001. Evolutionary and immunological implications of contemporary HIV-1 variation. *British medical bulletin*, 58, 19-42.
198. KOTHE, D. L., DECKER, J. M., LI, Y., WENG, Z., BIBOLLET-RUCHE, F., ZAMMIT, K. P., SALAZAR, M. G., CHEN, Y., SALAZAR-GONZALEZ, J. F. & MOLDOVEANU, Z. 2007. Antigenicity and immunogenicity of HIV-1 consensus subtype B envelope glycoproteins. *Virology*, 360, 218-234.
199. KOTHE, D. L., LI, Y., DECKER, J. M., BIBOLLET-RUCHE, F., ZAMMIT, K. P., SALAZAR, M. G., CHEN, Y., WENG, Z., WEAVER, E. A. & GAO, F. 2006. Ancestral and consensus envelope immunogens for HIV-1 subtype C. *Virology*, 352, 438-449.
200. KOTTILIL, S., JACKSON, J. O., REITANO, K. N., O'SHEA, M. A., ROBY, G., LLOYD, M., YANG, J., HALLAHAN, C. W., REHM, C. A. & ARTHOS, J. 2007. Innate immunity in HIV infection: enhanced susceptibility to CD95-mediated natural killer cell death and turnover induced by HIV viremia. *JAIDS Journal of Acquired Immune Deficiency Syndromes*, 46, 151-159.
201. KWON, Y. D., GEORGIEV, I. S., OFEK, G., ZHANG, B., ASOKAN, M., BAILER, R. T., BAO, A., CARUSO, W., CHEN, X. & CHOE, M. 2016. Optimization of the solubility of HIV-1-neutralizing antibody 10E8 through somatic variation and structure-based design. *Journal of virology*, JVI. 03246-15.
202. KWONG, P. D., WYATT, R., ROBINSON, J., SWEET, R. W., SODROSKI, J. & HENDRICKSON, W. A. 1998. Structure of an HIV gp120 envelope glycoprotein in complex with the CD4 receptor and a neutralizing human antibody. *Nature*, 393, 648-659.
203. LACKNER, A., LEDERMAN, M. M. & RODRIGUEZ, B. 2012. HIV pathogenesis: the host. *Cold Spring Harbor perspectives in medicine*, a007005.
204. LAFORGE, M., SILVESTRE, R., RODRIGUES, V., GARIBAL, J., CAMPILLO-GIMENEZ, L., MOUHAMAD, S., MONCEAUX, V., CUMONT, M.-C., RABEZANAHARY, H. & PRUVOST, A. 2018. The anti-caspase inhibitor Q-VD-OPH prevents AIDS disease progression in SIV-infected rhesus macaques. *The Journal of clinical investigation*, 128.
205. LASKEY, S. B. & SILICIANO, R. F. 2014. A mechanistic theory to explain the efficacy of antiretroviral therapy. *Nature Reviews Microbiology*, 12, 772.
206. LASKY, L. A., GROOPMAN, J. E., FENNIE, C. W., BENZ, P. M., CAPON, D. J., DOWBENKO, D. J., NAKAMURA, G. R., NUNES, W. M., RENZ, M. E. & BERMAN, P. W. 1986. Neutralization of the AIDS retrovirus by antibodies to a recombinant envelope glycoprotein. *Science*, 233, 209-212.
207. LAURENT-CRAWFORD, A., COCCIA, E., KRUST, B. & HOVANESSIAN, A. 1995. Membrane-expressed HIV envelope glycoprotein heterodimer is a powerful inducer of cell death in uninfected CD4+ target cells. *Research in virology*, 146, 5-17.
208. LECOEUR, H. & GOUGEON, M.-L. 1996. Comparative analysis of flow cytometric methods for apoptosis quantitation in murine thymocytes and human peripheral lymphocytes from controls and HIV-infected persons evidence for interference by granulocytes and erythrocytes. *Journal of immunological methods*, 198, 87-99.

209. LEE, J. H., OZOROWSKI, G. & WARD, A. B. 2016. Cryo-EM structure of a native, fully glycosylated, cleaved HIV-1 envelope trimer. *Science*, 351, 1043-1048.
210. LEMEY, P., PYBUS, O. G., WANG, B., SAKSENA, N. K., SALEMI, M. & VANDAMME, A.-M. 2003. Tracing the origin and history of the HIV-2 epidemic. *Proceedings of the National Academy of Sciences*, 100, 6588-6592.
211. LENASSI, M., CAGNEY, G., LIAO, M., VAUPOTIČ, T., BARTHOLOMEEUSEN, K., CHENG, Y., KROGAN, N. J., PLEMENITAŠ, A. & PETERLIN, B. M. 2010. HIV Nef is secreted in exosomes and triggers apoptosis in bystander CD4+ T cells. *Traffic*, 11, 110-122.
212. LI, C. J., FRIEDMAN, D. J., WANG, C., METELEV, V. & PARDEE, A. B. 1995. Induction of apoptosis in uninfected lymphocytes by HIV-1 Tat protein. *Science*, 268, 429-431.
213. LI, H. & PAUZA, C. D. 2011. HIV envelope-mediated, CCR5/ α 4 β 7-dependent killing of CD4-negative $\gamma\delta$ T cells which are lost during progression to AIDS. *Blood*, blood-2011-05-356535.
214. LI, L. Y., LUO, X. & WANG, X. 2001. Endonuclease G is an apoptotic DNase when released from mitochondria. *Nature*, 412, 95-99.
215. LI, Q., SMITH, A. J., SCHACKER, T. W., CARLIS, J. V., DUAN, L., REILLY, C. S. & HAASE, A. T. 2009. Microarray analysis of lymphatic tissue reveals stage-specific, gene expression signatures in HIV-1 infection. *The Journal of Immunology*, jimmunol. 0803222.
216. LI, S., JUAREZ, J., ALALI, M., DWYER, D., COLLMAN, R., CUNNINGHAM, A. & NAIF, H. M. 1999. Persistent CCR5 utilization and enhanced macrophage tropism by primary blood human immunodeficiency virus type 1 isolates from advanced stages of disease and comparison to tissue-derived isolates. *Journal of virology*, 73, 9741-9755.
217. LIU, J., BARTESAGHI, A., BORGNIA, M. J., SAPIRO, G. & SUBRAMANIAM, S. 2008. Molecular architecture of native HIV-1 gp120 trimers. *Nature*, 455, 109-113.
218. LIU, X., LIU, L., WANG, Y., WANG, X., MA, Y. & LI, Y. 2014. The study on the factors affecting transformation efficiency of E. coli competent cells. *Cell*, 5, x106.
219. LIU, Y. Q., LI, W. Q., MORRIS-NATSCHKE, S. L., QIAN, K., YANG, L., ZHU, G. X., WU, X. B., CHEN, A. L., ZHANG, S. Y. & NAN, X. 2015. Perspectives on biologically active camptothecin derivatives. *Medicinal research reviews*, 35, 753-789.
220. LOCKSLEY, R. M., KILLEEN, N. & LENARDO, M. J. 2001. The TNF and TNF receptor superfamilies: integrating mammalian biology. *Cell*, 104, 487-501.
221. LORETO, C., LA ROCCA, G., ANZALONE, R., CALTABIANO, R., VESPASIANI, G., CASTORINA, S., RALPH, D. J., CELLEK, S., MUSUMECI, G. & GIUNTA, S. 2014. The role of intrinsic pathway in apoptosis activation and progression in Peyronie's disease. *BioMed research international*, 2014.
222. LYUMKIS, D., JULIEN, J.-P., DE VAL, N., CUPO, A., POTTER, C. S., KLASSE, P.-J., BURTON, D. R., SANDERS, R. W., MOORE, J. P. & CARRAGHER, B. 2013. Cryo-EM structure of a fully glycosylated soluble cleaved HIV-1 envelope trimer. *Science*, 342, 1484-1490.
223. MAAS, J. J., GANGE, S. J., SCHUITEMAKER, H., COUTINHO, R. A., VAN LEEUWEN, R. & MARGOLICK, J. B. 2000. Strong association between failure of T cell homeostasis and the syncytium-inducing phenotype among HIV-1-infected men in the Amsterdam Cohort Study. *Aids*, 14, 1155-1161.

224. MACHO, A., CALZADO, M. A. & CEBALLOS, E. 1999. Susceptibility of HIV-1-TAT transfected cells to undergo apoptosis. Biochemical mechanisms. *Oncogene*, 18, 7543.
225. MADDON, P. J., DALGLEISH, A. G., MCDUGAL, J. S., CLAPHAM, P. R., WEISS, R. A. & AXEL, R. 1986. The T4 gene encodes the AIDS virus receptor and is expressed in the immune system and the brain. *Cell*, 47, 333-348.
226. MANES, T. L. & COTA-GOMEZ, A. 2016. Mechanisms of HIV-1 Tat-Mediated Regulation of the Manganese-Superoxide Dismutase Promoter. *Free Radical Biology and Medicine*, 100, S58.
227. MARKOSYAN, R. M., COHEN, F. S. & MELIKYAN, G. B. 2003. HIV-1 envelope proteins complete their folding into six-helix bundles immediately after fusion pore formation. *Molecular biology of the cell*, 14, 926-938.
228. MARTIN-VILLALBA, A., LLORENS-BOBADILLA, E. & WOLLNY, D. 2013. CD95 in cancer: tool or target? *Trends in molecular medicine*, 19, 329-335.
229. MARX, P. A., ALCABES, P. G. & DRUCKER, E. 2001. Serial human passage of simian immunodeficiency virus by unsterile injections and the emergence of epidemic human immunodeficiency virus in Africa. *Philosophical Transactions of the Royal Society of London B: Biological Sciences*, 356, 911-920.
230. MASUDA, T., SATO, Y., HUANG, Y.-L., KOI, S., TAKAHATA, T., HASEGAWA, A., KAWAI, G. & KANNAGI, M. 2015. Fate of HIV-1 cDNA intermediates during reverse transcription is dictated by transcription initiation site of virus genomic RNA. *Scientific reports*, 5, 17680.
231. MASUR, H. 2015. HIV-related opportunistic infections are still relevant in 2015. *Topics in antiviral medicine*, 23, 116.
232. MATRAJT, L., YOUNAN, P. M., KIEM, H.-P. & SCHIFFER, J. T. 2014. The majority of CD4+ T-cell depletion during acute SHIV89. 6P infection occurs in uninfected cells. *Journal of virology*, JVI. 03428-13.
233. MATTEI, S., GLASS, B., HAGEN, W. J., KRÄUSSLICH, H.-G. & BRIGGS, J. A. 2016. The structure and flexibility of conical HIV-1 capsids determined within intact virions. *Science*, 354, 1434-1437.
234. MCCLOSKEY, T. W., OTT, M., TRIBBLE, E., KHAN, S. A., TEICHBERG, S., PAUL, M. O., PAHWA, S., VERDIN, E. & CHIRMULE, N. 1997. Dual role of HIV Tat in regulation of apoptosis in T cells. *The Journal of Immunology*, 158, 1014-1019.
235. MCDUGAL, J., KENNEDY, M., SLIGH, J., CORT, S., MAWLE, A. & NICHOLSON, K. 1986. Binding of HTLV-III-LAV to T4plus T cells by a complex of the 110K viral protein and the T4 molecule. *Science*, 231, 382-386.
236. MEISSNER, E. G., COFFIELD, V. M. & SU, L. 2005. Thymic pathogenicity of an HIV-1 envelope is associated with increased CXCR4 binding efficiency and V5-gp41-dependent activity, but not V1/V2-associated CD4 binding efficiency and viral entry. *Virology*, 336, 184-197.
237. MEISSNER, E. G., ZHANG, L., JIANG, S. & SU, L. 2006. Fusion-induced apoptosis contributes to thymocyte depletion by a pathogenic human immunodeficiency virus type 1 envelope in the human thymus. *Journal of virology*, 80, 11019-11030.
238. MEYAARD, L., OTTO, S. A., JONKER, R. R., MIJNSTER, M. J., KEET, R. & MIEDEMA, F. 1992. Programmed death of T cells in HIV-1 infection. *Science*, 257, 217-219.
239. MEYTHALER, M., MARTINOT, A., WANG, Z., PRYPUTNIEWICZ, S., KASHETA, M., LING, B., MARX, P. A., O'NEIL, S. & KAUR, A. 2009. Differential

- CD4+ T-lymphocyte apoptosis and bystander T-cell activation in rhesus macaques and sooty mangabeys during acute simian immunodeficiency virus infection. *Journal of virology*, 83, 572-583.
240. MEYTHALER, M., PRYPUTNIEWICZ, S. & KAUR, A. 2008. Kinetics of T lymphocyte apoptosis and the cellular immune response in SIVmac239-infected rhesus macaques. *Journal of medical primatology*, 37, 33-45.
241. MILLER, M. D., FARNET, C. M. & BUSHMAN, F. D. 1997. Human immunodeficiency virus type 1 preintegration complexes: studies of organization and composition. *Journal of virology*, 71, 5382-5390.
242. MISTRY, B., D'ORSOGNA, M. R., WEBB, N. E., LEE, B. & CHOU, T. 2016. Quantifying the sensitivity of HIV-1 viral entry to receptor and coreceptor expression. *The Journal of Physical Chemistry B*, 120, 6189-6199.
243. MITRA, D., STEINER, M., LYNCH, D., STAIANO-COICO, L. & LAURENCE, J. 1996. HIV-1 upregulates Fas ligand expression in CD4+ T cells in vitro and in vivo: association with Fas-mediated apoptosis and modulation by aurintricarboxylic acid. *Immunology*, 87, 581-585.
244. MOORE, P. L., GRAY, E. S., SHEWARD, D., MADIGA, M., RANCHOBE, N., LAI, Z., HONNEN, W. J., NONYANE, M., TUMBA, N. & HERMANUS, T. 2011. Potent and broad neutralization of HIV-1 subtype C by plasma antibodies targeting a quaternary epitope including residues in the V2 loop. *Journal of virology*, 85, 3128-3141.
245. MORIKAWA, Y., BARSOV, E. & JONES, I. 1993. Legitimate and illegitimate cleavage of human immunodeficiency virus glycoproteins by furin. *Journal of virology*, 67, 3601-3604.
246. MORRISON, S. L. 1997. Transformation of *E. coli* by electroporation. *Current protocols in immunology*, 21, A. 3N. 1-A. 3N. 4.
247. MOULARD, M. & DECROLY, E. 2000. Maturation of HIV envelope glycoprotein precursors by cellular endoproteases. *Biochimica et Biophysica Acta (BBA)-Reviews on Biomembranes*, 1469, 121-132.
248. MOUTOUH, L., ESTAQUIER, J., RICHMAN, D. D. & CORBEIL, J. 1998. Molecular and cellular analysis of human immunodeficiency virus-induced apoptosis in lymphoblastoid T-cell-line-expressing wild-type and mutated CD4 receptors. *Journal of virology*, 72, 8061-8072.
249. MTAMBO, A., CHAN, K., SHEN, A., LIMA, V., HOGG, R., MONTANER, J. & MOORE, D. 2012. Treatment limitations imposed by antiretroviral drug resistance mutations: implication for choices of first line regimens in resource-limited settings. *HIV medicine*, 13, 141-147.
250. MUÑOZ, A., WANG, M.-C., BASS, S., TAYLOR, J. M., KINGSLEY, L. A., CHMIEL, J. S., POLK, B. F. & GROUP, M. A. C. S. 1989. Acquired immunodeficiency syndrome (AIDS)-free time after human immunodeficiency virus type 1 (HIV-1) seroconversion in homosexual men. *American Journal of Epidemiology*, 130, 530-539.
251. MURO-CACHO, C. A., PANTALEO, G. & FAUCI, A. S. 1995. Analysis of apoptosis in lymph nodes of HIV-infected persons. Intensity of apoptosis correlates with the general state of activation of the lymphoid tissue and not with stage of disease or viral burden. *The Journal of Immunology*, 154, 5555-5566.
252. MUTHUMANI, K., ZHANG, D., HWANG, D. S., KUDCHODKAR, S., DAYES, N. S., DESAI, B. M., MALIK, A. S., YANG, J.-S., CHATTERGOON, M. A. & MAGUIRE JR, H. C. 2002. Adenovirus encoding HIV-1 Vpr activates caspase 9

- and induces apoptotic cell death in both p53 positive and negative human tumor cell lines. *Oncogene*, 21, 4613.
253. MYSZKA, D. G., SWEET, R. W., HENSLEY, P., BRIGHAM-BURKE, M., KWONG, P. D., HENDRICKSON, W. A., WYATT, R., SODROSKI, J. & DOYLE, M. L. 2000. Energetics of the HIV gp120-CD4 binding reaction. *Proceedings of the National Academy of Sciences*, 97, 9026-9031.
 254. NAKANO, K. & VOUSDEN, K. H. 2001. PUMA, a novel proapoptotic gene, is induced by p53. *Molecular cell*, 7, 683-694.
 255. NARDACCI, R., ANTINORI, A., KROEMER, G. & PIACENTINI, M. 2005. Cell death mechanisms in HIV-associated dementia: the involvement of syncytia. *Cell death and differentiation*, 12, 855.
 256. NARDACCI, R., PERFETTINI, J., GRIECO, L., THIEFFRY, D., KROEMER, G. & PIACENTINI, M. 2015. Syncytial apoptosis signaling network induced by the HIV-1 envelope glycoprotein complex: an overview. *Cell death & disease*, 6, e1846.
 257. NAVIS, M., MATAS, D. E., RACHINGER, A., KONING, F. A., VAN SWIETEN, P., KOOTSTRA, N. A. & SCHUITEMAKER, H. 2008. Molecular evolution of human immunodeficiency virus type 1 upon transmission between human leukocyte antigen disparate donor-recipient pairs. *PloS one*, 3, e2422.
 258. NIE, Z., BREN, G. D., VLAHAKIS, S. R., SCHIMNICH, A. A., BRENCHLEY, J. M., TRUSHIN, S. A., WARREN, S., SCHNEPPLE, D. J., KOVACS, C. M. & LOUTFY, M. R. 2007. Human immunodeficiency virus type 1 protease cleaves procaspase 8 in vivo. *Journal of virology*, 81, 6947-6956.
 259. NISOLE, S. & SAÏB, A. 2004. Early steps of retrovirus replicative cycle. *Retrovirology*, 1, 9.
 260. NYAMWEYA, S., HEGEDUS, A., JAYE, A., ROWLAND-JONES, S., FLANAGAN, K. L. & MACALLAN, D. C. 2013. Comparing HIV-1 and HIV-2 infection: Lessons for viral immunopathogenesis. *Reviews in medical virology*, 23, 221-240.
 261. OH, S.-K., CRUIKSHANK, W. W., RAINA, J., BLANCHARD, G. C., ADLER, W. H., WALKER, J. & KORNFELD, H. 1992. Identification of HIV-1 envelope glycoprotein in the serum of AIDS and ARC patients. *Journal of acquired immune deficiency syndromes*, 5, 251-256.
 262. OTAKE, K., FUJII, Y., NAKAYA, T., NISHINO, Y., ZHONG, Q., FUJINAGA, K., KAMEOKA, M., OHKI, K. & IKUTA, K. 1994. The carboxyl-terminal region of HIV-1 Nef protein is a cell surface domain that can interact with CD4+ T cells. *The Journal of Immunology*, 153, 5826-5837.
 263. OYAIZU, N., MCCLOSKEY, T. W., CORONESI, M., CHIRMULE, N., KALYANARAMAN, V. S. & PAHWA, S. 1993. Accelerated apoptosis in peripheral blood mononuclear cells (PBMCs) from human immunodeficiency virus type-1 infected patients and in CD4 cross-linked PBMCs from normal individuals. *Blood*, 82, 3392-3400.
 264. OZOROWSKI, G., PALLESEN, J., DE VAL, N., LYUMKIS, D., COTTRELL, C. A., TORRES, J. L., COPPS, J., STANFIELD, R. L., CUPO, A. & PUGACH, P. 2017. Open and closed structures reveal allostery and pliability in the HIV-1 envelope spike. *Nature*, 547, 360.
 265. PANCERA, M., ZHOU, T., DRUZ, A., GEORGIEV, I. S., SOTO, C., GORMAN, J., HUANG, J., ACHARYA, P., CHUANG, G.-Y. & OFEK, G. 2014. Structure and immune recognition of trimeric pre-fusion HIV-1 Env. *Nature*, 514, 455-461.

266. PANTALEO, G., GRAZIOSI, C., DEMAREST, J. F., BUTINI, L., MONTRONI, M., FOX, C. H., ORENSTEIN, J. M., KOTLER, D. P. & FAUCI, A. S. 1993a. HIV infection is active and progressive in lymphoid tissue during the clinically latent stage of disease. *Nature*, 362, 355.
267. PANTALEO, G., GRAZIOSI, C. & FAUCI, A. S. 1993b. The immunopathogenesis of human immunodeficiency virus infection. *New England Journal of Medicine*, 328, 327-335.
268. PAPAMICHOS-CHRONAKIS, M. & PETERSON, C. L. 2013. Chromatin and the genome integrity network. *Nature Reviews Genetics*, 14, 62.
269. PERFETTINI, J.-L., NARDACCI, R., BOUROUBA, M., SUBRA, F., GROS, L., SÉROR, C., MANIC, G., ROSSELLI, F., AMENDOLA, A. & MASDEHORS, P. 2008. Critical involvement of the ATM-dependent DNA damage response in the apoptotic demise of HIV-1-elicited syncytia. *PLoS One*, 3, e2458.
270. PERFETTINI, J.-L., ROUMIER, T., CASTEDO, M., LAROCLETTE, N., BOYA, P., RAYNAL, B., LAZAR, V., CICCOSANTI, F., NARDACCI, R. & PENNINGER, J. 2004. NF- κ B and p53 are the dominant apoptosis-inducing transcription factors elicited by the HIV-1 envelope. *Journal of Experimental Medicine*, 199, 629-640.
271. PERFETTINI, J., CASTEDO, M., ROUMIER, T., ANDREAU, K., NARDACCI, R., PIACENTINI, M. & KROEMER, G. 2005a. Mechanisms of apoptosis induction by the HIV-1 envelope. *Cell Death & Differentiation*, 12, 916-923.
272. PERFETTINI, J., CASTEDO, M., ROUMIER, T., ANDREAU, K., NARDACCI, R., PIACENTINI, M. & KROEMER, G. 2005b. Mechanisms of apoptosis induction by the HIV-1 envelope. *Cell Death & Differentiation*, 12.
273. PERRY, S. W., NORMAN, J. P., LITZBURG, A., ZHANG, D., DEWHURST, S. & GELBARD, H. A. 2005. HIV-1 transactivator of transcription protein induces mitochondrial hyperpolarization and synaptic stress leading to apoptosis. *The Journal of Immunology*, 174, 4333-4344.
274. PETER, M. E., HADJI, A., MURMANN, A. E., BROCKWAY, S., PUTZBACH, W., PATTANAYAK, A. & CEPPI, P. 2015. The role of CD95 and CD95 ligand in cancer. *Cell death and differentiation*, 22, 549.
275. PETIT, F., ARNOULT, D., LELIÈVRE, J.-D., MOUTOUH-DE PARSEVAL, L., HANCE, A. J., SCHNEIDER, P., CORBEIL, J., AMEISEN, J. C. & ESTAQUIER, J. 2002. Productive HIV-1 infection of primary CD4⁺ T cells induces mitochondrial membrane permeabilization leading to a caspase-independent cell death. *Journal of Biological Chemistry*, 277, 1477-1487.
276. PIETRO, R. D. & ZAULI, G. 2004. Emerging non-apoptotic functions of tumor necrosis factor-related apoptosis-inducing ligand (TRAIL)/Apo2L. *Journal of cellular physiology*, 201, 331-340.
277. PILLAY, N. C. 2011. *HIV-1 subtype B and C GP120-mediated apoptosis of bystander CD4⁺ T lymphocytes*. Faculty of Health Sciences, University of the Witwatersrand.
278. PLANTIER, J.-C., LEOZ, M., DICKERSON, J. E., DE OLIVEIRA, F., CORDONNIER, F., LEMÉE, V., DAMOND, F., ROBERTSON, D. L. & SIMON, F. 2009. A new human immunodeficiency virus derived from gorillas. *Nature medicine*, 15, 871.
279. PLATT, E. J., WEHRLY, K., KUHMAN, S. E., CHESEBRO, B. & KABAT, D. 1998. Effects of CCR5 and CD4 cell surface concentrations on infections by macrophagetropic isolates of human immunodeficiency virus type 1. *Journal of virology*, 72, 2855-2864.

280. PODHORECKA, M., SKLADANOWSKI, A. & BOZKO, P. 2010. H2AX phosphorylation: its role in DNA damage response and cancer therapy. *Journal of nucleic acids*, 2010.
281. POLLARA, J., HART, L., BREWER, F., PICKERAL, J., PACKARD, B. Z., HOXIE, J. A., KOMORIYA, A., OCHSENBAUER, C., KAPPES, J. C. & ROEDERER, M. 2011. High-throughput quantitative analysis of HIV-1 and SIV-specific ADCC-mediating antibody responses. *Cytometry Part A*, 79, 603-612.
282. POONIA, B., PAUZA, C. D. & SALVATO, M. S. 2009. Role of the Fas/FasL pathway in HIV or SIV disease. *Retrovirology*, 6, 91.
283. POPOVIC, M., SARNGADHARAN, M. G., READ, E. & GALLO, R. C. 1984. Detection, isolation, and continuous production of cytopathic retroviruses (HTLV-III) from patients with AIDS and pre-AIDS. *Science*, 224, 497-500.
284. PORNILLOS, O., GANSER-PORNILLOS, B. K., KELLY, B. N., HUA, Y., WHITBY, F. G., STOUT, C. D., SUNDQUIST, W. I., HILL, C. P. & YEAGER, M. 2009. X-ray structures of the hexameric building block of the HIV capsid. *Cell*, 137, 1282-1292.
285. POWERS, K. A., KRETZSCHMAR, M. E., MILLER, W. C. & COHEN, M. S. 2014. Impact of early-stage HIV transmission on treatment as prevention. *Proceedings of the National Academy of Sciences*, 111, 15867-15868.
286. PRITCHARD, L. K., VASILJEVIC, S., OZOROWSKI, G., SEABRIGHT, G. E., CUPO, A., RINGE, R., KIM, H. J., SANDERS, R. W., DOORES, K. J. & BURTON, D. R. 2015. Structural constraints determine the glycosylation of HIV-1 envelope trimers. *Cell reports*, 11, 1604-1613.
287. PUGACH, P., OZOROWSKI, G., CUPO, A., RINGE, R., YASMEEN, A., DE VAL, N., DERKING, R., KIM, H. J., KORZUN, J. & GOLABEK, M. 2015. A native-like SOSIP. 664 trimer based on an HIV-1 subtype B env gene. *Journal of virology*, 89, 3380-3395.
288. RAMPAL, G., KHANNA, N., THIND, T. S., ARORA, S. & VIG, A. 2012. Role of isothiocyanates as anticancer agents and their contributing molecular and cellular mechanisms. *Med. Chem. Drug Discovery*, 3, 79-93.
289. RANKOVIC, S., VARADARAJAN, J., RAMALHO, R., AIKEN, C. & ROUSSO, I. 2017. Reverse transcription mechanically initiates HIV-1 capsid disassembly. *Journal of virology*, JVI. 00289-17.
290. RASOLA, A., GRAMAGLIA, D., BOCCACCIO, C. & COMOGLIO, P. M. 2001. Apoptosis enhancement by the HIV-1 Nef protein. *The Journal of Immunology*, 166, 81-88.
291. REED, J. C. 2000. Mechanisms of apoptosis. *The American journal of pathology*, 157, 1415-1430.
292. REEVES, J. D., GALLO, S. A., AHMAD, N., MIAMIDIAN, J. L., HARVEY, P. E., SHARRON, M., PÖHLMANN, S., SFAKIANOS, J. N., DERDEYN, C. A. & BLUMENTHAL, R. 2002. Sensitivity of HIV-1 to entry inhibitors correlates with envelope/coreceptor affinity, receptor density, and fusion kinetics. *Proceedings of the National Academy of Sciences*, 99, 16249-16254.
293. REINBERGER, S., SPRING, M., NIßLEIN, T., STAHL-HENNIG, C., HUNSMANN, G. & DITTMER, U. 1999. Kinetics of lymphocyte apoptosis in macaques infected with different simian immunodeficiency viruses or simian/human immunodeficiency hybrid viruses. *Clinical Immunology*, 90, 141-146.
294. RESHI, M. L., SU, Y.-C. & HONG, J.-R. 2014. RNA viruses: ROS-mediated cell death. *International journal of cell biology*, 2014.

295. REYNOLDS, S. J., MAKUMBI, F., NAKIGOZI, G., KAGAAYI, J., GRAY, R. H., WAWER, M., QUINN, T. C. & SERWADDA, D. 2011. HIV-1 transmission among HIV-1 discordant couples before and after the introduction of antiretroviral therapy. *AIDS (London, England)*, 25, 473.
296. RICHARD, J., PRÉVOST, J., BAXTER, A. E., VON BREDOW, B., DING, S., MEDJAHED, H., DELGADO, G. G., BRASSARD, N., STÜRZEL, C. M. & KIRCHHOFF, F. 2018. Uninfected Bystander Cells Impact the Measurement of HIV-Specific Antibody-Dependent Cellular Cytotoxicity Responses. *mBio*, 9, e00358-18.
297. RICHARD, J., VEILLETTE, M., DING, S., ZOUBCHENOK, D., ALSAHAFI, N., COUTU, M., BRASSARD, N., PARK, J., COURTER, J. R. & MELILLO, B. 2016. Small CD4 mimetics prevent HIV-1 uninfected bystander CD4+ T cell killing mediated by antibody-dependent cell-mediated cytotoxicity. *EBioMedicine*, 3, 122-134.
298. RINGE, R. P., OZOROWSKI, G., YASMEEN, A., CUPO, A., PORTILLO, V. M. C., PUGACH, P., GOLABEK, M., RANTALAINEN, K., HOLDEN, L. G. & COTTRELL, C. A. 2017. Improving the expression and purification of soluble, recombinant native-like HIV-1 envelope glycoprotein trimers by targeted sequence changes. *Journal of virology*, JVI. 00264-17.
299. ROGAKOU, E. P., PILCH, D. R., ORR, A. H., IVANOVA, V. S. & BONNER, W. M. 1998. DNA double-stranded breaks induce histone H2AX phosphorylation on serine 139. *Journal of biological chemistry*, 273, 5858-5868.
300. ROGGERO, R., ROBERT-HEBMANN, V., HARRINGTON, S., ROLAND, J., VERGNE, L., JALECO, S., DEVAUX, C. & BIARD-PIECHACZYK, M. 2001. Binding of Human Immunodeficiency Virus Type 1 gp120 to CXCR4 Induces Mitochondrial Transmembrane Depolarization and Cytochrome-c-Mediated Apoptosis Independently of Fas Signaling. *Journal of virology*, 75, 7637-7650.
301. ROUMIER, T., CASTEDO, M., PERFETTINI, J.-L., ANDREAU, K., MÉTIVIER, D., ZAMZAMI, N. & KROEMER, G. 2003. Mitochondrion-dependent caspase activation by the HIV-1 envelope. *Biochemical pharmacology*, 66, 1321-1329.
302. RUIZ, L., MARTINEZ-PICADO, J., ROMEU, J., PAREDES, R., ZAYAT, M. K., MARFIL, S., NEGREDO, E., SIRERA, G., TURAL, C. & CLOTET, B. 2000. Structured treatment interruption in chronically HIV-1 infected patients after long-term viral suppression. *Aids*, 14, 397-403.
303. RYCHERT, J., STRICK, D., BAZNER, S., ROBINSON, J. & ROSENBERG, E. 2010. Detection of HIV gp120 in plasma during early HIV infection is associated with increased proinflammatory and immunoregulatory cytokines. *AIDS research and human retroviruses*, 26, 1139-1145.
304. RYSAVY, N. M., SHIMODA, L. M., DIXON, A. M., SPECK, M., STOKES, A. J., TURNER, H. & UMEMOTO, E. Y. 2014. Beyond apoptosis: the mechanism and function of phosphatidylserine asymmetry in the membrane of activating mast cells. *Bioarchitecture*, 4, 127-137.
305. SAAG, M. S., BENSON, C. A., GANDHI, R. T., HOY, J. F., LANDOVITZ, R. J., MUGAVERO, M. J., SAX, P. E., SMITH, D. M., THOMPSON, M. A. & BUCHBINDER, S. P. 2018. Antiretroviral drugs for treatment and prevention of HIV infection in adults: 2018 recommendations of the International Antiviral Society–USA Panel. *Jama*, 320, 379-396.

306. SAELENS, X., FESTJENS, N., WALLE, L. V., VAN GURP, M., VAN LOO, G. & VANDENABEELE, P. 2004. Toxic proteins released from mitochondria in cell death. *Oncogene*, 23, 2861-2874.
307. SALVATO, M. S., YIN, C. C., YAGITA, H., MAEDA, T., OKUMURA, K., TIKHONOV, I. & PAUZA, C. D. 2007. Attenuated disease in SIV-infected macaques treated with a monoclonal antibody against FasL. *Clinical and Developmental Immunology*, 2007.
308. SAMBROOK, J. & RUSSELL, D. W. 2006. Transformation of E. coli by Electroporation. *Cold Spring Harbor Protocols*, 2006, pdb. prot3933.
309. SANDERS, R. W., DERKING, R., CUPO, A., JULIEN, J.-P., YASMEEN, A., DE VAL, N., KIM, H. J., BLATTNER, C., DE LA PEÑA, A. T. & KORZUN, J. 2013. A next-generation cleaved, soluble HIV-1 Env trimer, BG505 SOSIP. 664 gp140, expresses multiple epitopes for broadly neutralizing but not non-neutralizing antibodies. *PLoS Pathog*, 9, e1003618.
310. SANDERS, R. W., VAN GILS, M. J., DERKING, R., SOK, D., KETAS, T. J., BURGER, J. A., OZOROWSKI, G., CUPO, A., SIMONICH, C. & GOO, L. 2015. HIV-1 neutralizing antibodies induced by native-like envelope trimers. *Science*, 349, aac4223.
311. SANDERS, R. W., VESANEN, M., SCHUELKE, N., MASTER, A., SCHIFFNER, L., KALYANARAMAN, R., PALUCH, M., BERKHOUT, B., MADDON, P. J. & OLSON, W. C. 2002. Stabilization of the soluble, cleaved, trimeric form of the envelope glycoprotein complex of human immunodeficiency virus type 1. *Journal of virology*, 76, 8875-8889.
312. SANTOSUOSSO, M., RIGHI, E., LINDSTROM, V., LEBLANC, P. R. & POZNANSKY, M. C. 2009. HIV-1 envelope protein gp120 is present at high concentrations in secondary lymphoid organs of individuals with chronic HIV-1 infection. *Journal of Infectious Diseases*, 200, 1050-1053.
313. SAPHIRE, E. O., PARREN, P. W., PANTOPHLET, R., ZWICK, M. B., MORRIS, G. M., RUDD, P. M., DWEK, R. A., STANFIELD, R. L., BURTON, D. R. & WILSON, I. A. 2001. Crystal structure of a neutralizing human IGG against HIV-1: a template for vaccine design. *science*, 293, 1155-1159.
314. SARKAR, A., BALE, S., BEHRENS, A.-J., KUMAR, S., SHARMA, S. K., DE VAL, N., PALLESEN, J., IRIMIA, A., DIWANJI, D. C. & STANFIELD, R. L. 2018. Structure of a cleavage-independent HIV Env recapitulates the glycoprotein architecture of the native cleaved trimer. *Nature communications*, 9, 1956.
315. SASTRY, K. J., MARIN, M. C., NEHETE, P. N., MCCONNELL, K., EL-NAGGAR, A. K. & MCDONNELL, T. J. 1996. Expression of human immunodeficiency virus type I tat results in down-regulation of bcl-2 and induction of apoptosis in hematopoietic cells. *Oncogene*, 13, 487-493.
316. SCHÜLKE, N., VESANEN, M. S., SANDERS, R. W., ZHU, P., LU, M., ANSELMA, D. J., VILLA, A. R., PARREN, P. W., BINLEY, J. M. & ROUX, K. H. 2002. Oligomeric and conformational properties of a proteolytically mature, disulfide-stabilized human immunodeficiency virus type 1 gp140 envelope glycoprotein. *Journal of virology*, 76, 7760-7776.
317. SHARMA, S. K., DE VAL, N., BALE, S., GUENAGA, J., TRAN, K., FENG, Y., DUBROVSKAYA, V., WARD, A. B. & WYATT, R. T. 2015. Cleavage-independent HIV-1 Env trimers engineered as soluble native spike mimetics for vaccine design. *Cell reports*, 11, 539-550.
318. SHARP, P. M. & HAHN, B. H. 2011. Origins of HIV and the AIDS pandemic. *Cold Spring Harbor perspectives in medicine*, 1, a006841.

319. SHATTOCK, R. J. & MOORE, J. P. 2003. Inhibiting sexual transmission of HIV-1 infection. *Nature Reviews Microbiology*, 1, 25.
320. SHEDLOCK, D. J., HWANG, D., CHOO, A. Y., CHUNG, C. W., MUTHUMANI, K. & WEINER, D. B. 2008. HIV-1 viral genes and mitochondrial apoptosis. *Apoptosis*, 13, 1088-1099.
321. SILVESTRI, G., SODORA, D. L., KOUP, R. A., PAIARDINI, M., O'NEIL, S. P., MCCLURE, H. M., STAPRANS, S. I. & FEINBERG, M. B. 2003. Nonpathogenic SIV infection of sooty mangabeys is characterized by limited bystander immunopathology despite chronic high-level viremia. *Immunity*, 18, 441-452.
322. SILVESTRIS, F., NAGATA, S., CAFFORIO, P., SILVESTRIS, N. & DAMMACCO, F. 1996. Cross-linking of Fas By Antibodies to a Peculiar Domain of gp120 V3 Loop Can Enhance T Cell Apoptosis in HIV-1-infected Patients. *Journal of Experimental Medicine*, 184, 2287-2300.
323. SKEHEL, J. J. & WILEY, D. C. 2000. Receptor binding and membrane fusion in virus entry: the influenza hemagglutinin. *Annual review of biochemistry*, 69, 531-569.
324. SMITH, C. J., RYOM, L., WEBER, R., MORLAT, P., PRADIER, C., REISS, P., KOWALSKA, J. D., DE WIT, S., LAW, M. & EL SADR, W. 2014. Trends in underlying causes of death in people with HIV from 1999 to 2011 (D: A: D): a multicohort collaboration. *The Lancet*, 384, 241-248.
325. SNYDER, A., ALSAUSKAS, Z. C., LEVENTHAL, J. S., ROSENSTIEL, P. E., GONG, P., CHAN, J. J., BARLEY, K., HE, J. C., KLOTMAN, M. E. & ROSS, M. J. 2010. HIV-1 viral protein r induces ERK and caspase-8 dependent apoptosis in renal tubular epithelial cells. *AIDS (London, England)*, 24, 1107.
326. SOUGRAT, R., BARTESAGHI, A., LIFSON, J. D., BENNETT, A. E., BESS, J. W., ZABRANSKY, D. J. & SUBRAMANIAM, S. 2007. Electron tomography of the contact between T cells and SIV/HIV-1: implications for viral entry. *PLoS pathogens*, 3, e63.
327. SOURISSEAU, M., SOL-FOULON, N., PORROT, F., BLANCHET, F. & SCHWARTZ, O. 2007. Inefficient human immunodeficiency virus replication in mobile lymphocytes. *Journal of virology*, 81, 1000-1012.
328. SPIJKERMAN, I., DE WOLF, F., LANGENDAM, M., SCHUITEMAKER, H. & COUTINHO, R. 1998. Emergence of syncytium-inducing human immunodeficiency virus type 1 variants coincides with a transient increase in viral RNA level and is an independent predictor for progression to AIDS. *Journal of Infectious Diseases*, 178, 397-403.
329. SPIRA, S., WAINBERG, M. A., LOEMBA, H., TURNER, D. & BRENNER, B. G. 2003. Impact of clade diversity on HIV-1 virulence, antiretroviral drug sensitivity and drug resistance. *Journal of Antimicrobial Chemotherapy*, 51, 229-240.
330. STERJOVSKI, J., CHURCHILL, M. J., ELLETT, A., GRAY, L. R., ROCHE, M. J., DUNFEE, R. L., PURCELL, D. F., SAKSENA, N., WANG, B. & SONZA, S. 2007. Asn 362 in gp120 contributes to enhanced fusogenicity by CCR5-restricted HIV-1 envelope glycoprotein variants from patients with AIDS. *Retrovirology*, 4, 89.
331. STERJOVSKI, J., CHURCHILL, M. J., ROCHE, M., ELLETT, A., FARRUGIA, W., WESSELINGH, S. L., CUNNINGHAM, A. L., RAMSLAND, P. A. & GORRY, P. R. 2011. CD4-binding site alterations in CCR5-using HIV-1 envelopes influencing gp120-CD4 interactions and fusogenicity. *Virology*, 410, 418-428.

332. STERNFELD, T., SCHMID, M., TISCHLEDER, A., MUDRA, S., SCHLAMP, A., KOST, B. P., GRUBER, R., YOULE, M., BOGNER, J. R. & GOEBEL, F.-D. 2007. The influence of HIV infection and antiretroviral therapy on the mitochondrial membrane potential of peripheral mononuclear cells. *Antiviral therapy*, 12, 769.
333. STERNFELD, T., TISCHLEDER, A., SCHUSTER, M. & BOGNER, J. 2009. Mitochondrial membrane potential and apoptosis of blood mononuclear cells in untreated HIV-1 infected patients. *HIV medicine*, 10, 512-519.
334. STEVENSON, M., MEIER, C., MANN, A. M., CHAPMAN, N. & WASIAK, A. 1988. Envelope glycoprotein of HIV induces interference and cytolysis resistance in CD4+ cells: mechanism for persistence in AIDS. *Cell*, 53, 483-496.
335. STRACK, P. R., FREY, M. W., RIZZO, C. J., CORDOVA, B., GEORGE, H. J., MEADE, R., HO, S. P., CORMAN, J., TRITCH, R. & KORANT, B. D. 1996. Apoptosis mediated by HIV protease is preceded by cleavage of Bcl-2. *Proceedings of the National Academy of Sciences*, 93, 9571-9576.
336. STREBEL, K. 2014. HIV-1 Vpu—an ion channel in search of a job. *Biochimica et Biophysica Acta (BBA)-Biomembranes*, 1838, 1074-1081.
337. SUNILA, I., VACCAREZZA, M., PANTALEO, G., FAUCI, A. S. & ORENSTEIN, J. M. 1997. gp120 is present on the plasma membrane of apoptotic CD4 cells prepared from lymph nodes of HIV-1-infected individuals: an immunoelectron microscopic study. *Aids*, 11, 27-32.
338. SWANSTROM, R. & COFFIN, J. 2012. HIV-1 pathogenesis: the virus. *Cold Spring Harbor perspectives in medicine*, a007443.
339. TAIT, S. W. & GREEN, D. R. 2010. Mitochondria and cell death: outer membrane permeabilization and beyond. *Nature reviews Molecular cell biology*, 11, 621.
340. TANAKA, M., UENO, T., NAKAHARA, T., SASAKI, K., ISHIMOTO, A. & SAKAI, H. 2003. Downregulation of CD4 is required for maintenance of viral infectivity of HIV-1. *Virology*, 311, 316-325.
341. TANG, S., MURAKAMI, T., AGRESTA, B. E., CAMPBELL, S., FREED, E. O. & LEVIN, J. G. 2001. Human immunodeficiency virus type 1 N-terminal capsid mutants that exhibit aberrant core morphology and are blocked in initiation of reverse transcription in infected cells. *Journal of virology*, 75, 9357-9366.
342. TERAJ, C., KORNBLUTH, R., PAUZA, C. D., RICHMAN, D. D. & CARSON, D. A. 1991. Apoptosis as a mechanism of cell death in cultured T lymphoblasts acutely infected with HIV-1. *Journal of Clinical Investigation*, 87, 1710.
343. THALI, M., MOORE, J., FURMAN, C., CHARLES, M., HO, D., ROBINSON, J. & SODROSKI, J. 1993. Characterization of conserved human immunodeficiency virus type 1 gp120 neutralization epitopes exposed upon gp120-CD4 binding. *Journal of virology*, 67, 3978-3988.
344. THOMAS, E. R., DUNFEE, R. L., STANTON, J., BOGDAN, D., TAYLOR, J., KUNSTMAN, K., BELL, J. E., WOLINSKY, S. M. & GABUZDA, D. 2007. Macrophage entry mediated by HIV Envs from brain and lymphoid tissues is determined by the capacity to use low CD4 levels and overall efficiency of fusion. *Virology*, 360, 105-119.
345. THOMPSON, M. A., ABERG, J. A., HOY, J. F., TELENTI, A., BENSON, C., CAHN, P., ERON, J. J., GÜNTARD, H. F., HAMMER, S. M. & REISS, P. 2012. Antiretroviral treatment of adult HIV infection: 2012 recommendations of the International Antiviral Society—USA panel. *Jama*, 308, 387-402.

346. TINDALL, B. & COOPER, D. A. 1991. Primary HIV infection: host responses and intervention strategies. *Aids*, 5, 1-14.
347. TRAN, E. E., BORGNIA, M. J., KUYBEDA, O., SCHAUDER, D. M., BARTESAGHI, A., FRANK, G. A., SAPIRO, G., MILNE, J. L. & SUBRAMANIAM, S. 2012. Structural mechanism of trimeric HIV-1 envelope glycoprotein activation. *PLoS pathogens*, 8, e1002797.
348. TSAO, L.-C., GUO, H., JEFFREY, J., HOXIE, J. A. & SU, L. 2016. CCR5 interaction with HIV-1 Env contributes to Env-induced depletion of CD4 T cells in vitro and in vivo. *Retrovirology*, 13, 22.
349. ULLRICH, C. K., GROOPMAN, J. E. & GANJU, R. K. 2000. HIV-1 gp120-and gp160-induced apoptosis in cultured endothelial cells is mediated by caspases. *Blood*, 96, 1438-1442.
350. VALLARI, A., HOLZMAYER, V., HARRIS, B., YAMAGUCHI, J., NGANSOP, C., MAKAMCHE, F., MBANYA, D., KAPTUÉ, L., NDEMBI, N. & GÜRTLER, L. 2011. Confirmation of putative HIV-1 group P in Cameroon. *Journal of virology*, 85, 1403-1407.
351. VAN GILS, M. J., EDO-MATAS, D., BOWLES, E. J., BURGER, J. A., STEWART-JONES, G. B. & SCHUITEMAKER, H. 2011. Evolution of human immunodeficiency virus type 1 in a patient with cross-reactive neutralizing activity in serum. *Journal of virology*, JVI. 05214-11.
352. VARGA, T. & APLAN, P. D. 2005. Chromosomal aberrations induced by double strand DNA breaks. *DNA repair*, 4, 1038-1046.
353. VASHISTHA, H., HUSAIN, M., KUMAR, D. & SINGHAL, P. C. 2009. Tubular cell HIV-1 gp120 expression induces caspase 8 activation and apoptosis. *Renal failure*, 31, 303-312.
354. VAUX, D. L. & STRASSER, A. 1996. The molecular biology of apoptosis. *Proceedings of the National Academy of Sciences*, 93, 2239-2244.
355. VENDEVILLE, A., RAYNE, F., BONHOURE, A., BETTACHE, N., MONTCOURRIER, P. & BEAUMELLE, B. 2004. HIV-1 Tat enters T cells using coated pits before translocating from acidified endosomes and eliciting biological responses. *Molecular biology of the cell*, 15, 2347-2360.
356. VLAHAKIS, S. R., ALGECIRAS-SCHIMNICH, A., BOU, G., HEPPELMANN, C. J., VILLASIS-KEEVER, A., COLLMAN, R. G. & PAYA, C. V. 2001. Chemokine-receptor activation by env determines the mechanism of death in HIV-infected and uninfected T lymphocytes. *The Journal of clinical investigation*, 107, 207-215.
357. WADE, J., STERJOVSKI, J., GRAY, L., ROCHE, M., CHIAVAROLI, L., ELLETT, A., JAKOBSEN, M. R., COWLEY, D., DA FONSECA PEREIRA, C. & SAKSENA, N. 2010. Enhanced CD4+ cellular apoptosis by CCR5-restricted HIV-1 envelope glycoprotein variants from patients with progressive HIV-1 infection. *Virology*, 396, 246-255.
358. WAJANT, H. 2002. The Fas signaling pathway: more than a paradigm. *Science*, 296, 1635-1636.
359. WALCZAK, H. & KRAMMER, P. H. 2000. The CD95 (APO-1/Fas) and the TRAIL (APO-2L) apoptosis systems. *Experimental cell research*, 256, 58-66.
360. WANG, H., ZHONG, C.-Y., WU, J.-F., HUANG, Y.-B. & LIU, C.-B. 2010a. Enhancement of TAT cell membrane penetration efficiency by dimethyl sulphoxide. *Journal of Controlled Release*, 143, 64-70.

361. WANG, X. M., NADEAU, P. E., LO, Y.-T. & MERGIA, A. 2010b. Caveolin-1 modulates HIV-1 envelope-induced bystander apoptosis through gp41. *Journal of virology*, 84, 6515-6526.
362. WARD, M., BUEHLER, M. J. W., JAFFE, M. H. W. & BERKELMAN, R. L. 1993. 1993 revised classification system for HIV infection and expanded surveillance case definition for AIDS among adolescents and adults.
363. WEI, P., GARBER, M. E., FANG, S.-M., FISCHER, W. H. & JONES, K. A. 1998. A novel CDK9-associated C-type cyclin interacts directly with HIV-1 Tat and mediates its high-affinity, loop-specific binding to TAR RNA. *Cell*, 92, 451-462.
364. WENSING, A. M., CALVEZ, V., GÜNTARD, H. F., JOHNSON, V. A., PAREDES, R., PILLAY, D., SHAFER, R. W. & RICHMAN, D. D. 2016. 2017 update of the drug resistance mutations in HIV-1. *Topics in antiviral medicine*, 24, 132.
365. WESTENDORP, M. O., FRANK, R., OCHSENBAUER, C., STRICKER, K., DHEIN, J., WALCZAK, H., DEBATING, K.-M. & KRAMMER, P. H. 1995. Sensitization of T cells to CD95-mediated apoptosis by HIV-1 Tat and gp120. *Nature*, 375, 497.
366. WILD, C., DUBAY, J. W., GREENWELL, T., BAIRD, T., OAS, T. G., MCDANAL, C., HUNTER, E. & MATTHEWS, T. 1994. Propensity for a leucine zipper-like domain of human immunodeficiency virus type 1 gp41 to form oligomers correlates with a role in virus-induced fusion rather than assembly of the glycoprotein complex. *Proceedings of the National Academy of Sciences*, 91, 12676-12680.
367. WILEN, C. B., TILTON, J. C. & DOMS, R. W. 2012. HIV: cell binding and entry. *Cold Spring Harbor perspectives in medicine*, a006866.
368. WILLEY, R. L., BONIFACINO, J. S., POTTS, B. J., MARTIN, M. A. & KLAUSNER, R. D. 1988. Biosynthesis, cleavage, and degradation of the human immunodeficiency virus 1 envelope glycoprotein gp160. *Proceedings of the National Academy of Sciences*, 85, 9580-9584.
369. WITTIG, I., BRAUN, H.-P. & SCHÄGGER, H. 2006. Blue native PAGE. *Nature protocols*, 1, 418.
370. WOLF, D., WITTE, V., LAFFERT, B., BLUME, K., STROMER, E., TRAPP, S., D'ALOJA, P., SCHÜRMAN, A. & BAUR, A. S. 2001. HIV-1 Nef associated PAK and PI3-kinases stimulate Akt-independent Bad-phosphorylation to induce anti-apoptotic signals. *Nature medicine*, 7, 1217.
371. WU, Y. 2004. HIV-1 gene expression: lessons from provirus and non-integrated DNA. *Retrovirology*, 1, 13.
372. WYATT, R. & SODROSKI, J. 1998. The HIV-1 envelope glycoproteins: fusogens, antigens, and immunogens. *Science*, 280, 1884-1888.
373. XU, X.-N., LAFFERT, B., SREATON, G. R., KRAFT, M., WOLF, D., KOLANUS, W., MONGKOLSAPAY, J., MCMICHAEL, A. J. & BAUR, A. S. 1999. Induction of Fas Ligand Expression by HIV Involves the Interaction of Nef with the T Cell Receptor Chain.
374. YAN, X., CHU, F., PURI, A. W., FU, Y. & LIDSTROM, M. E. 2016. Electroporation-based genetic manipulation in type I methanotrophs. *Applied and environmental microbiology*, AEM. 03724-15.
375. YANG, X., FARZAN, M., WYATT, R. & SODROSKI, J. 2000a. Characterization of stable, soluble trimers containing complete ectodomains of

- human immunodeficiency virus type 1 envelope glycoproteins. *Journal of virology*, 74, 5716-5725.
376. YANG, X., FLORIN, L., FARZAN, M., KOLCHINSKY, P., KWONG, P. D., SODROSKI, J. & WYATT, R. 2000b. Modifications that stabilize human immunodeficiency virus envelope glycoprotein trimers in solution. *Journal of virology*, 74, 4746-4754.
377. YANG, Y., BAILEY, J., VACCHIO, M. S., YARCHOAN, R. & ASHWELL, J. D. 1995a. Retinoic acid inhibition of ex vivo human immunodeficiency virus-associated apoptosis of peripheral blood cells. *Proceedings of the National Academy of Sciences*, 92, 3051-3055.
378. YANG, Y., MERČEP, M., WARE, C. F. & ASHWELL, J. D. 1995b. Fas and activation-induced Fas ligand mediate apoptosis of T cell hybridomas: inhibition of Fas ligand expression by retinoic acid and glucocorticoids. *Journal of Experimental Medicine*, 181, 1673-1682.
379. YORK, V., MILUSH, J., LÓPEZ-VERGÈS, S., DEEKS, S., MARTIN, J., HECHT, F., LANIER, L. & NIXON, D. 2013. CD56negCD16+ NK cells are mature NK cells generated from CD56+ CD16+ NK cells during HIV-1 infection (P4438). *Am Assoc Immunol*.
380. ZHANG, J. & CRUMPACKER, C. S. 2001. Human immunodeficiency virus type 1 RNA in peripheral blood mononuclear cells of patients receiving prolonged highly active antiretroviral therapy. *The Journal of infectious diseases*, 184, 1341-1344.
381. ZHANG, M., LI, X., PANG, X., DING, L., WOOD, O., CLOUSE, K., HEWLETT, I. & DAYTON, A. I. 2001a. Identification of a potential HIV-induced source of bystander-mediated apoptosis in T cells: upregulation of trail in primary human macrophages by HIV-1 tat. *Journal of biomedical science*, 8, 290-296.
382. ZHANG, W., GODILLOT, A. P., WYATT, R., SODROSKI, J. & CHAIKEN, I. 2001b. Antibody 17b binding at the coreceptor site weakens the kinetics of the interaction of envelope glycoprotein gp120 with CD4. *Biochemistry*, 40, 1662-1670.
383. ZHAO, G., PERILLA, J. R., YUFENYUY, E. L., MENG, X., CHEN, B., NING, J., AHN, J., GRONENBORN, A. M., SCHULTEN, K. & AIKEN, C. 2013. Mature HIV-1 capsid structure by cryo-electron microscopy and all-atom molecular dynamics. *Nature*, 497, 643.
384. ZHOU, Q. & YIK, J. H. 2006. The Yin and Yang of P-TEFb regulation: implications for human immunodeficiency virus gene expression and global control of cell growth and differentiation. *Microbiology and Molecular Biology Reviews*, 70, 646-659.
385. ZHOU, T., XU, L., DEY, B., HESSELL, A. J., VAN RYK, D., XIANG, S.-H., YANG, X., ZHANG, M.-Y., ZWICK, M. B. & ARTHOS, J. 2007. Structural definition of a conserved neutralization epitope on HIV-1 gp120. *Nature*, 445, 732.
386. ZIMMERMAN, C., KLEIN, K. C., KISER, P. K., SINGH, A. R., FIRESTEIN, B. L., RIBA, S. C. & LINGAPPA, J. R. 2002. Identification of a host protein essential for assembly of immature HIV-1 capsids. *Nature*, 415, 88.

APPENDIX G- ethics waiver

UNIVERSITY OF THE
WITWATERSRAND,
JOHANNESBURG



HUMAN RESEARCH ETHICS
COMMITTEE (MEDICAL)

Human Research Ethics Committee (Medical)

Research Office Secretariat:

Faculty of Health Sciences, Phillip Tobias Building, 3rd Floor, Office 301/2/4, 29 Princess of Wales Terrace, Parktown, 2193
Tel +27 (0)11-717-1252 /1234/2656/2700

Private Bag 3, Wits 2050

Office email: HREC-Medical.ResearchOffice@wits.ac.za

Website: www.wits.ac.za/research/about-our-research/ethics-and-research-integrity/

Ref: W-CBP-190409-1

09/04/2019

TO WHOM IT MAY CONCERN:

Waiver: This certifies that the following research does not require clearance from the Human Research Ethics Committee (Medical)

Investigator: Nelia Phuti Manamela (Student Number: 736237)

Supervisor: Prof Maria Papathanasopoulos and Miss Thuli Khanyile

Department: Molecular Medicine and Haematology

Project title: Contribution of HIV-1 subtype C envelope glycoprotein conformations in apoptosis of uninfected bystander CD4+ T lymphocytes

Reason: *In vitro* lab study. No human participation or information is required.

A handwritten signature in cursive script, reading "CB Penny", written over a horizontal line.

Doctor CB Penny

Chairperson: Human Research Ethics Committee (Medical)

Copy – HREC (Medical) Secretariat: Rhulani Mkansi and Zanele Ndlovu.